NASA CONTRACTOR REPORT

NASA CR-928

NASA CR-928
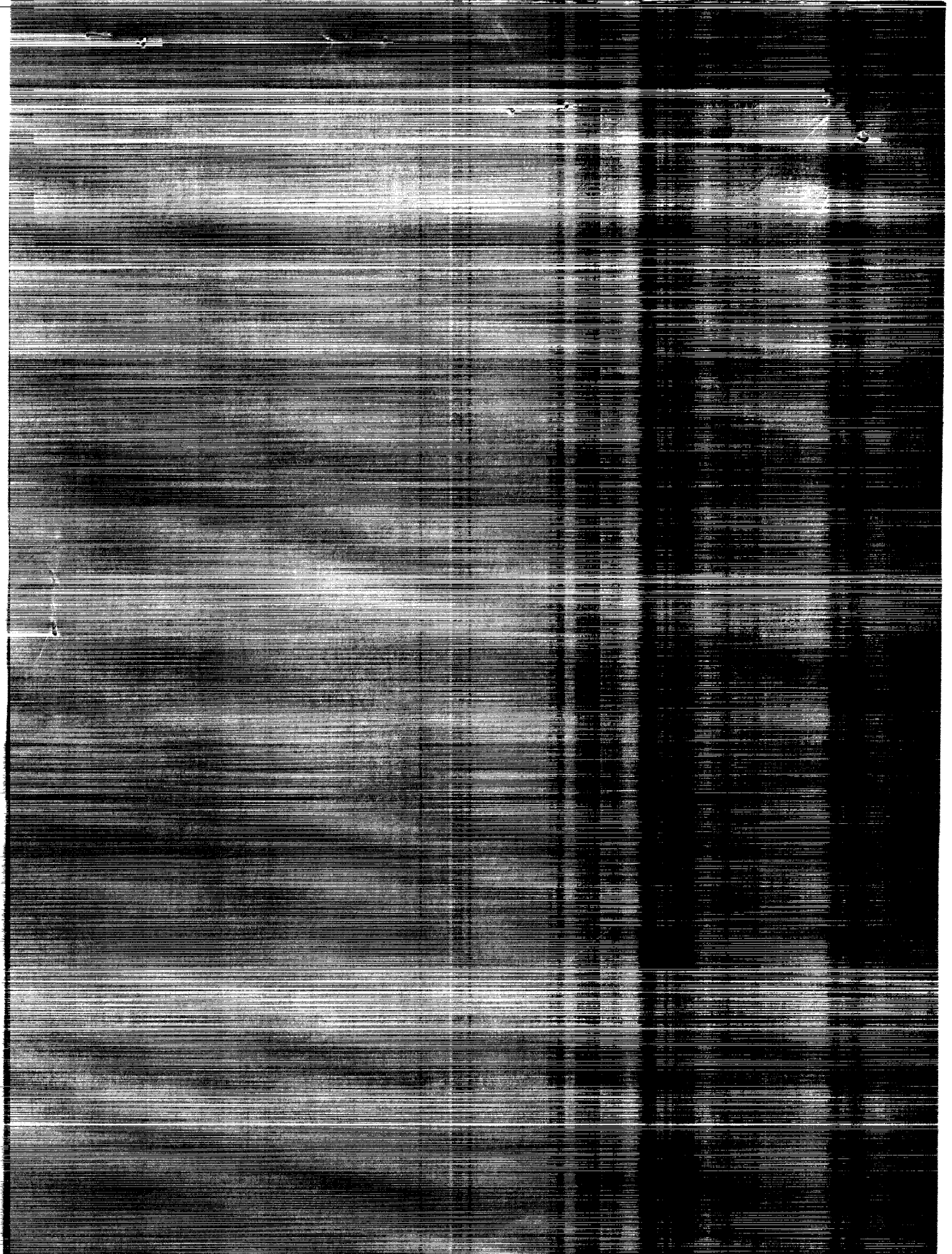
PROPULSION SYSTEM DYNAMIC SIMULATION

THEORY AND EQUATIONS

By Arnold W. Martin

Distribution of this report is provided in the interest of information exchange. Responsibility for the contents resides in the author or organization that prepared it.

Issued by Originator as Report No. NA-67-384

NATIONAL AERONAUTICS AND SPACE ADMINISTRATION

TABLE OF CONTENTS

TABLE OF CONTENTS (Continued)

PROPULSION SYSTEM DYNAMIC SIMULATION

THEORY AND EQUATIONS

By Arnold W. Martin

North American Aviation, Inc.

SUMMARY

This report presents the theory, equations and assumptions for a propulsion system dynamic simulation program with emphasis on the air induction system.

Although the simulation program was developed and used primarily for the XB-70, the theory and equations are sufficiently general to be applicable to a wide range of inlet configurations and flight conditions. Similarly, while the majority of simulation runs have utilized a digital computer in conjunction with the General Electric Company's "Dynasyar" program, the simulation is adaptable to other computing systems, and to analog computers.

INTRODUCTION

In the development of any propulsion system dynamics simulation, a choice must inevitably be made between accuracy, and cost and complexity. Almost as inevitably, the optimum compromise of these conflicting requirements will differ from simulation run to simulation run. Therefore, the simulation program provided as part of contract NAS2-3268, reference 1, has been based on a "building block" concept wherein each of the building blocks can be as sophisticated or as simple as is appropriate. The same concept is used here in describing the logic and equations for various portions of the simulation program.

Air Induction System Simulation:

For illustrative purposes, the simulation theory and equations presented here are of an intermediate degree of sophistication, and assume an air induction system similar to that of the XB-70. In particular, it is assumed that 1) inlet boundary layer air is bled through porous material covering appreciable portions of the throat and internal contraction sections of the inlet, and 2) bypass air is extracted from the duct immediately upstream of the engine face. Details of any specific configuration can usually be accounted for by minor changes in the equations.

The overall air induction system simulation program is capable of simulating almost any mode of inlet operation, from static conditions to high supersonic Mach numbers, from all external to all internal shock compression, and from small disturbances to hammershock. Usually, the event to be simulated and the associated mode of inlet operation will be

known prior to making a simulation run. Consequently the portions of the simulation not applicable to the run can be eliminated. Similarly, many of the options within each phase or mode of inlet operation can be eliminated for a given simulation run.

Air Induction Control System and Engine System Simulations:

Both the air induction control system and the engines for a given aircraft tend to be highly dependent on the specific configuration. Consequently, only highly simplified control system and engine system simulations are presented.

On first acquaintance, these representations may seem to be simplified to the extent of being useless. Experience with the simulation program has shown, however, that such representation can be extremely useful, for example, in 1) mapping areas where detailed testing is required or where a high degree of simulation accuracy is required, 2) simulating malfunctions, 3) analyzing test data, and 4) determining the necessary dynamics response characteristics for various elements of a control system. Such representations have the very appreciable advantage of being easily interpreted, readily changed, and economically run.

3

AIR INDUCTION SYSTEM

Air Induction System Phases of Operation

From both logic and convenience considerations, the air induction system simulation program is divided into phases or modes of operation. These phases have been arbitrarily designated as Started, Unstarting, Empty-Fill, Subcritical, and Hammershock.

Started Phase:

In the Started Phase, an inlet operates with either a combination of external and internal shock compression or all internal shock compression. The terminal normal shock is located downstream of the effective throat as illustrated in figure 1. If the terminal shock were initially at position "a" and the engine or bypass airflow demand decreased, pressure in the duct would increase and the terminal shock would move forward. Maximum total pressure recovery is obtained with the terminal normal shock at the effective throat. Figure 2 shows the typical rise in engine-face total pressure recovery as the terminal shock moves from "a" to "b" with decrease in airflow demand. Should the terminal shock move forward of the effective throat, the inlet unstarts.

Unstarting Phase:

Once the terminal normal shock moves forward of the effective throat, continuity of mass, energy and momentum requires that it continue to move forward past the cowl lip. As the terminal shock moves from "b" to "c" figure 3, engine face total pressure recovery drops as shown in figure 2.

4

Inlet operation during the terminal shock travel from the effective throat to the cowl lip is termed the Unstarting Phase.

The unstart just described was caused by the airflow demand downstream of the inlet throat being less than the airflow captured by the started inlet. Unstart also results when the inlet throat area becomes insufficient to pass the captured airflow. Such a condition can arise because of a decrease in throat area, a reduction in Mach number, or an increase in captured airflow caused by attitude or inlet geometry changes. Whichever the cause, a normal shock forms in the throat and moves upstream as illustrated in figure 4. (It is to be noted that this shock is in addition to the existing terminal normal shock.) Depending on the terminal shock location at the instant of throat choking, the terminal normal shock may move upstream fast enough to catch and coalesce with the forward normal shock before it reaches the cowl lip.

Empty-Fill Phase:

As the terminal normal shock moves forward of the cowl lip, the large static pressure rise across the shock tends to cause massive separation of the boundary layer on the external compression surfaces. Figure 5 illustrates how the flow separation restricts the effective inlet throat area to a fraction of the geometric area. With inflow greatly reduced and outflow (engine and bypass demand) proportional to the instantaneous duct total pressure, engine face total pressure will drop rapidly from condition "d" to "e" as shown in figure 2. During this emptying phase, a terminal shock forms in the effective throat and moves downstream as the duct pressure drops. (Note that there is an external and an internal normal shock during this phase.)

5

After duct pressure drops to a critical level, the separated flow reattaches as shown in figure 6. With outflow low because of the low duct pressure, inflow exceeds outflow, duct pressure rises; and the terminal normal shock moves upstream. Depending on the engine and bypass demand, the terminal shock will either 1) proceed forward of the cowl lip, triggering boundary layer separation and a new emptying phase, or 2) stabilize in a supercritical positions downstream of the inlet throat, point "g" of figure 2.

The Empty-Fill Phase described above is applicable to all of the unstart cycle subsequent to the Unstarting Phase, and to buzz, and supercritical stabilized operation.

Subcritical Phase:

Subcritical and stable inlet operation at subsonic and supersonic flight speeds is shown schematically in figure 7. This mode of operation is designated the Subcritical Phase.

Hammershock Phase:

When duct outflow is abruptly reduced, say by an engine stall, the large excess of inflow over outflow causes a sharp rise in pressure at the engine face. The pressure propagates upstream at a speed, relative to the local flow, somewhat greater than sound. The interface between the undisturbed upstream flow and the high-pressure, low-velocity downstream flow is termed a hammershock. Pressure behind the hammershock can appreciably exceed free-stream total pressure.

Figure 8a shows a typical pressure trace during a hammershock transient. The pressure is that which would be seen just behind the hammershock front.

6

Points on the trace correspond to the hammershock wave positions shown in figure 8b.

Phase changes:

Both the physical and the simulation processes of changing from one Phase to another are continuous and smooth. Logic is contained in each Phase to initiate the change to the next Phase. Special "Initial Conditions" logic computes those properties required to accomplish a smooth transition.

In the subject inlet simulation, logic is provided to automatically accomplish the following Phase changes.

Started	Unstarting
Started	Hammershock
Unstarting	Empty-Fill
Empty-Fill	Hammershock
Empty-Fill	Subcritical
Empty-Fill	Started
Subcritical	Empty-Fill (supercritical, stable)
Subcritical	Hammershock

STARTED PHASE

Inlets having internal shock compression are characterized by low external drag, clean internal lines, and high pressure recovery. These advantages are realized, however, only when the inlet is controlled to near peak performance where small transients in airflow supply or demand can result in the rather violent transient, inlet unstart. Consequently, simulation accuracy is particularly important for the Started Phase of inlet operation.

Started Inlet Geometry

Figure 9 is a schematic diagram of a typical air induction system with a mixed (part external, part internal) shock compression inlet. Principal components are the shock compression surfaces, the subsonic diffuser, a boundary layer bleed system, and a bypass system.

The simulation model configuration for the physical system of figure 9 is shown in figure 10. Also shown are the flow stations with the symbols used in the simulation logic.

Simulation Concept

The simulation model can be considered as either 1) a system of two somewhat arbitrarily defined volumes to which are applied the continuity relationships of mass, energy, and momentum, or 2) a modified Helmholtz resonator superimposed on the internal flow. A mechanical analogy to the Helmholtz resonator concept is a spring-mass system wherein the low

8

velocity air in the aft-duct-volume (Duct Volume) serves as the spring as it is compressed or expanded, and, the high velocity air in the throat section (Helmholtz Volume) acts as a mass whose kinetic energy is changing. Figure 10 illustrates the division between the Duct Volume and the Helmholtz Volume. Note that the upstream face of the Helmholtz Volume is the terminal shock.

In essence, the simulation logic computes the acceleration of the "Helmholtz Volume" resulting from the instantaneous flow conditions at the upstream and downstream faces of this volume. The Helmholtz Volume acceleration is integrated to obtain velocity; then, velocity is integrated to obtain position. Inasmuch as the terminal shock is the upstream face of the Helmholtz Volume, the acceleration, velocity, and position of the terminal shock are also determined.

Two different basic concepts have been used in computing the acceleration, velocity and position of the Helmholtz Volume. The concept designated "Frozen Plug" is presented in the text. This concept is simpler and less sensitive to the arbitrary input of Helmholtz Volume length. Because it is more sensitive to the assumed Helmholtz Volume length, the alternate concept (Appendix A) is sometimes preferable when test data are available to help in the length selection.

Flow properties at the upstream face of the Helmholtz Volume are determined entirely by conditions upstream of the terminal shock. Specifically, these conditions are aircraft Mach number, angle of attack, angle of yaw (- sideslip) and inlet geometry. The simplifying assumption is made that the flow is essentially one-dimensional at the terminal shock, although empirical factors can be used to account for non-uniformity. It

is further assumed that aircraft attitude and inlet geometry rates of
change are such that the compression surfaces are seen as quasi-stationary
by the supersonic flow.

Flow conditions at any station in the Helmholtz Volume (figure 10)
are computed from one-dimensional flow relationships proceeding aft from
the upstream face. Mass and energy enter through the upstream face
(terminal normal shock), and leave through the boundary layer bleed exits
in the Helmholtz Volume and through the interface with the Duct Volume.

The Duct Volume is considered to be a lumped volume in that changes
in density and total temperature are assumed to occur simultaneously
throughout the volume. However, flow properties are assumed to vary from
station to station in the Duct Volume in accordance with quasi-steady
state, one-dimensional flow relationships. Mass and energy enter the Duct
Volume through the interface with the Helmholtz Volume, and leave through
the boundary layer bleed openings in the Duct Volume, through the bypass
openings, and through the engine(s).

Details of the Started Phase are given in the several "logic block"
subdivisions which together form the simulation program. These arbitrary
subdivisions, corresponding in general to the logic block diagrams and
card decks of Reference 1, are as follows: Upstream Properties, Properties
at the Terminal Shock, Properties Behind the Terminal Shock, Boundary Layer
Bleed Flows, Subsonic Flow Total Pressure Losses, Duct Volume Mass, Duct
Volume Total Temperature, Duct Volume Pressures, Bypass and Engine System
Airflows, Helmholtz Volume Properties, Helmholtz Volume Acceleration, Phase
Switches and Outputs to the Air Induction Control Systems.

Upstream Properties

The outputs computed in the Upstream Properties logic block are T_{to}, P_{tx}, and W_{II}; and local Mach number, M_A. Figure 11 is a flow diagram showing the equations used in calculating these outputs.

It will be noticed that γ has been assumed to be a constant, 1.4, in these and subsequent calculations. The error introduced by this assumption is far outweighed by the greater simplicity and time saved in the numerous calculations involving γ. It might be noted that while the specific values selected for such frequently used parameters as γ, g, and R are not critical, it is important that the exact value selected for a term be used in all equations using that term. In particular, the motion of the Helmholtz Volume (and therefore the terminal shock) is a function of the small difference between large numbers, one computed for the flow conditions proceeding from the freestream aft to the Helmholtz Volume-Duct Volume interface, the other computed from the engine face forward to the interface. A small difference in the value of a constant as used in the upstream calculations from that used in the downstream calculations results in a residual error.

The flight conditions, P_o, T_o, M_o, α_o and ψ_o are usually input as independent functions of time as shown in figure 11. They can, however, be expressed as functions of other parameters or computed in further simulation logic blocks.

$\dfrac{P_{tx}}{P_{to}}$, total pressure recovery just upstream of the terminal shock, is expressed as a function of flight conditions and inlet geometry. This permits the use of either test data or data computed from theoretical shock equations for steady state flow. Note that test data must not include

losses across the terminal normal shock or in the subsonic diffuser. Total pressure recovery upstream of the terminal normal shock is surprisingly insensitive to small changes in geometry for high-performance mixed-compression inlets. Consequently, it is frequently possible to express P_{tx}/P_{to} as a function of M_o, α_o, and ψ_o only.

The mass flow ratio, $\dfrac{W_{II}}{W_o}$, is also expressed as a function of flight conditions and inlet geometry. Either test data, calculated values, or a combination of both can be used. Note that:

$$\frac{W_{II}}{W_o} = \frac{W_I}{W_o} - \sum_1^N \left(\frac{W_{bb}}{W_o}\right)_n$$

where $\dfrac{W_{bb}}{W_o}$ is the boundary layer bleed mass flow ratio for a bleed zone entirely in a supersonic flow field. Because the mass flow ratios $\dfrac{W_I}{W_o}$ and $\dfrac{W_{bb}}{W_o}$ can be uniquely defined by the same parameters, it is convenient to combine them into the single term, W_{II}/W_o.

Inasmuch as there is no work or heat addition to the flow between the freestream and the terminal shock, T_{tx} is equal to T_{to}.

Properties at the Upstream Face of the Terminal Shock

Those properties uniquely determined by the upstream flow conditions and the area at the terminal shock station are A_x, W_x, M_x, P_x, T_x, $\overline{P_{ty}}$ and $\overline{P_y}$. Equations used in computing these properties are shown in figure 12. In brief, supersonic Mach number at the shock is computed by iteration from the known quantities of weight flow, total pressure, total temperature, and area. The iteration routine used in the digital computer simulation program is given in Reference 1.

Total flow at the shock station, W_x , is the total captured flow less the boundary layer bleed flow up to the shock. Details of how bleed flow in the throat region is computed are given in the section, Inlet Boundary Layer Bleed Flow.

$\overline{P_{ty}}$ and $\overline{P_y}$ are calculated on the assumption that the terminal shock is stationary. These parameters are used in secondary calculations where it is convenient to make the calculations before determining the shock velocity and then apply corrections to account for the shock velocity.

Properties Behind the Terminal Shock

Properties behind the terminal shock are a function of shock velocity as well as upstream flow conditions and area. Calculations to obtain these parameters, (U_x'/U_x , M_y , T_y , T_{ty} , P_y , P_{ty} , and W_y) are shown in figure 13.

The calculations are based on the fact that the ratios of static pressure and temperature across a normal shock depend only on the Mach number of the supersonic flow relative to the shock wave. The procedure consists of: 1) calculating M_x' , the Mach number of the upstream flow relative to the shock from the supersonic flow Mach number relative to the duct; 2) calculating downstream static pressure, static temperature, and Mach number relative to the shock using conventional normal shock equations; 3) calculating downstream Mach number relative to the flow; and 4) calculating airflow, total pressure, and total temperature downstream of the terminal shock and relative to the duct using the Mach number relative to the duct, static pressure and static temperature.

13

Inlet Boundary Layer Bleed Flow

Boundary layer bleed flow is considered in three parts. First, there is boundary layer bleed from zones that are always and completely upstream of the terminal shock during started operation. This bleed flow has been subtracted from the total captured airflow to give the mass flow ratio, W_{II}/W_0 , as described in the section, Upstream Properties. Second, there is the bleed flow upstream of the terminal shock from a zone (or zones) wherein the bleed flow is affected by the terminal shock position. This bleed flow is designated W_{bbx} . Third, there is the bleed flow downstream of the terminal shock. This flow, W_{bby} , varies both with terminal shock postion and, to a lesser degree, with terminal shock velocity.

Local conditions in the supersonic flow upstream of the terminal shock are dependent only on the flight conditions and inlet geometry. Consequently W_{bbx} is identical to that under steady state conditions with the same terminal shock position.

Local conditions in the subsonic flow downstream of the terminal shock vary with terminal shock velocity as well as position. This factor is accounted for in the boundary layer bleed flow calculations as follows:

1) $\overline{W_{bby}}$ is computed for steady state conditions, assuming the steady state terminal shock to be at the instantaneous shock position.

2) The ratio of instantaneous to steady state bleed flow is assumed to be equal to the ratio of instantaneous to steady state static pressure behind the terminal shock. That is,

$$W_{bby} = \overline{W_{bby}} \; \frac{P_y}{\overline{P_y}}$$

W_{bbx} and $\overline{W_{bby}}$ can be determined for a given flight condition, inlet geometry, boundary layer bleed configuration and terminal shock position from either or both analytical considerations and model test data. The best procedure will vary depending on the details of the specific boundary layer bleed configuration and the test data available. The simulation format used for the XB-70 is described for illustrative purposes.

In the XB-70, inlet boundary layer air bled from a "throat bleed zone" extending from slightly forward of the geometric throat aft to the end of the porous material varies with terminal shock position. Bleed flow through from this zone is collected in a single compartment as shown in figure 14. Also shown is typical 0.25 scale model test data showing boundary layer bleed mass flow ratio in this zone as a function of terminal shock position.

Inspection of the data shows total bleed flow to vary approximately linearly with terminal shock position. Bleed flow from forward of the terminal shock, W_{bbx} , is zero with the shock at X_{II} and equal to the total measured bleed flow with the terminal shock at or aft of X_{III} . Conversely, the steady state bleed flow from aft of the terminal shock, W_{bby} , is equal to the total measured bleed flow with the terminal shock at X_{II} , and zero with the terminal shock at or aft of X_{III} . Further, the throat area variation and bleed area distribution for the XB-70 inlet make it reasonably accurate to assume that W_{bbx} and $\overline{W_{bby}}$ also vary linearly with terminal shock position between X_{II} and X_{III} .

Based on these observations, the following equations were used to compute the bleed flow upstream of the terminal shock position.

$$\frac{W_{bbx}}{W_{II}} = \phi_X \, \Delta X$$

where

$$\phi_x = \left[\frac{d}{dX} \left(\frac{W_{bbx}}{W_{II}} \right) \right]_{\substack{\text{test} \\ \text{data}}} = f(M_A, A_T)$$

When the terminal shock is upstream of X_{II} , ΔX is set to zero inasmuch as W_{bbx} will then be zero. Similarly, when the terminal shock is between X_{II} and X_{III}

$$\Delta X = X - X_{II} \quad .$$

When the terminal shock is downstream of station X_{III} ,

$$\Delta X = X_{III} - X_{II}$$

inasmuch as there is no further increase in W_{bbx} as the shock moves aft of the bleed zone.

Equations for computing bleed flows downstream of the terminal shock are based on similar reasoning. Detailed equations for bleed flows both upstream and downstream of the terminal shock are presented in figure 15. Note that the bleed flow slope, ϕ_y , is negative as illustrated in figure 14.

In the XB-70 simulation program, ϕ_x and ϕ_y are expressed as table look-up functions of local Mach number M_A , and throat area, factors indirectly defining local flow Mach number realtive to each exposed bleed outlet.

Subsonic Flow Total Pressure Losses

Air induction system total pressure losses can be categorized as those occurring across the shock waves, and those resulting from friction and vorticity. The latter, of course, can be strongly influenced by shock-boundary layer interactions.

Assumptions made in simulating total pressure losses other than shock

losses are as follows:

1) There are no expansion losses in the supersonic flow in the inlet.

2) There are negligible friction losses in the supersonic flow in the inlet.

3) The magnitude and distribution of total pressure losses through the subsonic diffuser are those for quasi-steady state flow.

The assumption of negligible friction losses in the supersonic inlet flow is justified by the fact that air in the boundary layer where such losses occur is usually bled-off to prevent boundary layer-shock inter-actions.

Losses in the subsonic flow downstream of the terminal shock are functions of the subsonic diffuser geometry, duct Mach number, Reynolds number, and the location and strength of the terminal shock. The latter become significant particularly during highly supercritical operation when the terminal shock tends to be both strong and downstream of the region having boundary layer bleed.

The format for simulating the subsonic flow total pressure losses permits use of various representations without affecting other portions of the simulation program. Losses can be calculated from test-derived factors or theoretical considerations. The basic requirement for the simulation program is that subsonic diffuser total pressure losses be computed for three sections, y - z, z - d, and d - 2 as shown in figure 16. Total pressure losses in each section are assumed to vary linearly from zero at the upstream face to the full loss at the downstream face.

Most of the representations that have been used have the form

$$\Delta P_t = \epsilon (P_t - P)$$

ϵ is an empirically or theoretically-derived loss coefficient, usually a function of one or more variables defining the inlet geometry and/or the terminal shock location. The compressible dynamic pressure, $q_c \cong P_t - P$, may, depending on the logic selected, be that at 1) station X, immediately upstream of the terminal shock, 2) station Y, immediately downstream of the terminal shock, or 3) stations Y, Z, and d, the upstream stations for each of the three sections.

The representation selected usually depends on the form, quantity and quality of test data available. The following observations may be of help in selecting the representation for a specific simulation.

1) The representation must give a continuous variation in total pressure losses with changes in terminal shock position and inlet geometry. For example, one of the most accurate representations for small shock excursions is that which bases losses on q_c at the station where the porous bleed material ended. Losses upstream of this station are eliminated by boundary layer bleed. Duct flow aft of this station is constant. However, a large and troublesome step change in q_c occurs when the terminal shock crosses this station.

2) Basing losses on the subsonic q_c just downstream of the terminal shock is both logical and probably the most conventional method of computing subsonic diffuser total pressure losses. A subtle disadvantage, whose importance depends on the details of the simulation program, is a feedback between subsonic total pressure losses and q_c through the terminal shock velocity.

3) Basing losses on the supersonic q_c just upstream of the terminal

18

shock is particularly appropriate when the terminal shock moves appreciably downstream of the throat. The shock-boundary layer interaction then becomes a dominant factor in determining subsonic diffuser losses. The supersonic q_c is related to the strength of the terminal shock, and is therefore more nearly proportioned to the shock-boundary layer interaction losses than is q_c downstream of the terminal shock. A further advantage is that the supersonic q_c is independent of the terminal shock velocity.

4) In most tests, only the overall total pressure losses are measured; and, engineering judgement must be used to determine what proportion of the overall loss occurs in each section. Basing losses for each section on q_c at the upstream face of that section would, therefore, seem to be questionable refinement, except under special circumstances.

Two of the representations which have been used in the XB-70 program are shown in figures 17 and 18. The equations of figure 17 illustrate the use of the quasi-steady state static and total pressures downstream of the terminal shock to eliminate the redundancy loop between the dynamic total pressure and total pressure losses in the Duct Volume. The representation of figure 18, wherein losses are based on the dynamic head upstream of the terminal shock, was found convenient for simulation runs investigating the effects of abnormal bypass door settings. The terminal shock was then far downstream, and losses were strongly affected by the strength of the terminal shock.

Duct Volume Mass

Air in the Duct Volume at any instant is

$$\bar{W}_d = \bar{W}_{d_{initial}} + \int_{t_{initial}}^{t} \frac{d\bar{W}_d}{dt} \, dt$$

where $\frac{d\bar{W}_d}{dt}$ is the difference between flow into and out of the Duct Volume.

Flow out of the Duct Volume, depending on the configuration, may include the engine primary airflow, engine secondary airflow, bypass air-flow, and auxiliary airflow for cooling or other purposes. If the auxiliary airflow is negligible as for the XB-70,

$$W_e = W_2 + W_s + W_{bp}$$

During steady state operation, inflow is W_z where

$$W_z = W_{II} - W_{bbx} - W_{bby} = g\rho_z A_z U_z$$

During non-steady state operation, the inflow differs from W_z because the upstream face of the Duct Volume is moving. Inflow under such conditions can be envisioned to consist of two parts - the flow relative to the duct at station z, and the flow swept by the area A_z moving at a velocity $\frac{dX}{dt}$ relative to the duct through air of density ρ_z .

$$W_z' = g\rho_z A_z U_z - g\rho_z A_z \frac{dX}{dt} = W_z \frac{U_z'}{U_z}$$

where

$$U_z' = U_z - dX/dt$$

The calculation of $\bar{W}_d$ is shown in detail in figure 19.

Duct Volume Temperature

Total temperature is computed from the instantaneous total enthalpy and air quantity in the Duct Volume assuming that the air within this

20

volume is at a uniform total temperature. Airflow out of the Duct Volume is assumed to be at this uniform total temperature. Airflow into the Duct Volume is assumed to be at the total temperature just downstream of the terminal shock, T_{ty}. Therefore:

$$\frac{d}{dt}\left(\overline{W}_d\ C_p\ T_{td}\right) = W_z'\ C_p\ T_{ty} - W_e\ C_p\ T_{td} + \frac{P_z\ A_z}{J}\ \frac{dX}{dt}$$

Dividing by C_p and differentiating:

$$\frac{d\overline{W}_d}{dt}\ T_{td} + \overline{W}_d\ \frac{dT_{td}}{dt} = W_z'\ T_{tz} - W_e T_{td} + \frac{P_z A_z}{JC_p}\ \frac{dX}{dt}$$

Substituting $(W_z' - W_e)$ for $\dfrac{d\overline{W}_d}{dt}$,

$$\frac{dT_{td}}{dt} = \frac{1}{\overline{W}_d}\left[W_z'\ (T_{tz} - T_{td}) + \frac{P_z\ A_z}{JC_p}\ \frac{dX}{dt}\right]$$

Further,

$$W_z' = W_z\ (1 - \frac{dX/dt}{U_z}) = W_z\ \frac{U_z'}{U_z}$$

and,

$$\frac{P_z\ A_z}{JC_p}\ \frac{dX}{dt} = W_z\ \frac{(\gamma - 1)}{\gamma}\ \frac{dX/dt}{U_z}\ T_z$$

therefore,

$$\frac{d\ T_{td}}{dt} = \frac{W_z}{\overline{W}_d\ U_z}\left[U_z'\ (T_{ty} - T_{td}) + \frac{(\gamma - 1)}{\gamma}\ \frac{dX}{dt}\ T_z\right]$$

The final equations for computing T_{td} are presented in figure 20.

Duct Volume Pressures

At any instant, the average density in the Duct Volume is

$$ g \rho_d = \frac{\overline{W}_d}{\overline{V}_d} = \frac{P_d}{RT_d} $$

Therefore

$$ P_d = \frac{\overline{W}_d}{\overline{V}_d} RT_d $$

and

$$ P_{td} = P_d (1 + .2M_d^2)^{3.5} $$

where M_d is the Mach number at the station d where the density is equal
to the average density in the Duct Volume. Several methods of varying
degrees of accuracy and complexity have been developed for computing Mach
number at the average density station. The simplest approximation, reason-
ably accurate for all but extremely large terminal shock excursions, is
defined by the equations of figure 21.

The first step in this approximate method consists of determining
the ratio of the area at the average density station to the geometric
average area in the Duct Volume during the initial steady state conditions.
This ratio is then assumed to remain constant during the transient conditions.

During the initial steady state conditions,

$$ g \rho_d = \frac{\overline{W}_d}{\overline{V}_d} $$

and

$$ g \rho_{td} = \frac{P_{td}}{RT_{td}} $$

Therefore

$$\frac{\rho_{td}}{\rho_d} = \frac{P_{td}}{RT_{td}} \Big/ \frac{\overline{W_d}}{V_d} = (1 + .2M_d^2)^{5/2}$$

or

$$M_d = \left(5\left[\left(\frac{P_{td}}{RT_{td}} \Big/ \frac{\overline{W_d}}{V_d}\right)^{2/5} - 1\right]\right)^{\frac{1}{2}}$$

Further, flow at the average density station will be equal to W_z , the flow at the end of the boundary layer bleed system. Inasmuch as

$$W_z = W_d = \frac{P_{td}}{\sqrt{T_{td}}}\sqrt{\frac{\gamma g}{R}} \frac{M_d}{(1 + .2M_d^2)^3} A_d$$

the flow area at the average density station is

$$A_d = \frac{W_z\sqrt{T_{td}}}{P_{td}} \sqrt{\frac{R}{\gamma g}} \frac{(1 + .2M_d^2)^3}{M_d}$$

The geometric average area is computed as

$$A_{d_{geo}} = \frac{V_d}{X_e - X_z}$$

Consequently, the ratio of area at the average density station to the geometric average area is

$$K_a = \frac{A_d}{A_{d_{geo}}} = \frac{A_d}{\left(\frac{V_d}{X_e - X_z}\right)}$$

During subsequent transient conditions, M_d is determined by iterative solution of the equation:

$$\frac{M_d}{(1 + .2M_d^2)^3} = \frac{W_{zH}\sqrt{T_{td}}}{P_{td_H} K_a A_{d_{geo}}} \sqrt{\frac{R}{\gamma g}}$$

23

where

$$P_{td_H} = P_{ty} - \Delta P_{tyz} - \Delta P_{tzd}$$

and W_{zH} is the flow at station z computed on the assumption that the flow is in equilibrium with the instantaneous value of terminal shock velocity. A more correct assumption would be that the flow at the average density station was the average of the instantaneous flows at the upstream and the downstream faces of the Duct Volume. This however, introduces a redundancy loop (P_{td} is a function of W_d which is a function of P_{td}) which introduces more problems than the change in accuracy usually merits.

To repeat,

$$P_{td} = P_d(1 + .2M_d^2)^{3.5} = \frac{\bar{W}_d \, RT_{td}}{V_d} (1 + .2M_d^2)^{3.5}$$

Total pressures at the upstream and downstream faces of the Duct Volume are, respectively,

$$P_{tzD} = P_{td} + \Delta P_{tzd}$$

and

$$P_{te} = P_{t2} = P_{td} - \Delta P_{tde} \quad .$$

Static pressure at the upstream face of the Duct Volume is

$$P_{zD} = P_{tzD}/(1 + .2M_{zD}^2)^{3.5}$$

where M_{zD} is obtained by iterative solution of the equation

$$\frac{M_{zD}}{(1 + .2M_{zD}^2)^3} = \frac{W_z \sqrt{T_{td}}}{P_{tzD} \, A_z} \sqrt{\frac{R}{\gamma g}}$$

Note that P_{zD} is static pressure at station z computed from properties in the Duct Volume. Later, pressure at station z is computed from properties in the Helmholtz Volume. It is the difference between these two pressures

that acts to accelerate the Helmholtz Volume.

Bypass and Engine System Airflows

The optimum format for computing bypass and engine system airflows will vary with details of the specific configuration to be simulated. In the XB-70 configuration, duct air enters a plenum chamber immediately forward of the engines from where it is exhausted either or both through the bypass doors and the engine secondary flow system. The system is shown schematically in figure 22.

Each inlet has two sets of bypass doors, Trim and Main. Both the Trim and Main bypass doors form convergent-divergent nozzles at low bypass exit area and convergent nozzles at high bypass exit areas. The Trim bypass doors have high movement rate capabilities but low flow capacity; conversely, the Main doors have low rate capabilities but high flow capacity. Total bypass flow is the summation of the flow through the two sets of bypass doors. Bypass flow is computed as

$$W_{bp} = \frac{K_{bp} \, P_{t2}}{\sqrt{T_{t2}}} \sqrt{\frac{\gamma g}{R} \left(\frac{M_{bp}}{(1 + .2M_{bp}^2)^3} \right)} C_{bp}A_{bp}$$

where

$$K_{bp} = \frac{P_{tbp}}{P_{t2}}$$

M_{bp} = bypass throat Mach number.

$C_{bp}A_{bp}$ = bypass effective throat area.

During most flight conditions, M_{bp} is sonic or near sonic, and

$$W_{bp} = K_{bp}P_{t2} \, \lambda \, C_{bp}A_{bp}$$

Further, the pressure ratio, $K_{bp} = \dfrac{P_{bp}}{P_{t2}}$, usually varies with bypass flow quantity which in turn varies with $C_{bp}A_{bp}$. It is often convenient, therefore, to include the K_{bp} term in the C_{bp} term.

XB-70 engine secondary airflow is, depending on flight conditions, supplied by either the boundary layer bleed system or the bypass compartment. In the latter situation, secondary airflow is scheduled as a function of primary engine flow. The engine system airflow can then be express as

$$W_2 + W_8 = W_2 \left(1 + \left(\frac{W_s}{W_2} \right)_{scheduled} \right)$$

Equations for computing bypass and engine system airflows are presented in figure 23.

Helmholtz Volume Properties

In the "frozen plug" simulation concept, properties throughout the Helmholtz Volume at any instant are assumed to be dependent on, and in equilibrium with conditions just downstream of the terminal shock (station y of figure 10). For example, at station z of the Helmholtz Volume, the instantaneous total temperature is T_{ty} ; the instantaneous total pressure is P_{ty} less the subsonic diffuser losses between stations y and z; and, the instantaneous flow is W_y less any flow removed from the duct between stations y and z.

Total air quantity in the Helmholtz Volume is the initial quantity plus the difference between flow into and out of the volume. That is,

$$\bar{W}_H = \bar{W}_{H_i} + \int_i^t \frac{d\bar{W}_H}{dt}\, dt$$

where,

$$\frac{d\bar{W}_H}{dt} = W_x' - W_z' - W_{bby}$$

In an analogous concept to that described in the section, Duct Volume Mass, flow into the Helmholtz Volume can be expressed as

$$W_x' = g\rho_x A_x U_x - g\rho_x A_x \frac{dX}{dt} = W_x \frac{U_x'}{U_x}$$

where

$$U_x' = U_x - dX/dt$$

Similarly, outflow through the downstream face of the Plug Volume is

$$W_z' = W_z \frac{U_z'}{U_z} = (W_y - W_{bby}) \frac{U_z'}{U_z}$$

Total outflow is

$$W_z' + W_{bby}$$

Should there be a bypass in the throat region, the total outflow would become

$$W_z \frac{U_z'}{U_z} + W_{bby} + W_{bp_{THROAT}} \quad .$$

Equations for computing Helmholtz Volume properties are summarized in figure 24.

Helmholtz Volume Acceleration

The approximation is made in the "frozen plug" concept that instantaneous properties throughout the Helmholtz Volume are related to those at station y by steady state flow relationships. For the instantaneous terminal shock position, X, and velocity, dX/dt, the equilibrium pressure at the downstream face of the "frozen" Helmholtz Volume is P_{zH} .

The instantaneous pressure at the upstream face of the Duct Volume, computed from Duct Volume properties, is P_{zD}. During steady state operation, P_{zH} equals P_{zD}; and, there is no inbalance of forces at the interface. During non-equilibrium conditions, P_{zH} will not equal P_{zD}; and, there will be an unbalanced force of $(P_{zH} - P_{zD})A_z$. The unbalanced force is assumed to act on the Helmholtz Volume as follows:

$$\frac{d}{dt}\left(\frac{\bar{W}_H}{g}\frac{dX}{dt}\right) = (P_{zH} - P_{zD})A_z$$

or

$$\frac{d(\bar{W}_H/g)}{dt}\frac{dX}{dt} + \frac{\bar{W}_H}{g}\frac{d^2X}{dt^2} = (P_{zH} - P_{zD})A_z$$

Figure 25 is a diagram of the equations used to determine Helmholtz Volume terminal shock acceleration, velocity, and position.

It might be noted that there is no "dead time" factor introduced into the equations of motions (dead time being that time required for a disturbance traveling through the airflow at local sonic velocities to go from, say, the engine face to the terminal shock). While dead time may logically be considered a limiting minimum time for a disturbance to be sensed at another station, it is hypothesized that any disturbance propagated through the Duct Volume will be attenuated to insignificance until there has been a significant rise in Duct Volume pressure. Further, the mass accumulation causing Duct Volume pressure change and the disturbance "wave" propagation take place coincidentally rather than sequentially. Consequently, the addition of a "dead time" would not be logical.

Phase Switches

The phase switch logic continually monitors various inlet parameters to determine whether and when a switch should be made:

1) to the Unstarting Phase because the terminal normal shock has passed forward of the aerodynamic throat,

2) to the Unstarting Phase because the throat area is too small to pass the captured flow,

3) to the Hammershock Phase because of an abrupt decrease in outflow from the duct.

Logic for each of these checks is outlined in figure 26 and described below.

Unstart Inititated by the Terminal Shock Moving Upstream of the Throat:

In discussing the initiation of unstart due to the terminal normal shock moving forward of the inlet aerodynamic throat, it should be noted that the aerodynamic throat can be appreciably forward of the geometric throat. This is illustrated in figure 27.

Three checks are made to determine when this type of unstart has been initiated. First, the terminal shock must be moving upstream. Second, the supersonic Mach number upstream of the terminal shock must be increasing. These checks indicate that the terminal shock is moving upstream of an aerodynamic throat. Finally, the terminal shock must be forward of the geometric throat. This check has been found necessary because there may be one or more secondary throats (area contraction) downstream of the primary inlet throat. Even small area discontinuities associated with the area calculation procedure can result in a false unstart without this check.

Unstart Initiated by Insufficient Throat Area:

Inlet unstart is also initiated when the throat area becomes insufficient to pass the captured airflow. This condition may result from a variety of causes including attitude changes, Mach number changes, and throat area changes. Whatever the cause, the phase switching logic compares the captured airflow (less the boundary layer bleed upstream of the throat) to the flow that can pass through the throat at the instantaneous total pressure and temperature. An empirical constant, K_u , is used to reduce the flow that could theoretically pass through the throat at Mach 1.0. This factor accounts for such items as non-uniform Mach number in the throat, and differences between effective flow area and geometric area.

Hammershock:

The large and abrupt decrease in duct outflow associated with engine stall results in the formation of a hammershock wave at the engine face and subsequent forward motion of this wave. Inasmuch as an airflow decrease of any magnitude will cause a hammershock disturbance of some magnitude, the decision as to how large the airflow decrease must be before the Hammershock Phase is applicable is necessarily arbitrary. Consequently, the phase switching logic computes proportional rate of change of duct outflow, $\frac{dWe}{We}/dt$, and compares this with an arbitray critical rate of change, K_{HS} , above which the Hammershock Phase is considered more appropriate. Selection of K_{HS} is made by comparing both Hammershock Phase and Started Phase simulation data for a series of duct outflow reduction rates. K_{HS} is that value giving an appreciably higher duct pressure with the Hammershock Phase than with the Started Phase.

Outputs to the Air Induction Control System

One of the most difficult problems in the design and development of an air induction system is finding signals suitable for control of the system. Differences in inlet geometry, performance requirements, maneuvering rates, and similar factors will undoubtedly make the control system and signals used unique for each aircraft. However, several procedures used in computing control signals for the XB-70 demonstrate some of the methods which can be used in simulating control signals. Locations of the various air induction control system signal pick-ups are shown in figure 28.

Local Mach Number:

Mach number on the first ramp of the inlet, M_A , is used to arm the Restart Control and to schedule throat area. Local Mach number is used as a control system input in preference to freestream Mach number because, ideally, it eliminates the need to know angle of attack and angle of yaw. M_A is computed by interpolation of tables of M_A versus M_O , α_O , and ψ_O . Such tables can be generated either from test data or analytical data.

Local Static Pressure Ratio:

The ratio of local static pressure to the static or total pressure at another duct station is a widely used control signal. During the "Low Performance" mode of inlet operation of the XB-70 for example, the bypass doors are opened to pull the terminal shock aft to the "Downstream Shock Position Signal" station, thereby providing tolerance to larger airflow transients.

Figure 29 shows theoretical and test observed variation in the DSPS static pressure, P_{DSS} , with terminal shock position. Also shown is a

reference static pressure, P_{DSR} , at a station close to the engine face
where flow is always subsonic. The static pressure ratio curve, $\frac{P_{DSS}}{P_{DSR}}$,
indicates terminal shock position in units independent of absolute total
pressure. When "Low Performance" is called for, the bypass doors open until
the ratio $\frac{P_{DSS}}{P_{DSR}}$ reaches a scheduled value.

Several procedures can be used to simulate the air induction system
signals of figure 29. The most appropriate method depends on the control
system design and the empirical data available.

Where the control system reacts only to the information that the
pressure ratio is above or below the scheduled value, it is sufficient to
use the shock position as a signal. That is:

if $\qquad$ $X > X_{DSS}$

$\qquad$ $\frac{P_{DSS}}{P_{DSR}} <$ scheduled value

$\qquad$ bypass doors move in closing direction;

if $\qquad$ $X < X_{DSS}$

$\qquad$ $\frac{P_{DSS}}{P_{DSR}} >$ scheduled value

$\qquad$ bypass doors move in opening direction.

Where the bypass rate depends on the difference between the observed
and scheduled values of $\frac{P_{DSS}}{P_{DSR}}$, it becomes appropriate to use empirical
data tables of $\frac{P_{DSS}}{P_{DSR}}$ as a function of terminal shock position and inlet
throat area. This introduces the slopes shown in the test data of figure
29, associated with pressure feed back through the boundary layer and finite
width of both the pressure sensor and the terminal shock.

When pressure sensor lines are relatively long and perhaps of dissimilar

32

lengths, simulation of the line phase and amplitude response characteristics may require that the absolute static pressure at the sensor pressure taps be computed. This can be done as follows. If $X > X_{DPS}$, M_{DSS} is obtained by iterative supersonic solution of the equation

$$\frac{M_{DSS}}{(1 + .2M_{DSS}^2)^3} = \frac{W_{DSS}}{\frac{P_{tx}}{\sqrt{T_{to}}}\sqrt{\frac{\gamma g}{R}} A_{DSS}}$$

Then

$$P_{DSS} = \frac{P_{tx}}{(1 + .2M_{DSS}^2)^{3.5}}$$

If $X \leq X_{DSPS}$, M_{DSPS} is obtained by iterative subsonic solution of the equation

$$\frac{M_{DSPS}}{(1 + .2M_{DSPS}^2)^{3.5}} = \frac{W_{DSPS}}{\frac{P_{tDSPS}}{\sqrt{T_{td}}}\sqrt{\frac{\gamma g}{R}} A_{DSPS}}$$

Then

$$P_{DSPS} = \frac{P_{tDSPS}}{(1 + .2M_{DSPS}^2)^{3.5}}$$

Assuming total pressure losses in the subsonic flow to be proportional to duct length,

$$\frac{P_{ty} - P_{tDSPS}}{P_{ty} - P_{t2}} = \frac{X_{DSPS} - X}{X_2 - X}$$

or

$$P_{tDSPS} = P_{ty} - (P_{ty} - P_{t2})\left(\frac{X_{DSPS} - X}{X_2 - X}\right).$$

33

The value of W_{DSPS} can best be determined by consideration of the specific geometry. For the XB-70 configuration, X_{DSPS} is slightly downstream of the porous bleed section, and, ignoring secondary dynamics effects, $W_{DSPS} = W_z$.

Duct Overpressure:

To minimize air induction system weight, it may be desirable to have a control function which opens the bypass doors when necessary to limit differential pressure across the duct wall to a scheduled maximum. The signal pressures required are P_{OP} and P_0 where the control maintains $P_{OP} - P_0 \leq \Delta P$ scheduled. P_0 is obtained from flight conditions. P_{OP} is obtained in a manner similar to that described above for computing P_{DSS}.

Shock Position Pressure Ratio:

The terminal shock positioning parameter, SPP, for the B-70 inlet is the ratio of the shock position manifold pressure P_{SPM}, to a throat total-pressure-probe pressure, P_{SPR}. The shock position manifold and the throat-total-pressure probe are shown schematically in figure 28.

As the terminal shock moves forward, the number of manifold static pressure taps exposed to the high static pressure downstream of the terminal shock increases, and therefore the manifold pressure increases. The total probe pressure, which does not change with terminal shock position, serves to eliminate the effect of absolute pressure level. By properly spacing the holes in the manifold, the ratio of manifold to total probe pressure, SPP, can be shaped to give a near linear variation with, say, corrected weight flow, $W_e/(P_{t2}/P_{to})$.

In the B-70 inlet simulation, SPP is obtained by interpolation of model test values of SPP tabulated as a function of terminal shock position,

throat area, and $\dfrac{W_{TT}\sqrt{T_{to}}}{A_T \, P_{tx}}$. These factors define the terminal shock position, inlet geometry, and inlet throat Mach number.

Examples of the equations used to obtain inlet signals to the control system are presented in figure 30. The representation for determining the Downstream Shock Parameter, DSP, is a compromise between the several methods discussed previously. P_{DSS} is set equal to P_y when the terminal shock is forward of the sensing station, and equal to P_x when the shock is aft of the sensing station. P_{DSR} is set equal to P_d . While not precise, these values give reasonable approximations of the signal pressures with a minimum of calculations. A similar simplification is used for the Overpressure signal.

UNSTARTING PHASE

The mode of inlet operation wherein a normal shock travels upstream from the aerodynamic throat to the cowl lip, figures 3 and 4, is termed the Unstarting Phase. Figure 2 shows the typical pressure drop during this phase and its relationship to the remainder of the unstart transient.

Unstarting can be initiated by either of two conditions. In one, later referred to as Insufficient Demand Unstarting, the airflow demand downstream of the inlet throat becomes less than the airflow through the throat section. In the other, called Choked Throat Unstarting, the captured airflow exceeds the airflow that can pass through the throat at the existing total pressure and temperature. The separate sets of logic for simulating Insufficient Demand Unstarting and Choked Throat Unstarting have been combined in the mutually-inclusive Unstarting Phase.

Insufficient Demand Unstarting Simulation Concept

Figure 31 is a schematic representation of the Insufficient Demand Unstarting simulation model. The model differs from that for the Started Phase in that it has one rather than two "lumped volumes" with distributed properties. This simplification is justified both by the lesser accuracy requirements for this phase and by the agreement between the simulation and model test data.

In brief, properties downstream of the terminal shock are determined from the instantaneous total mass and total temperature in the Duct Volume; and, the properties upstream of the terminal shock are determined from the instantaneous flight conditions and inlet geometry. The terminal shock

velocity is that value required to satisfy the upstream and downstream conditions at any instant. Shock position is obtained by integration of the shock velocity.

Choked Throat Unstarting Simulation Concept

Inlet unstart because of insufficient throat area to pass the captured airflow can result 1) from attitude changes increasing the captured airflow, 2) from decreases in throat area, and 3) from flight Mach number reductions. Whatever the cause, the excess of inflow over that which can pass through the throat results in the formation of a normal shock in the throat.

In the simulation program, this mode of operation is initiated by arbitrarily locating a normal shock a small but finite distance forward of the throat. The volume between this normal shock and the throat then becomes the control volume for the Choked Throat Unstarting Phase as illustrated in figure 32. Inflow to the "Throat Volume" is a function of the supersonic flow conditions just upstream of the normal shock and the normal shock velocity. Flow leaves the control volume through the choked throat and through any boundary layer bleed exits in the control volume. Outflow is a function of the total pressure and temperature in the control volume and the effective throat and bleed areas. Total pressure and temperature are computed from the instantaneous values of volume, mass, enthalpy and average velocity in the control volume. Shock velocity is determined by iteration to obtain that value necessary to satisfy the instantaneous flow conditions usptream and downstream of the normal shock.

It is emphasized that the normal shock described above is in addition to the originally existing terminal shock. That is, there are two simultaneous normal shocks in the inlet. During the unstarting transient, the

upstream normal shock motion is independent of conditions downstream of the inlet throat (unless the terminal shock moves forward of the throat). The terminal normal shock motion is, however, very much a function of the upstream conditions and therefore of the upstream normal shock.

Figure 33 illustrates the dependency of the terminal normal shock motion on the choked-throat-induced transient. As the upstream normal shock forms at the throat and moves out of the supersonic diffuser portion of the inlet, the ratio of total temperature across the shock rises and the ratio of total pressure drops rapidly. The associated change in pressure, temperature, and flow just upstream of the terminal normal shock then cause it to move upstream. Depending on such factors as the position of the terminal normal at the time of throat choking, the terminal normal shock may overtake and coalesce with the upstream normal shock before it reached the cowl lip.

Because of their interdependency, the Insufficient demand and the Choked Throat Unstarting Phases have been combined in the single Unstarting Phase. In those cases where an unstart is induced by throat choking, the throat total pressure, temperature and flow computed by that Phase logic become the upstream conditions for the terminal shock. Switching to the Empty-Fill Phase occurs when either the upstream normal shock, the terminal normal shock, or the coalesced shock pass the cowl lip. This procedure assumes that the Unstarting Upstream transient is independent of the terminal normal shock, or to be more specific, that there is sonic flow through the effective throat area. If and when the terminal shock passes forward of the throat, flow in the throat will in actuality be subsonic. The error in computed outflow does not, however, appreciably affect the overall transient.

More details of the simulation logic are presented in the discussions of the various portions of the Unstarting Phase.

Upstream Properties

The simulation model for the Unstarting Phase is presented in figure 34. During the Unstarting Downstream transient, the Upstream Volume becomes vanishingly small and does not affect the upstream properties relative to the Duct Volume.

Upstream properties for the Upstream Volume are computed as shown in figure 35. The equations used to compute P_{tx} , T_{tx} , W_{II} , and M_A are identical to those used in the Started Phase, figure 11. The data tables used in calculating these properties are also identical and interchangeable with the Started Phase Tables.

P_{tx} is, by definition, the total pressure just downstream of the oblique compression shock waves in the supersonic diffuser but upstream of any normal shock within the inlet. P_{tx} increases, therefore, as the normal shock moves forward and eliminates part of the oblique shock system total pressure loss. Generally speaking, the oblique shock losses from the cowl to the throat are small, and the assumption that the oblique shock losses (and therefore P_{tx}) do not vary with normal shock position is considered adequate for the Unstarting Phase of inlet simulation.

Properties Upstream of the Upstream Normal Shock

Equations for computing properties just forward of the upstream normal shock are presented in figure 36. Note that W_{xu} exceeds W_{II} inasmuch as W_{II} is defined as the total captured airflow less the bleed flow up to station X_{II} during started operation as illustrated in figure 37. Duct

airflow and cumulative bleed flow are plotted as a function of inlet station for four terminal shock positions. At a given normal shock position, X_u, flow just upstream of the shock will be $W_{II} + \Delta W_{bbx}$ as expressed graphically in figure 37. Note that while there is less bleed flow forward of the normal shock as it moves upstream in the supersonic diffuser, the total bleed flow increases as more of the bleed area is exposed to higher-static-pressure subsonic flow.

Properties Behind the Upstream Normal Shock

Properties just downstream of the normal shock are determined by 1) computing the Mach number of the upstream flow relative to the moving normal shock, 2) computing static pressure and temperature from the upstream static pressure and temperature and the upstream Mach number relative to the shock, 3) calculating the downstream Mach number relative to the moving shock, 4) calculating the downstream Mach number relative to the duct, and 5) computing total temperature relative to the duct from the downstream static temperature and the Mach number relative to the duct. Figure 38 is a diagram of the equations used for these calculations.

Boundary Layer Bleed Forward of the Throat

Illustrative curves of total boundary layer bleed flow, bleed flow upstream of the normal shock, and bleed flow downstream of the normal shock as a function of shock position are presented in figure 39. These characteristic curves may be determined from analytical considerations or by interpolation of test data. The curves shown were obtained by straight-line interpolation of data such as shown in figure 37. Each particular inlet and bleed configuration will have its own characteristics. Those of the

XB-70 configuration are essentially linear as shown.

Supersonic flow at a station upstream of normal shock between stations X_{II} and X_I, figure 37, is equal to W_{II} plus and increment, ΔW_{bbx}. For the bleed characteristics shown in figure 39,

$$\Delta W_{bbx} = \left(\frac{dW_{bbx}}{dx}\right)\left(X_{II} - X_u\right)$$

In a non-dimensional form

$$\Delta W_{bbx} = \frac{dW_{bbx}/W_{II}}{dx}\left(X_{II} - X_u\right)\left(W_{II}\right)$$

$$= \phi_{xu}(X_{II} - X_u)\,W_{II}$$

where ϕ_{xu} is the slope $\dfrac{dW_{bbx}/W_{II}}{dx}$ between stations X_I and X_{II}.

Bleed flow, W_{bbyu} in the subsonic flow region between the normal shock station, X_u, and the throat is computed in a similar method as that described for computing ΔW_{bbx}. Equations for computing W_{bbyu} and ΔW_{bbx} are listed in figure 40. As in the Started Phase, quasi-steady state bleed flow, $\overline{W_{bbyu}}$, is corrected to the dynamic conditions by the ratio of instantaneous to quasi-steady state static pressures aft of the normal shock. That is

$$W_{bbyu} = \overline{W_{bbyu}}\ \frac{P_{yu}}{\overline{P_{yu}}}$$

The equation for computing $\overline{W_{bbyu}}$ used in figure 40,

$$\overline{W_{bbyu}} = \phi_{yu}(X_u - X_T)W_{II}$$

would more properly be

$$\overline{W_{bbyu}} = \left[\phi_{yu}(X_u - X_{II}) + \phi_y(X_{II} - X_T)\right]W_{II}$$

because the aerodynamic throat station and the bleed zone boundary station,

41

X_{II} , will usually differ slightly. The error introduced is trivial for most configurations.

Upstream Volume Mass and Total Temperature

Inflow to the Upstream Volume can be envisioned to consist of two parts, flow relative to the duct at station X_u and the quantity of air swept by the shock face moving through air at a density ρ_{xu} with a velocity $\frac{dX_u}{dt}$ relative to the duct. That is

$$W_{xu} = g\rho_{xu} A_{xu} U_{xu} - g\rho_{xu} A_{xu} \frac{dX_u}{dt} = W_{xu} \frac{U'_{xu}}{U_{xu}}$$

where

$$U'_{xu} = U_{xu} - \frac{dX_u}{dt}$$

Outflow is the summation of flow out of the boundary layer bleed exits in the Upstream Volume and flow through the choked throat. The latter is

$$W_T = \frac{K_u P_{tu}}{\sqrt{T_{tu}}} A_T \lambda$$

where the throat Mach number is assumed to be unity and K_u is an empirical flow coefficient which accounts for non-uniformity in Mach number at the throat.

The quantity of air in the Upstream Volume at any time, t, is

$$\bar{W}_u = \bar{W}_{ui} + \int_i^t \frac{dW_u}{dt} dt$$

where i denotes the initial value and $\frac{dW_u}{dt}$ is the difference between inflow, W_{xu} , and outflow, $W_{bby_u} + W_T$. Detailed equations are presented in figure 41.

Total temperature in the Upstream Volume is computed on the assumption

42

that total temperature is uniform throughout the volume at any instant. Flow crossing the shock face enters the volume at the total temperature, T_{tyu} . Flow leaving the volume is at the uniform total temperature, T_{tu} . Therefore,

$$W'_{xu} \, C_p \, T_{tyu} - (W_T + W_{bbyu}) \, C_p T_{tu} = \frac{d(W_u \, C_p \, T_{tu})}{dt}$$

Replacing $\dfrac{dW_u}{dt}$ by $W'_{xu} - (W_T + W_{bbyu})$ and dividing by C_p ,

$$W'_{xu} \, T_{tyu} - (W_T + W_{bbyu}) T_{tu} = W'_{xu} \, T_{tu} - (W_T + W_{bbyu}) T_{tu} + \overline{W}_u \, \frac{dT_{tu}}{dt}$$

or

$$\frac{dT_{tu}}{dt} = \frac{W_{xu}}{\overline{W}_u} \, (T_{tyu} - T_{tu}) \, .$$

These equations are summarized in figure 41.

Upstream Volume Total Pressure

Calculation of total pressure in the Upstream Volume is based on the simplifying assumption that the average density is the same as that at a flow area which is the average of the upstream and downstream faces of the Upstream Volume. Mach number M_u is computed at this station where $A_u = \frac{1}{2}(A_{xu} + A_T)$ assuming that the flow quantity, total pressure, and total temperature are equal to those at the throat. (The error introduced by these assumptions is small when the shock is near the throat. The effect of any error on the overall transient is small as the shock approaches the cowl lip).

Total pressure, P_{tu} , is then computed from the relationships

$$g\rho u = \frac{P_u}{RT_u} = \frac{\overline{W}_u}{\overline{V}_u}$$

and

$$\frac{P_{tu}}{P_u} \bigg/ \frac{T_{tu}}{T_u} = (1 + .2M_u^2)^{2.5}$$

Figure 42 is a flow diagram showing all the equations required to compute P_{tu}. Inasmuch as subsonic total pressure losses in the Upstream Volume are extremely small, total pressure is assumed to be uniform throughout the volume.

Upstream Normal Shock Position

The upstream normal shock position is obtained by integration of the shock velocity. Shock velocity is determined by iteration as that value necessary to satisfy the instantaneous pressure ratio across the shock, P_{tu}/P_{txu}, where P_{tu} is obtained from continuity in the Upstream Volume and P_{tx} is computed from upstream properties.

Various computer approaches may be used to determine the shock velocity necessary to satisfy the instantaneous pressure ratio across the shock. All are variations of the following general procedure.

1) Static pressure, P_{xu}, and static temperature, T_{xu} are computed from M_{xu}, P_{txu}, and T_{txu} which are supersonic flow properties relative to the duct at the instantaneous shock position.

2) A shock velocity relative to the duct, dX_u/dt, is assumed and the corresponding Mach number of the flow relative to the shock is computed as

$$M_{xu}' = M_{xu} - \frac{dX_u/dt}{a_{xu}}$$

3) Subsonic flow static pressure, P_{yu}, static temperature T_{yu} and Mach number relative to the shock, M_{yu}', are computed from conventional

44

normal shock equations and the quantities $M_{xu}^!$, P_{xu} , and T_{xu} . Note that the static properties are not dependent on whether the duct or the shock is used as the reference. That is, $P_{xu} = P_{xu}^!$, $T_{xu} = T_{xu}^!$, $P_{yu} = P_{yu}^!$, and $T_{yu} = T_{yu}^!$.

4) Downstream Mach number relative to the duct is computed as

$$M_y = M_y^! + \frac{dXu/dt}{a_{yu}}$$

5) Downstream total pressure relative to the duct, P_{tyu} , is computed as

$$P_{tyu} = P_{yu}(1 + .2M_{yu}^2)^{3.5} \ .$$

6) P_{tyu} is then composed to P_{tu} (or $\dfrac{P_{tyu}}{P_{txu}}$ is compared with $\dfrac{P_{tu}}{P_{txu}}$)

If P_{tyu} equals P_{tu} , the total pressure ratio across the normal shock is satisfied, and the assumed shock velocity, dXu/dt , is correct. If P_{tyu} does not equal P_{tu} , the procedure is repeated with a different assumed shock velocity.

A graphical solution of the foregoing equations is presented in figure 43. For example, if $\dfrac{P_{tu}}{P_{txu}} = \dfrac{P_{tyu}}{P_{txu}} = 0.95$, and M_x is 1.5, the normal shock Mach number relative to the duct is -0.135. It can be seen that for many conditions there are two shock Mach numbers which can satisfy the total pressure ratio across the shock. The simulation program is arbitrarily restricted to the solid line portions of the curves to the left of the minimums of P_{ty}/P_{tx} .

The equation used for iterative shock velocity solution in the digital computer simulation program of Reference 1 is

$$\frac{P_{ty}}{P_{tx}} = \left\{ 1 + .2 \left[\sqrt{\frac{\left(M_x - \frac{dX/dt}{a_x}\right)^2 + 5}{7\left(M_x - \frac{dX/dt}{a_x}\right)^2 - 1}} + \frac{6\,dX/dt\left(M_x - \frac{dX/dt}{a_x}\right)}{\sqrt{\left[\left(M_x - \frac{dX/dt}{a_x}\right)^2 + 5\right]\left[7\left(M_x - \frac{dX/dt}{a_x}\right)^2 - 1\right]}} \right] \right\}^{2} 3.5$$

$$\left\{ \left[\frac{7\left(M_x - \frac{dX/dt}{a_x}\right)^2 - 1}{6} \right] \left[\frac{1}{(1 + .2 M_x^2)^{3.5}} \right] \right\}$$

Inaccuracies during the initial portion of the transient occassionally result in P_{ty}/P_{tx} values below the minimum for the associated Mach number, M_x . While this condition exists, the shock Mach number, $(dX/dt)/a_x$ is set equal to the "Lower Limit" value, that is, the value where the slope of P_{ty}/P_{tx} versus $(dX/dt)/a_x$ is zero as shown in figure 43. Initial inaccuracies can also result in a momentary downstream excursion of the shock. Because the upstream normal shock is initially located just upstream of the throat station, a small downstream excursion could eliminate the Upstream Volume, and therewith, the simulation logic. Consequently, the iteratively computed shock Mach number is checked; and, if it is positive, its value is set to zero.

The equations for computing upstream normal shock position are listed in figure 44.

Upstream Properties for the Duct Volume

It will be recalled that the Started Phase contains logic to determine when a switch should be made to either the Choked Throat Unstarting Phase or the Insufficient Demand Unstarting Phase. To review, if the captured airflow (less bleed to the throat) exceeds the airflow that can pass through the throat at sonic conditions, the Choked Throat Unstarting Phase is initiated. If the total airflow demand is less than the captured airflow

and the terminal normal shock moves forward of the aerodynamic throat, Insufficient Demand Unstarting is initiated.

Choked Throat Unstarting:

Knowledge as to which phase is applicable is carried over to the Unstarting Phase which incorporates both phases of unstarting logic in a single phase. If the Choked Throat Unstarting Phase is applicable, the total temperature and total pressure in the Upstream Volume become the total temperature and pressure upstream of the terminal shock. That is,

$$T_{tx} = T_{tu}$$

$$P_{tx} = P_{tu}$$

If the terminal shock is aft of the throat, the flow just upstream of the terminal shock is

$$W_x = W_T - W_{bbx}$$

If the terminal shock is forward of the throat, the flow just upstream of the terminal shock is

$$W_x = W_T + \Delta W_{bby}$$

The above flow relationships are shown schematically in figure 45. Once the terminal shock moves forward of the throat, the assumption of sonic velocity in the throat used in computing W_T is no longer valid. However, the error is considered acceptable for this transient.

Insufficient Demand Unstarting:

If the Insufficient Demand Unstarting Phase is applicable, the Upstream Volume vanishes and the properties upstream of the terminal shock are identical to those forward of the now non-existent upstream normal shock. That is,

47

$$T_{tx} = T_{txu} = T_{to}$$

$$P_{tx} = P_{txu}$$

Flow upstream of the shock is

$$W_x = W_{II} + \Delta W_{bbx}$$

as illustrated in figure 37. The equations used in computing properties upstream of the terminal shock are presented in figure 46.

Properties Behind the Terminal Shock

Equations for computing properties just aft of the terminal normal shock are presented in figure 47. The equations and logic are identical to those for the upstream normal shock, figure 38.

Boundary Layer Bleed for the Duct Volume

When the terminal shock is aft of the throat during the Choked Throat Unstarting transient, flow between the throat and the terminal shock is supersonic. Consequently, the slope of bleed flow ratio per unit length of duct, $d(W_{bbx}/W_{II})/dx = \phi_x$, derived from started inlet data can be used to compute bleed flow between the throat and the terminal shock with sufficient accuracy for the Unstarting transient.
That is,

$$W_{bbx} = \phi_x(X - X_{II})(W_{II})$$

Similarly, bleed flow from the Duct Volume is

$$W_{bby} = (\phi_y)\ (X - X_{III})W_{II}\ \frac{P_y}{P_y}$$

When the terminal shock is forward of station X_{II} , bleed flow forward of the terminal shock will be less by an amount ΔW_{bbx} than it would be with the terminal shock at X_{II} . Using the logic discussed previously for the

Upstream Volume and shown graphically in figures **37 and 39,**

$$\Delta W_{bbx} = (\phi_{xu})(X_{II} - X)W_{II} .$$

Similarly, bleed flow out of the Duct Volume is

$$W_{bby} = \left[(\phi_y)(X_{II} - X_{III}) + (\phi_{yu})(X - X_{II}) \right] W_{II} \frac{P_y}{P_y}$$

If ϕ_{yu} is approximately equal to ϕ_y, the latter equation can be reduced to

$$W_{bby} = (\phi_y)(X - X_{III})(W_{II}) \frac{P_y}{P_y}$$

When the terminal shock is forward of the inlet throat, flow just upstream of the terminal shock will exceed the flow at the throat station by the bleed flow, ΔW_{bby} between the terminal shock and the throat (see figure 45) where

$$\Delta W_{bby} = (\phi_{yu})(X - X_T)(W_{II})$$

The equations and logic used to compute bleed flows relevant to the Duct Volume are summarized in figure 48.

Duct Losses

Both simulation accuracy requirements and the effect of small inaccuracies on the overall transient are less for the Unstarting Phase than for the Started Phase. The logic for determining total pressure losses other than shock losses is, therefore, less critical than for the Started Phase. Assumptions made in the total pressure loss calculations presented in figure 49 are as follows:

1) Total pressure losses from the cowl lip to the terminal shock are negligible.

2) Losses aft of the terminal shock are proportional to the quasi-steady state dynamic head, $\bar{P}_{ty} - \bar{P}_y$, just downstream of the terminal shock. Use of $\bar{P}_{ty} - \bar{P}_y$ rather than the actual dynamic head, $P_{ty} - P_y$, eliminates a redundancy in the shock motion equations with little loss in accuracy. The empirical loss factor can be expressed as the function of any appropriate parameters, for example M_A as used in the equations of figure 49.

3) Losses from the terminal shock to the average density station, d, and the losses from station d to the engine face are assumed to be equal.

Bypass and Engine System Airflows

The duct airflow demand, W_e , is the summation of the bypass airflow and the engine system primary and secondary airflows. Figure 50 shows typical equations used in computing W_e for the XB-70 configuration wherein the bypass total pressure is sufficient during the Unstarting Phase to ensure sonic flow in the minimum area section of the "Main" and "Trim" bypass doors.

Duct Volume Mass and Total Temperature

Air quantity in the Duct Volume at any instant is the initial quantity of air in the volume plus the difference between inflow and outflow from the volume over the given time interval. As described in the Started Phase section, inflow is the flow crossing the moving terminal shock face of the Duct Volume,

$$W_x' = W_x \frac{U_x'}{U_x} = W_x \frac{M_x'}{M_x}$$

where $U_x^!$ is the velocity of the flow relative to the shock,

$$U_x^! = U_x - dx/dt$$

Flow out of the duct is the summation of the exit flow, W_e and the flow out of the boundary layer bleed exits, W_{bby} . As in the Started Phase,

$$W_e = W_2 + W_s + W_{bp} + W_{aux}$$

Total temperature in the Duct Volume is computed in a procedure identical to that used for the Upstream Volume except that the total temperature of the flow crossing the terminal shock face is T_{ty} and the temperature of the outflow is T_{td} , the instantaneous total temperature throughout the Duct Volume. Equations are summarized in figure 51.

Duct Volume Total Pressure

Total pressure in the Duct Volume at any instant can be expressed as

$$P_{td} = P_d(1 + .2M_d^2)^{3.5} = \frac{\bar{W}_d}{V_d} RT_d(1 + .2M_d^2)^{3.5}$$

where all the necessary quantities except M_d have been computed previously. For the Unstarting Phase, the simplifying assumption that M_d remains constant at the value existing at initiation of the phase has been found adequate. Equations used to determine the initial M_d are presented in the Initial Conditions description. In essence, M_d is computed from the relationship,

$$(1 + .2M_d^2)^{2.5} = \left[\left(\frac{P_{td}}{RT_{td}} \right) \Big/ \left(\frac{\bar{W}_d}{\bar{V}_d} \right) \right]_{initial}$$

Figure 52 shows the sequence of equations used in calculating instantaneous P_{td} , P_{t2} , and P_{ty} .

Terminal Shock Position

The terminal shock velocity and position are computed in procedures identical to those described in the section, <u>Upstream Normal Shock</u> position These procedures are indicated by the equations of figure 53.

Phase Switches

The Unstarting Phase almost invariably terminates by switching to the Empty-Fill Phase when either the terminal shock or the "upstream normal shock" move forward of the cowl lip. However, conditions can be such that the transient will reverse and operation revert to the Started Phase. This occurrence is recognized by the switching logic when the following conditions are satisfied:

1) the transient was initiated by insufficient demand

2) the terminal shock moves aft of the geometric throat.

The fact that the inlet geometric throat is usually downstream of the effective throat provides hysteresis, so as to speak, to prevent small initial errors from causing repeated switching between the Started Phase and the Unstarting Phase.

The Phase Switching logic equations are presented in figure 54.

Outputs to the Air Induction Control System

Logic possibilities for simulating control system signals are basically identical to those described for the Started Phase. In fact, the control system simulation usually requires that the same logic be used in all phases of inlet operation to provide a consistent and continuous signal.

Inasmuch as the inlet signal logic to be selected will vary widely with the simulation objectives, only the unstart signal parameters used on the

.XB-70 are discussed for the Unstarting Phase.

Figure 55 shows the location of the two pressure taps used to sense unstart, and how the pressures vary during an unstart. The ratio of the signal to reference pressure, P_{US}/P_{UR} , is also shown. As the terminal normal shock moves forward of the tap, P_{US} , there is an abrupt increase in local static pressure and in the non-dimensional pressure ratio, P_{US}/P_{UR} . As far as the controller is concerned, unstart occurs when the pressure ratio increases to a pre-selected value as illustrated in figure 55. Note that it is the first normal shock to cross the static pressure tap, P_{US} , that signals an unstart. This may be either the terminal shock or, in event the unstart was initiated by throat choking, by the upstream normal shock.

Depending on the degree of simulation refinement desired, either 1) the unstart pressure ratio can be simply represented as a value above or below the controller scheduled value indicating unstart depending on whether the normal shock is forward or aft of the P_{US} tap; or 2) the individual static pressures at P_{US} and P_{UR} can be computed by the methods similar to those described in the Started Phase Section.

53

EMPTY-FILL PHASE

Simulation Concept

The Empty-Fill Phase, as suggested by the title, consists of two
distinct modes of inlet operation. Inspection of a typical buzz pressure
trace, figure 56 reveals the similarity of the characteristic pressure drop
to that of a container having negligible inflow, and outflow proportional
to the pressure (or mass) in the container. The "filling" portion of the
trace shows a corresponding similarity to the filling process of a container
having constant inflow, and outflow proportional to the pressure (or mass)
in the container.

Schlieren photographs and static pressure data obtained during buzz
show extreme separation during the emptying mode of operation, but reattach-
ment of the flow during the filling process. Further, pressure taps in
several inlet models have shown static pressures during the emptying process
to be quite close to values computed assuming sonic velocity in the flow
downstream of an external normal shock. This region of near sonic pressure
is in the vicinity of but is more extensive than the geometric throat region.

A simulation model for the Empty-Fill Phase which is compatible with the
foregoing observations is illustrated by figure 57.

The governing mechanism during the Empty-Fill mode of operation is flow
separation, both in actuality and in the simulation model. Because the
separation process is not readily amenable to theoretical treatment (nor
is the process overly consistent in Nature), various arbitrary assumptions
as to separation characteristics are required inputs to the simulation

. program. These assumptions include the rate and pattern of the separation, the duct pressure at which reattachment is initiated, and the rate and pattern of reattachment. Trial and error variation of these characteristics have shown 1) the simulation results are not overly sensitive to the separation characteristics assumed, and 2) non-dimensionalized separation characteristics based on test data give simulation results in good agreement with test data for inlets of quite varied scale and configuration, Reference 3. (Agreement is considered good if the differences between a simulated and a test transient are of the same magnitude as the differences between several test transients.)

The single control volume and the associated flow stations and terminology used in the Empty-Fill Phase simulation are defined in figure 57. Properties in the Duct Volume are "lumped" in that changes are assumed to occur simultaneously throughout the Duct Volume; however, properties differ from station to station in the volume. Terminal shock motion is determined by iterative solution of the motion required to satisfy the independently computed properties upstream and downstream of the shock. Further details of the equations and logic are discussed in accordance with the several functional blocks which make up the simulation program.

Upstream Properties

The calculations for determining properties upstream of the terminal shock, figure 58, are nearly identical to those for the Started Phase. The one difference is that $(P_{tx}/P_{to})_E$ is the total pressure recovery downstream of the external oblique shocks and the external normal shock. Total pressure recovery for the Started Phase, P_{tx}/P_{to} , was the total pressure in

the inlet downstream of the oblique compression waves but upstream of any normal shock. $(P_{tx}/P_{to})_E$ is determined with the external normal shock close to the cowl where it will be during the "Fill" phase. During the Empty Phase (where forward motion of the external normal shock will eliminate portions of the geometry-created oblique shock waves and flow separation will create new oblique waves) accuracy of the total pressure calculations is not critical. Consequently, the total pressure recovery, $(P_{tx}/P_{to})_E$, computed for the Fill mode is satisfactory.

The started inlet flow, W_{II} , is a fictitious flow during unstarted operation, but is used in the simulation phase switching logic to determine when an inlet restart occurs.

Properties at the Terminal Shock Station

Properties at the terminal shock station are computed from one-dimensional flow relationships using airflow, area, total pressure, and total temperature at the terminal shock station. In addition, intelligence is required as to whether flow just upstream of the terminal shock is subsonic or supersonic. Flow conditions are illustrated in figure 59 for the three possible conditions during the Empty-Fill Phase: 1) terminal normal shock aft of the throat during the Fill mode of operation, 2) terminal shock forward of the throat during the Fill mode of operation (similar in many respects to the Unstarting Phase), and 3) terminal shock aft of the throat during the Empty mode.

The Empty-Fill Phase differs from the previous Phases in that W_x is no longer a unique function of inlet geometry, flight conditions, and terminal shock position. Rather, the known factor during the Empty-Fill Phase is that the flow is sonic in the effective throat for conditions 1

56

and 3 above, and near sonic for the short-duration condition 2. Therefore,

$$W_T = \frac{P_{tT}}{\sqrt{T_{tT}}} \, A_{Tef} \sqrt{\frac{\gamma g}{R}} \, \frac{M_T}{(1 + .2M_T^2)^{3.0}}$$

$$= \frac{P_{tx}}{\sqrt{T_{to}}} \, A_{Tef} \, \lambda$$

By inspection of figure 59, it can be seen that if:

$$X > X_T : \quad W_x = W_T - W_{bbx}$$

$$X < X_T : \quad W_x = W_T + \Delta W_{bby}$$

The equations of figure 60 show the logic used in determining the applicable condition and how the required properties are computed. Note that the equation for W_x in figure 60,

$$W_x = W_T + \Delta W_{bbyu} - W_{bbx}$$

degenerates to the forms shown in figure 59 inasmuch as ΔW_{bbyu} vanishes with the terminal shock aft of the throat and W_{bbx} vanishes with the terminal shock forward of the throat.

Properties Behind the Terminal Shock

Calculations shown in figure 61 to compute properties just downstream of the terminal shock are identical to those previously discussed for the Unstarting Phase.

Effective Throat Area

The general concept of flow separation and reattachment which results in a time-varying effective flow area at a given geometric station has been indicated in figure 57. In absence of detailed information, a flow separation pattern is arbitrarily selected to give simple equations for effective

flow area at a given station as a function of time.

Figure 62 depicts the assumptions made in deriving the equations of figure 63. The assumptions are made that 1) the effective throat area is at the geometric throat station, and 2) the effective flow area varies linearly with station in the detached flow region. It can be seen that, from purely geometric considerations, effective flow area at any station X between X_T and X_{RA} is

$$A_{X_{ef}} = A_{T_{ef}} + \frac{(X - X_T)}{(X_{RA} - X_T)} (A_{X_{RA}} - A_{T_{ef}})$$

Effective flow area aft of X_{RA} is identical to the geometric area.

Note that the only parameter that must be expressed as a function of time during the period of separation is effective throat area, $A_{T_{ef}}$. Specifically, $A_{T_{ef}}$ during the separation process is expressed as a function of time from the initiation of the separation; and, $A_{T_{ef}}$ during the reattachment process is expressed as a function of time from the initiation of the reattachment. Separation is initiated if:

1) Operation switches from the Unstarting Phase to the Empty-Fill Phase

2) The terminal normal shock moves upstream past the cowl lip in the Empty-Fill Phase

3) Operation switches from the Subcritical Phase to the Empty-Fill Phase because the mass flow ratio becomes less than the buzz-limit mass flow ratio.

The simulation input curves of $A_{T_{effective}}/A_{T_{geometric}}$ versus time after the initiation of separation were initially determined by trial and error. Various curves were assumed, and the curve giving best agreement between simulation and test data was selected. This curve was then converted

to a non-dimensional form by assuming that the rate of separation is pro-
portional to the square root of the throat total temperature (velocity),
and inversely proportional to the square root of the throat area (length).
This non-dimensional curve has been used with good results for quite varied
inlet sizes and configurations; however, better values for a specific con-
figuration can be determined by trial and error if sufficient test data are
available.

As pressure in the duct drops during the emptying mode of operation,
a value is reached where the flow reattaches. XB-70 model test data show
that the reattachment usually occurs when the duct total to ambient static
pressure ratio, P_{td}/P_o , reaches a critical value, K_{EF} . XB-70 test data
indicate that K_{EF} was essentially independent of Mach number and that a
K_{EF} value of 6.4 is appropriate for "average severity" unstart and buzz.
A K_{EF} value of 4 was found appropriate for severe unstarts and buzz.

A procedure similar to that described above for separation was used
to obtain a curve of $A_{T_{effective}}/A_{T_{geometric}}$ versus time after $P_{td}/P_o \leq K_{EF}$.
During this reattachment, however, $A_{T_{ef}}/A_{T_{geo}}$ increases with increasing
time.

Although not essential, it has been found convenient, and in keeping
with the actual flow phenomena, to assume a constant area throat section
extending from the geometric throat station to the cowl lip.

The logic used in determining effective throat area is summarized in
the flow diagram of figure 63. Equations for computing effective flow area
at any station are presented in figure 64.

Effective volume is computed in a procedure similar to that used in
obtaining effective flow area. Equations are shown in figure 65.

Boundary Layer Bleed Flow

Logic for computing boundary layer bleed flows is similar in general format to that used in the Started Phase. It differs primarily in that bleed flow has been made non-dimensional by using the parameter W_{bb}/W_T rather than W_{bb}/W_{II} . (W_{II} is not a measurable parameter during tests with unstarted supercritical operation.)

The validity and importance of the bleed flow calculation during separated flow conditions might well be questioned inasmuch as the bleed effects can be readily absorbed in the gross assumption of effective throat area. However, it is convenient, if not necessary, that a continuous and consistent calculation be made during all of the Empty-Fill Phase so that the bleed flow will be known when the flow reattaches. Because the accuracy of the bleed flow calculation is of little concern during operation with separated flow (emptying mode), the parameters W_{bb}/W_T are determined by test or calculations for unstarted, supercritical inlet conditions.

Assuming linear variation in bleed with shock position as illustrated in figure 14, and referring to the sketches of figure 59, it can be seen that bleed flows can be calculated as follows:

$$X > X_{III} : \quad W_{bbx}/W_T = \phi_x(X_{III} - X_T)$$
$$W_{bby}/W_T = 0$$
$$\Delta W_{bby}/W_T = 0$$

$$X_T < X < X_{III} : \quad W_{bbx}/W_T = \phi_x(X - X_T)$$
$$W_{bby}/W_T = \phi_y(X - X_{III})$$
$$\Delta W_{bby}/W_T = 0$$

60

$$X < X_T : \quad W_{bbx}/W_T = 0 \quad \text{(no supersonic flow upstream of shock)}$$

$$W_{bby}/W_T = \phi_y(X - X_{III})$$

$$\Delta W_{bby}/W_T = \phi_y(X - X_T)$$

Note that the reference flow is W_T , while the reference flow in the Started and Unstarting Phases is W_{II} .

Detailed equations are shown in figure 66.

Duct Volume Total Pressure Losses

Figure 67 presents the equations for computing Duct Volume total pressure losses. They are identical to those used in the Unstarting Phase.

Bypass and Engine System Airflows

The equations and logic for computing bypass and engine system airflows, figure 68, are identical to those for the Started and Unstarting Phases.

Duct Volume Mass and Total Temperature

The quantity of air in the Duct Volume at any instant is the initial quantity plus the difference between inflow and outflow. Inflow is the flow relative to the shock face of the Duct Volume, W_X' , where

$$W_X' = W_X \ \frac{U_X'}{U_X} = W_X\left(\frac{U_X - dX/dt}{U_X}\right)$$

Outflow from the duct volume, as in the Started and Unstarting Phase, is the summation of W_{bby} and W_e .

The logic for computing Duct Volume total temperature is identical to that used in the Unstarting Phase. Note that total temperature behind the external normal shock (and therefore upstream of the terminal shock) is

assumed to be equal to freestream total temperature. This assumption in effect says that the velocity of the external normal shock relative to the inlet is trivial. Model test data confirm that, although the external normal shock does move during the Empty-Fill transient, the total excursion of the external normal shock is small (most of the motion in the external shock field during buzz is in the oblique shock portion of separated-flow lambda shock).

Figure 69 is an equation flow diagram for computing Duct Volume mass and total temperature.

Duct Volume Total Pressure

The logic and equations for computing Duct Volume total pressure are identical to those used for the Unstarting Phase. The simplifying assumption is again made that the Mach number at the average density station, M_d , remains constant at its initial value. Fortunately, this assumption is most nearly correct when greatest accuracy is desired during supercritical, attached-flow operation with the terminal shock near the throat. Equations are listed in figure 70.

Terminal Shock Position

The terminal shock position and velocity are calculated in a procedure identical but for two exceptions to that described in the Unstarting Phase section, Upstream Normal Shock Position.

The first exception is associated with the terminal shock which 1) forms at the throat upon initiation of the Phase, and 2) moves aft as a consequence of subsequent events. The simulation logic assumes this terminal shock forms initially at a station slightly downstream of the throat.

62

Velocity of this terminal shock is then determined from the instantaneous total pressures upstream and downstream of the terminal shock. To eliminate the possibility of the terminal shock being driven forward of the throat because of small errors in the initial conditions, the program logic sets the shock velocity to zero until the total pressure ratio across the shock results in a positive (downstream) velocity.

The second exception recognizes the fact that when the terminal shock moves aft, the increasing shock strength and appreciable boundary layer result in shock-boundary layer interactions. These are evidenced by a series of oblique shocks rather than a single, clean terminal shock. This effect is approximated in the simulation program by introducing an effective Mach number, $M_{xe} = K_{MX}M_x$, where K_{MX} is an empirical function of X. Physically, M_{xe} can be envisioned as the component M_x normal to a pseudo-oblique shock having total pressure losses equal to the oblique shock train. When test data to evaluate K_{MX} are not available, its value is assumed to be unity.

Figure 71 gives the equations for computing terminal shock velocity and position.

Phase Switches

The phase switching logic in the Empty-Fill Phase continually checks as to when a switch should be made to the Started Phase, the Hammershock Phase, or the Subcritical Phase. A further check is made as to when a new Empty-Fill Phase should be initiated.

Inlet operation switches to the Started Phase, (a restart is made) when flow through the throat becomes equal to the captured flow. An empirical constant is used to account for differences between actual and

theoretical restart conditions.

A switch is made to the Hammershock Phase when the rate of change of the duct outflow exceeds a specified rate. The method of selecting the specified rate is discussed in the description of the Started Phase switch logic.

A switch is made to the Subcritical Phase when the conditions are satisfied concurrently that 1) the terminal shock moves forward of the cowl lip, and 2) the duct mass flow ratio exceeds the empirical minimum value for buzz-free inlet operation.

A new Empty-Fill Phase is initiated (flow separation is triggered) when, concurrently, 1) the terminal shock moves forward of the cowl lip, and 2) the duct mass flow ratio is less than the empirical minimum value for buzz-free inlet operation.

The phase switching equations are presented in figure 72.

Outputs to the Air Induction Control System

The logic used to determine local pressure signals to the AICS for the Started and the Unstarting Phases are equally applicable to the Empty-Fill Phase. It is to be remembered, however, that flow is subsonic from the cowl lip to the throat, and that effective rather than geometric areas must be used during separated flow conditions.

SUBCRITICAL PHASE

An inlet operates in the Subcritical Phase when flow from the cowl lip
to the engine face is subsonic and stable. The Subcritical Phase encom-
passes flight with stable, unstarted (all external shock compression) inlet
operation.

Subcritical Phase Concept

The Subcritical Phase simulation model is based on the reasoning pre-
sented in reference 4 for determining the approximate position of an
external normal shock. The top portion of figure 73 illustrates the general
procedure. Known quantities are Mach number upstream of the normal shock,
and the captured flow. The airflow spilled by the inlet is assumed to be
diverted around the cowl lip by a pseudo-surface originating at the cowl
lip and having the maximum angle possible without flow detachment. The
normal shock stands at the intersection of the pseudo-surface and the
stream tube just entering the inlet. The bottom portion of figure 73 shows
the change in shock position, ΔX , when the captured stream-tube is reduced
from h_1 to h_2 .

The simulation model is shown in figure 74. The lumped volume concept
described for the Unstarting and Empty-Fill Phases is again used but with
the external normal shock and the pseudo-surface now serving, respectively,
as the upstream face and part of the bounding surface of the Duct Volume.
Again, iteration is used to determine the shock velocity required to satisfy
the instantaneous values of total pressure upstream and downstream of the
shock. Shock velocity is integrated to determine instantaneous shock

position. If the shock moves forward, the pseudo-ramp surface spills more flow and less flow enters the inlet. If the shock moves aft, more flow enters the inlet.

During subsonic and low supersonic speeds, the simulation concept has no physical significance. However, the simulation procedure can be extended to such conditions by the assumption of a pseudo-Mach number, M_{xp} , and its associated pseudo-shock. Use of the pseudo-Mach number provides a mechanism for closing the loop between airflow supply and demand at subsonic flight conditions. The validity of this procedure has not been checked against test data. However, a high degree of simulation accuracy is generally not required at subsonic flight speeds.

Upstream Properties

Equations for computing properties upstream of the terminal shock (external normal shock) are presented in figure 75. The equations are similar to those for the other Phases except that M_x , previously computed from one-dimensional flow continuity relationships, is now a function of flight conditions and inlet geometry. Further, when M_x is less than 1.1, a pseudo-Mach number of 1.1 is assumed to permit use of the simulation logic at subsonic Mach numbers.

Inflow

By hypothesis, the angle between the flow just upstream of the terminal shock and the pseudo-surface which deflects the spillage air is the maximum angle not causing flow detachment. Variation of this angle, δ_{max} , with upstream Mach number is shown in figure 76 for both two-dimensional and conical flow. Generally, two-dimensional values are used because flow at

66

the cowl lip approaches two-dimensional flow even for axi-symmetric inlets. δ_{max} can be obtained from tables, as in figure 76 or by the following equations.

$$\sin^2\theta_{MAX} = \frac{.6M_x^2 - 1 + \left[2.4(1 + \frac{\gamma-1}{2}M_x^2 + .15M_x^4)\right]^{\frac{1}{2}}}{1.4M_x^2}$$

$$\cot\theta_{MAX} = \sqrt{\frac{1 - \sin^2\theta_{MAX}}{\sin^2\theta_{MAX}}}$$

$$\tan\delta_{MAX} = \frac{2\cot\theta_{MAX}(M_x^2\sin\theta_{MAX} - 1)}{2 + M_x^2(\gamma + 1 - 2\sin^2\theta_{MAX})}$$

From the geometry of figure 73 it can be seen that

$$\frac{\Delta W_x}{\Delta t} = \left(\frac{\Delta h}{h}\right)\left(W_x\right)\left(\frac{1}{\Delta t}\right) = \frac{W_x}{h}\frac{\Delta h}{\Delta t}$$

and

$$\frac{\Delta h}{\Delta t} = \frac{\Delta X\tan\delta_{max}}{\Delta t} = \left(\frac{\Delta X}{\Delta t}\Big/a_x\right)a_x\tan\delta_{max}$$

Further,

$$\frac{W_x}{h} = \frac{A_x}{h}\frac{P_{tx}}{\sqrt{T_x}}\sqrt{\frac{\gamma g}{R}}\frac{M_x}{(1 + .2M_x^2)^{3.5}}$$

and

$$a_x = \sqrt{\gamma g R T_x}$$

Combining terms and converting to a derivative format,

$$\frac{dW_x}{dt} = \gamma g\left(\frac{A_x}{h}\right)P_{tx}\frac{M_x}{(1 + .2M_x^2)^{3.5}}\tan\delta_{max}\left(\frac{dX}{dt}\Big/a_x\right)$$

Finally, inflow to the Duct Volume is

$$W_x = W_{x_i} + \int_i^t \frac{dW_x}{dt} \, dt$$

The foregoing equations are summarized in figure 77.

Boundary Layer Bleed Flows

Inasmuch as the terminal shock is always forward of the cowl lip in the Subcritical Phase, the only bleed flow to be calculated is W_{bby} . To maintain similarity with the calculations in the other Phases, bleed flow is

$$W_{bby} = \phi_y \, (X_I - X_{III}) \, (W_x)$$

Where ϕ_y is $\frac{dW_{bby}}{W_x}/dx$, the non-dimensionalized bleed flow per unit length of bleed surface exposed to subsonic flow. The procedure for non-dimensionalizing the bleed flow slope is not particularly appropriate for the Subcritical Phase (in actuality, W_{bby} tends to increase with decreasing W_x at a given flight condition). However, both the bleed flow quantity and its effect on inlet dynamics are small in this flight regime. The bleed flow equations are listed in figure 78.

Duct Volume Total Pressure Loss

Total pressure loss in the Duct Volume is assumed to be proportional to the dynamic head at the end of the bleed section. Half of the total pressure loss is assumed to occur between the end of the bleed section and the average density station, and half between the average density station and the engine face. The required equations are shown in figure 79. Note that these calculations assume a quasi-stationary terminal shock, making $\overline{T_{tIII}} = T_{to}$ and $\overline{P_{tIII}} = \overline{P_{ty}}$. This assumption having negligible effect

68

on the simulation accuracy, eliminates a redundancy loop.

Bypass and Engine System Airflows

The bypass and engine system airflow calculations, figure 80, are identical to those for the other phases.

Duct Volume Mass and Total Temperature

The logic and equations for computing the instantaneous quantity of air and the total temperature in the Duct Volume are similar to those discussed in the Unstarting and Empty-Fill Phases. The equations are presented in figure 81.

Duct Volume Total Pressure

The equations for computing total pressure in the Duct Volume, figure 82, are identical to those described for the Unstarting Phase except for the additional equations required to determine the portion of the Duct Volume forward of the cowl lip. From consideration of the two-dimensional geometry of figure 73, area at station X is

$$A_X = h_X \frac{A_L}{h_L}$$

where A_L and h_L are the flow area and height respectively at the cowl lip station. Further,

$$h_X = h_L - (X_L - X)\tan\delta_{min}$$

so that

$$A_X = A_L \left[1 - \left(\frac{X_L - X}{h_L}\right) \tan\delta_{max} \right]$$

The increment of Duct Volume between the terminal shock and the cowl lip

is, therefore,

$$\Delta V = \left(\frac{A_x + A_L}{2}\right)\left(X_L - X\right) = A_L\left[1 - \left(\frac{X_L - X}{2h_L}\right)\tan\delta_{max}\right]\left(X_L - X\right)$$

Mach number at the average density station is assumed to remain constant at the value existing at the beginning of the Phase.

Terminal Shock Velocity and Position

The iteration for the terminal shock velocity required to satisfy the instantaneous total pressures upstream and downstream of the shock is shown in figure 83. As in the other Phases, shock velocity is integrated to obtain shock position. A further portion of the logic prevents any appreciable travel of the terminal shock aft of the cowl lip.

During subsonic conditions, there will, of course, be no actual terminal shock, and the pseudo-shock is nothing more than a convenient fiction.

Phase Switches

Three conditions can cause a switch from the Subcritical Phase to another mode of inlet operation. First, an abrupt decrease in duct out-flow can result in hammershock. Second, reduction of the inlet mass flow ratio to the value where buzz occurs causes a switch to the Empty-Fill Phase. Third, an increase in airflow demand to the point where inlet operation becomes supercritical causes a switch to the Empty-Fill Phase. The logic for determining when a switch to another Phase should be made and what the new Phase should be is presented in figure 84.

Air Induction System Signals to the Control System

The same simulation techniques used to generate inlet signals to the

control system in other Phases can be used in the Subcritical Phase.

A typical hammershock pressure transient induced by engine stall is shown in figure 85. Hammershock can occur during any of the various modes of inlet operation, and at any flight speed. In fact, the hammershock pressure trace of figure 85 was recorded during ground operation of XB-70 Ship 1.

Hammershock Phase Concept

A schematic representation of the simulation model for the Hammershock Phase is presented in figure 86. While the model shown is for hammershock initiated in the Started Phase, the simulation logic is also capable of simulating hammershocks initiated in the Empty-Fill and the Subcritical Phases.

The Hammershock Phase logic is based on the fact that the pressure disturbance is propoagated at a velocity in the airflow somewhat higher than the local speed of sound. Consequently, flow upstream of the disturbance front is unaffected by the disturbance. That is, upstream flow relative to the disturbance front is supersonic, and the disturbance front becomes a normal shock wave.

The same concept of a control volume used in the Unstarting and Empty-Fill Phases is used in the hammershock logic. Now, the upstream face of the control volume is the terminal shock; and, the downstream face is the engine face. Upon initiation of the Hammershock Phase, a hammershock wave front is arbitrarily located slightly forward of the engine face. With outflow drastically reduced, inflow to the control volume (Hammershock Volume)

, greatly exceeds outflow; pressure in the volume rises; and, the hammer-shock wave front moves upstream at the velocity required to satisfy the instantaneous total pressures upstream and downstream of the shock. If pressure in the duct is sufficiently high upon expulsion of the hammershock wave, there will be flow out of the duct into the external flow field until the static pressure at the cowl lip drops to the total pressure downstream of the external shock system. The simulation run is terminated at this time.

Upstream Properties

The equations for computing the upstream properties, presented in figure 87, are identical to those for the Started, Empty-Fill and Sub-critical Phases except for the additions required to determine which Phase was in effect when the hammershock was initiated and what the corresponding upstream properties are.

Properties at Station X

Flow conditions for hammershock initiated in the Started, Empty-Fill, and Subcritical Phases are illustrated in figures 88 and 89. To reduce the logic required to compute properties at station X, it has been assumed that hammershock will not be initiated during the Unstarting Phase, or during the portion of the Empty-Fill Phase when the normal shock is moving from the throat to the cowl lip station. Because the pressure gradients are not overly severe and the duration is small, the probability of engine stall and hammershock occuring at such times is also small.

The logic and equations for computing properties at station X are presented in figure 90. Inasmuch as flow is subsonic throughout the duct

during subcritical operation, there is no internal normal shock (except for the hammershock); and therefore, station X as previously defined does not exist. However, it is convenient to maintain a similar computing format for all phases by arbitrarily setting X equal to the cowl lip station. The simulation program then knows that flow is subsonic at any station downstream of the cowl lip.

To further promote similarity in computing format, the concept of a base flow, W_{base} , is introduced. Using this concept, W_X can be expressed as

$$W_X = W_{base}\left(1 - \frac{W_{bbx}}{W_{base}} + \frac{\Delta W_{bb}}{W_{base}}\right)$$

W_{base} is the flow at some base point station, X_b . W_{bbx} is the bleed flow between the terminal shock (other than the hammershock) and the base station when the terminal shock is aft of the base station. At a station upstream of X_b , flow will be greater than W_{base} by ΔW_{bb} , the amount of bleed flow from that station to X_b . Note that this bleed flow increment must be computed for the flow conditions existing when W_{base} was obtained. In the Started Phase, for example, $W_{base} = W_{II}$ is obtained with supersonic flow upstream of X_{II} . Consequently the bleed-flow increment, ΔW_{bb} , must be computed on the basis of supersonic flow upstream of the base point station.

Inspection of figures 88 and 89 show that the components of the flow are as follows according to the Phase in which the hammershock transient was initiated.

Started Phase:

$$W_{base} = W_{II}$$

$$W_{bbx}/W_{base} = W_{bbx}/W_{II}$$

$$\Delta W_{bb}/W_{base} = \Delta W_{bbx}/W_{II}$$

Empty-Fill Phase

$$W_{base} = W_T$$

$$W_{bbx}/W_{base} = W_{bbx}/W_T$$

$$\Delta W_{bb}/W_{base} = \Delta W_{bby}/W_T$$

Subcritical Phase

$$W_{base} = W_{III}$$

$$W_{bbx}/W_{base} = 0$$

$$\Delta W_{bb}/W_{base} = \Delta W_{bby}/W_{III}$$

Further details are given in figure 90.

Properties Upstream of the Hammershock

Properties just upstream of the hammershock are computed on the simplifying assumption that the terminal shock (other than the hammershock) remains stationary from the initiation of the hammershock transient until the hammershock wave overtakes and coalesces with it. During this period, the total pressure downstream of the terminal shock is $\overline{P_{ty}}$ inasmuch as the shock is assumed to be stationary. Similarly, flow at the hammershock station, W_{xHS} , is equal to W_x less any bleed flow between the terminal shock and the hammershock. After the shocks coalesce, the properties upstream of the hammershock are, of course, identical to those upstream of the terminal shock.

Details of the logic and equations used can be seen in figure 91. Note that when the hammershock reaches the cowl lip, flow at the cowl lip can

became negative as described in the section, _Forward Outflow_.

Properties Behind the Hammershock

The equations for computing properties immediately downstream of the hammershock are identical to those used in the Unstarting and Empty-Fill Phases. The equations are shown in figure 92.

Effective Flow Area and Volume

In event the hammershock transient is initiated during the portion of the Empty-Fill Phase when flow is separated, the effective flow area and volume differ from the geometric values. The logic used to compute effective area and volume is the same as that used in the Empty-Fill Phase except that it is assumed that the degree of separation remains constant through the hammershock transient. That is, the ratio of effective to geometric throat area, $A_{T_{ef}}/A_T$, is constant at the value existing at initiation of the Hammershock Phase. The equations for computing effective area and volume are presented in figures 93 and 94 respectively.

Boundary Layer Bleed Flows

The logic used in computing bleed flows is similar to that described for the previous Phases except for the complications introduced by the fact that the hammershock transient may be initiated in any of the three Phases, Started, Empty-Fill, and Subcritical. By reference to figure 89, it can be seen that the following relationships apply where $\phi_x = \left(\dfrac{W_{bbx}}{W_{base}}\right)\!\Big/\!\Delta X$, and $\phi_y = \left(\dfrac{W_{bby}}{W_{base}}\right)\!\Big/\!\Delta X$ are the bleed flow slopes for supersonic and subsonic flow respectively.

Started Phase:

	W_{bbx}/W_{II}	$\Delta W_{bbx}/W_{II}$	$\overline{W_{bby}}/W_{II}$
$X > X_{III}$	$\phi_x(X_{III} - X_{II})$	0	0
$X_{II} < X < X_{III}$	$\phi_x(X - X_{II})$	0	$\phi_y(X - X_{III})$
$X < X_{II}$	0	$\phi_x(X_{II} - X)$	$\phi_y(X - X_{III})$

	$\overline{W_{bbyHS}}/W_{III}$
$X_{HS} > X_{III}$	0
$X_{II} < X_{HS} < X_{III}$	$\phi_y(X_{HS} - X_{III})$
$X_{HS} < X_{II}$	$\phi_y(X_{HS} - X_{III})$

Empty-Fill Phase

	W_{bbx}/W_T	$\Delta W_{bby}/W_T$	$\overline{W_{bby}}/W_T$
$X > X_{III}$	$\phi_x(X_{III} - X_T)$	0	0
$X_T < X < X_{III}$	$\phi_x(X - X_T)$	0	$\phi_y(X - X_{III})$
$X < X_T$	0	$\phi_y(X - X_T)$	$\phi_y(X - X_{III})$

	$\overline{W_{bbyHS}}/W_T$
$X_{HS} > X_{III}$	0
$X_T < X_{HS} < X_{III}$	$\phi_y(X_{HS} - X_{III})$
$X_{HS} < X_T$	$\phi_y(X_{HS} - X_{III})$

77

Subcritical Phase

	W_{bbx}/W_{III}	W_{bby}/W_{III}
$X \leq X_I$	0	$\phi_y(X_I - X_{III})$

	$\overline{W_{bbyHS}}/W_{III}$
$X_{HS} > X_{III}$	0
$X_{HS} < X_{III}$	$\phi_y(X_{HS} - X_{III})$

The logic for determining the various bleed flow quantities is shown in the equation flow diagram of figure 95.

Bypass and Engine System Airflows

Bypass and engine airflow calculations, figure 96, are identical to those used for the other phases.

Duct Volume Total Pressure Losses

To determine subsonic flow total pressure losses, a pseudo total pressure loss from the terminal shock to the engine face station is first calculated as

$$\Delta P_{ty2} = \epsilon(\overline{P_{ty}} - \overline{P_y})$$

With losses assumed to be distributed linearly with duct length, the total pressure loss from the terminal shock to the hammershock becomes

$$\Delta P_{tyxHS} = \left(\frac{X_{HS} - X}{X_2 - X}\right)\Delta P_{ty2}$$

Subsonic flow total pressure losses in the Hammershock Volume are assumed to

78

.be negligible inasmuch as the exit flow and Mach number are low during the hammershock transient. Subsonic flow total pressure loss equations are presented in figure 97.

Hammershock Volume Mass and Total Temperature

Air in the Hammershock Volume is that initially in the volume plus the difference between inflow and outflow in the ensuing interval. Inflow is the flow crossing the hammershock face of the Hammershock Volume. Outflow is the summation of the bleed flow from the Hammershock Volume, the bypass flow, and the engine system flow. Engine System flow can be negative (inflow) should there be flow reversal during engine stall.

Flow entering the Hammershock Volume is at the total temperature immediately downstream of the hammershock, T_{tyHS} . This flow is assumed to mix instantaneously with the air the Hammershock Volume to give a uniform total temperature, T_{tHS} . Outflow is at the temperature T_{tHS} (if reverse flow occurs during engine stall, the negative engine airflow will be at the appropriate temperature rather than T_{tHS}).

Figure 98 shows the equations used to compute Hammershock Volume mass and total temperature.

Hammershock Volume Total Pressure

The basic logic for calculating Duct Volume total pressure in the Unstarting and Empty-Fill Phases is used to compute Hammershock Volume total pressure. M_{HS} , the Mach number at the average density station in the Hammershock Volume, is assumed to remain constant at its initial value. Equations are presented in figure 99.

Hammershock Velocity and Position

The hammershock velocity is determined by iteration for the shock velocity satisfying the instantaneous upstream and downstream total pressures. Shock velocity is then integrated to determine shock position. The required equations, figure 100, are identical in form to those used for computing terminal shock motion in the Unstarting and Empty-Fill Phases. A function, which sets hammershock velocity to zero until $P_{tHS} \geq P_{txHS}$, has been added to minimize the effects of small inaccuracies in the initial conditions.

As discussed previously, the terminal shock, if one exists, is assumed to be stationary until it is overtaken by the hammershock. The two shocks then become one shock having the velocity and position computed for the hammershock.

Forward Outflow

As the hammershock moves forward of the cowl lip, duct total pressure is frequently higher than total pressure in the external flow just forward of the cowl station. Under such conditions, there will be flow from the duct into the external flow.

With outflow from the inlet, the local external flow will be brought to essentially stagnation conditions. Therefore static pressure at the cowl lip will be P_{txE} where P_{txE} is the total pressure behind the external normal shock for supersonic flight conditions or the freestream total pressure for subsonic flight conditions.

If the Mach number at the throat station is subsonic during outflow, the outflow quantity can be computed from total temperature, total pressure,

. static pressure, and area at the cowl station. That is,

$$W_{fo} = \frac{P_{tHS}}{\sqrt{T_{tHS}}} \sqrt{\frac{\gamma_L}{R}} \frac{A}{144} \frac{M_L}{(1 + .2M_L^2)^3}$$

where M_L is determined from the ratio of total to static pressure at the cowl lip, P_{tHS}/P_{txE} .

The flow calculated in the above method may exceed the maximum possible flow through the throat area, particularly at high inlet area contraction ratios. Outflow is then the flow computed for sonic velocity at the throat,

$$W_{fo} = \frac{P_{tHS}}{\sqrt{T_{tHS}}} A_T \lambda$$

Outflow at any instant will be the lesser of the two flows computed above. Outflow will continue until P_{tHS} drops to P_{txE} . Equations for computing forward outflow are presented in figure 101.

Phase Switches

The Hammershock Phase is terminated when the hammershock moves forward of the cowl lip and duct total pressure becomes equal to or less than external flow total pressure at the cowl lip. Physically, inlet operation would then change to either the Empty-Fill Phase or the Subcritical Phase. In practice, it is usually desireable to terminate the simulation run following a hammershock transient. The Phase switching logic of figure 102 terminates the entire simulation run at the end of the Hammershock Phase.

Attention is called to the fact that the combination of a mild engine stall initiated during highly supercritical started inlet operation can

result in a hammershock transient wherein the coalesced hammershock-terminal shock will become stabilized before reaching the cowl lip. That is, the inlet will remain started. This possibility is not considered in the Phase switching logic of figure 102.

Outputs to the Air Induction Control System

Inlet signals to the control system are generated using the same basic logic described for the previous Phases.

INITIAL CONDITIONS

Certain initial conditions must be computed at the beginning of each Phase of inlet operation. With the exception of the Unstarting Phase, each Phase may be initiated either in a steady state condition or in a transient condition carried over from the previous Phase. In either event, it is usually desirable to keep those equations required only to compute initial conditions outside of the main body of the simulation program. Then, only those equations needed in the dynamics calculations need be carried along continually. Care must be used, of course, to ensure that the initial conditions calculations are consistent with the dynamics equations.

Started Phase

Quantities which must be known upon initiation of the Started Phase are $\bar{W}_H$, $\bar{W}_d$, T_{td} , K_A , $C_{bp}A_{bp}$, and X.

$\bar{W}_{Hi}$, the air quantity initially in the Helmholtz Volume, is evaluated by use of Simpson's Rule. That is

$$\bar{W}_{Hi} = \int_{X}^{Z} (g^\rho A)\,dX$$

$$= \frac{Z-X}{3n}\left((g^\rho A)_0 + 4(g^\rho A)_1 + 2(g^\rho A)_2 + 4(g^\rho A)_3 + 2(g^\rho A)_4 \right.$$

$$\left. + \cdots + 4(g^\rho A)_{n-1} + (g^\rho A)_n \right)$$

Where n is the even number of equal length increments into which the Helmholtz Volume is divided and the stations 0, 1, ---n are as shown in figure 103.

83

At any station j,

$$(g\rho A)_j = \frac{W_j}{U_j}$$

At a station $x_j < X_{III}$

$$W_j = W_{II} - W_{bbx} - \overline{W_{bby}}\left(\frac{X_j - X}{X_{III} - X}\right)$$

At a station $X_j \geq X_{III}$

$$W_j = W_{II} - W_x - \overline{W_{bby}}$$

M_j is obtained by iteration to determine the subsonic solution of the equation.

$$\frac{M_j}{(1 + .2M_j{}^2)^3} = \frac{W_j\sqrt{T_{tj}}}{A_j \; P_{tj}}\sqrt{\frac{R}{\gamma g}}$$

where

$$T_{tj} = T_{tx} = T_{to}$$

and

$$P_{tj} = \overline{P_{ty}} - \frac{j}{n}\left(\Delta P_{tyz}\right)$$

Finally,

$$U_j = M_j\sqrt{\gamma g R T_j} = M_j\sqrt{\frac{T_{tj}}{1 + .2M_j}}\sqrt{\gamma g R}$$

In the XB-70 program, the Helmholtz Volume has usually been divided into 10 equal-length segments for the $\overline{W}_H$ calculation. The same basic logic is used to determine the air quantity initially in the Duct Volume. Because it is considerably larger, the Duct Volume is usually divided into 100

equal-length segments. Further, because the upstream face of the Duct volume will almost invariably be aft of the boundary layer bleed section, flow at each station will be the same value. That is,

$$W_j = W_{II} - W_{bbx} - W_{bby}$$

For steady state initial conditions,

$$T_{td} = T_{to}$$

The procedure for computing K_A is described in the section, Duct Volume Pressures, of the Started Phase. To review,

$$M_d = \left(5 \left[\left(\frac{P_{td}}{RT_{td}} \bigg/ \frac{\bar{\bar{W}}_d}{\bar{V}_d} \right)^{2/5} - 1 \right] \right)^{\frac{1}{2}}$$

$$A_d = W_z \; \frac{\sqrt{T_{td}}}{P_{td}} \sqrt{\frac{R}{\gamma g}} \; \frac{(1 + .2M_d^2)^3}{M_d}$$

$$A_{dgeo} = \frac{V_d}{X_e - X_z}$$

$$K_A = A_d/A_{dgeo}$$

The effective bypass area required for the steady state initial terminal shock position is that value required to balance the airflow supply and demand. With supply and demand being, respectively,

$$W_{II} - W_{bbx} - W_{bby}$$

and

$$W_{bp} + W_2 + W_s$$

the effective bypass area is

$$C_{bp} \; A_{bp} = \frac{W_{bp}\sqrt{T_{to}}}{P_{tbp} \; \lambda} = \frac{\sqrt{T_{to}}}{P_{tbp} \; \lambda} \; (W_{II} - W_{bbx} - W_{bby} - W_2 - W_s)$$

where

$$P_{tbp} = K_{bp} \; P_{t2} = K_{bp} \; (\overline{P_{ty}} - \Delta P_{tyz} - \Delta P_{tzd} - \Delta P_{td2})$$

and W_2 and W_s are functions of P_{t2}, T_{t2}, and throttle position. Note that P_{t2} is uniquely defined by the initial geometry, upstream properties, and the terminal shock position during steady state conditions.

The initial steady state terminal shock position is either input directly by specifying X, or indirectly by specifying the Shock Position Parameter, SPP. If SPP is input, the initial conditions program assumes a value of X, computes the resulting value of SPP and compares this with the input (scheduled) value of SPP. This procedure is repeated until SPP - SPP$_{Sched.}$ is within a specified tolerance. This trial and error procedure has usually been accomplished by use of the "Slope Method" in the XB-70 program as illustrated in figure 104. In this method SPP is computed for the maximum and minimum anticipated values of X, and the error between the scheduled and computed SPP is determined. A straight line, Chord 1 of figure 104, is then drawn. The intercept of the chord with the zero error line determines the value of X, to be used in computing the error, (ΔSPP). The procedure is continued as illustrated until X gives an error, ΔSPP, within the allowable tolerance.

The preceding calculations are all based on the assumption of steady state conditions. Consequently, $\overline{W}_H = \overline{\overline{W}}_H$, $\overline{W}_d = \overline{\overline{W}}_d$, $T_{td} = \overline{T_{td}}$, and $P_{td} = \overline{P_{td}}$. If the Started Phase is initiated from non-steady state

86

• conditions, the same calculations described above are used to compute the quasi-steady state parameters. These are then corrected to the non-steady state initial conditions as follows:

$$\underline{\bar{W}}_H = \frac{P_{td} \, T_{to}}{\bar{P}_{td} \, T_{td}} \, \underline{\bar{\bar{W}}}_H$$

$$\underline{\bar{W}}_d = \frac{P_{td} \, T_{to}}{\bar{P}_{td} \, T_{td}} \, \underline{\bar{\bar{W}}}_d$$

where P_{td} and T_{td} are the instantaneous values carried over from the previous phase. Practically, the changes in geometry, attitude, and/or airflow demand required to restart an inlet are generally slow relative to the duct dynamics. Consequently instantaneous values of the required parameters will be close to the quasi-steady state values.

Unstarting Phase

Properties which must be known at the initiation of the Unstarting Phase are M_d , $\bar{W}_d$, T_{td} , $\bar{W}_u$, and T_{tu} . Generally, the Unstarting Phase will be initiated as a continuation of the Started Phase. At the Phase change, the simulation model changes in that the Helmholtz Volume and the Duct Volume of the Started Phase are combined to form the single Duct Volume of the Unstarting Phase. That is,

$$(V_d)_{\substack{\text{Unstarting} \\ \text{Phase}}} = (V_d + V_H)_{\substack{\text{Started} \\ \text{Phase}}}$$

similarly

$$(\bar{W}_d)_{\substack{\text{Unstarting} \\ \text{Phase}}} = (\bar{W}_d + \bar{W}_H)_{\substack{\text{Started} \\ \text{Phase}}}$$

Further, the total pressure and total temperature at the engine face are

87

continuous functions through the Phase change so that,

$$(P_{t2})_{\substack{\text{Unstarting} \\ \text{Phase}}} = (P_{t2})_{\substack{\text{Started} \\ \text{Phase}}}$$

and,

$$(T_{t2})_{\substack{\text{Unstarting} \\ \text{Phase}}} = (T_{td})_{\substack{\text{Unstarting} \\ \text{Phase}}} = (T_{t2})_{\substack{\text{Started} \\ \text{Phase}}}$$

M_d , the Mach number at the average density station in the Duct Volume will change because the Duct Volume changed. Inasmuch as

$$\bar{W}_d = g\rho_d \; V_d = \frac{P_{td} \; V_d}{R \; T_{td}} \; \frac{1}{(1 + .2M_d{}^2)^{2.5}}$$

M_d is

$$M_d = \left(5\left[\left(\frac{P_{td}V_d}{RT_{td} \; \underline{W}_d}\right)^{.4} - 1\right]\right)^{\frac{1}{2}}$$

where

$$P_{td} = P_{t2} + \Delta P_{td2}$$

At the Phase switch, the Upstream Normal Shock, arbitrarily located a small but finite distance upstream of the throat, will not yet be in motion. Consequently

$$T_{tu} = T_{to}$$

and
$$P_{tu} = \overline{P_{ty}}$$

Air quantity in the Upstream Volume is

$$\bar{W}_u = \frac{P_{tyu} \; V_u}{RT_{to} \; (1 + .2M_u{}^2)^{2.5}}$$

, where

$$\overline{P_{tyu}} = \left(\frac{6\ M_{xu}^2}{M_{xu}^2 + 5}\right)^{3.5} \left(\frac{6}{7\ M_{xu}^2 - 1}\right)^{2.5} P_{txu}$$

and M_{xu} , V_u , and P_{txu} are calculated in accordance with the dynamics equations.

Empty-Fill Phase

Initial conditions which must be calculated for the Empty-Fill Phase are M_d , T_{td} and $\overline{W}_d$. When the Phase is initiated as a continuation of the Unstarting Phase, the Mach number, M_d , computed at the initiation of the Unstarting Phase is carried over and used during the Empty-Fill Phase. While an approximation, this value is reasonably correct inasmuch as the terminal shock is close to the throat station upon initiation of both the Unstarting Phase and the Empty-Fill Phase. Further, the simulation is not overly sensitive to the accuracy of M_d .

Engine face total pressure and temperature are continuous functions through the Phase switch. Consequently

$$(P_{t2})_{\substack{\text{Empty-Fill} \\ \text{Phase}}} = (P_{t2})_{\substack{\text{Unstarting} \\ \text{Phase}}}$$

and,

$$(T_{t2})_{\substack{\text{Empty-Fill} \\ \text{Phase}}} = (T_{td})_{\substack{\text{Empty-Fill} \\ \text{Phase}}} = (T_{t2})_{\substack{\text{Unstarting} \\ \text{Phase}}}$$

Air in the Duct Volume is

$$\overline{W}_d = \frac{P_{td}\ V_{def}}{RT_{td}\ (1 + .2M_d^2)^{2.5}}$$

where

$$P_{td} = P_{t2} + \Delta P_{td2}$$

In event a simulation run is initiated in the Empty-Fill Phase, the initial terminal shock position is specified and the value of $\bar{W}_d$ is computed in the same procedure used for the Started Phase. M_d is then computed as

$$M_d = \left(5 \left[\left(\frac{P_{td} \, V_d}{RT_{td} \, \underline{W}_d} \right)^{.4} - 1 \right] \right)^{\frac{1}{2}}$$

Subcritical Phase

Required initial conditions for the Subcritical Phase are T_{td} , M_d , and $\underline{\bar{W}}_d$. When the Subcritical Phase is initiated as a continuation of the Empty-Fill Phase, M_d is carried over from the Empty-Fill Phase to the Subcritical Phase. As engine face total temperature and total pressure are continuous during the Phase switch,

$$(T_{t2})_{\substack{\text{Subcritical} \\ \text{Phase}}} = (T_{td})_{\substack{\text{Subcritical} \\ \text{Phase}}} = (T_{t2})_{\substack{\text{Empty-Fill} \\ \text{Phase}}}$$

and

$$(P_{t2})_{\substack{\text{Subcritical} \\ \text{Phase}}} = (P_{t2})_{\substack{\text{Empty-Fill} \\ \text{Phase}}}$$

Air in the Duct Volume is

$$\bar{W}_d = \frac{P_{td} \, V_d}{RT_{td} \, (1 + .2M_d^2)^{2.5}}$$

where

$$P_{td} = P_{t2} + \Delta P_{td2}$$

90

If the Subcritical Phase is initiated from steady state conditions, $\overline{W}_d$ is computed by use of Simpson's Rule in a procedure similar to that used in the Started Phase. M_d is then calculated as

$$M_d = \left(5 \left[\left(\frac{P_{td} \, V_d}{RT_{td} \, \overline{W}_d}\right)^{.4} - 1\right]\right)^{\frac{1}{2}}$$

Hammershock Phase

Initial conditions which must be computed or input for the Hammershock Phase are M_{HS}, $\overline{W}_{HS}$, and T_{tHS}.

By the nature of the transient, M_{HS}, the Mach number at the average density station in the Hammershock Volume will be low during the Hammershock Phase. Consequently an assumed constant value is input, usually between 0 and 0.2.

The hammershock wave is initially located just far enough upstream of the engine face to create a finite Hammershock Volume. Initial total pressure and temperature in the volume will, therefore, be equal to the engine face total pressure and temperature at the instant of the Phase switch. Then,

$$\overline{W}_{HS} = \frac{P_{t_{HS}} \, V_{HS}}{RT_{t_{HS}}(1 + .2M_{HS}^2)^{2.5}}$$

where

$$P_{t_{HS}} = P_{t2}$$

$$T_{t_{HS}} = T_{t2}$$

SYMBOLS AND NOTATION

Primary Symbols

Symbol	Definition
a	speed of sound
A	flow area at the station designated by the subscript
A_{dgeo}	average geometric area, volume/length
c_p	specific heat at constant pressure
C_{bm}	main bypass area flow coefficient
C_{bp}	bypass area flow coefficient
C_{bt}	trim bypass area flow coefficient
DSP	Downstream Shock Parameter, P_{DSS}/P_{DSR}
g	acceleration due to gravity
h	stream tube height
J	mechanical equivalent of heat
K_a	ratio of flow area at the average density station to the average geometric area in the Duct Volume, A_d/A_{dgeo}
K_{bp}	P_{tbp}/P_{t2}
K_{EF}	value of P_{td}/P_o at which separated boundary layer flow reattaches
K_{HS}	input constant - if $(dW_e/W_e)/dt \geqslant K_{HS}$, inlet operation switches to the Hammershock Phase
K_{MX}	empirical factor to account for boundary layer-shock interaction effects
K_{RS}	empirical value of W_T/W_{II} at which inlet restart occurs
K_u	flow coefficient for the inlet throat area under sonic-flow conditions
K_{yz}	portion of the subsonic total pressure loss between stations Y and Z

K_{z2}	portion of the subsonic total pressure loss between stations Z and 2
l	length of the Helmholtz Volume
M	Mach number at the station designated by the subscript
P	static pressure at the flow station designated by the subscript
P_t	total pressure at the flow station designated by the subscript
P_{tx}/P_{to}	local to freestream total pressure ratio immediately upstream of the terminal normal shock in the started and the Unstarting Phases
$(P_{tx}/P_{to})_E$	local to freestream total pressure ratio downstream of the external normal shock and upstream of the terminal shock in the Empty-Fill Phase
$(P_{tx}/P_{to})_S$	local to freestream total pressure ratio upstream of the external normal shock or pseudo-normal shock in the Subcritical Phase
q_c	compressible flow dynamic head, $P_t - P$
R	gas constant
SPP	shock position parameter, P_{SPM}/P_{SPR}
t	time
T	static temperature at the flow station designated by the subscript
T_t	total temperature at the flow station designated by the subscript
U	velocity relative to the duct
U'	velocity relative to the associated normal shock
V	volume
W	airflow at the station designated by the subscript, weight/time

W_{bbx}	bleed flow downstream of X_{II} and upstream of the terminal shock (supersonic flow region)
W_{bbxu}	bleed flow upstream of X_{II} and the terminal shock (supersonic flow region)
W_{bby}	bleed flow downstream of X_{II} and the terminal shock (subsonic flow region)
W_{bbyu}	bleed flow upstream of X_{II} and downstream of the terminal shock (subsonic flow region)
W_T	flow through throat under sonic-flow conditions
$\bar{W}$	air quantity in the volume designated by the subscript, weight
$(W_I/W_o)_{buzz}$	empirical value of mass flow ratio below which buzz occurs
X	terminal shock station, upstream face
$X_{(\ )}$	flow station as designated by the subscript
Y	terminal shock station, downstream face
Z	flow station at the interface between the Helmholtz Volume and the Duct Volume in the Started Phase simulation model
α_o	angle of attack
γ	ratio of specific heats, c_p/c_v
δ_{max}	maximum deflection angle for attached flow
$\Delta P_{t(\ )}$	subsonic flow total pressure loss between the stations indicated by the subscripts
Δt_R	non-dimensionalized time after flow reattachment begins
Δt_S	non-dimensionalized time after flow separation begins
ϵ	subsonic flow total pressure loss coefficient $\epsilon = \Delta P_t/(P_t - P)$
λ	sonic flow constant, $\sqrt{\dfrac{\gamma g}{R}}\dfrac{M}{(1 + .2M^2)^3}$ where $M = 1.0$

94

ρ	mass density at the station designated by the subscript
ϕ_x	bleed flow ratio slope, $(W_{bbx}/W_{base})/dX$, Supersonic
ϕ_y	bleed flow ratio slope, $(W_{bby}/W_{base})/dX$, Subsonic
ϕ_{yu}	bleed flow ratio slope, $(W_{bbyu}/W_{base})/dX$
ψ_0	angle of yaw

Subscripts

Subscript	Description
base	reference or base value of parameter
bm	main bypass
bp	bypass
bt	trim bypass
d	station in the Duct Volume where the density is equal to the average density in the Duct Volume - also, parameters associated with the Duct Volume
dH	property at station d as computed from the Helmholtz Volume side
e	station just upstream of where the bypass and engine system airflows divide
E	parameter applicable to Empty-Fill Phase
ef	effective value of parameter as distinguished from the geometric value
H	property in the Helmholtz Volume
HS	property in the Hammershock Volume
i	value at the initiation of the Phase
L	cowl lip station

<u>Subscripts</u> (Continued)

n	nth value or element
o	freestream value
R	downstream station where flow separation ends and where flow reattachment begins
s	property of the engine secondary airflow
S	parameter applicable to the Subcritical Phase
T	throat station
TAB	parameters applicable to the test data used for empirical tables of boundary layer separation and reattachment characteristics
u	properties in the Upstream Volume
x	immediately upstream of the terminal shock
xu	immediately upstream of the Upstream Normal Shock
xHS	immediately upstream of the hammershock
y	immediately downstream of the terminal shock
yu	immediately downstream of the Upstream Normal Shock
yHS	immediately downstream of the hammershock
z	property at the interface between the Helmholtz Volume and the Duct Volume
zD	property at the interface between the Helmholtz Volume and the Duct Volume as computed from the Duct Volume side
zH	property at the interface between the Helmholtz Volume and the Duct Volume as computed from the Helmholtz Volume side
2	engine face station
I	upstream end of the boundary layer bleed area

II   boundary layer bleed compartment station, usually
                            located slightly forward of the geometric throat
                            station - bleed flow forward of this station is not
                            affected by the position of the terminal shock during
                            started operation

III   downstream end of the boundary layer bleed area

Superscripts

Superscript   Description

$\overline{(\ )}$ quasi-steady state value for the instantaneous terminal
                            shock position

$(\ )'$ parameter relative to the non-geometric station
                            designated by the subscript

LIST OF FIGURES

LIST OF FIGURES (Continued)

100

102

As the terminal shock moves upstream from "a" to "b" total pressure recovery increases as shown in figure 2.

Figure 1. Started Phase of Inlet Operation

$$\frac{P_{t2}}{P_{t0}}$$

TERMINAL SHOCK POSITION   PHASE

TERMINAL SHOCK POSITION	PHASE
a - b	STARTED
b - c	UNSTARTING
d - e	EMPTY PORTION OF EMPTY-FILL
e - f	FILL PORTION OF EMPTY-FILL
g	STABILIZED, SUPERCRITICAL OPERATION IN EMPTY-FILL

Figure 2. Total Pressure Recovery Versus Time
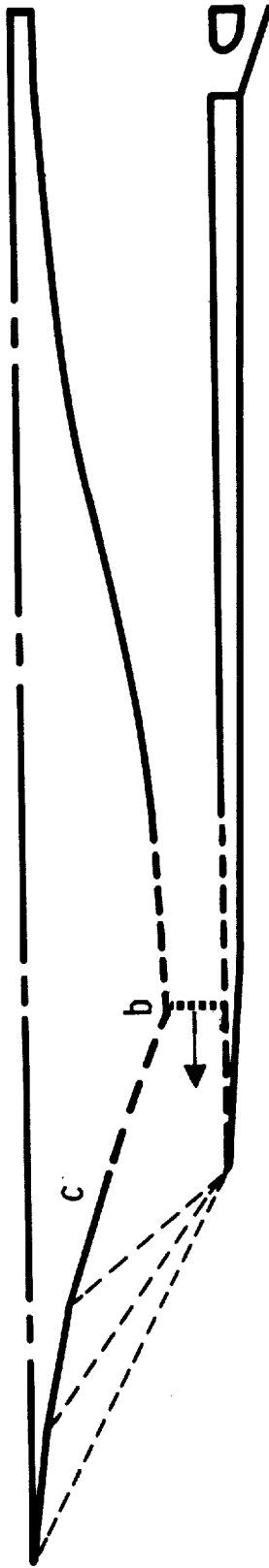
Terminal shock moves from "b" to "c"

Figure 3. Insufficient Demand – Induced Unstarting Phase of Inlet Operation
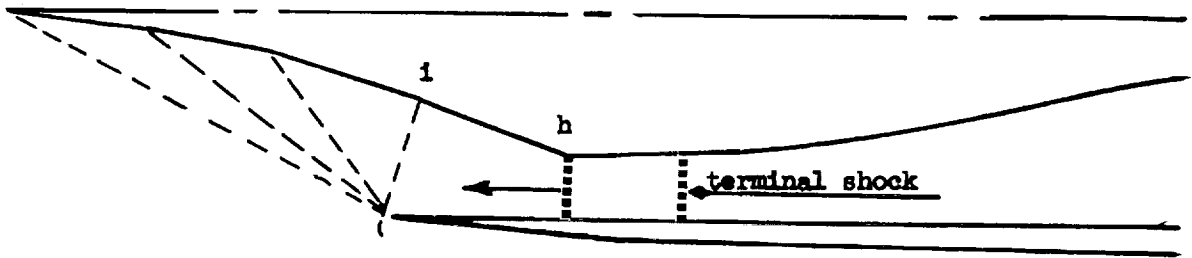
Unstart caused by throat choking begins with the
formation of a normal shock in the throat, "h".
As this shock moves forward, the terminal normal
shock moves forward, and may catch and coalesce
with the upstream normal shock before it reaches "i"

Figure 4. Choked Throat-Induced Unstarting Phase of Inlet Operation
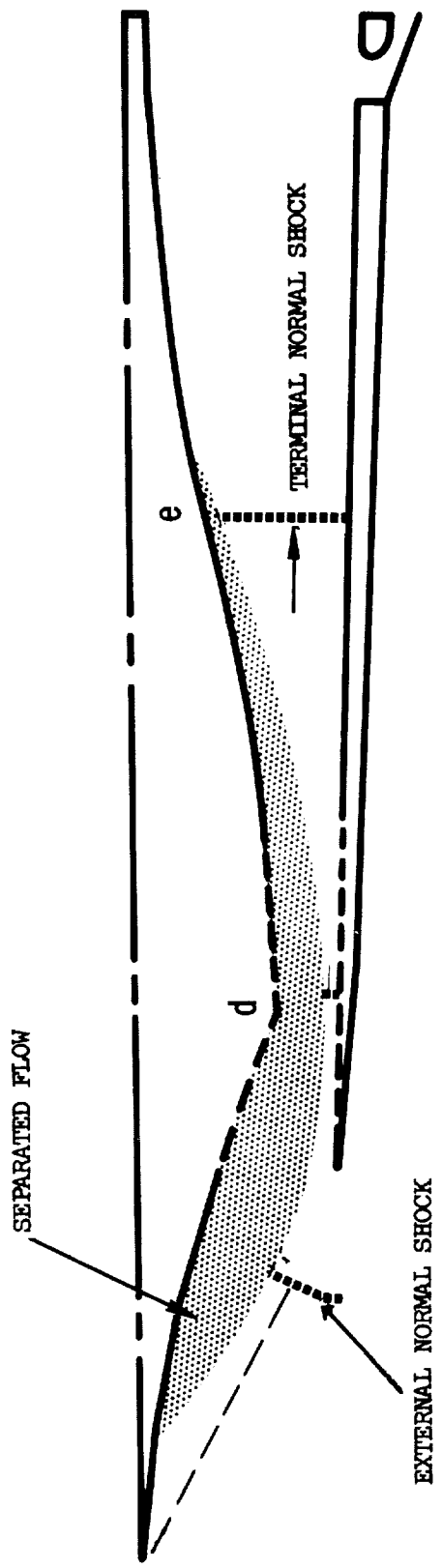
Terminal shock moves from "d" to "e"

Figure 5. Emptying Portion of Empty-Fill Phase
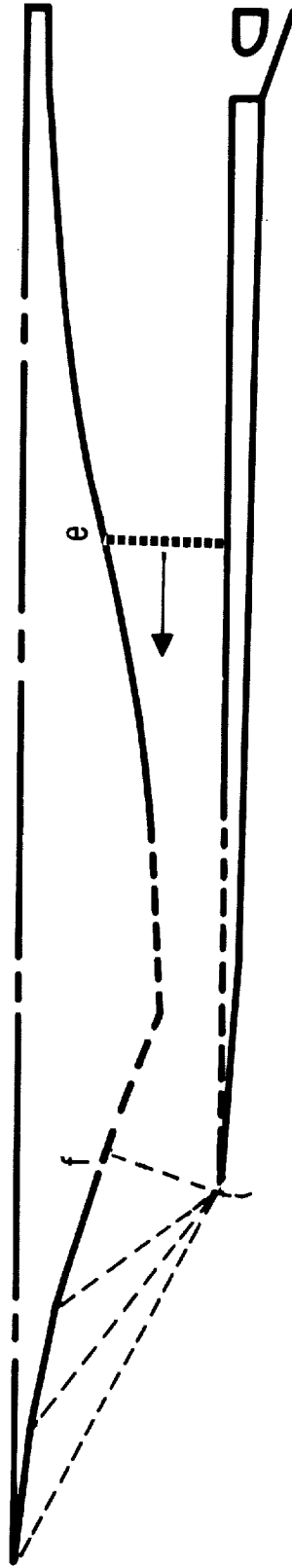
Terminal shock moves from "e" to "f"

Figure 6. Filling Portion of Empty-Fill Phase

108
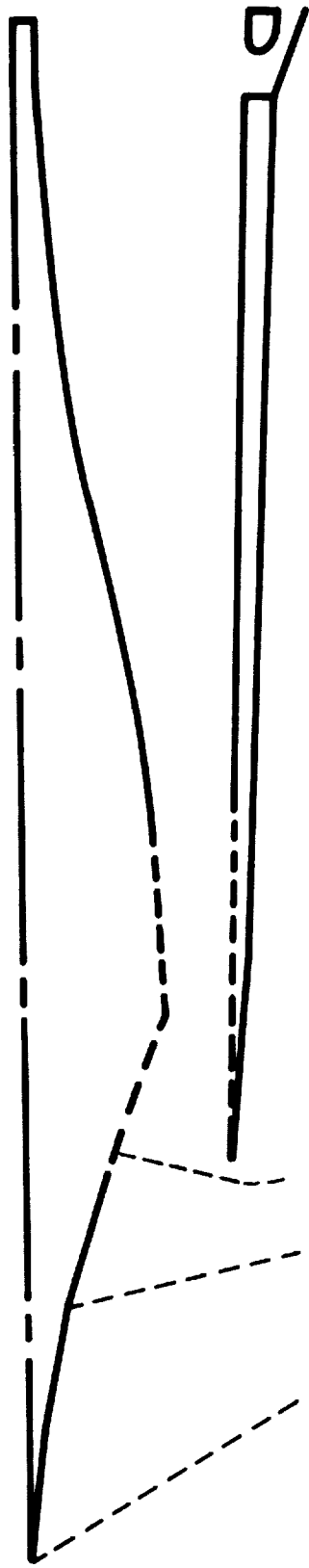
SUPERSONIC FLIGHT SPEEDS
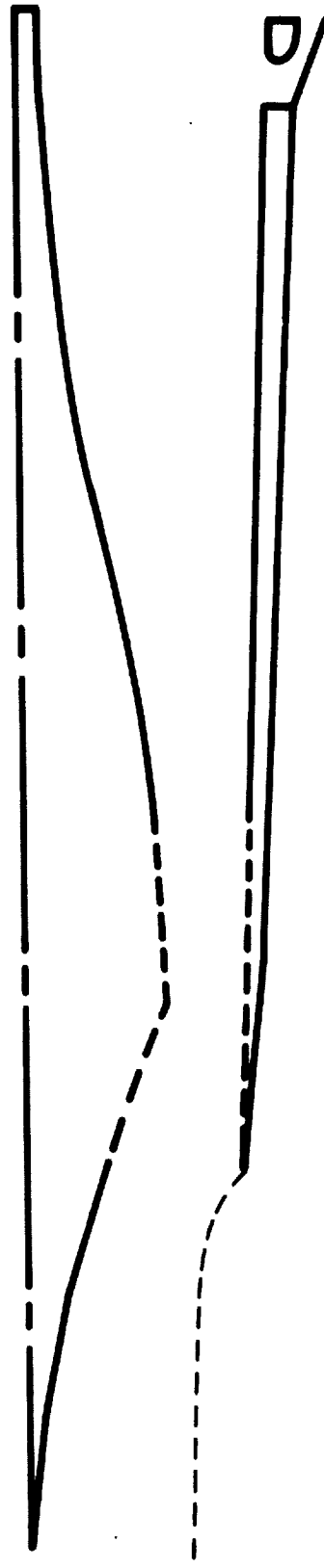
SUBSONIC FLIGHT SPEEDS

Figure 7. Subcritical Phase of Inlet Operation
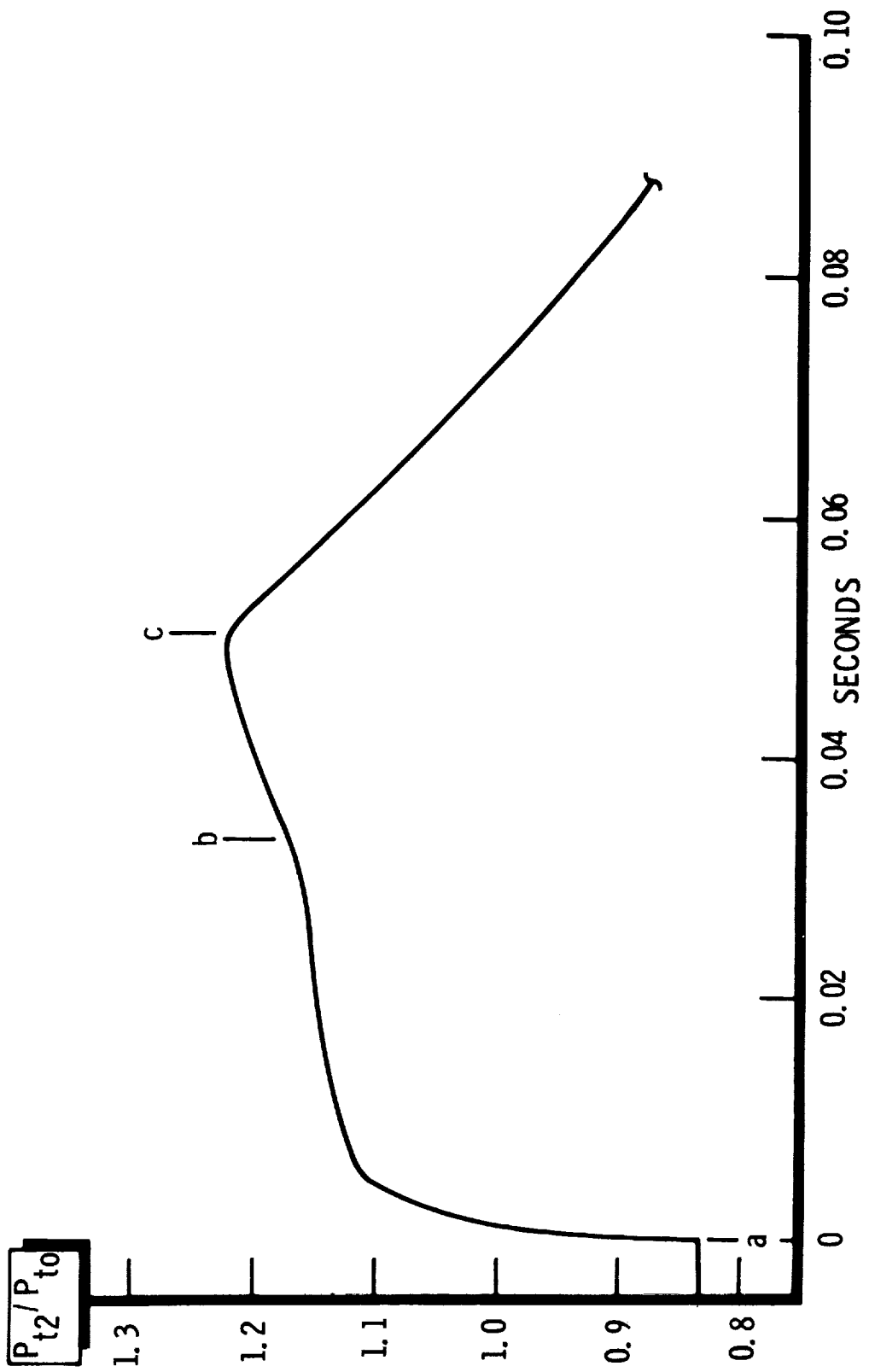
Figure 8a. Hammershock Phase of Inlet Operation

110

HAMMERSHOCK
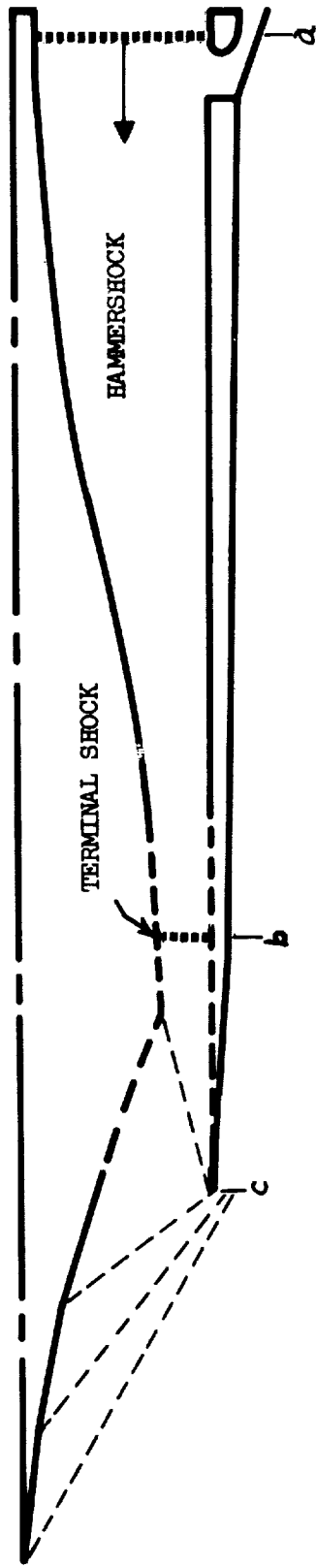
TERMINAL SHOCK

Hammershock wave forms at engine face and moves upstream

Figure 8b. Hammershock Phase of Inlet Operation

111
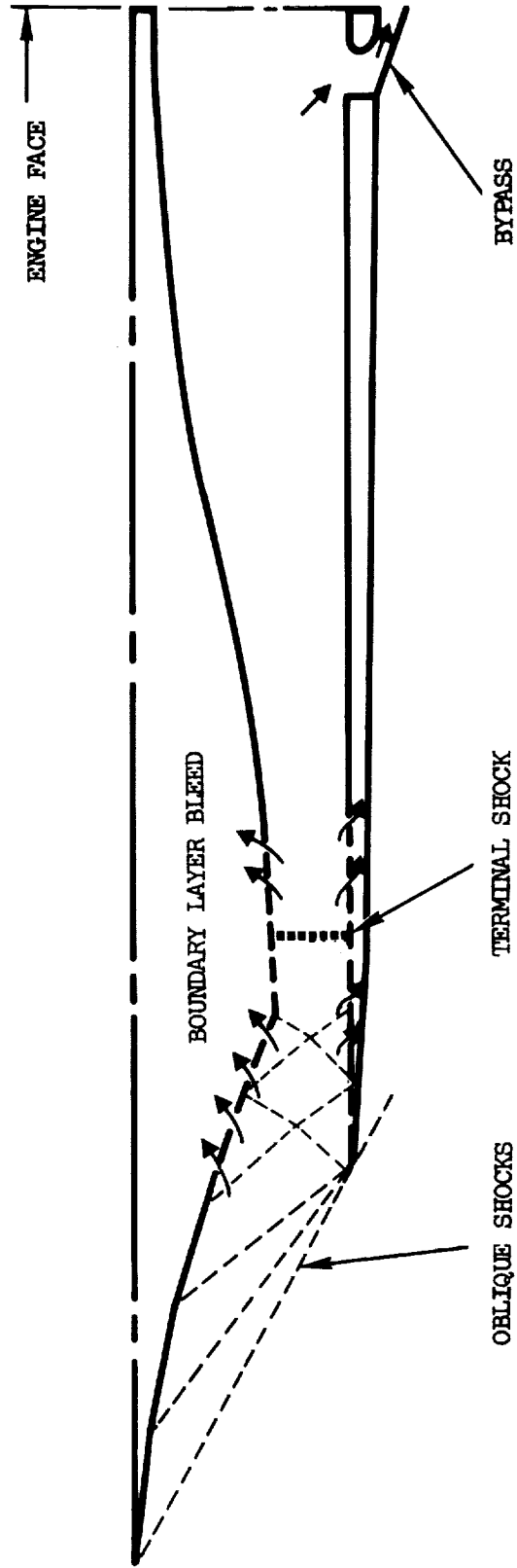
Figure 9. Typical Air Induction System

See "SYMBOLS AND NOTATION" for Station and Subscript definitions.

Figure 10. Started Phase Simulation Model

113
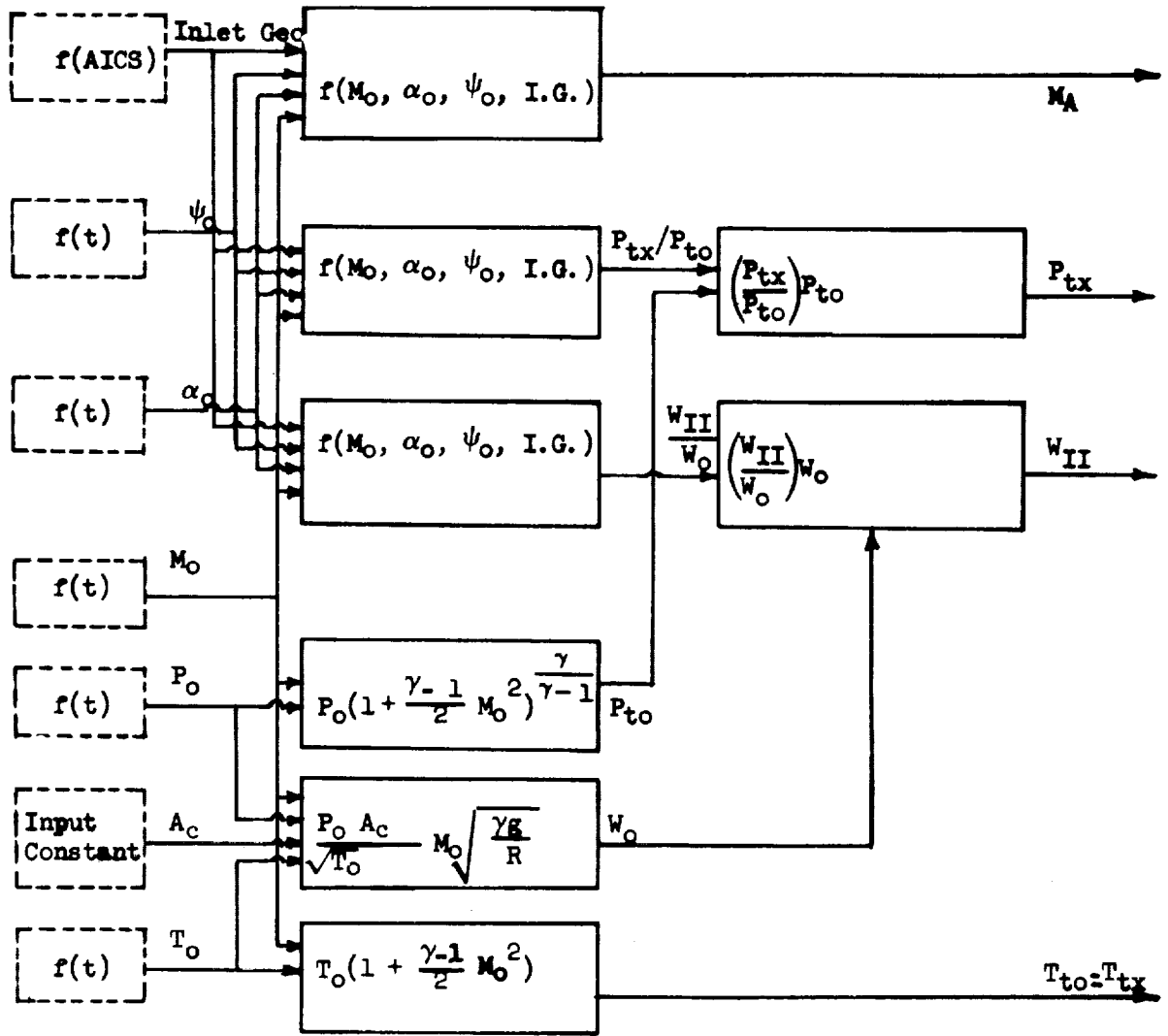
Figure 11. Started Phase Upstream Properties

114
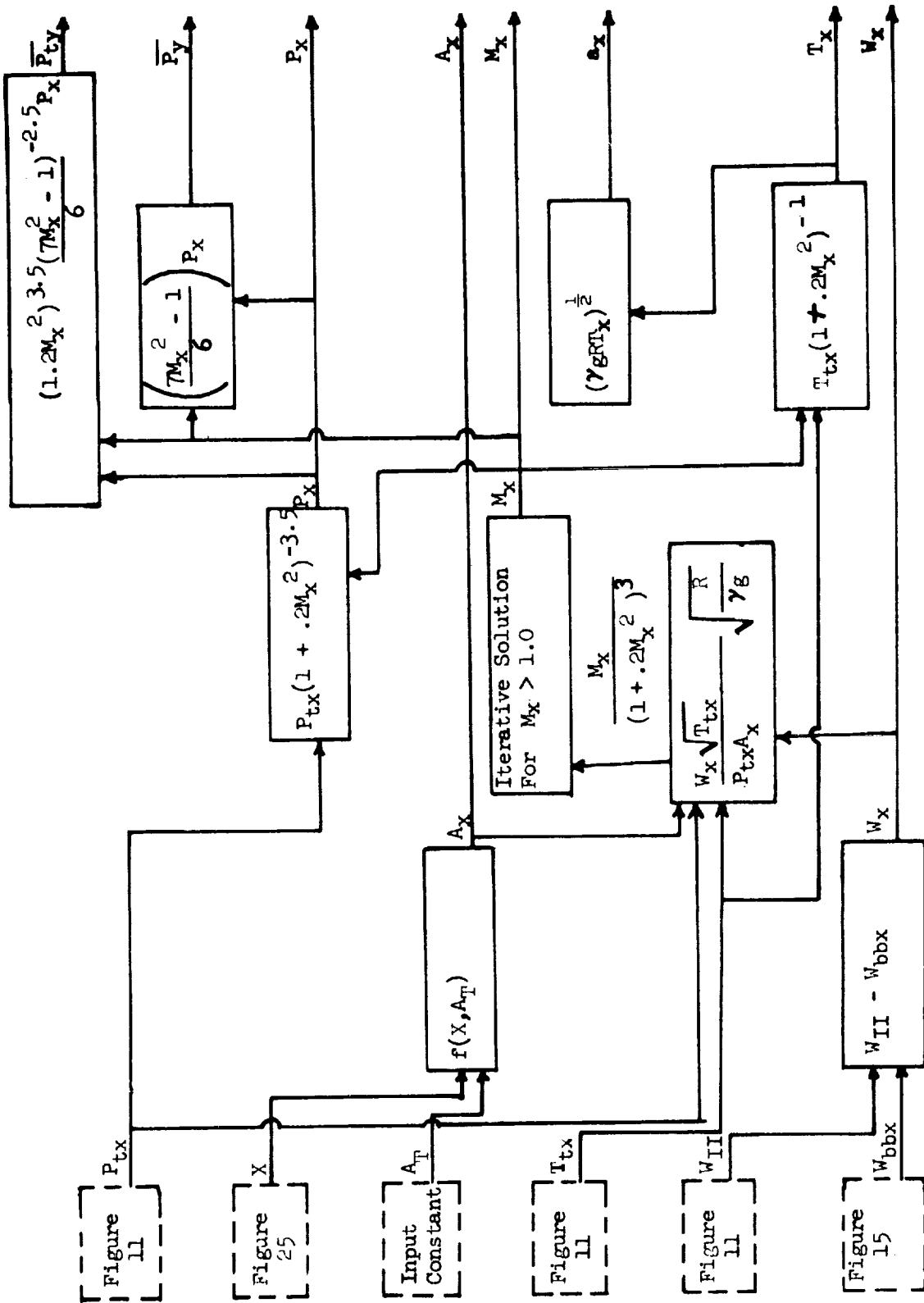
Figure 12. Started Phase Properties at the Terminal Shock

115

Figure
12   M_x

Figure
12   a_x

Figure
12   T_x

Figure
25   dx/dt

Figure
12   P_x

Figure
12   A_x

$$\frac{U_x'}{U_x} = \frac{M_x'}{M_x}$$ U_x'/U_x

$$M_x - \frac{dx/dt}{a_x}$$ M_x'

$$T_y(1 + .2M_y^2)$$ T_{ty}

$$\frac{(M_x'^2 + 5)(7M_x'^2 - 1)}{36M_x'^2} T_x$$ T_y T_y

$$\sqrt{\frac{M_x'^2 + 5}{7M_x'^2 - 1}}$$ M_y'

$$M_y' + \frac{dx/dt}{\sqrt{\gamma g R T_y}}$$ M_y

$$\frac{7M_x'^2 - 1}{6}$$ P_y P_y

$$P_y(1 + .2M_y^2)^{3.5}$$ P_{ty}

$$\sqrt{\frac{\gamma g}{R}} M_y \frac{P_y A_x}{\sqrt{T_y}}$$ W_y
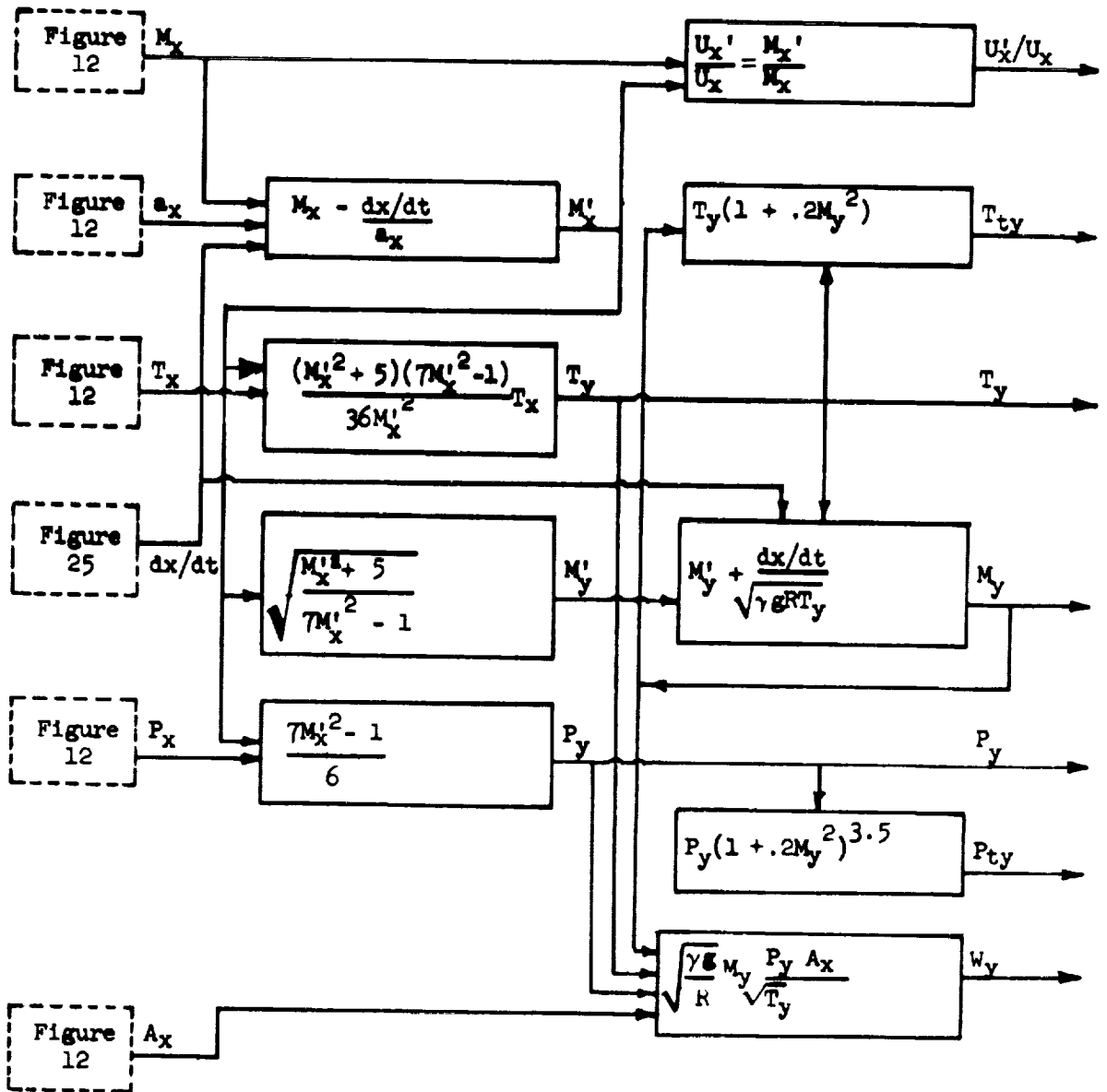
Figure 13.   Started Phase Properties Behind the Terminal Shock

116
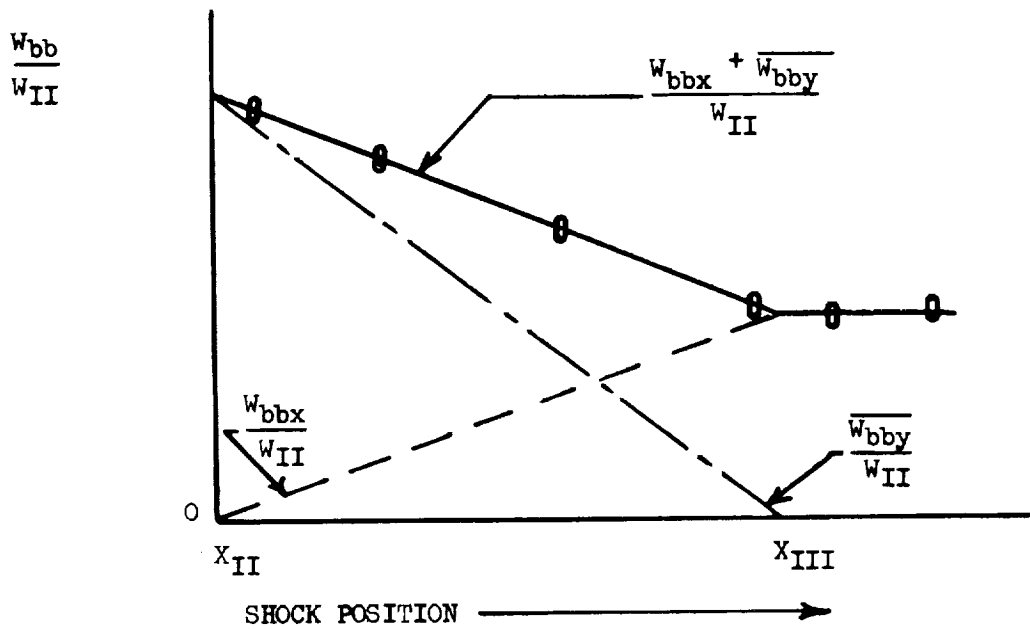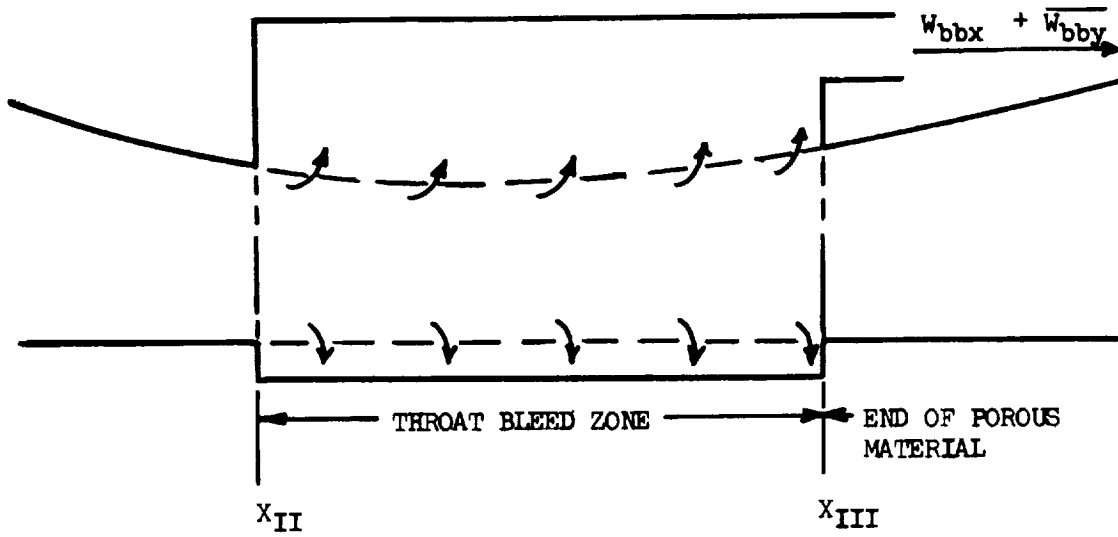
Figure 14. Started Phase Boundary Layer Bleed From Zones Affected by the Terminal Shock Position
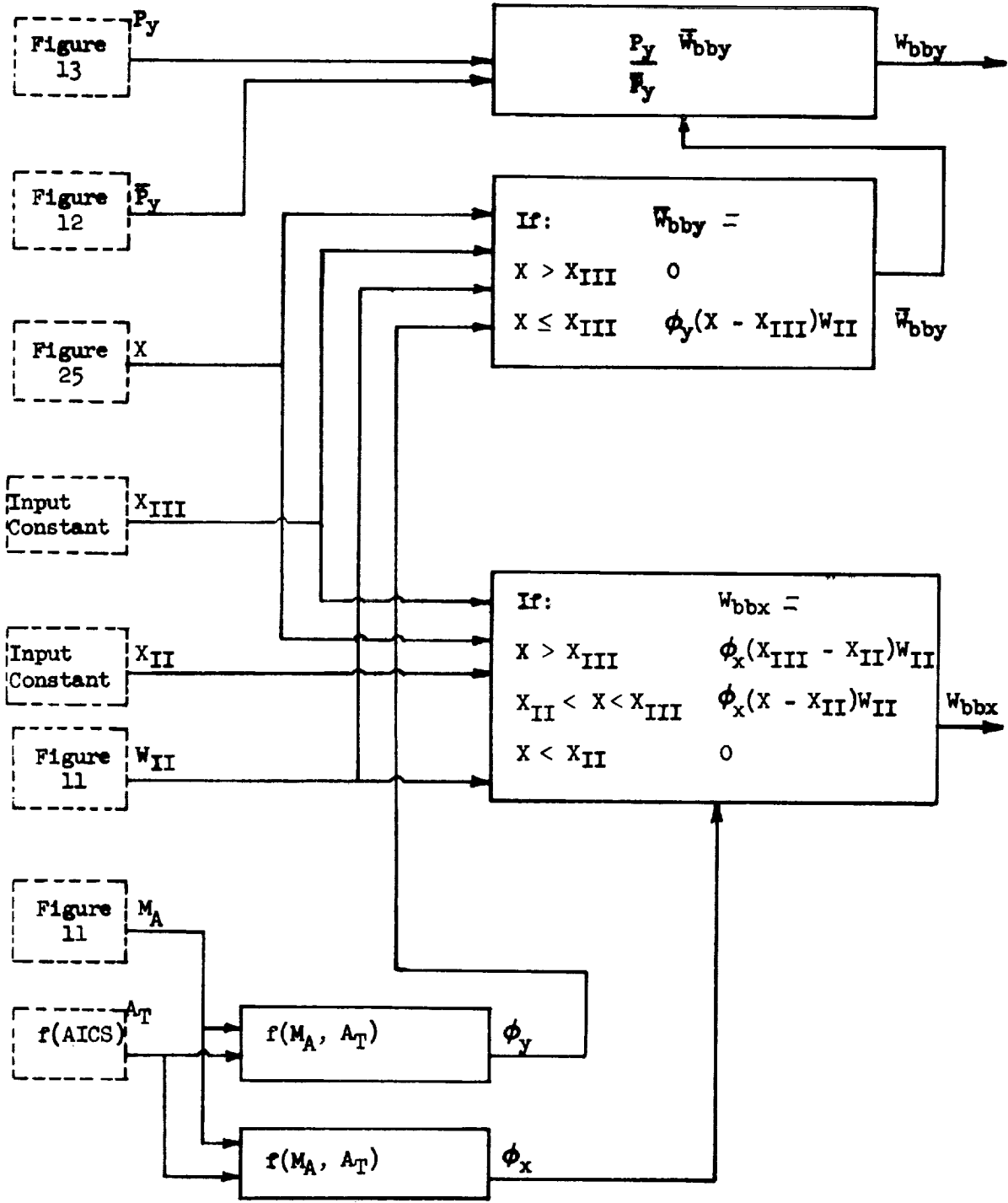
Figure 15. Started Phase Boundary Layer Bleed Flows
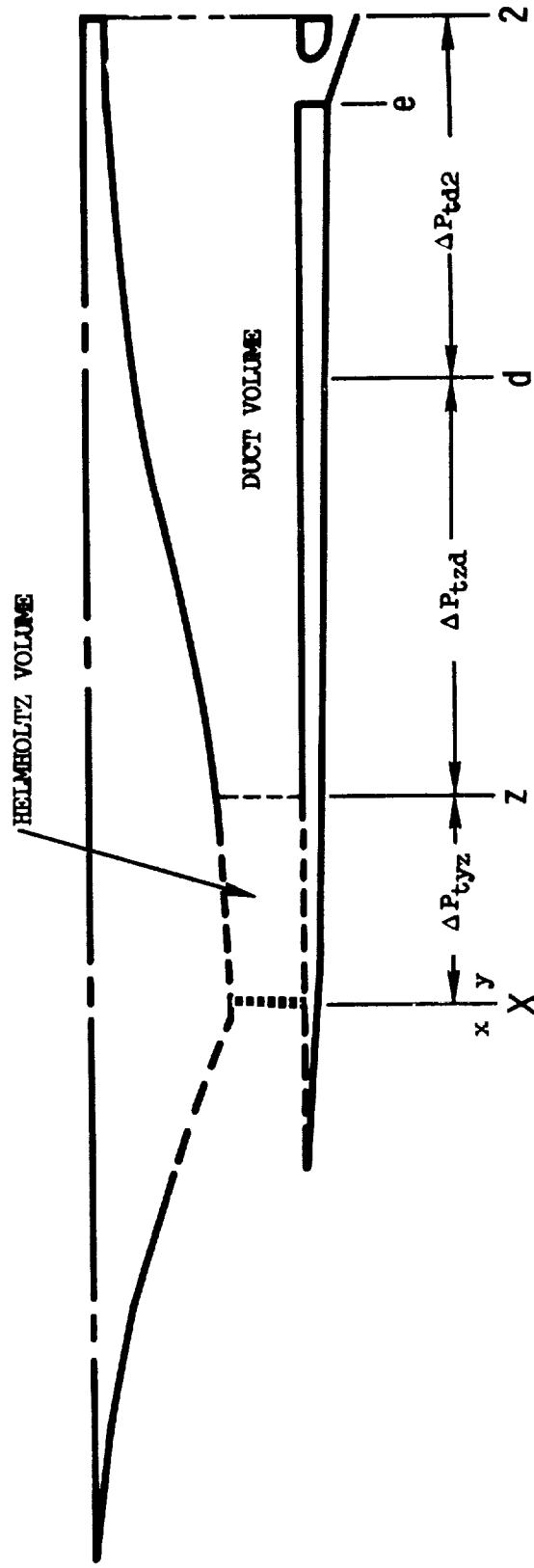
Figure 16. Started Phase Subsonic Flow Total Pressure Losses Diagram

119
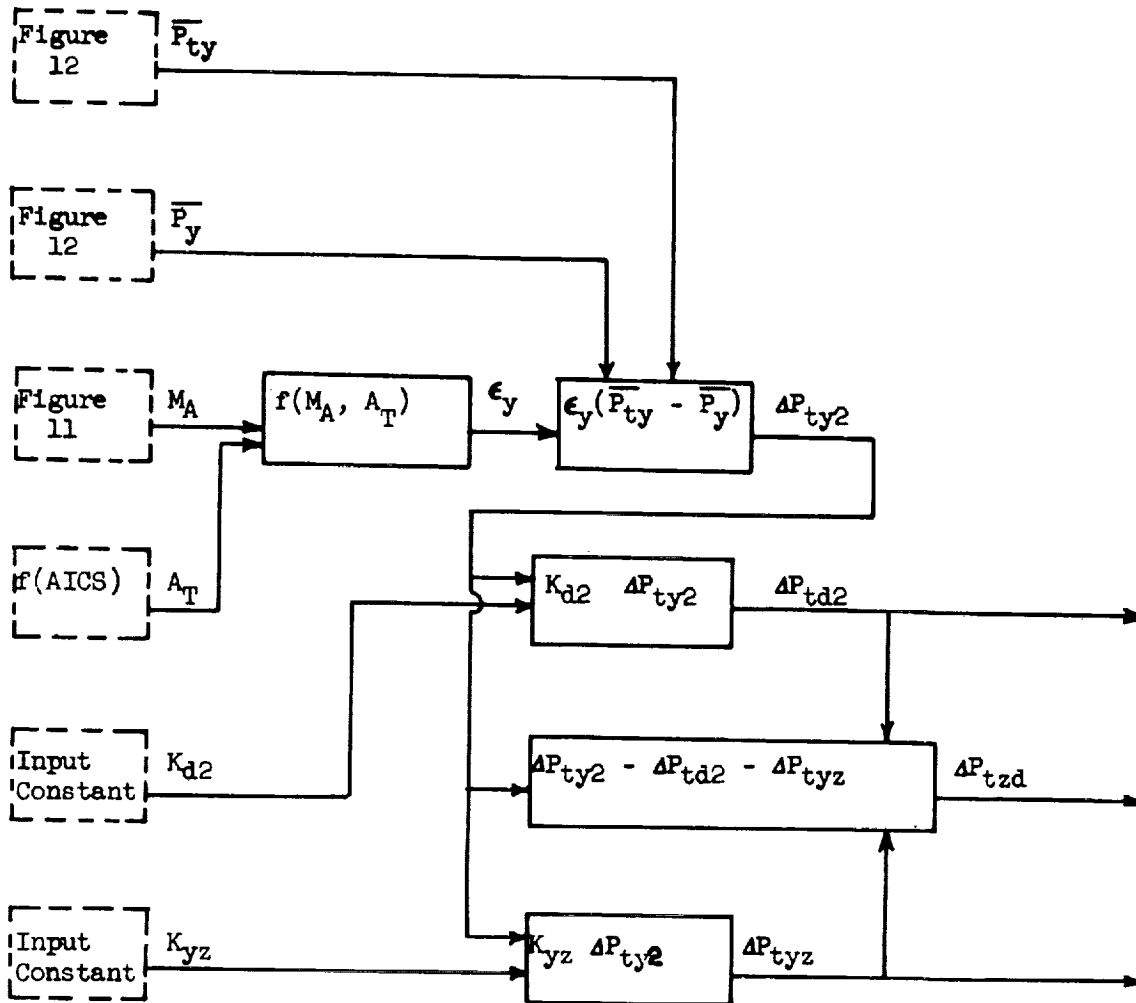
Figure 17. Started Phase Subsonic Flow Total Pressure Losses

120
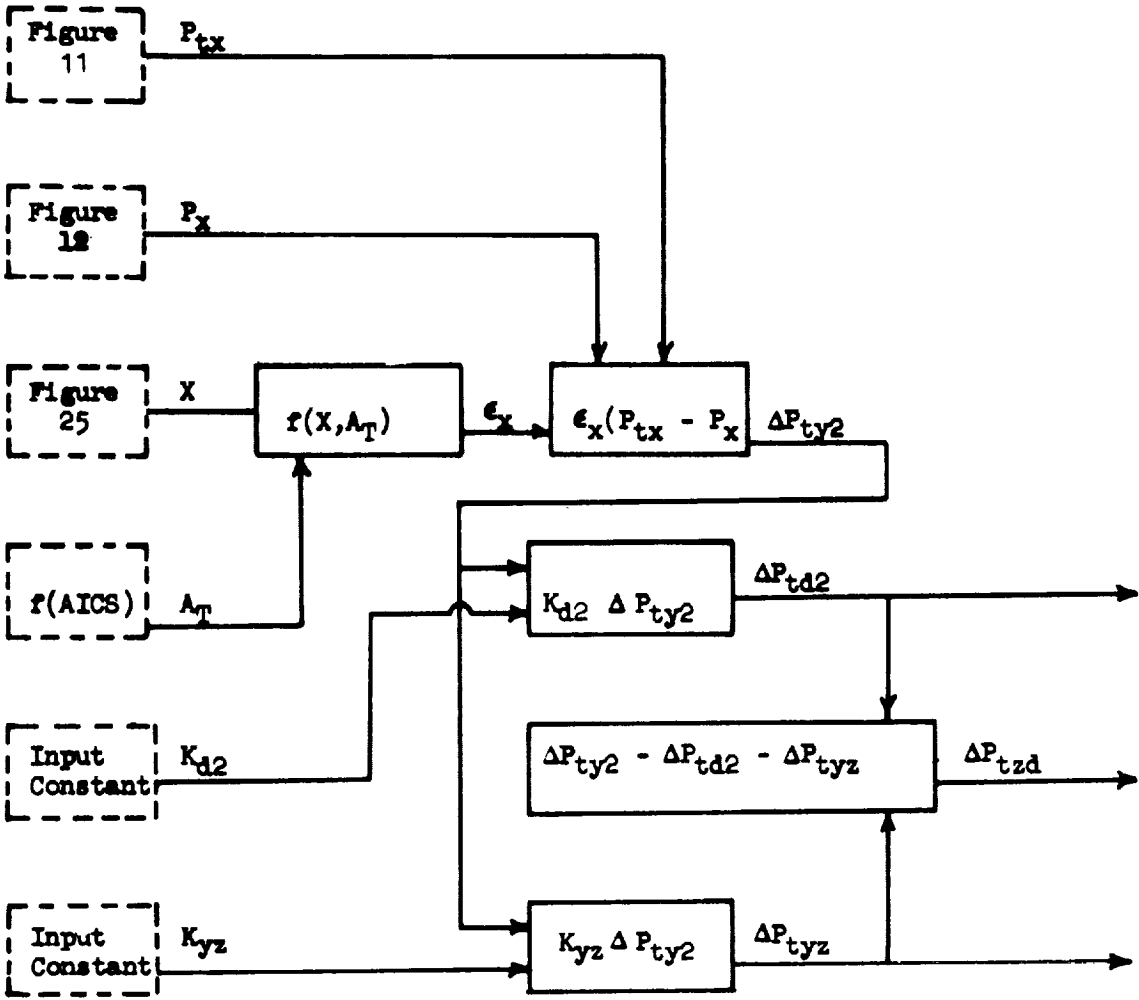
Figure 18. Started Phase Alternate Method Subsonic Flow Total Pressure Losses
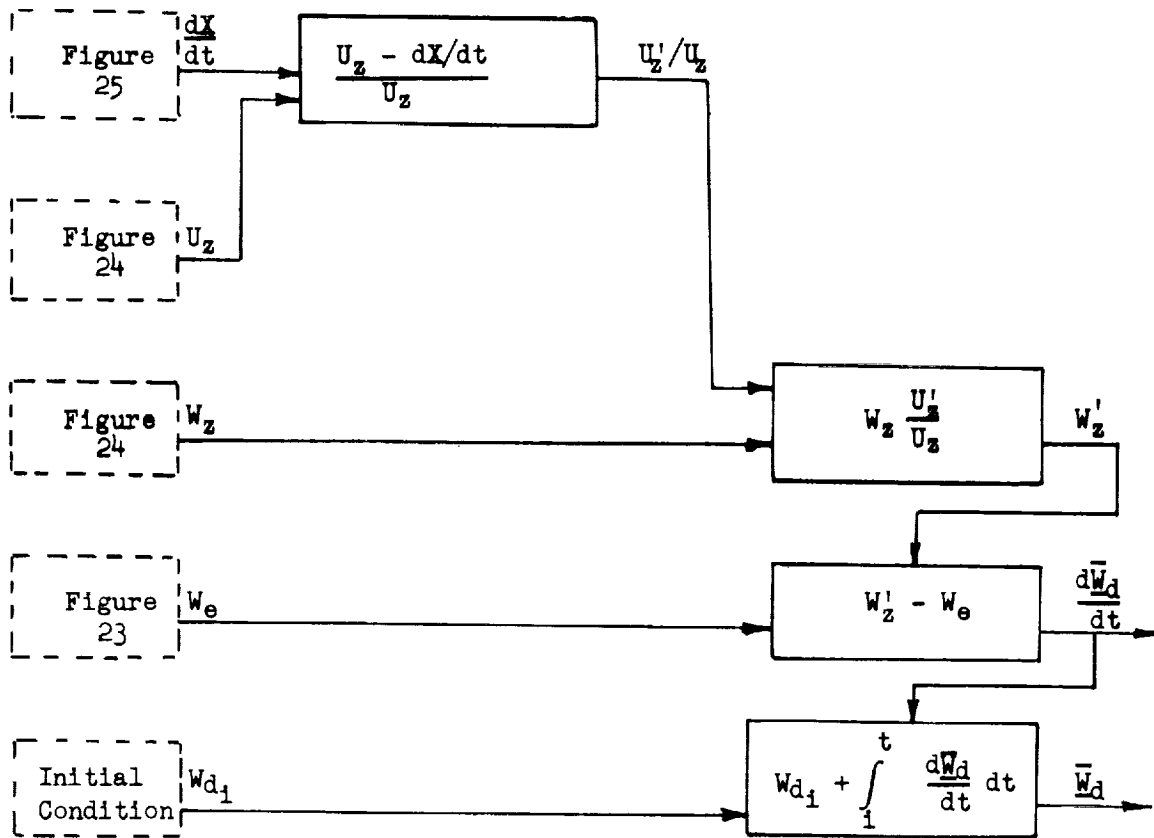
Figure 19. Started Phase Duct Volume Mass
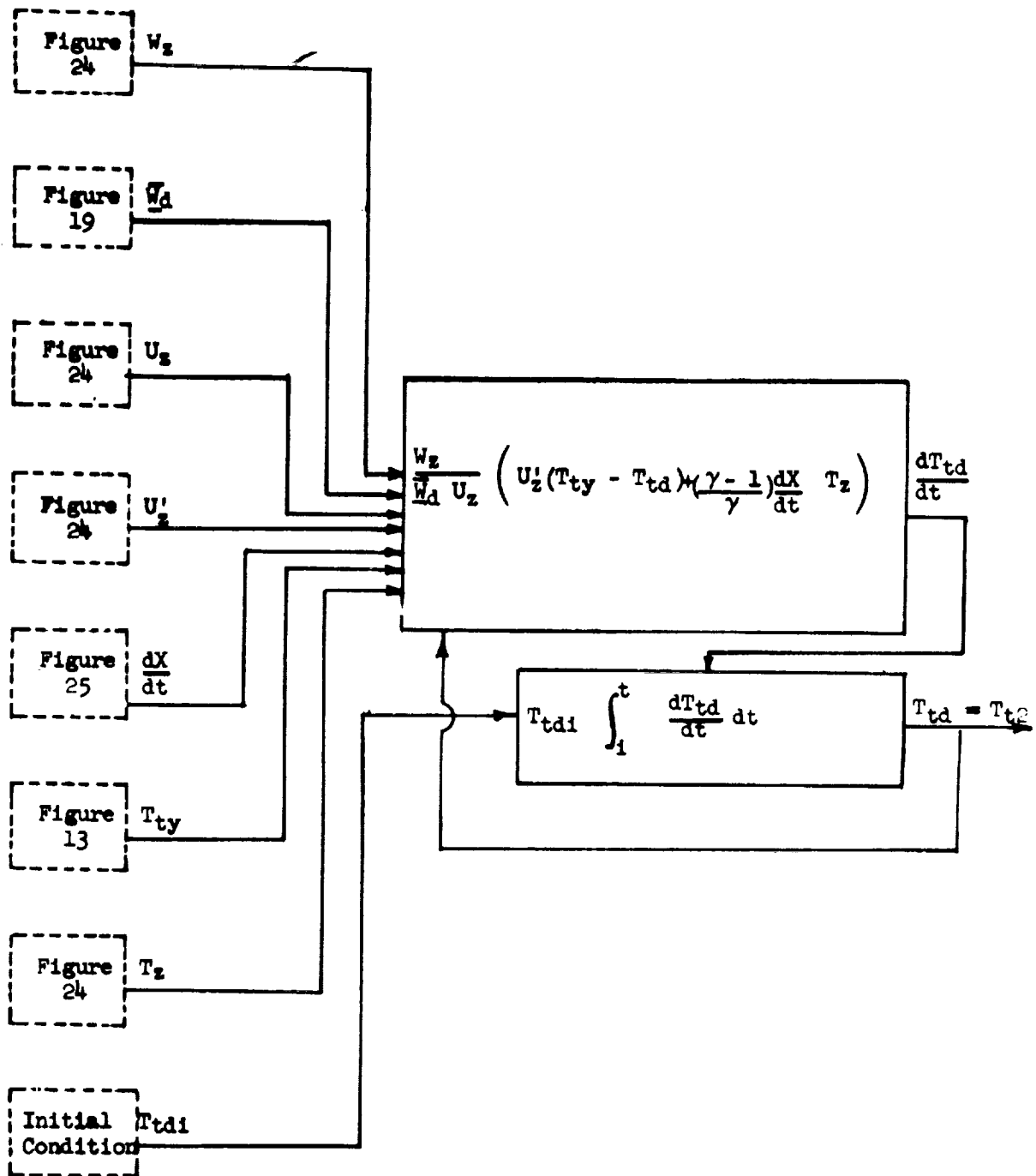
Figure 20. Started Phase Duct Volume Total Temperature

123
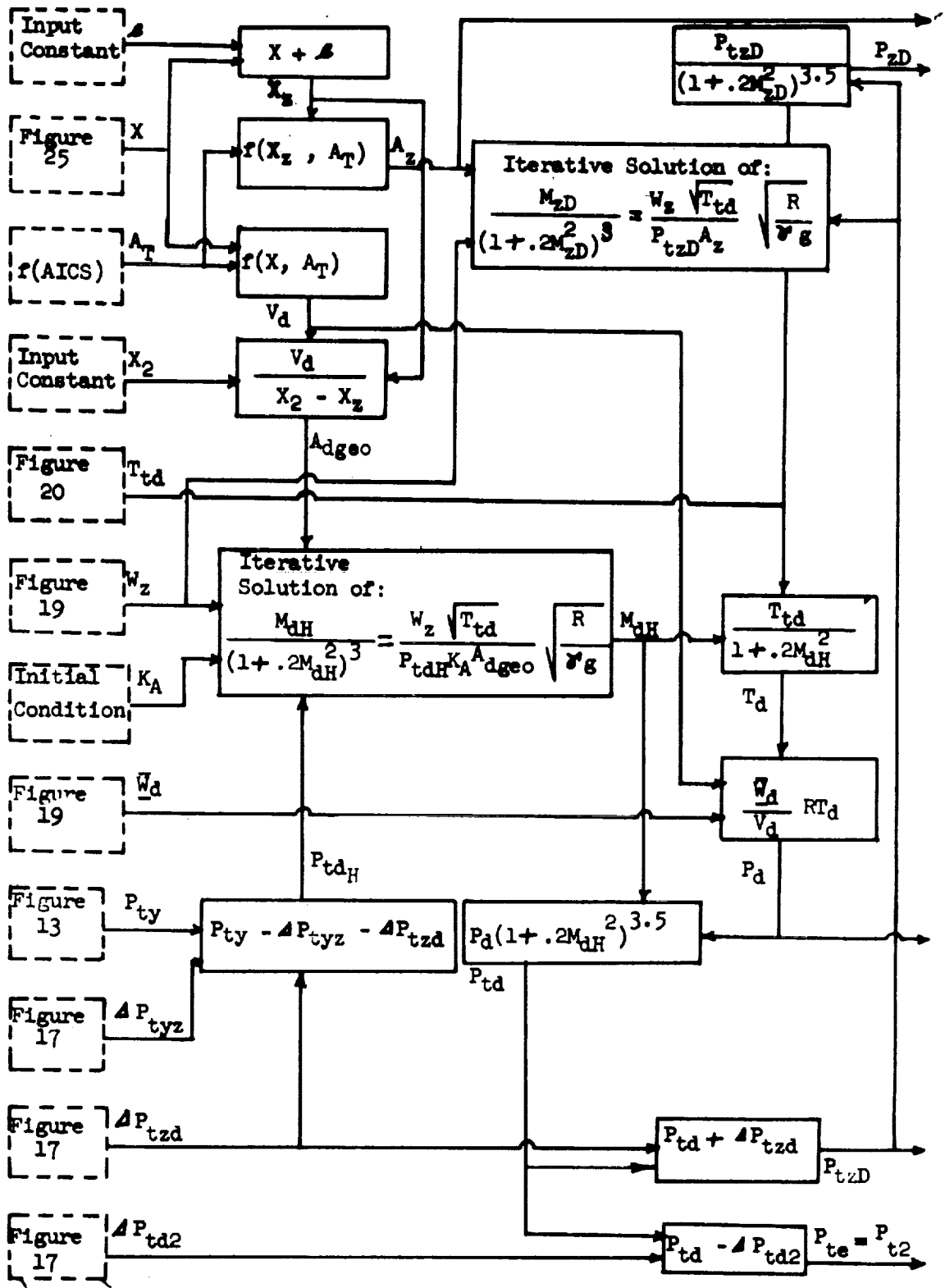
Figure 21. Started Phase Duct Volume Pressures

WING SURFACE

BYPASS FLOW

PLENUM

DUCT FLOW

ENGINE FACE

SCHEDULED
SECONDARY
FLOW

e

2
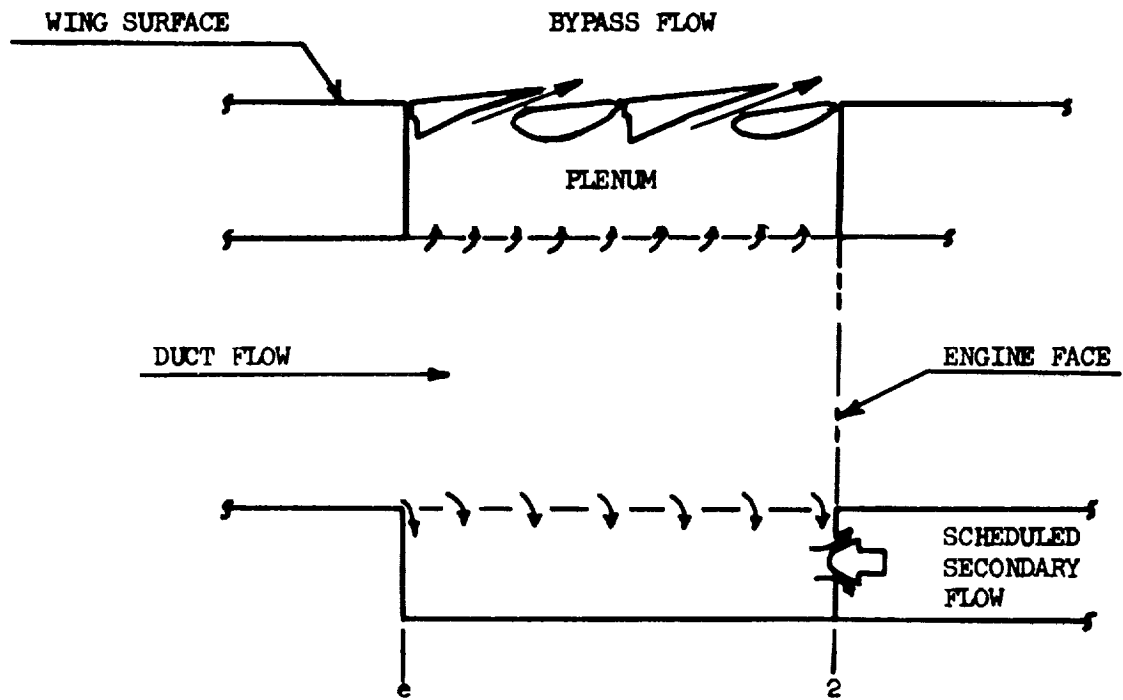
Figure 22. Started Phase Bypass and Secondary Airflow System
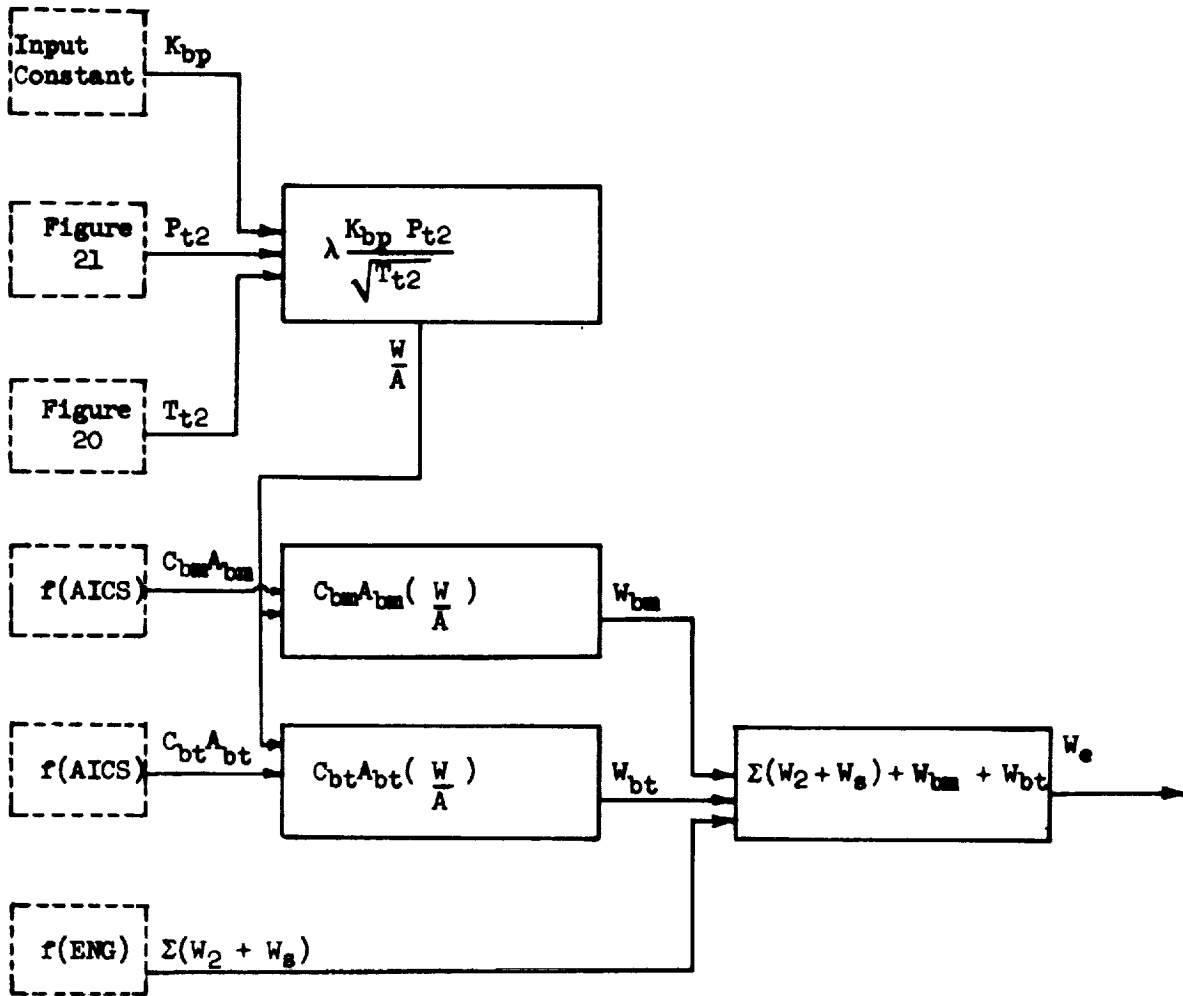
Figure 23. Started Phase Bypass and Engine System Airflows

Figure 13 — P_{ty}

Figure 17 — ΔP_{tyz}

$$P_{ty} - \Delta P_{tyz}$$

P_{tz}

$$P_{tz}/(1 + .2M_z^2)^{3.5}$$

P_{zH}

Figure 21 — A_z

Figure 13 — T_{ty}

Iterative solution
for $M_z < 1.0$

$$\frac{M_z}{(1 + .2M_z^2)^3} = \frac{W_z \sqrt{T_{ty}}}{A_z P_{tz}} \sqrt{\frac{R}{\gamma_g}}$$

M_z

$$T_{ty}/(1 + .2M_z^2)$$

T_z

$$M_z \sqrt{\gamma_g R T_z}$$

U_z

Figure 13 — W_y

$$W_y - W_{bby}$$

W_z

Figure 25 — $\dfrac{dX}{dt}$

$$U_z - \frac{dX}{dt}$$

U_z'

Figure 15 — W_{bby}

$$W_z \frac{U_z'}{U_z}$$

W_z'

Figure 12 — W_x

$$W_x \frac{U_x'}{U_x}$$

W_x'

$$W_x' - W_z' - W_{bby}$$

$\dfrac{d\overline{W}_H}{dt}$

Figure 13 — $\dfrac{U_x'}{U_x}$

Initial Condition — $\overline{W}_{Hi}$

$$\overline{W}_{H_1} + \int_1^t \frac{dW_H}{dt}\, dt$$

$\overline{W}_H$

Figure 24. Started Phase Helmholtz Volume Properties

127

$$\frac{g}{\bar{W}_H}\left[A_z(P_{zH}-P_{zD})-\frac{d\bar{W}_H}{dt}\frac{1}{g}\frac{dX}{dt}\right]$$

$$\frac{d^2X}{dt^2}$$

Figure 24 — $\bar{W}_H$

Figure 21 — A_z

Figure 24 — P_{zH}

Figure 21 — P_{zD}

Figure 24 — $\frac{d\bar{W}_H}{dt}$

Initial Condition — $\left(\frac{dX}{dt}\right)_1$

Initial Condition — X_1

$$\left(\frac{dX}{dt}\right)_1+\int_1^t \frac{d^2X}{dt^2}\,dt$$

$$\frac{dX}{dt}$$

$$X_1+\int_1^t \frac{dX}{dt}\,dt$$

$$X$$

Figure 25. Started Phase Helmholtz Volume Acceleration
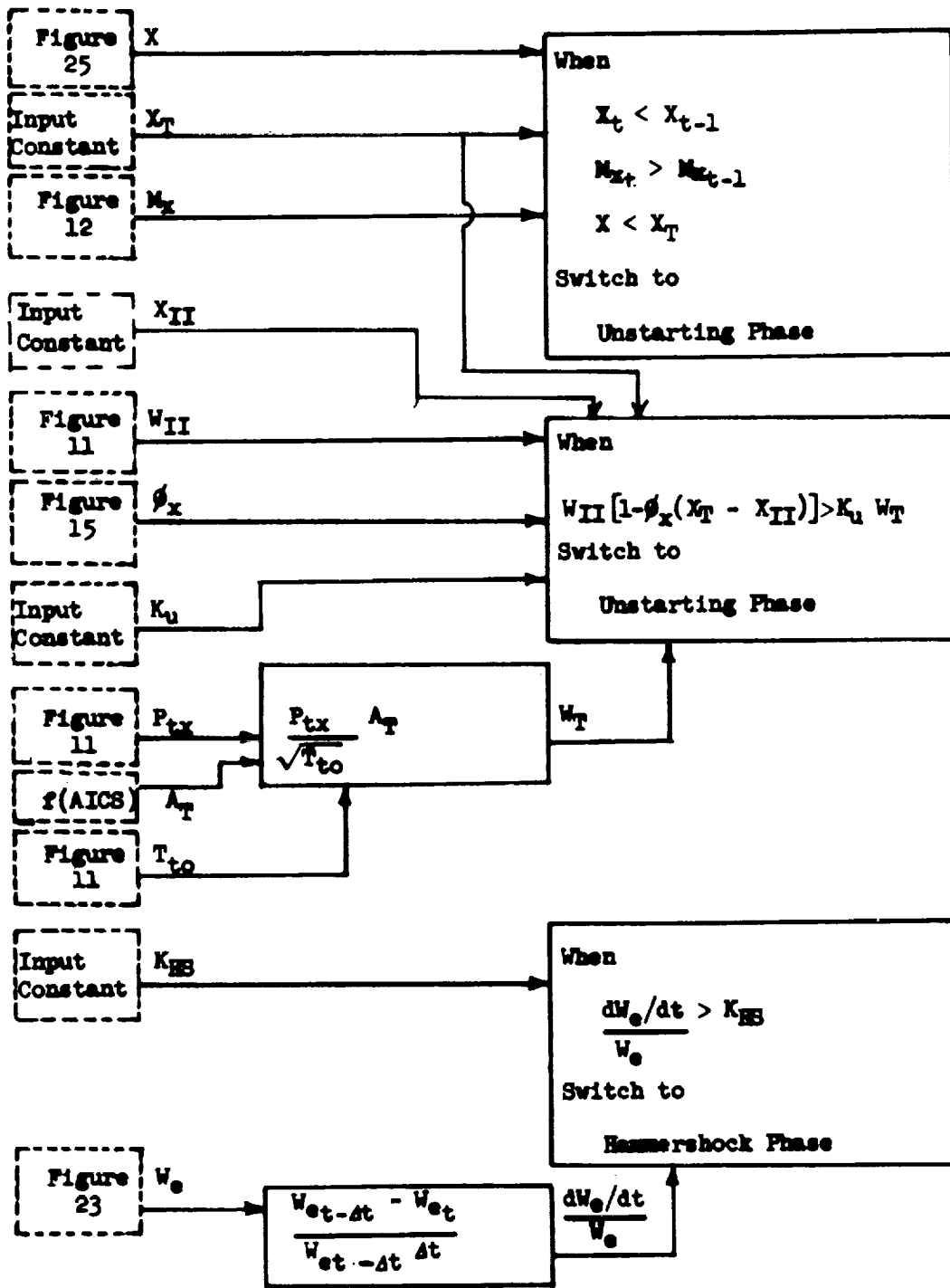
Figure 26. Started Phase Phase Switches
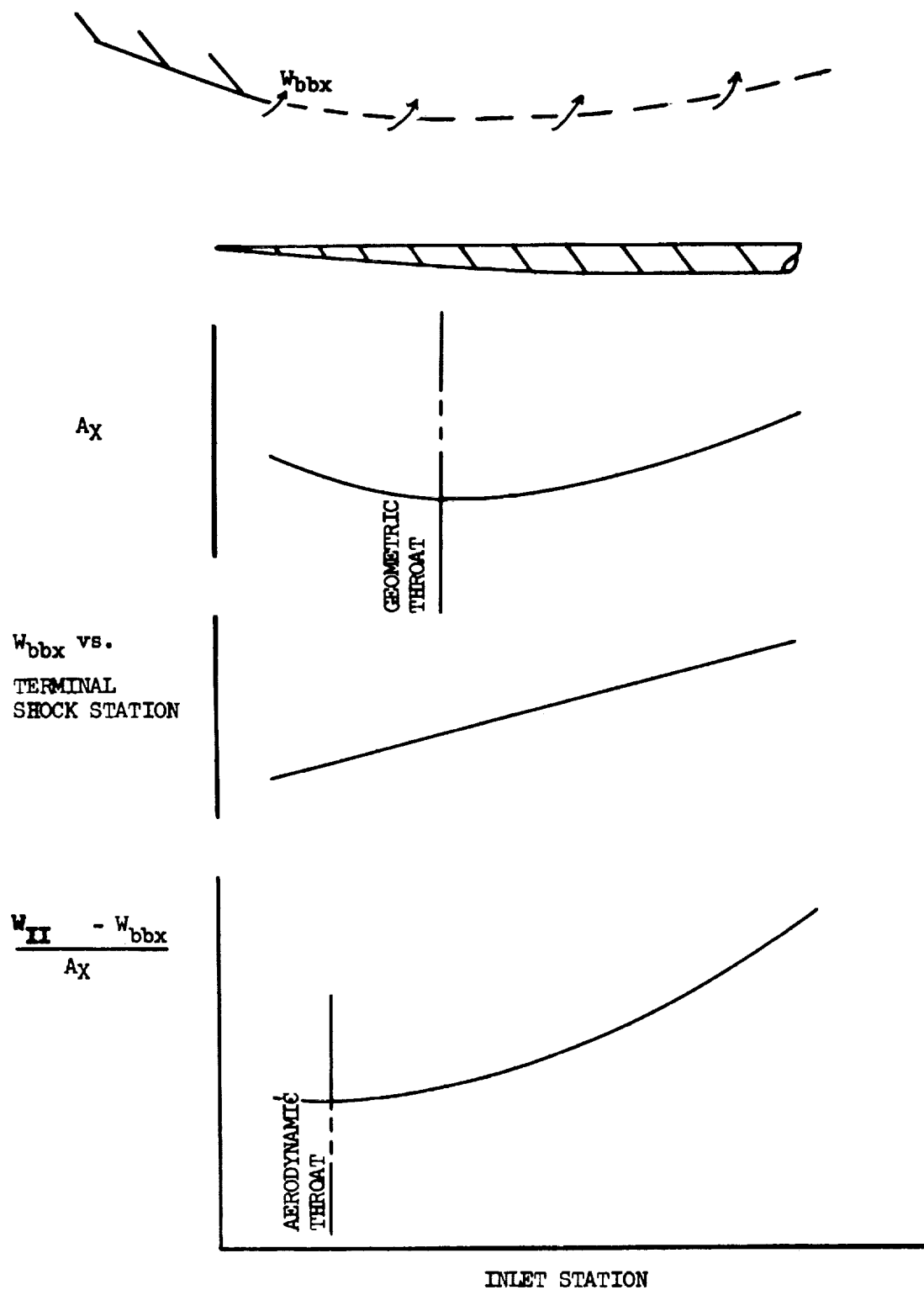
Figure 27. Started Phase Aerodynamic Throat
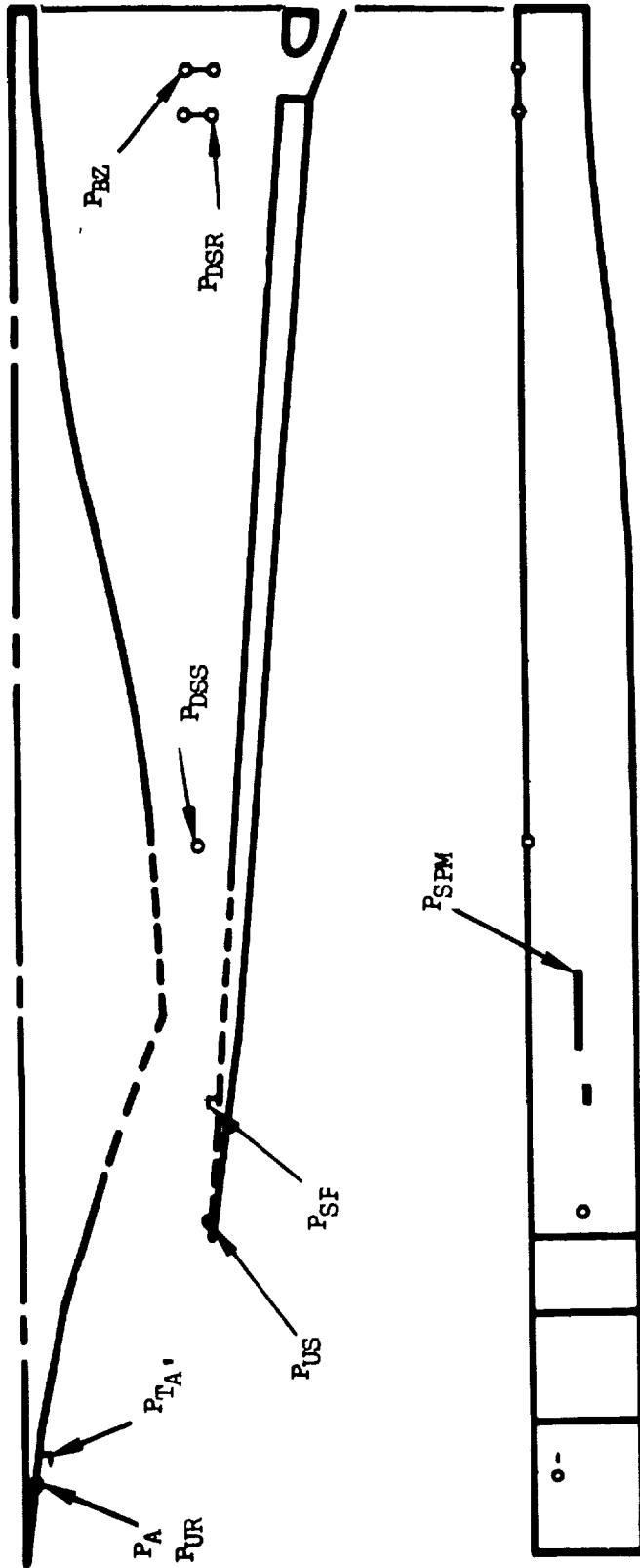
PARAMETER | DESCRIPTION
M_A = LOCAL MACH PARAMETER | = $f(P'_{TA}/P_A)$
USP = UNSTART PARAMETER | = P_{US}/P_{UR}
SPP = SHOCK POSITION PARAMETER | = P_{SPM}/P_{SPR}
BSP = BUZZ SIGNAL PARAMETER | = $\Delta P_{BZ}/P_{BZ}$
DSP = DOWNSTREAM SHOCK PARAMETER | = P_{DSS}/P_{DSR}

Figure 28. XB-70 Signals to the Air Induction Control System

131
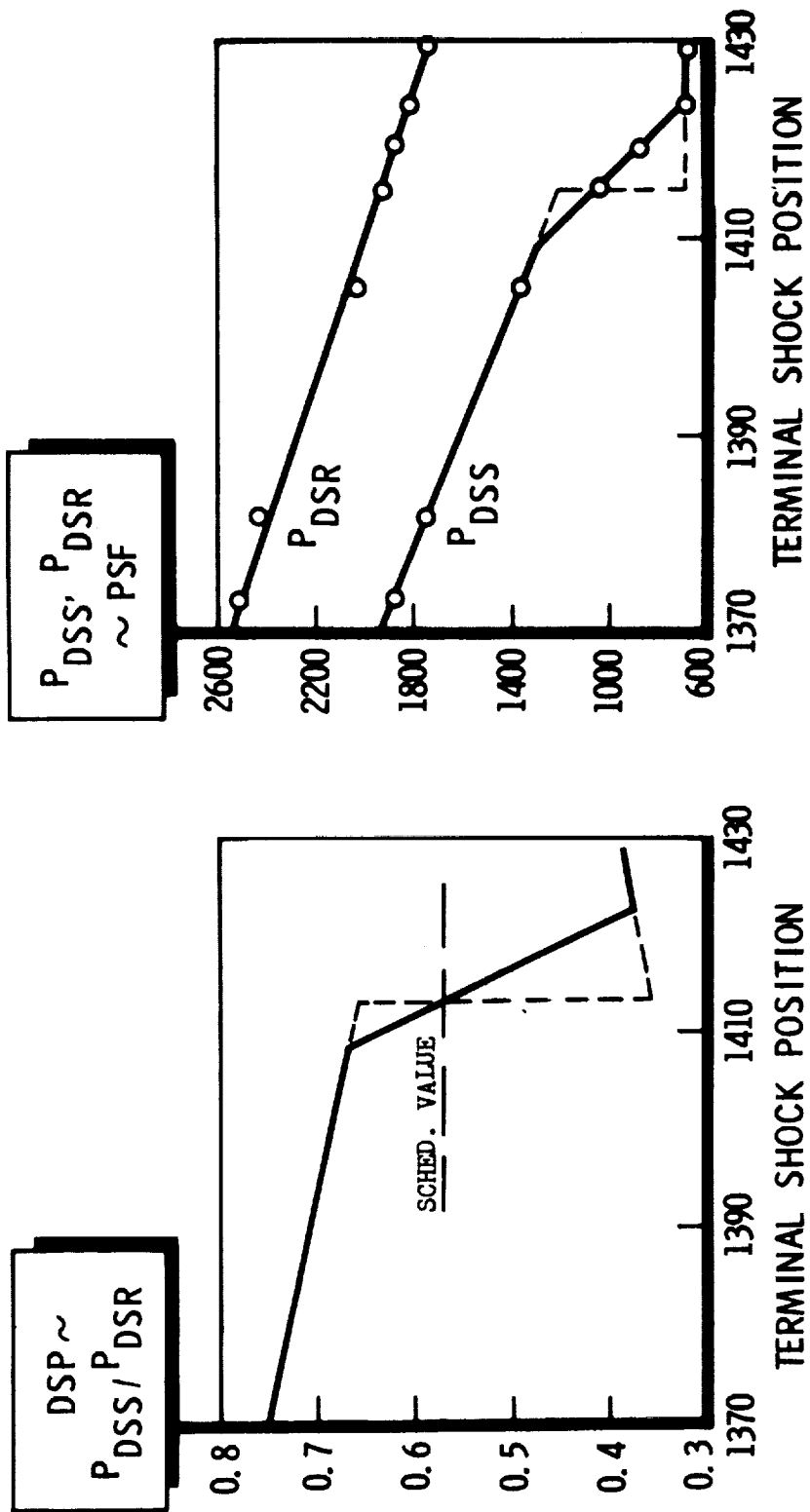
Figure 29. Started Phase DSP Signal Vs. Terminal Shock Position

132

$f(t)$ M_o

$f(t)$ α_o

$f(t)$ ψ_o

$f(M_o, \alpha_o, \psi_o)$ M_A

$f(t)$ P_o

$P_d - P_o$ $P_{OP} - P_o$

Figure 21 P_d

Input Constant X_{DSS}

Figure 12 P_x

Figure 13 P_y

Figure 25 X

$$\text{If}: \qquad DSP =$$
$$X \leq X_{DSS} \qquad \frac{P_y}{P_d}$$
$$X > X_{DSS} \qquad \frac{P_x}{P_d}$$

DSP

$f(AICS)$ A_T

Figure 11 W_{II}

Figure 11 T_{to}

Figure 11 P_{tx}

$$f\left(X, A_T, \frac{W_{II}\sqrt{T_{to}}}{A_T P_{tx}}\right)$$

SPP
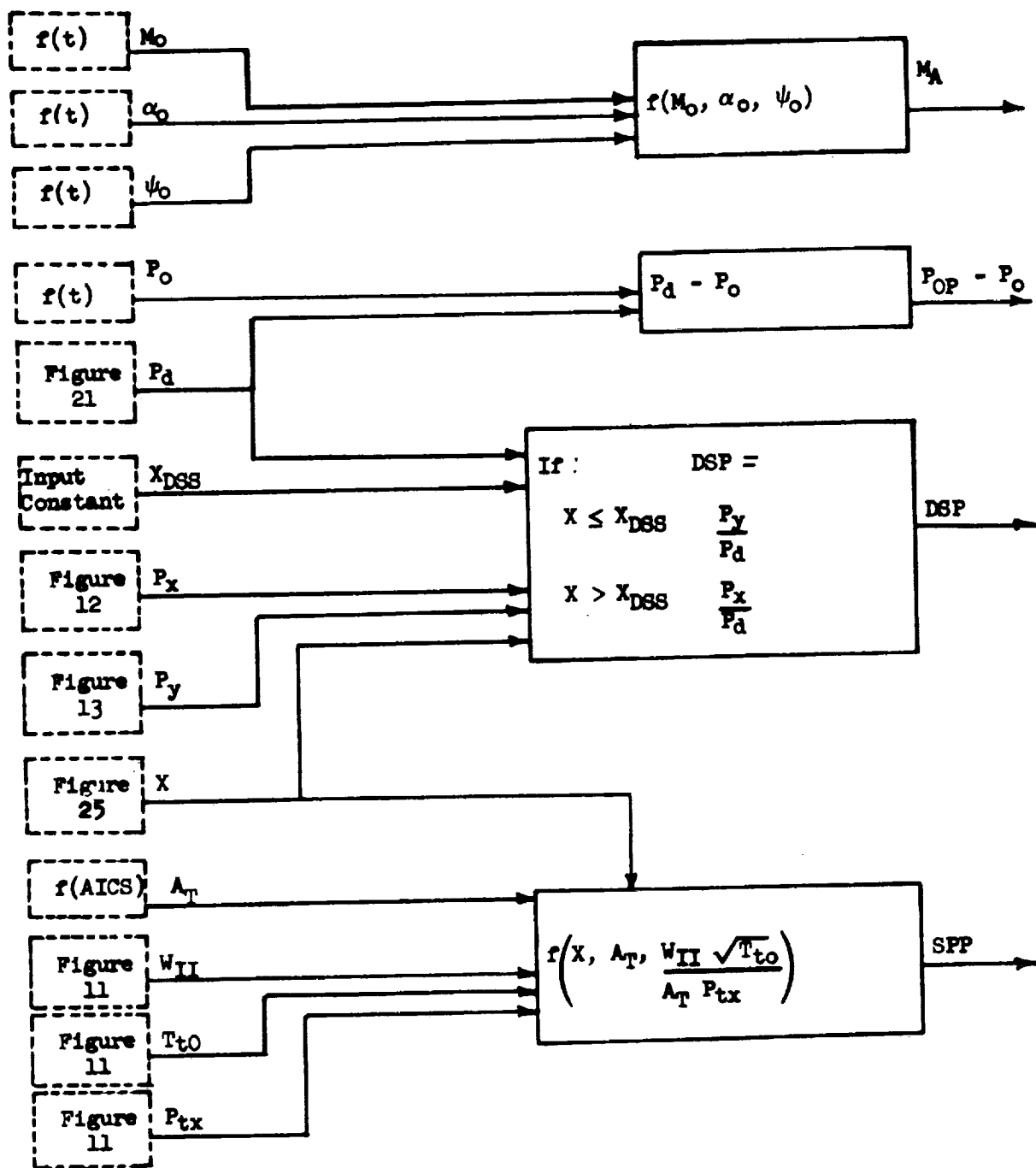
Figure 30. Started Phase Outputs to the Air Induction Control System
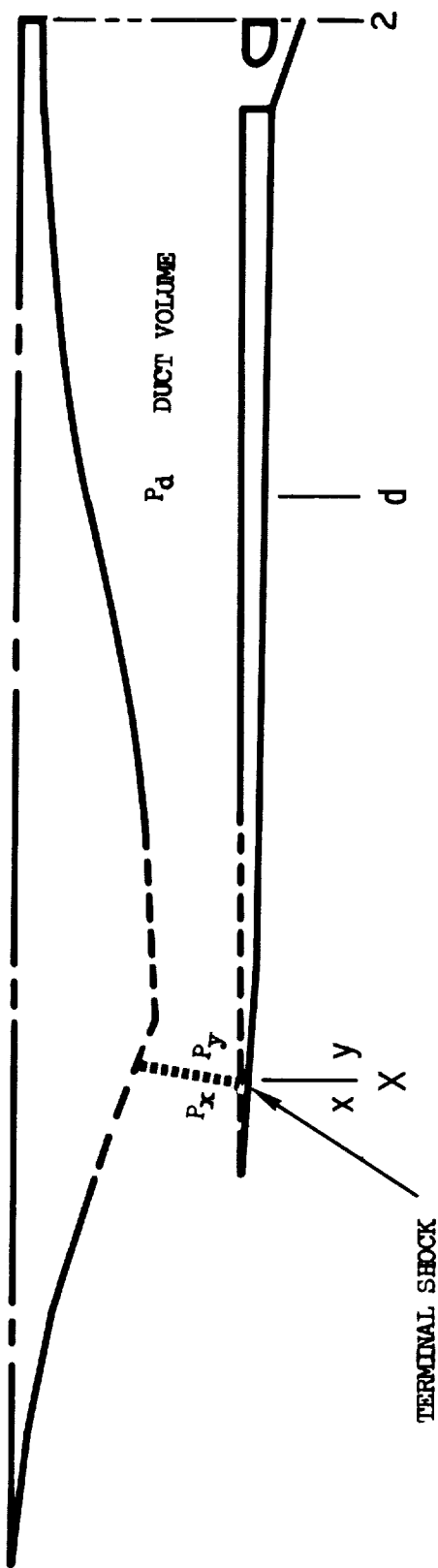
Figure 31. Insufficient Demand – Induced Unstarting Phase Simulation Model

134

UPSTREAM NORMAL SHOCK (forms just forward of throat and moves upstream)

UPSTREAM VOLUME (P_u)

TERMINAL SHOCK

P_{xu} P_{yu}

X_u

X_T

$M_T = 1$
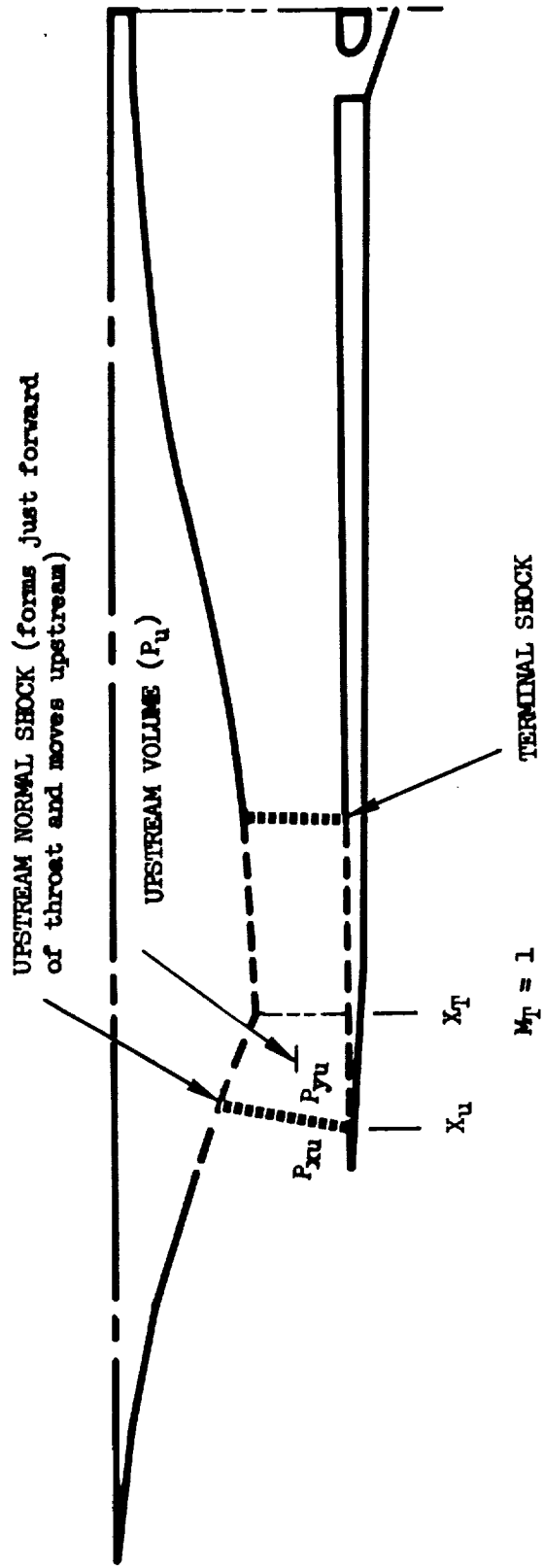
Figure 32. Choked Throat - Induced Unstarting Phase Simulation Model
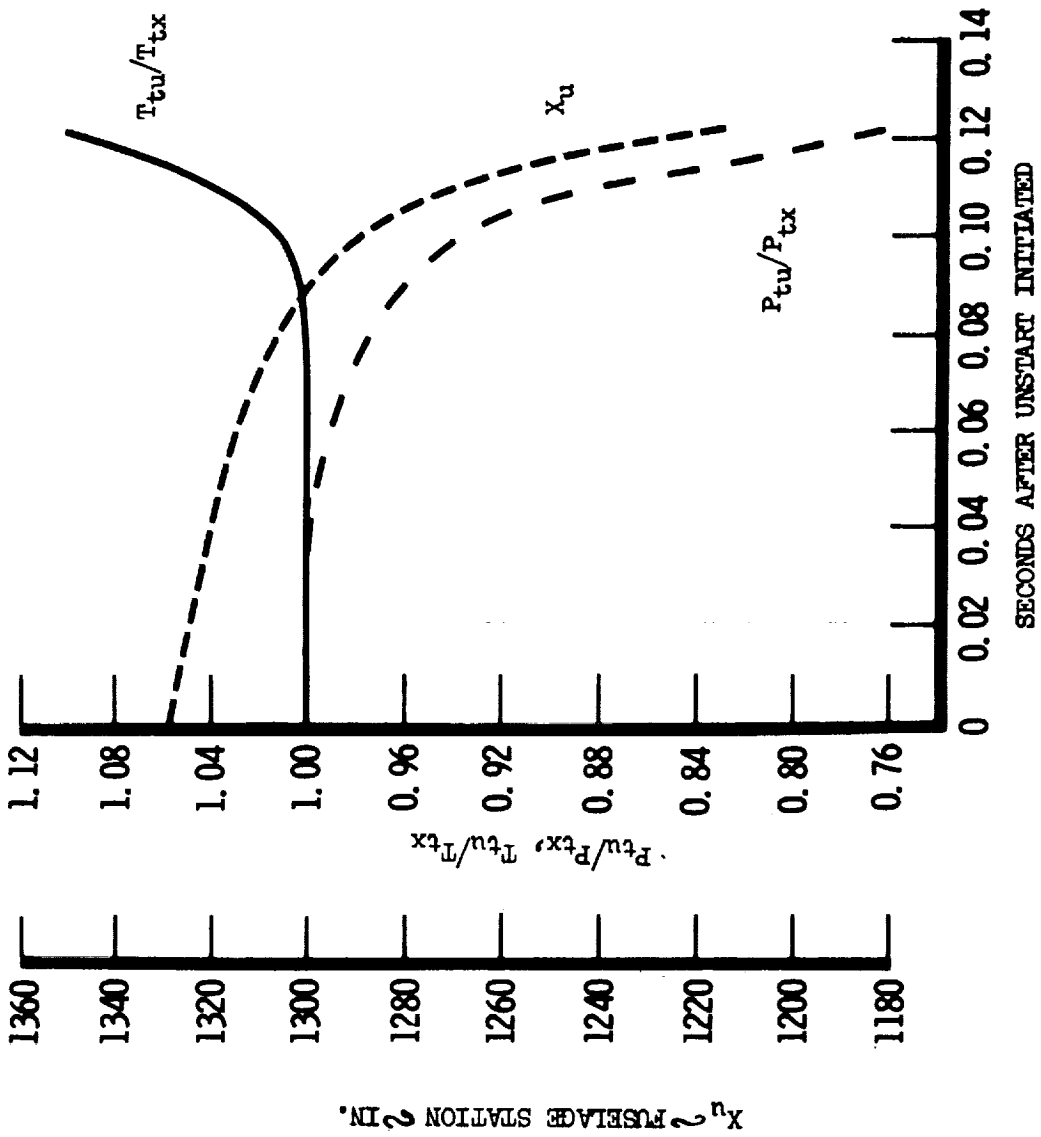
Figure 33. Choked Throat – Induced Unstart, P_{tu}/P_{tx}, T_{tu}/T_{tx}, and X_u Versus Time

136

Figure 34. Unstarting Phase Simulation Model

137

$f(AICS)$

Inlet Geo,

$f(M_o, \alpha_o, \psi_o, I.G.)$ → M_A

$f(t)$ ψ_o

$f(M_o, \alpha_o, \psi_o, I.G.)$ → P_{tx}/P_{to} → $\dfrac{P_{tx}}{P_{to}} P_{to}$ → P_{txu}

$f(t)$ α_o

$f(t)$ M_o

$f(M_o, \alpha_o, \psi_o, I.G.)$ → $\dfrac{W_{II}}{W_o}$ → $\dfrac{W_{II}}{W_o} W_o$ → W_{II}

$f(t)$ P_o

$P_o\left(1 + \dfrac{\gamma - 1}{2} M_o^2\right)^{\frac{\gamma}{\gamma - 1}}$ P_{to}

Input Constant A_c

$\dfrac{P_o A_c}{\sqrt{T_o}} M_o \sqrt{\dfrac{\gamma g}{R}}$ W_o

$f(t)$ T_o

$T_o\left(1 + \dfrac{\gamma - 1}{2} M_o^2\right)$ T_{to}, T_{txu}
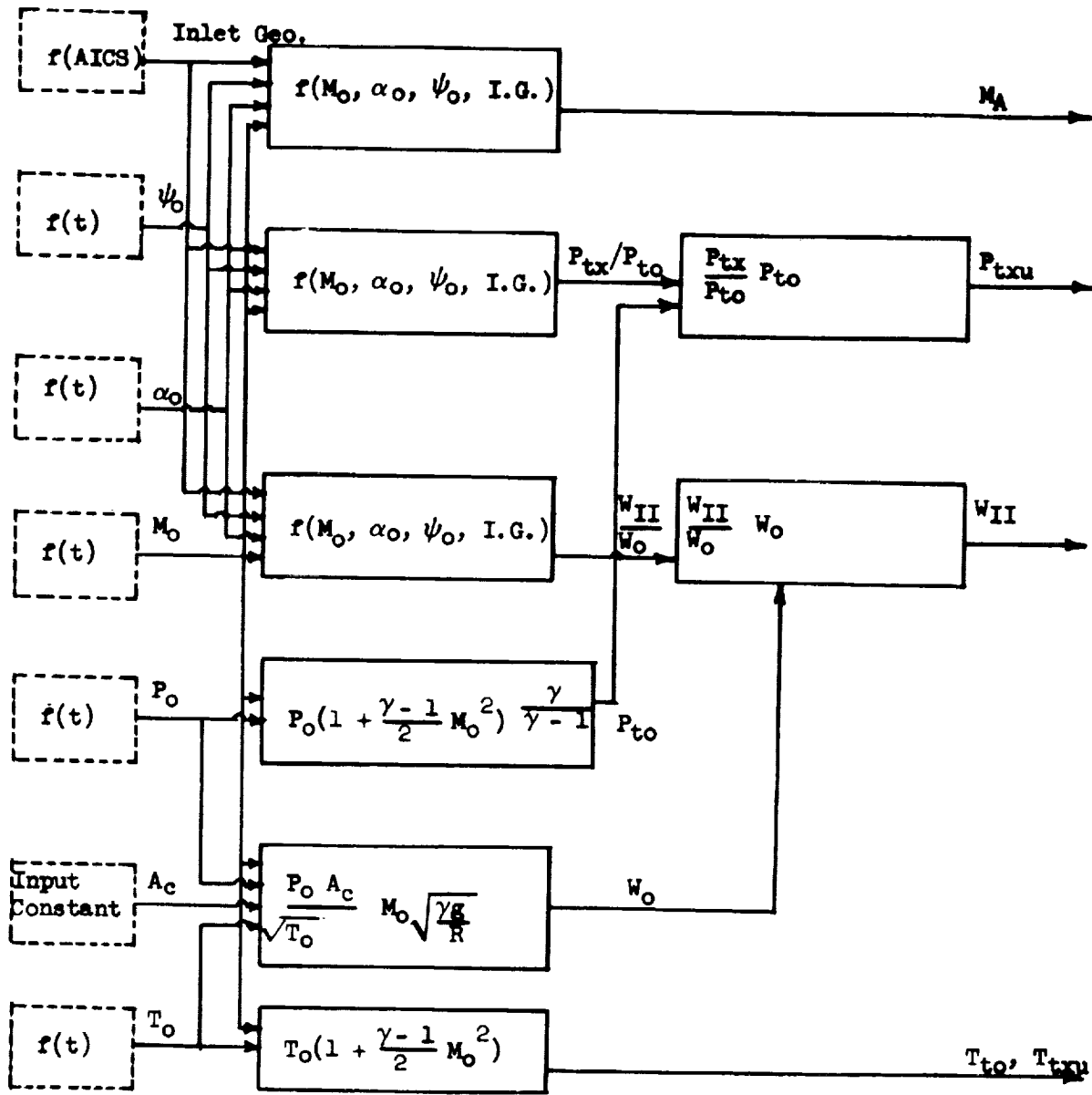
Figure 35. Unstarting Phase Upstream Properties for the Upstream Volume

138

Figure 35 P_{txu}

$$P_{txu}(1 + .2M_{xu}^2)^{-3.5} \quad P_{xu}$$

Figure 35 W_{II} $W_{II} + \Delta W_{bbx}$ W_{xu}

$$\left(\frac{7M_{xu}^2 - 1}{6}\right)P_{xu} \quad P_{yu}$$

Figure 40 ΔW_{bbx}

Iterative
Solution of: $M_{xu} > 1.0$

$$\frac{M_{xu}}{(1 + .2M_{xu}^2)^3} = \frac{W_{xu}\sqrt{T_{to}}}{P_{txu}A_{xu}}\sqrt{\frac{R}{\gamma_g}} \quad M_{xu}$$

Figure 35 T_{to}

$$T_{to}(1 + .2M_{xu}^2)^{-1} \quad T_{xu}$$

A_{xu}

Figure 44 X_u $f(X_u, A_T)$

$$\sqrt{\gamma_g R T_{xu}} \quad a_{xu}$$

$f(AICS)$ A_T
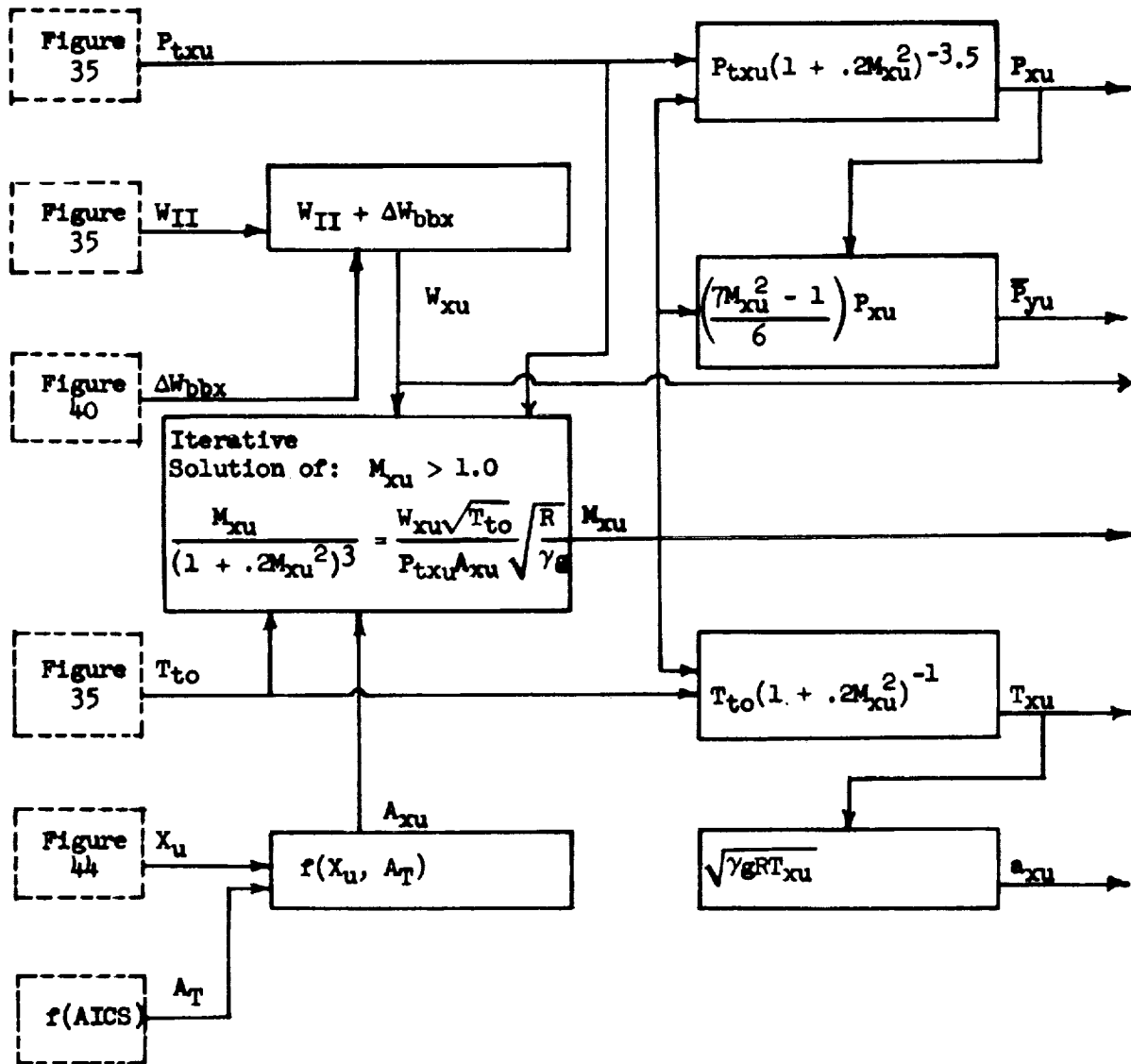
Figure 36. Unstarting Phase Properties Forward of the Upstream Normal Shock

BLEED FLOW IN THIS ZONE INDEPENDENT OF TERMINAL SHOCK POSITION DURING STARTED OPERATION

BLEED FLOW IN THIS ZONE VARIES WITH TERMINAL SHOCK POSITION DURING STARTED OPERATION

NO BLEED PAST THIS POINT

X_I X_u X_{II} X_{III}

W_1 ΔW_{bbx} W_{xu} W_{II}

NORMAL SHOCK AT X_{III}

X_{II}

X_u

X_I

DUCT FLOW

NORMAL SHOCK AT

X_I

X_u

X_{II}

X_{III}

CUMULATIVE BLEED FLOW

ΔW_{bbx}

X_I X_u X_{II} X_{III}

INLET STATION
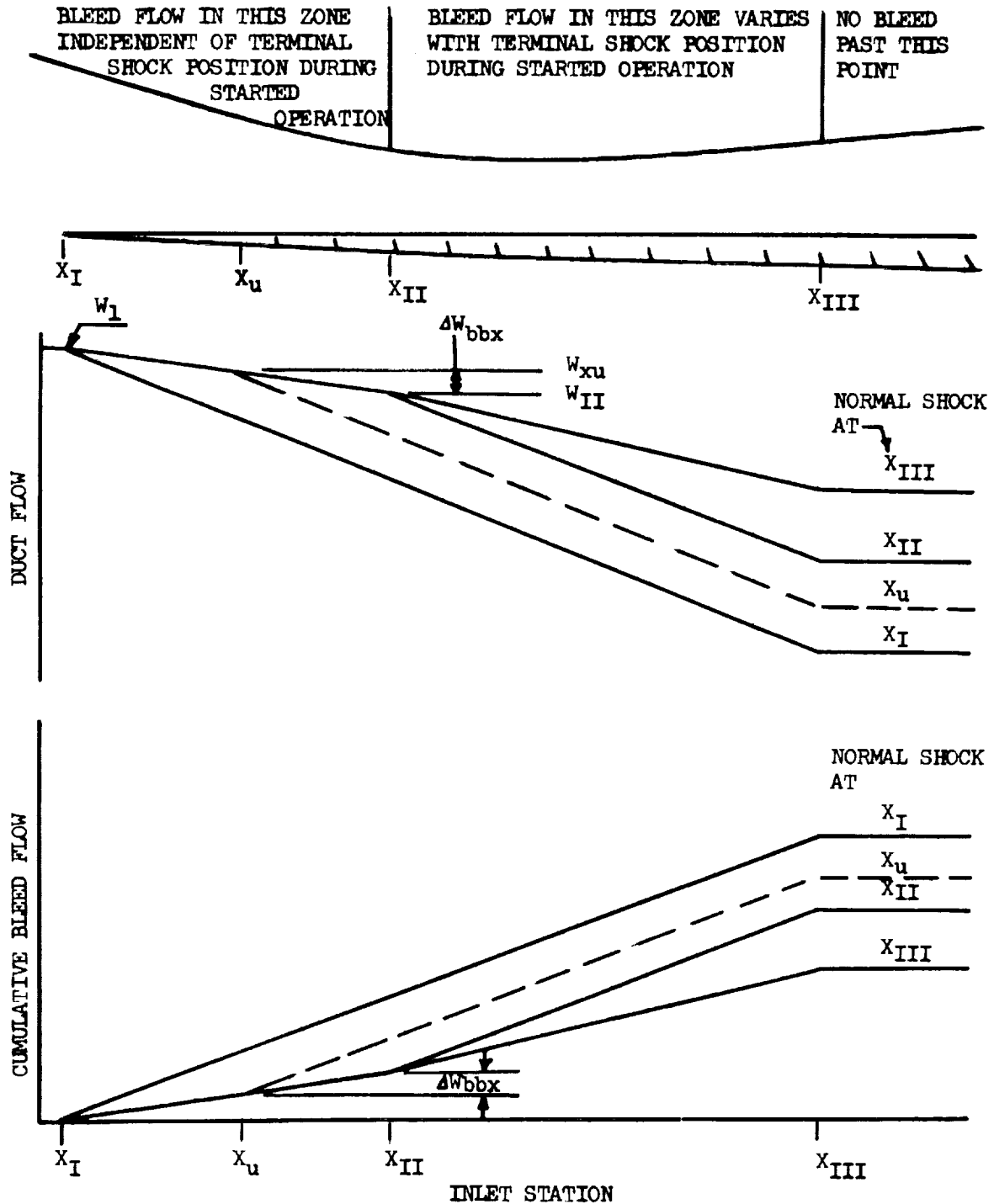
Figure 37. Duct & Cumulative Bleed Flows During Started & Unstarting Phases

Figure 36 | M_{xu}

$\dfrac{M'_{xu}}{M_{xu}}$ | U'_{xu}/U_{xu}

Figure 36 | a_{xu}

$M_{xu} - \dfrac{dXu/dt}{a_{xu}}$ | M'_{xu}

$T_{yu}(1 + .2M_{yu}^2)$ | T_{tyu}

Figure 36 | T_{xu}

$\dfrac{(M'^2_{xu} + 5)(7M'_{xu} - 1)}{36\, M'^2_{xu}} T_{xu}$ | T_{yu} | T_{yu}

Figure 44 | $\dfrac{dXu}{dt}$

$\sqrt{\dfrac{M^2_{xu} + 5}{7M^2_{xu} - 1}}$ | M_{yu}

$M'_{yu} + \dfrac{dXu/dt}{\sqrt{\gamma g R T_{yu}}}$ | M_{yu}

Figure 36 | P_{xu}

$\left(\dfrac{7M'^2_{xu} - 1}{6}\right) P_{xu}$ | P_{yu}
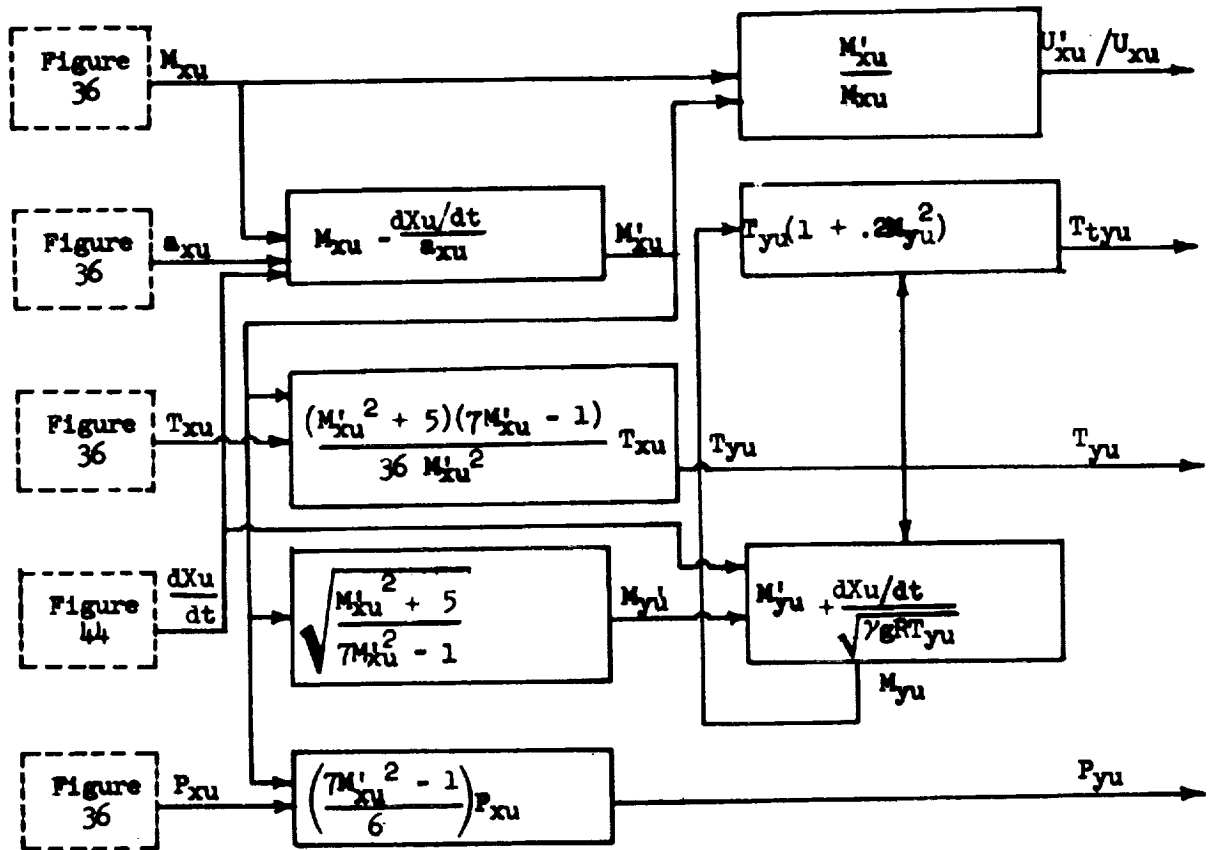
Figure 38. Unstarting Phase Properties Behind the Upstream Normal Shock

141
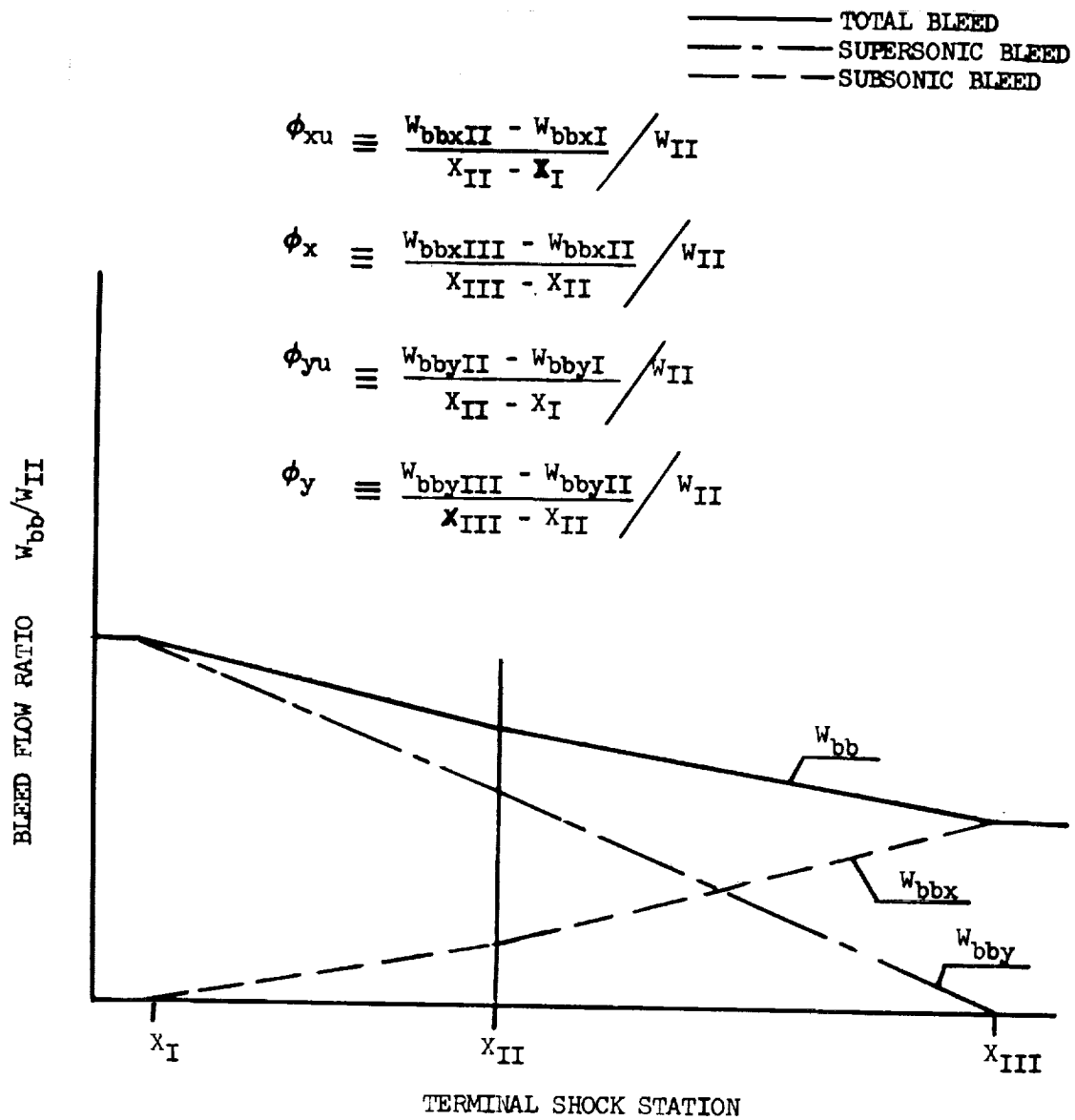
Figure 40. Unstarting Phase Bleed Flows in the Upstream Volume

143
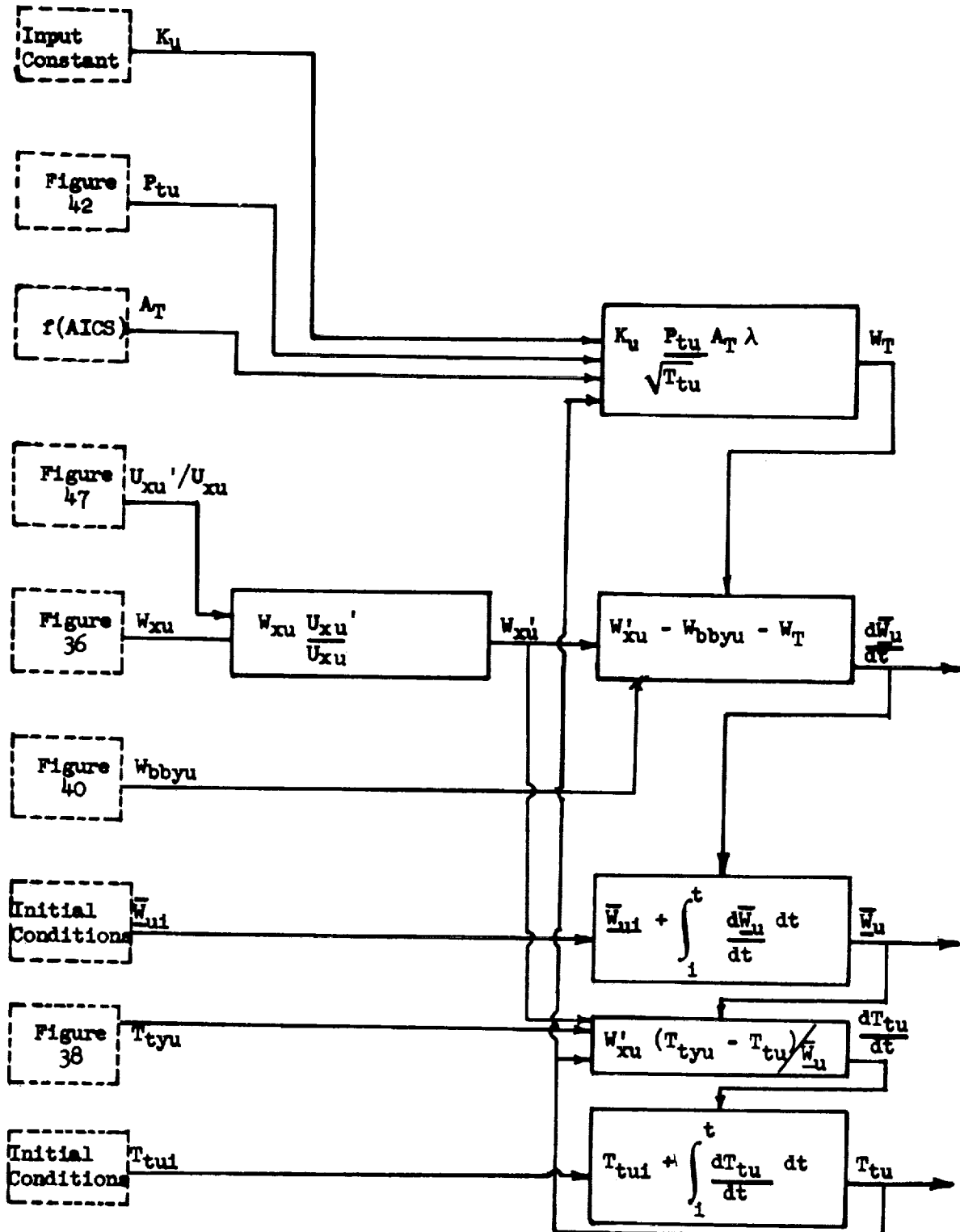
Figure 41. Unstarting Phase Upstream Volume Mass & Total Temperature
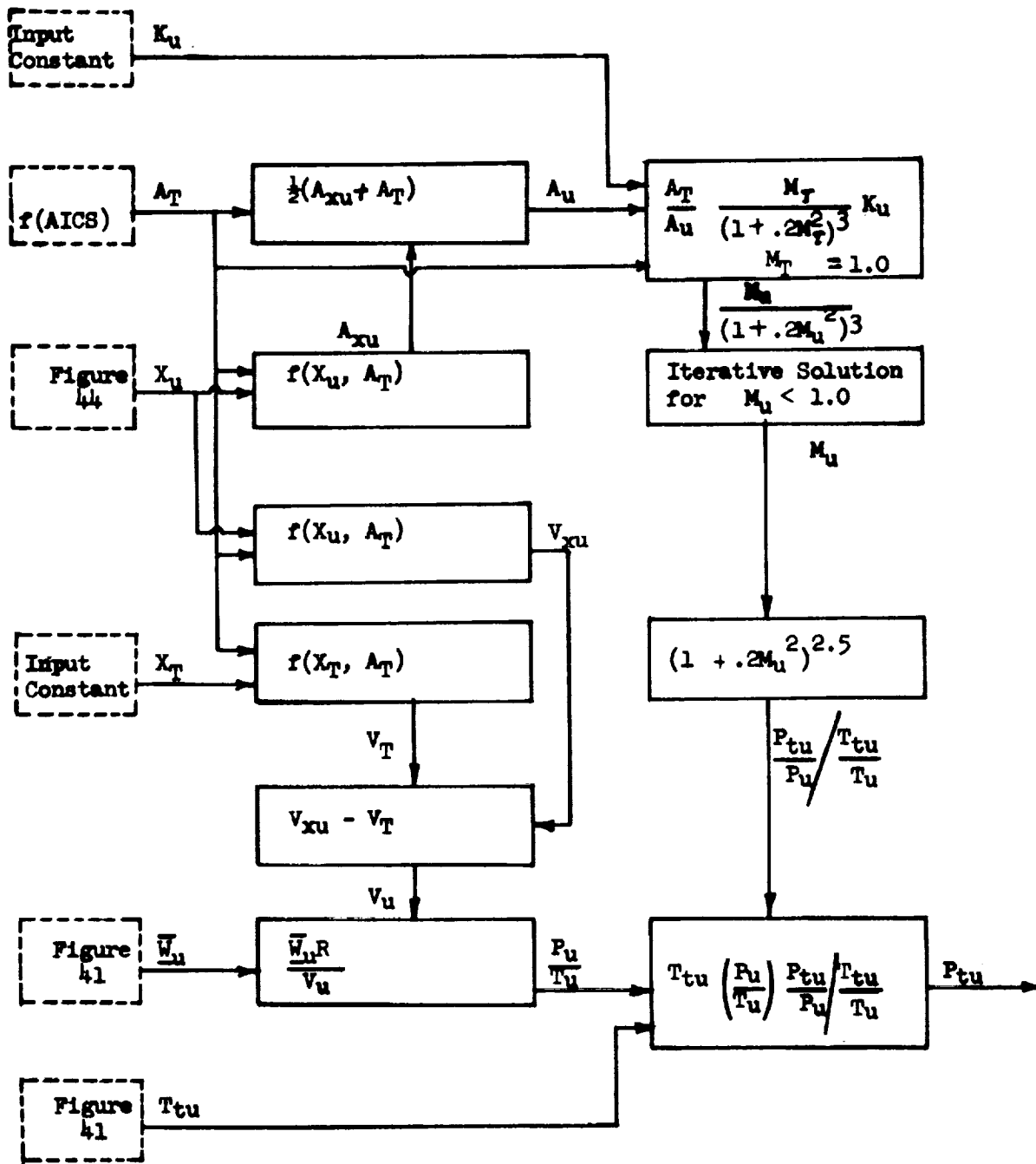
Figure 42. Unstarting Phase Upstream Volume Total Pressure
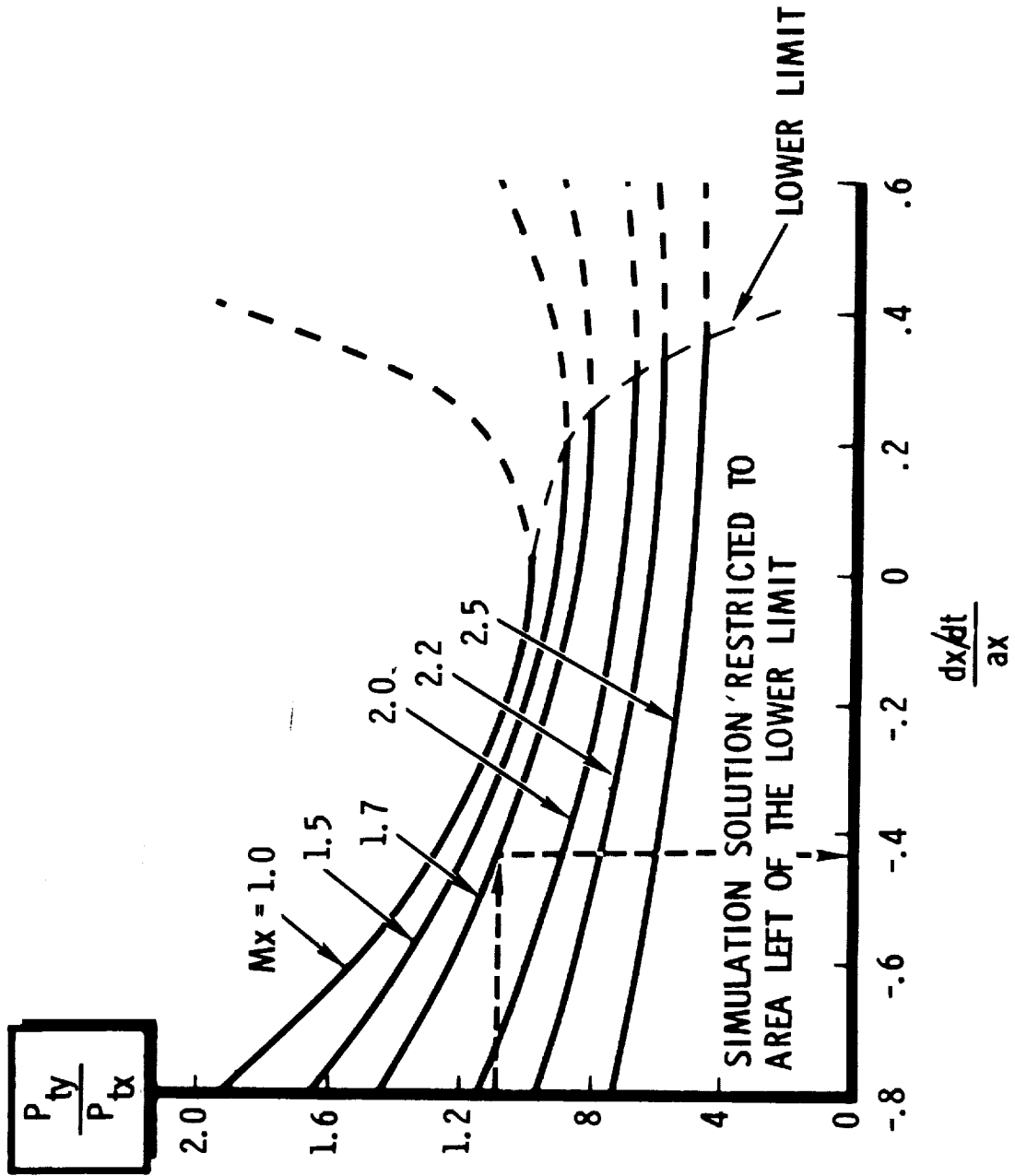
Figure 43. Unstarting Phase Variation of Shock Pressure Ratio With Shock Mach Number

146
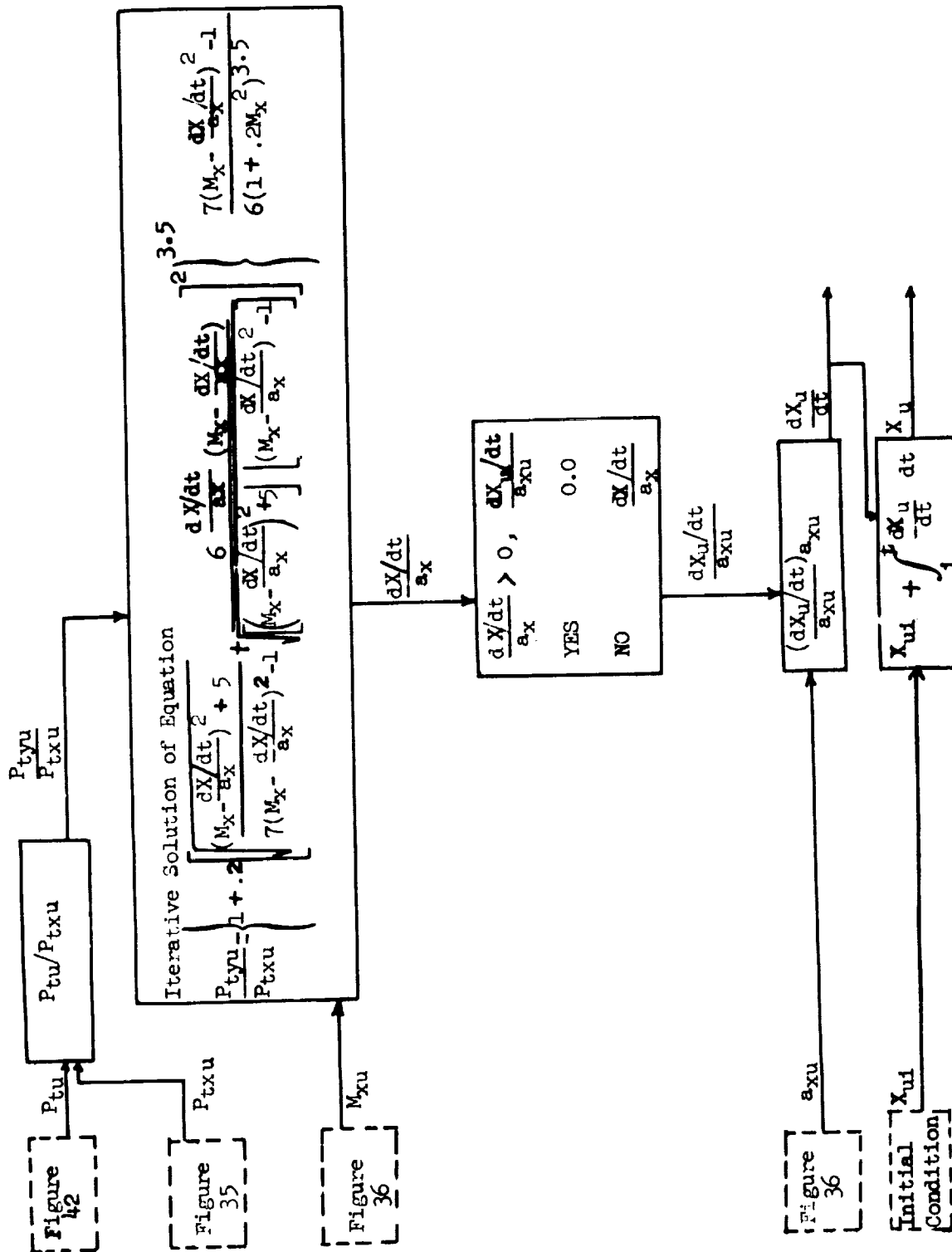
Figure 44. Unstarting Phase Upstream Normal Shock Velocity & Position

147
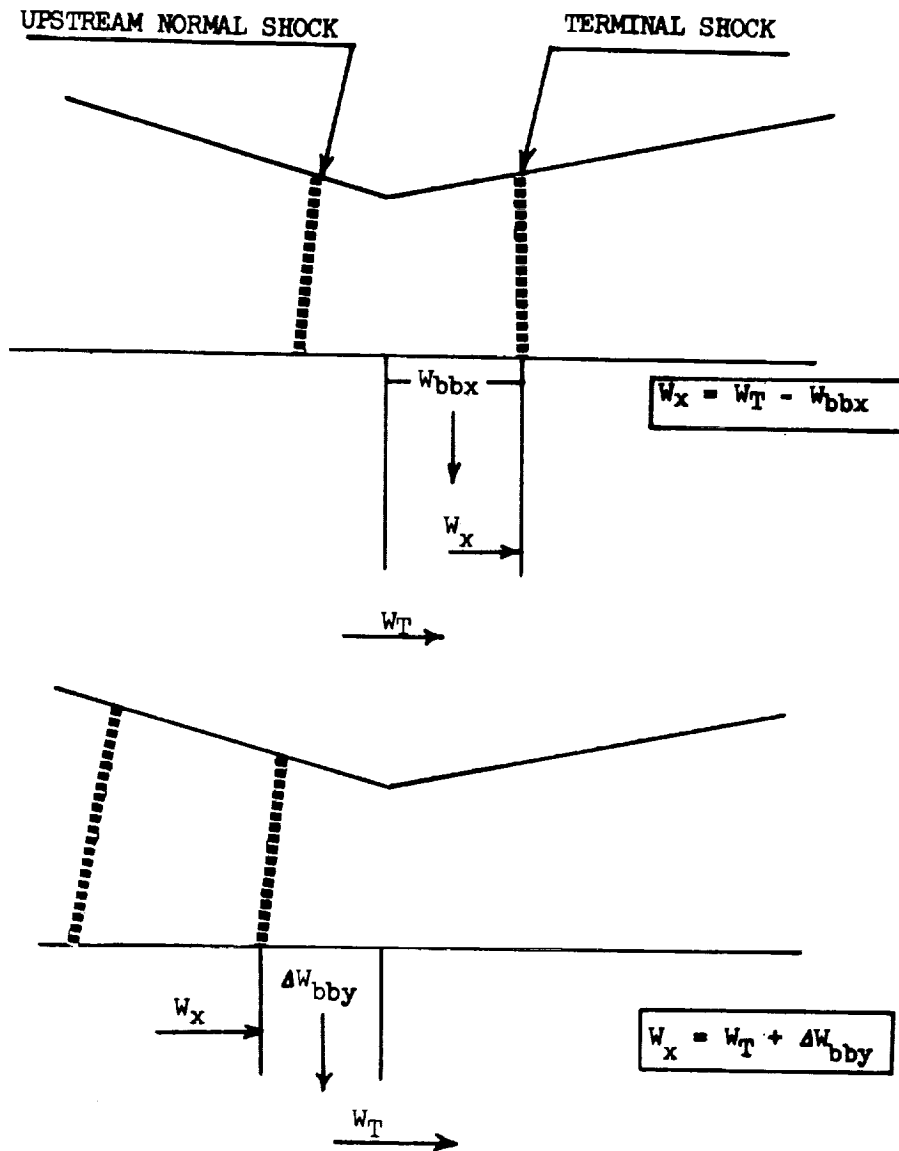
Figure 45. Unstarting Phase W_x During Choked Throat Unstarting
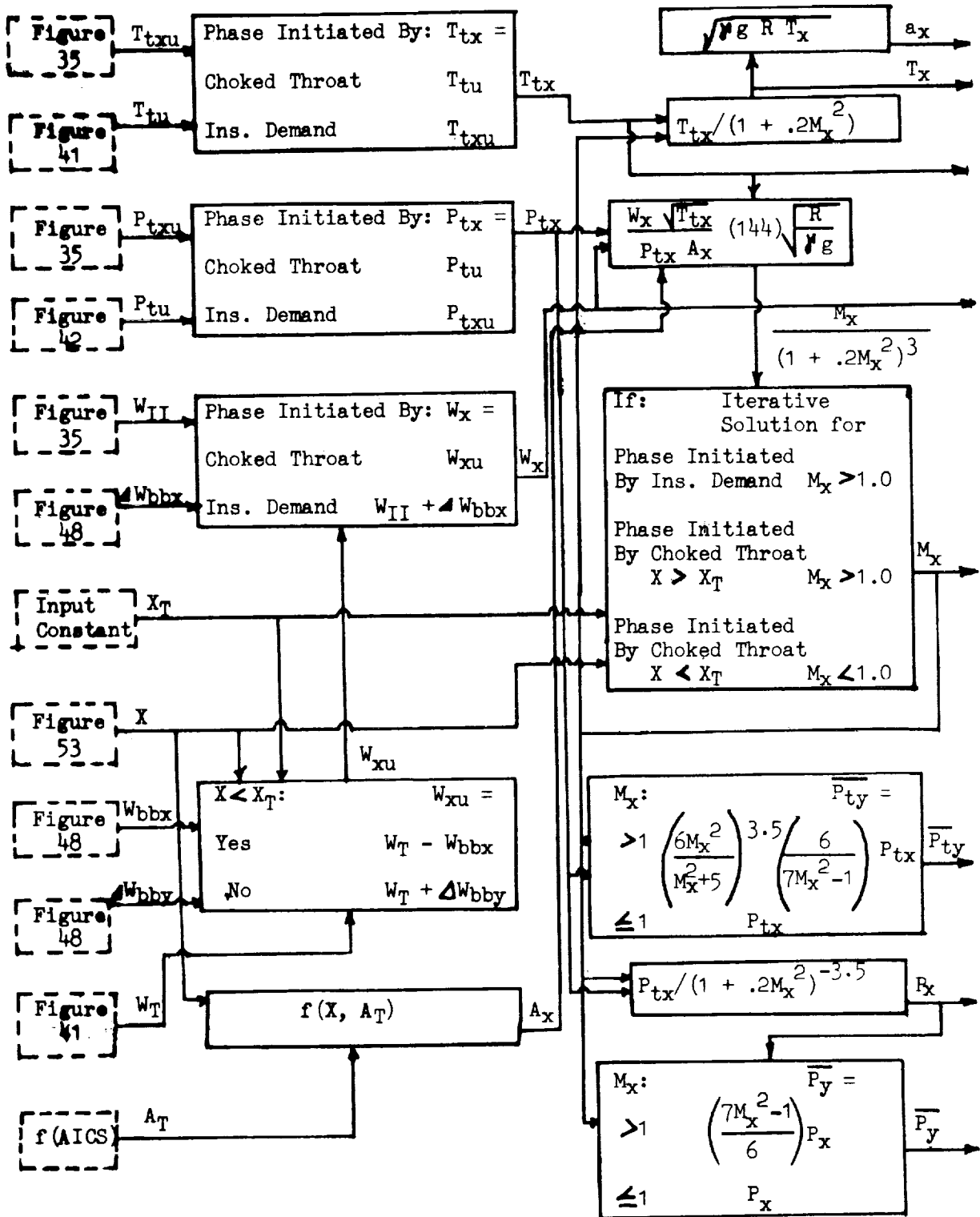
Figure 46. Unstarting Phase Properties at the Terminal Shock Station
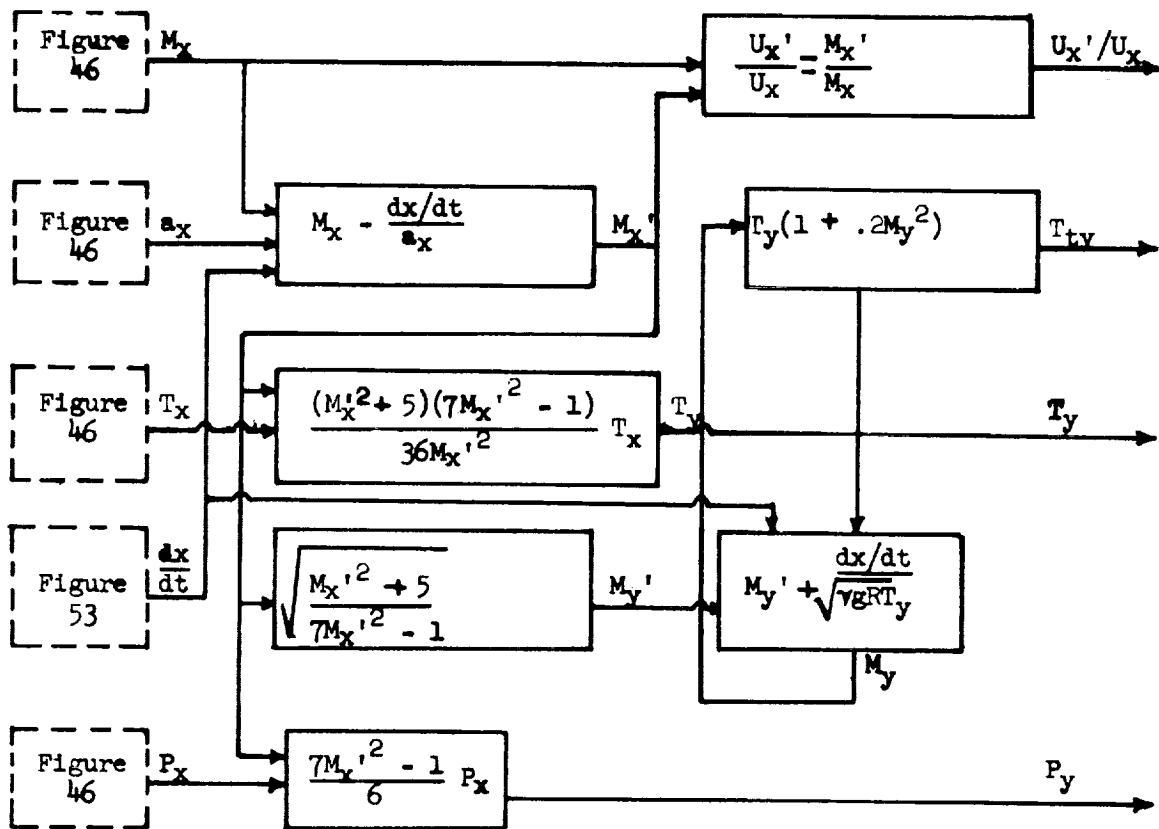
Figure 47. Unstarting Phase Properties Behind the Terminal Shock
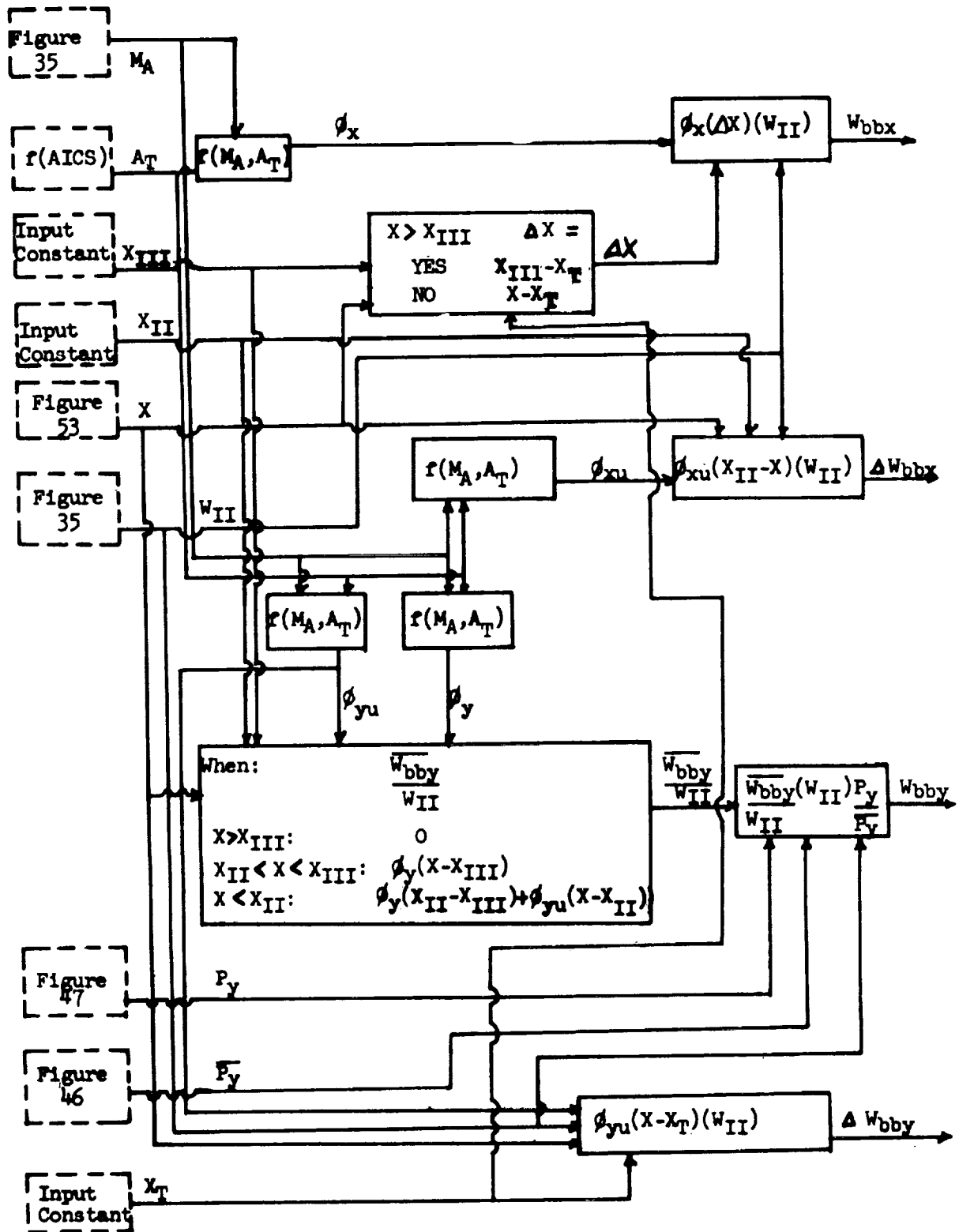
Figure 48. Bleed Flows for the Duct Volume
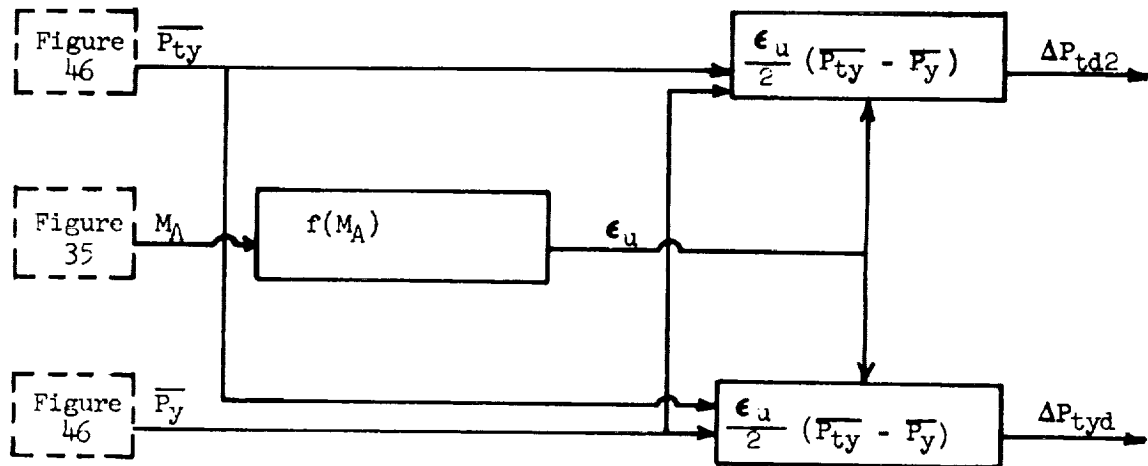
Figure 49. Unstarting Phase Duct Volume Total Pressure Losses
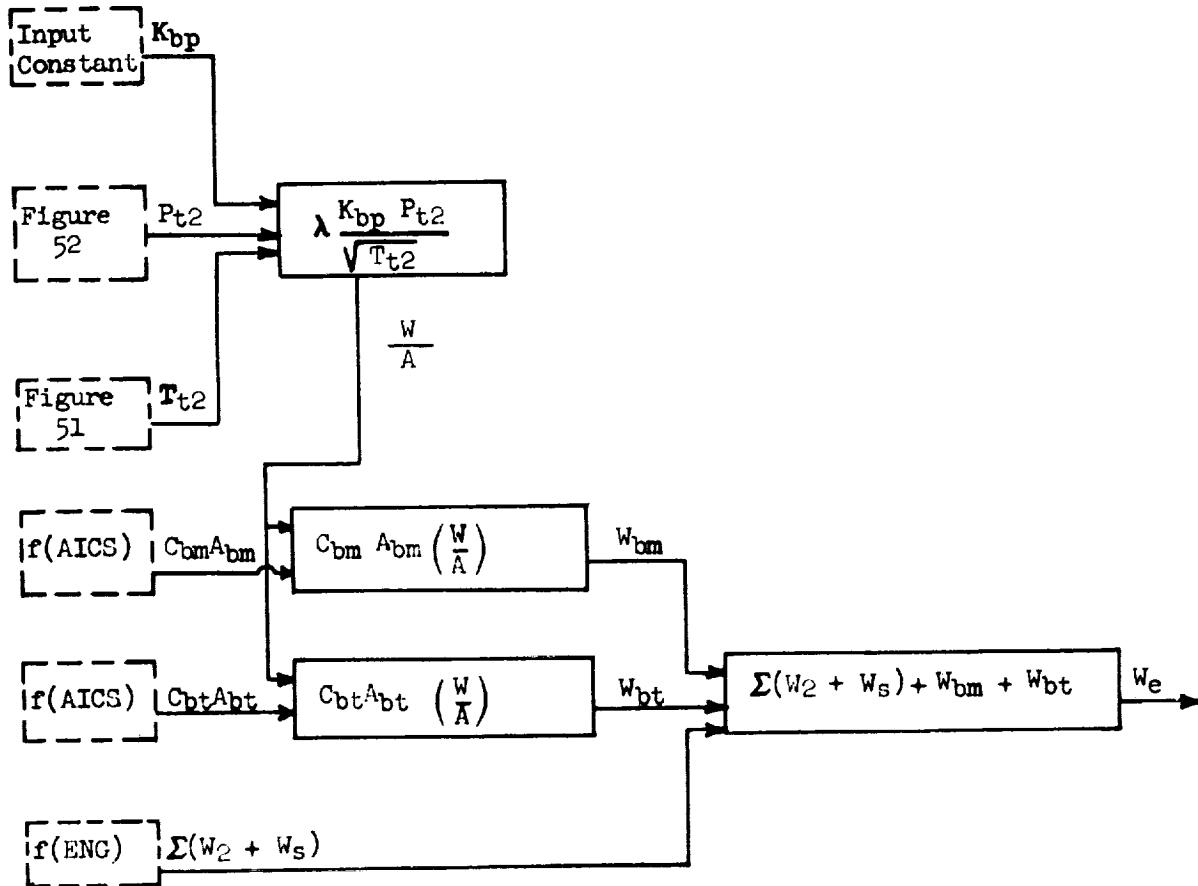
Figure 50. Unstarting Phase Bypass and Engine System Airflows
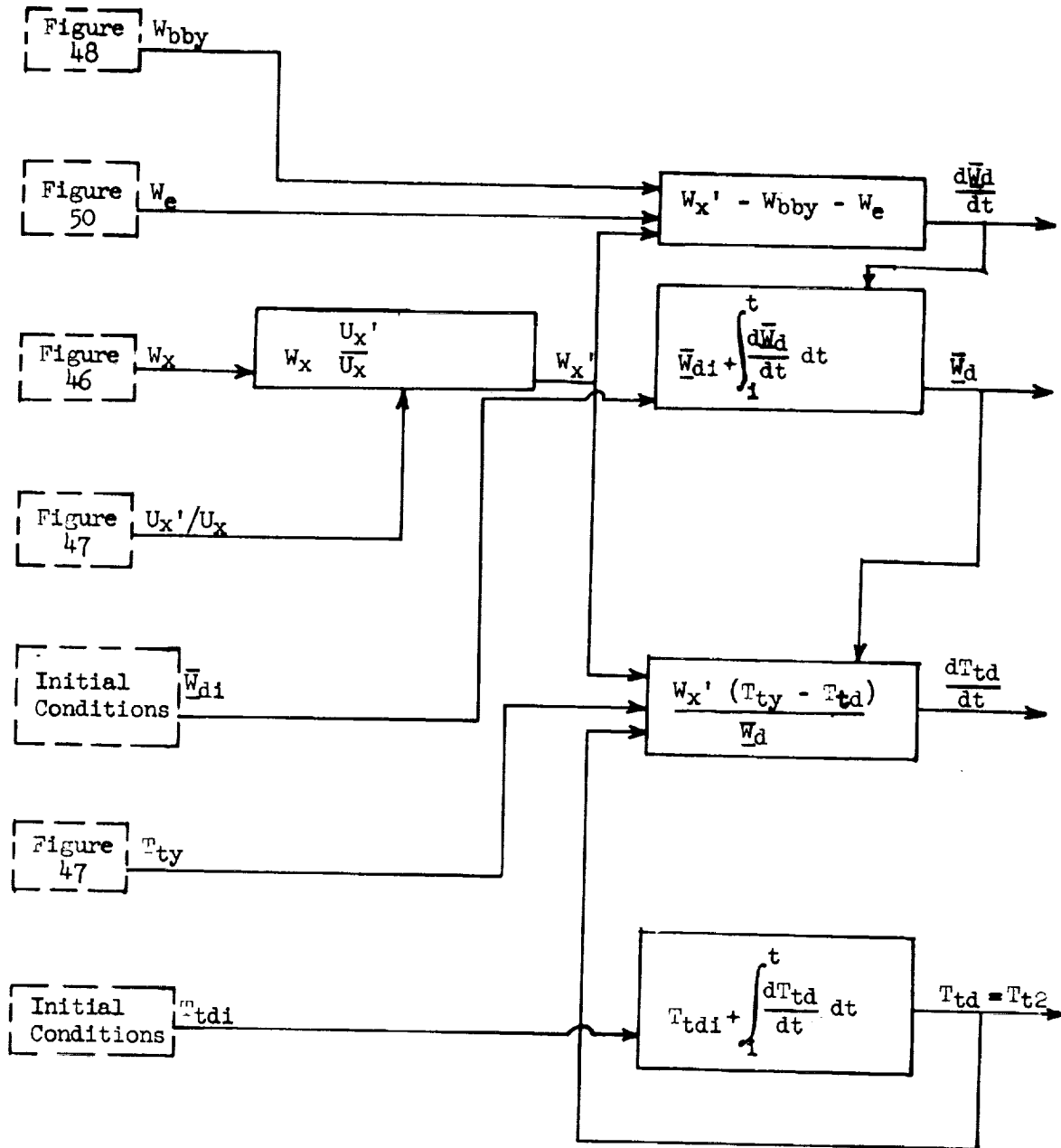
Figure 51. Unstarting Phase Duct Volume Mass and Total Temperature
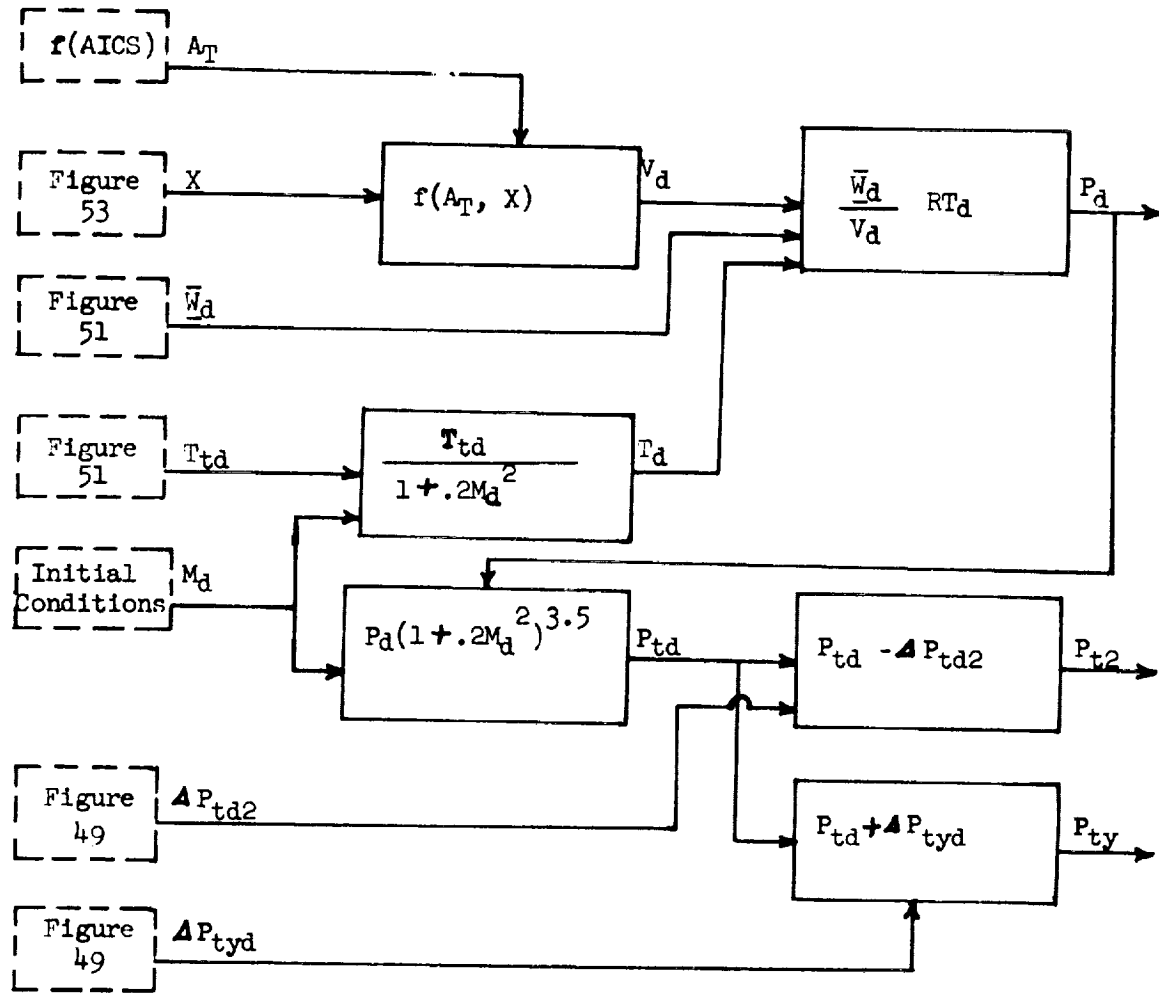
Figure 52. Unstarting Phase Duct Volume Total Pressure
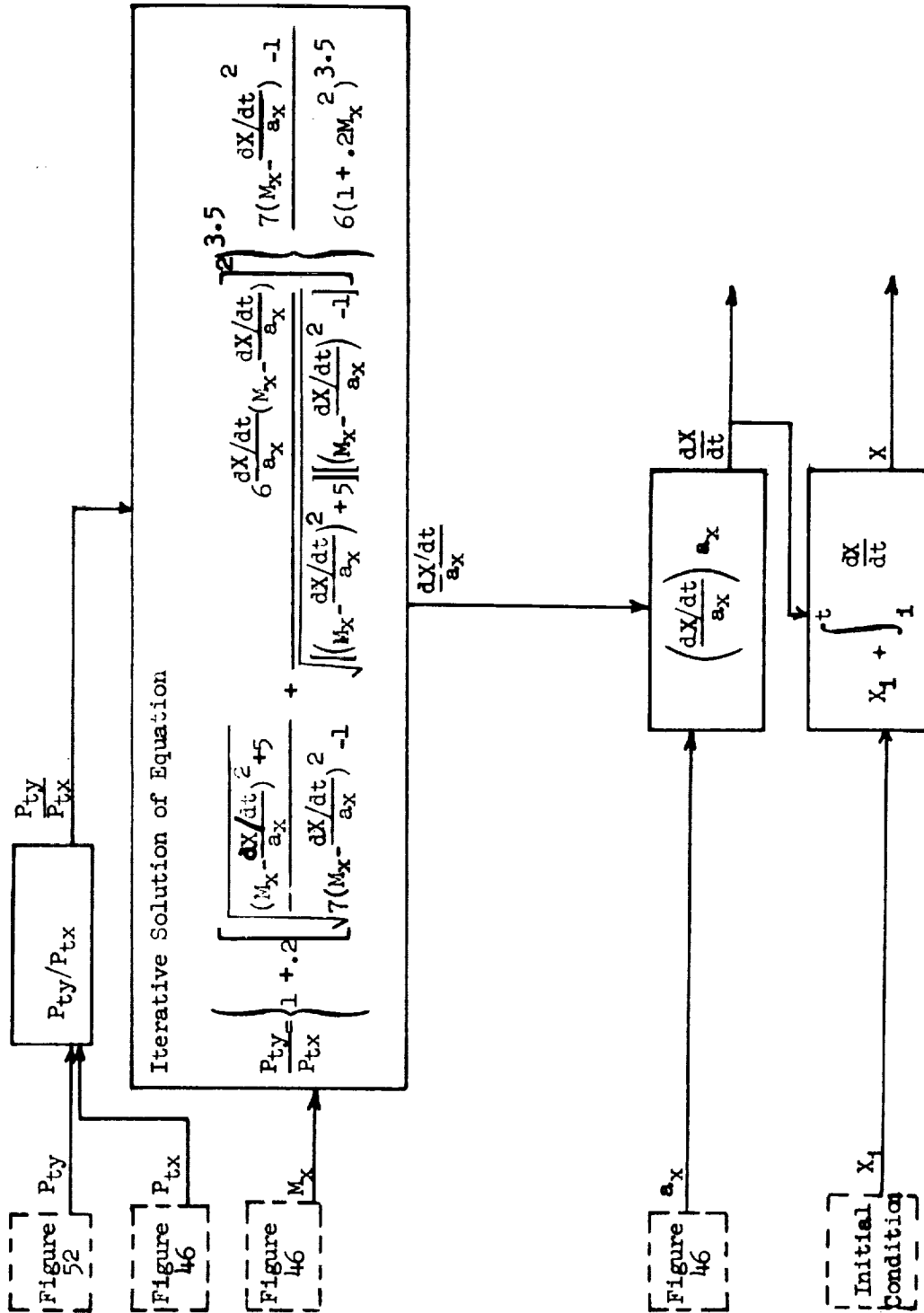
Figure 53. Unstarting Phase Terminal Shock Velocity and Position

Figure 54. Unstarting Phase Phase Switching Logic
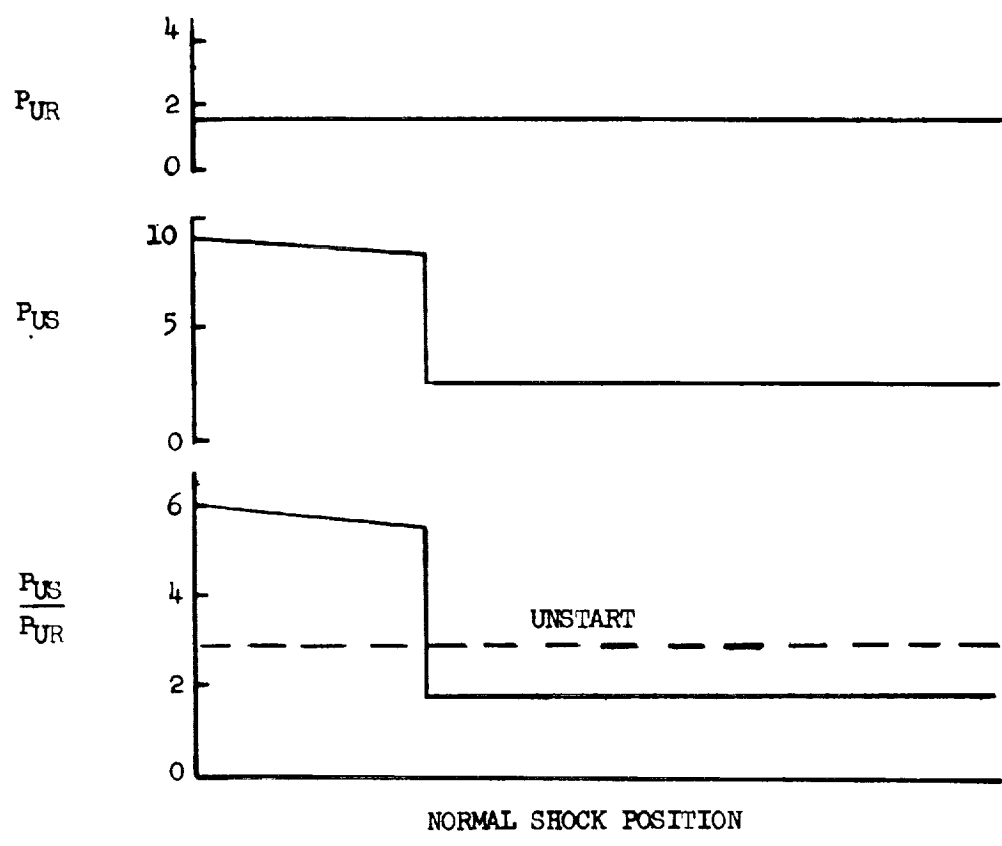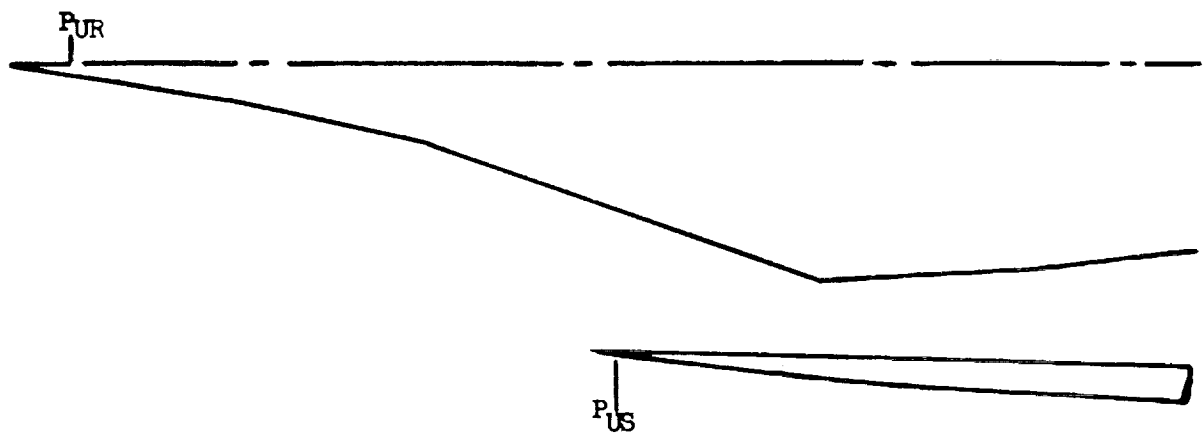
Figure 55. Unstarting Phase Inlet Unstart Pressure Signals
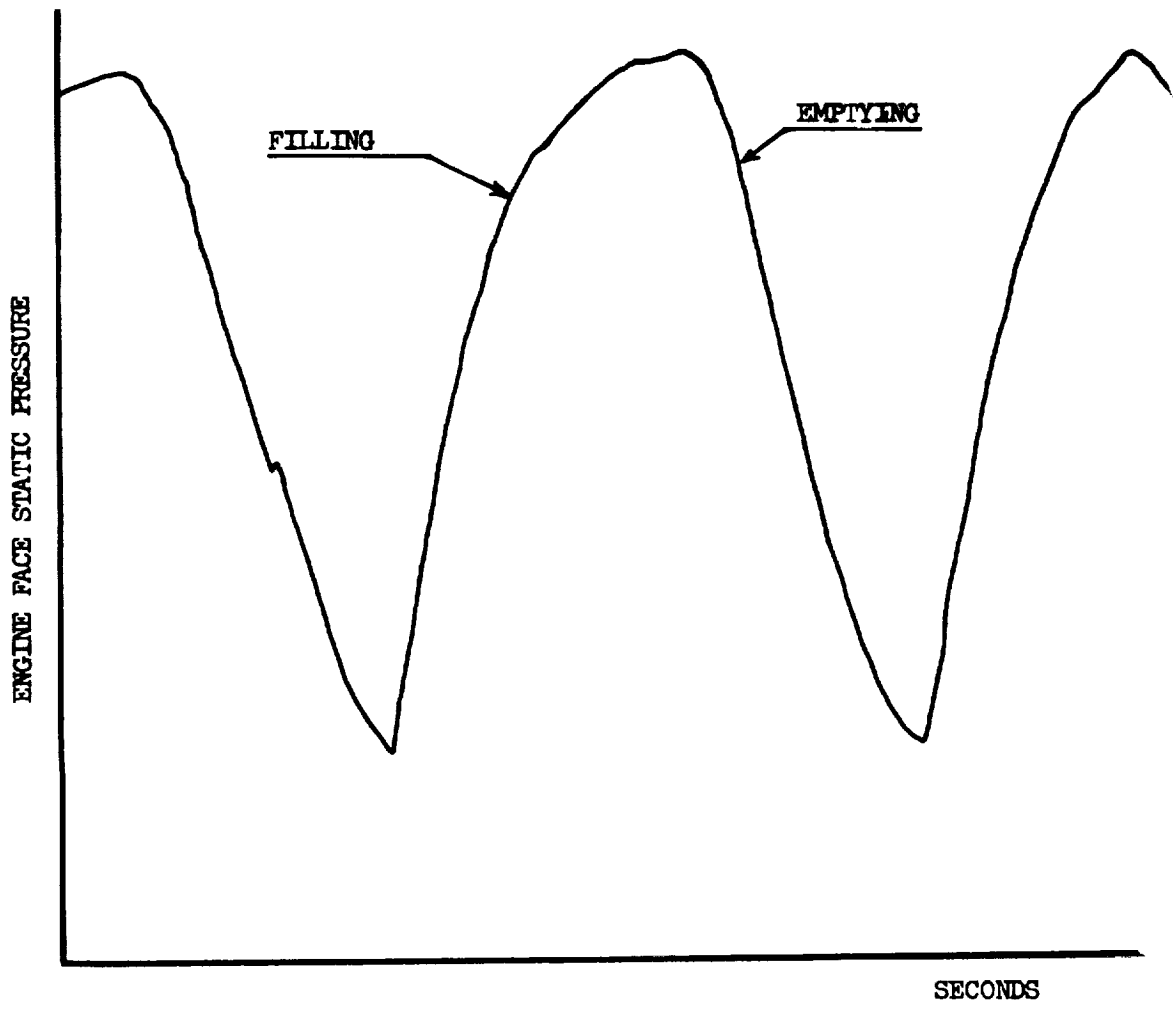
Figure 56. Empty-Fill Phase Typical Buzz Trace

160
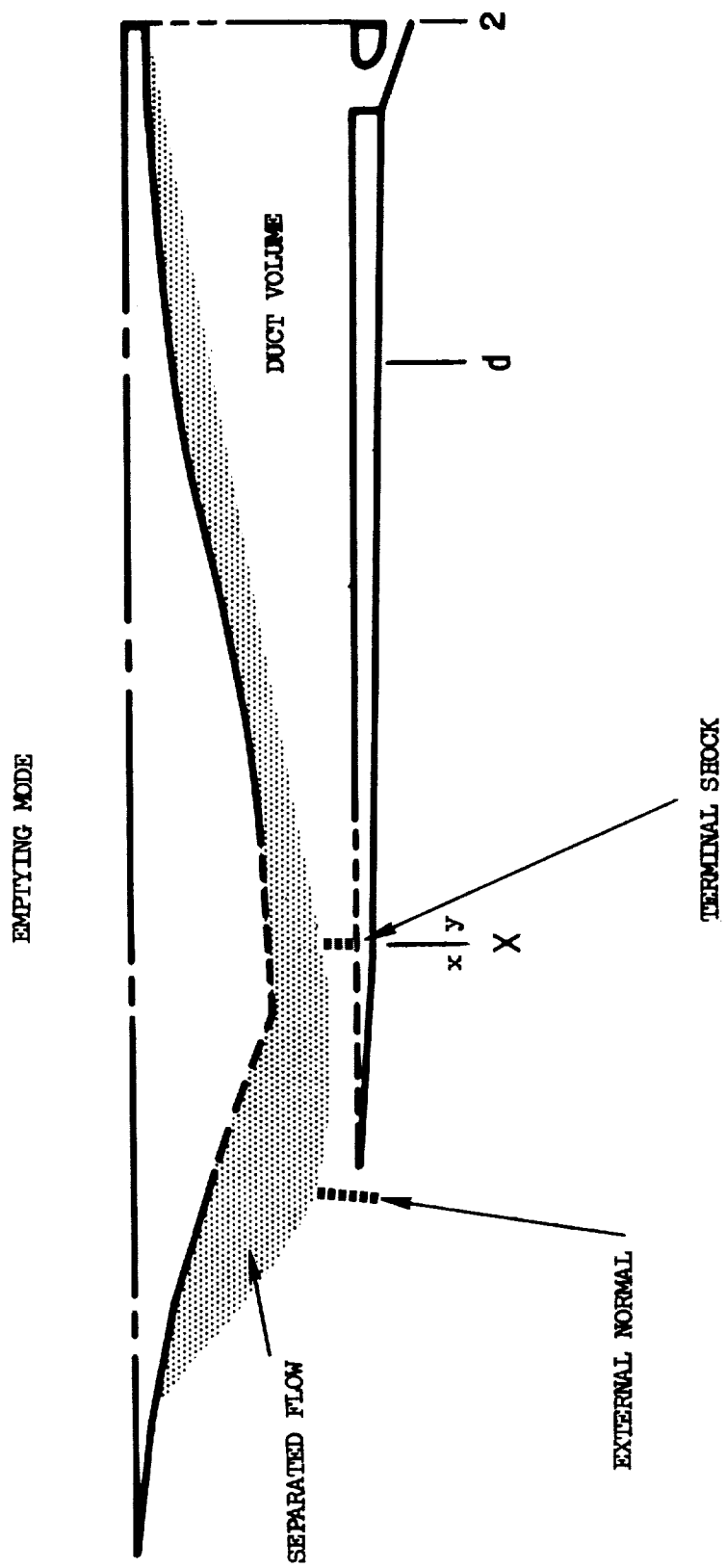
Figure 57a. Empty-Fill Phase Simulation Model

FILLING MODE

TERMINAL SHOCK

DUCT VOLUME

EXTERNAL NORMAL

x|y
X

d

2

161
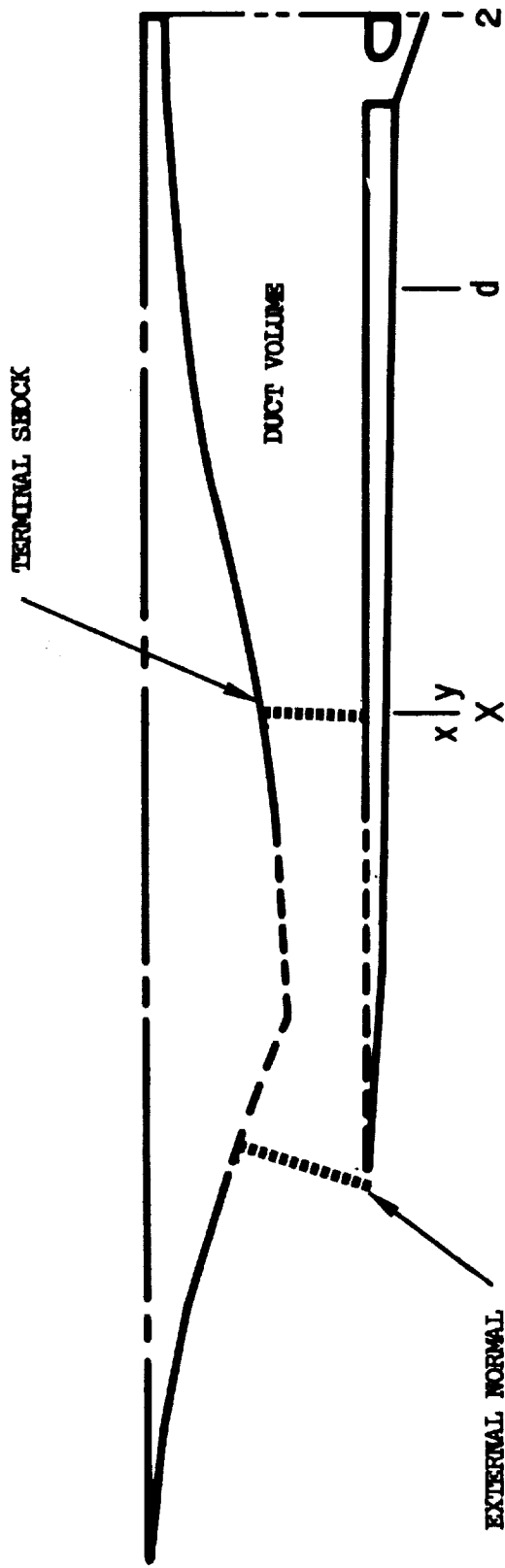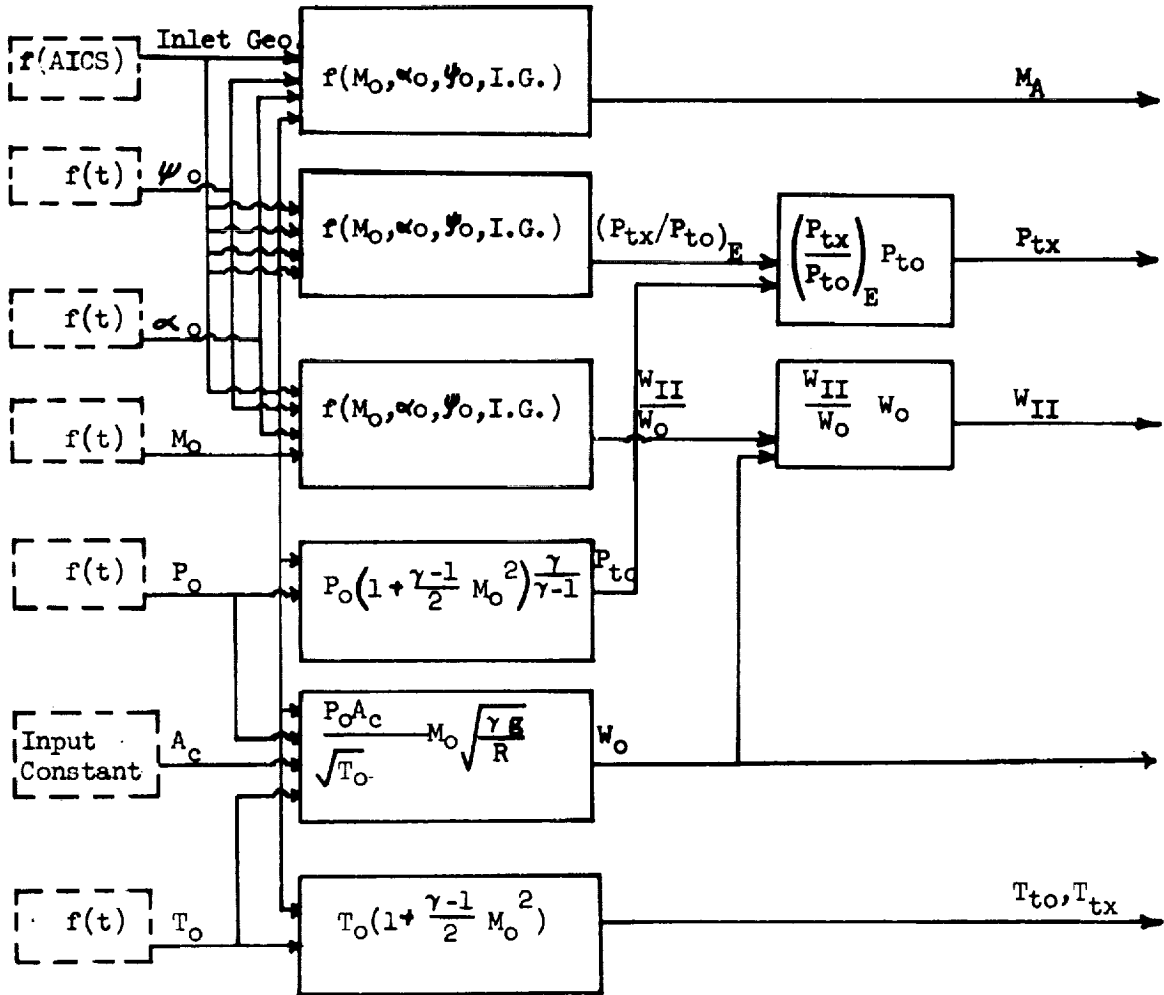
Figure 58. Empty-Fill Phase Upstream Properties
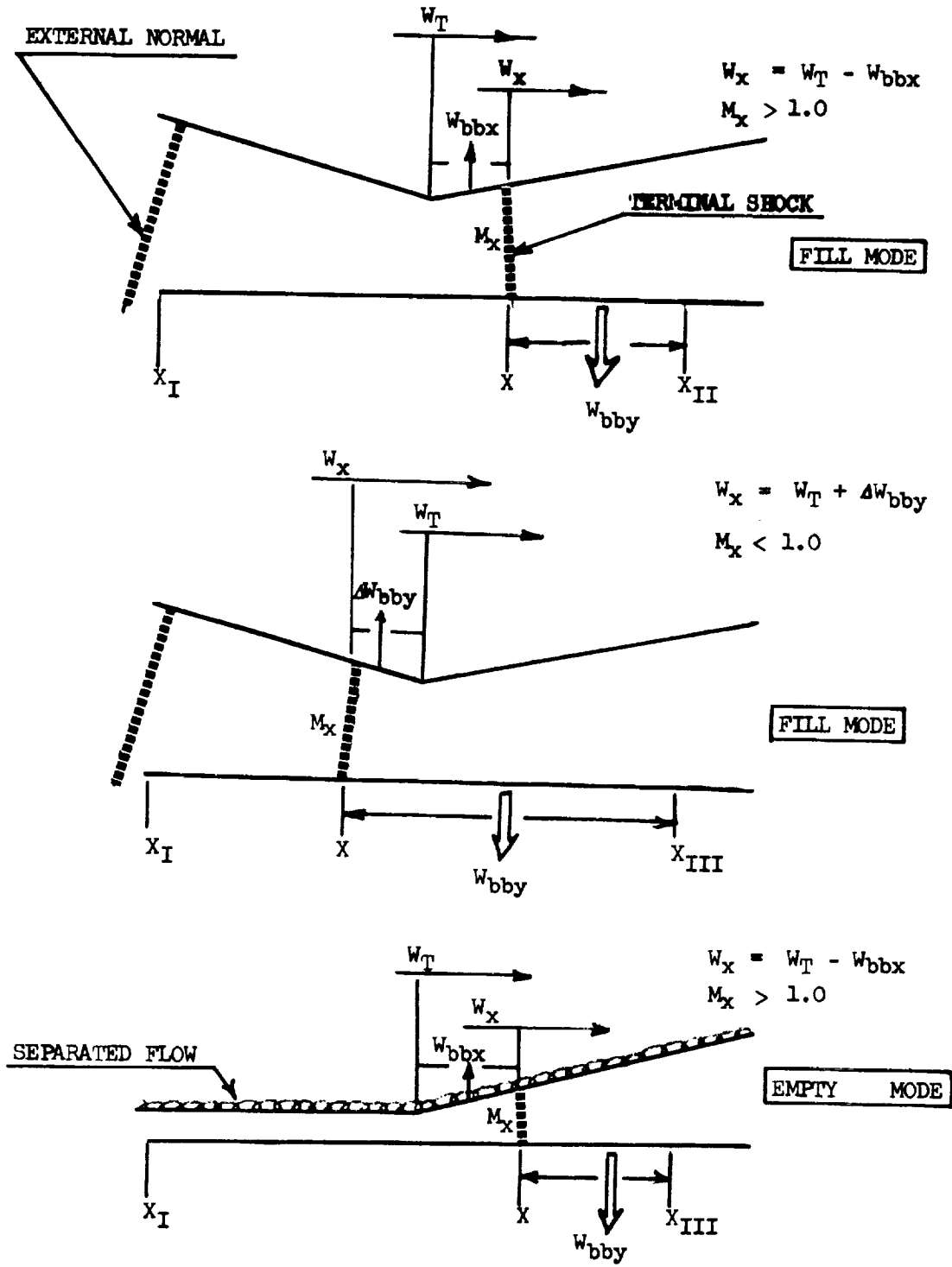
Figure 59. Empty-Fill Phase Airflow at the Terminal Shock
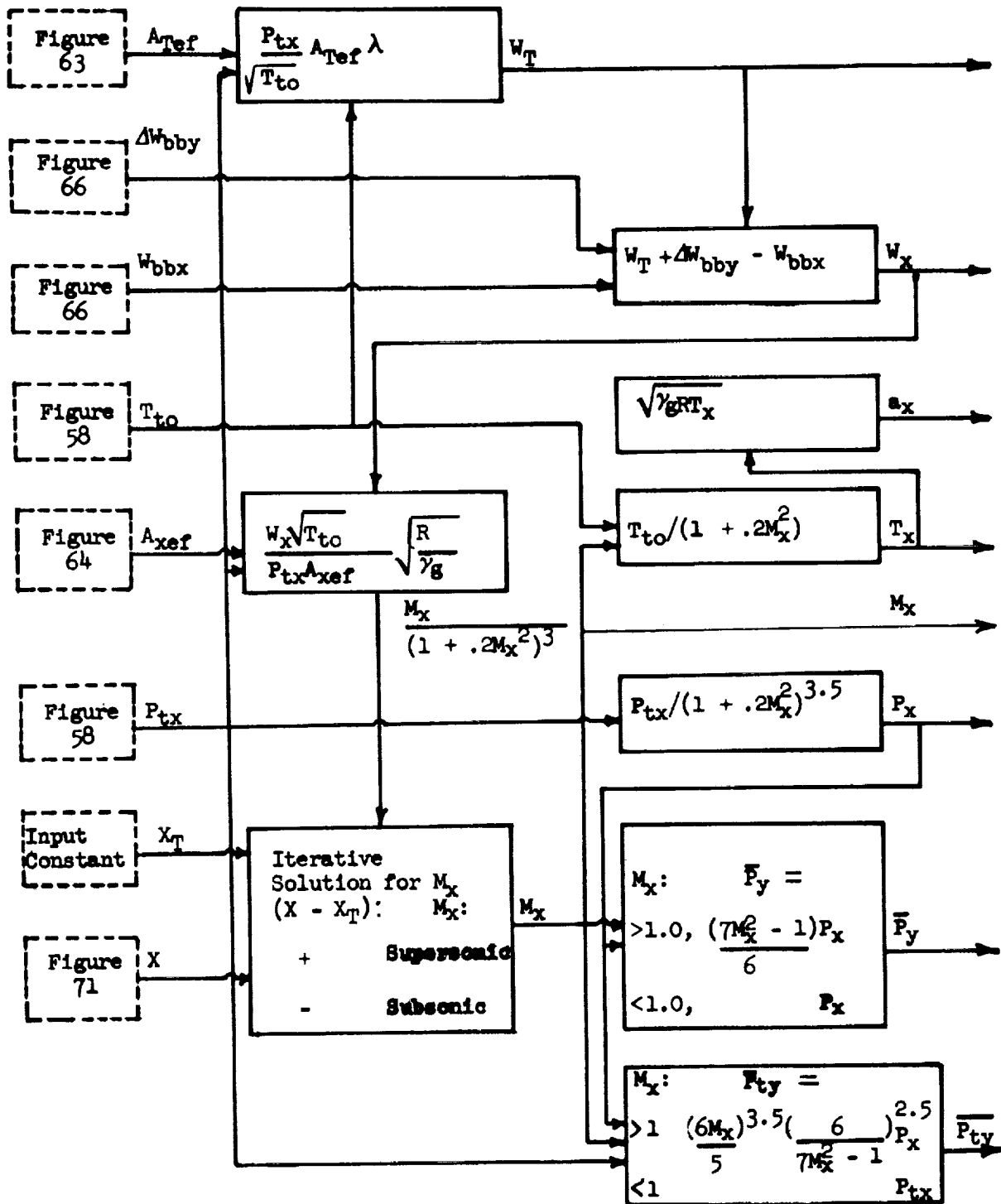
Figure 60. Empty-Fill Phase Properties at the Terminal Shock Station
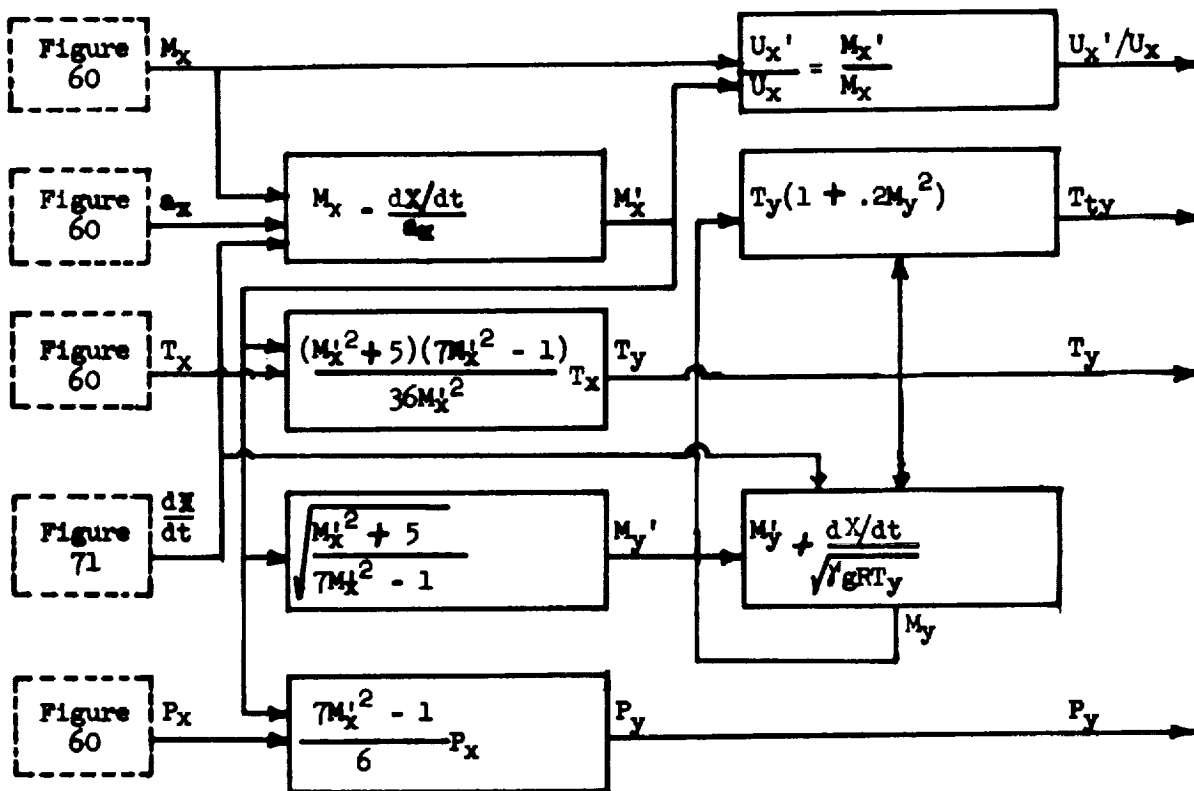
Figure 61. Empty-Fill Phase Properties Behind the Terminal Shock
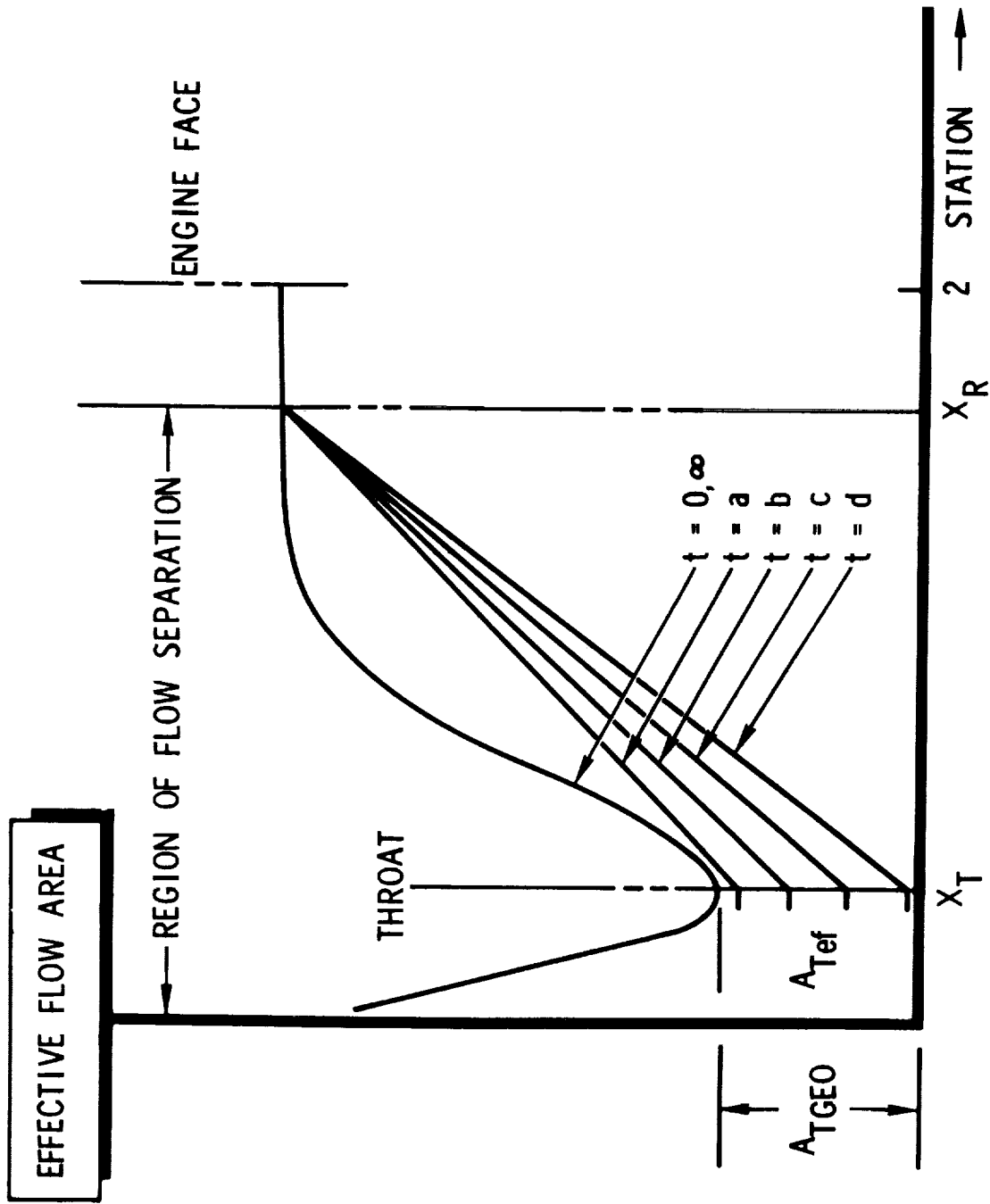
Figure 62. Empty-Fill Phase Effective Flow Area During Separation
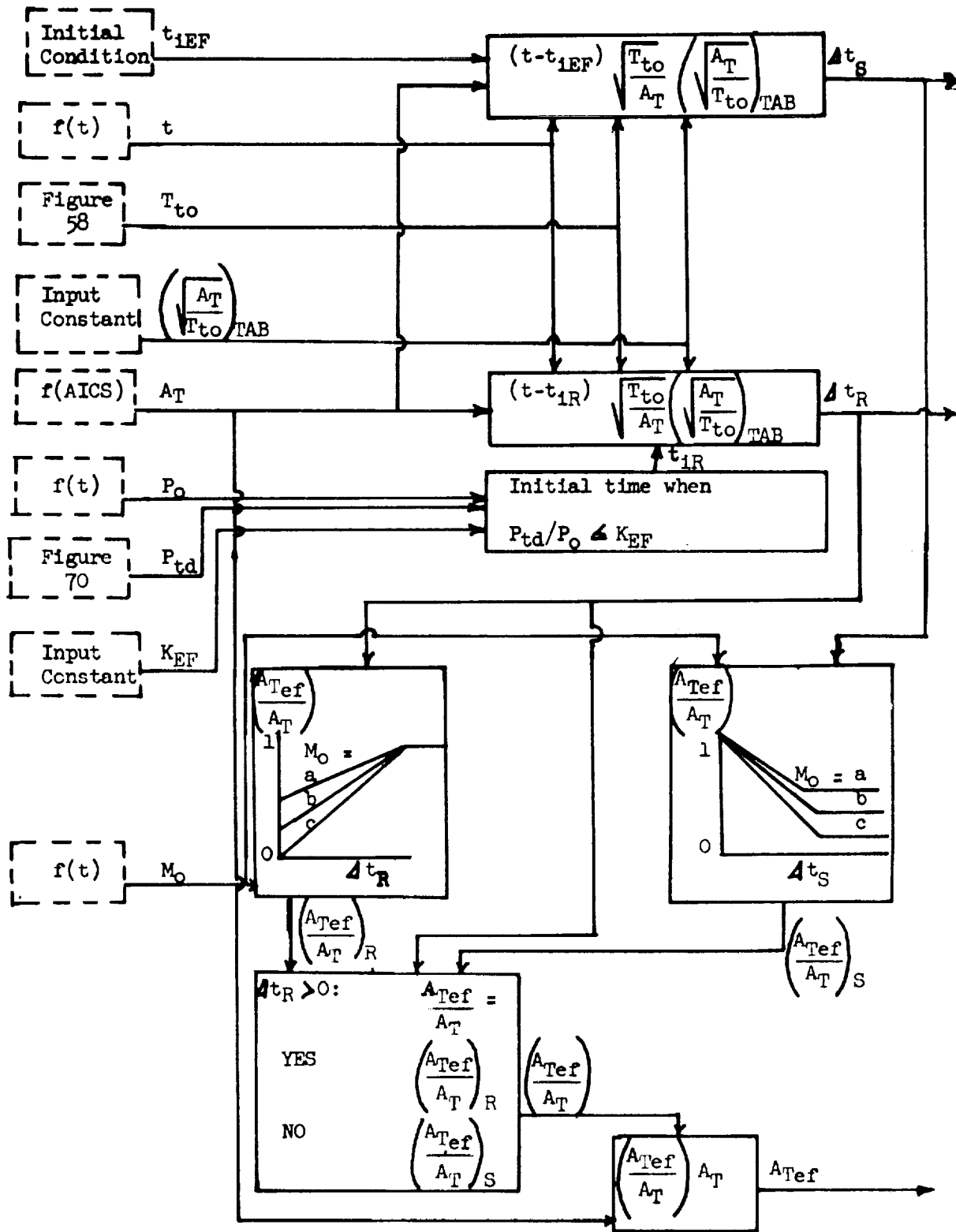
Figure 63. Empty-Fill Phase Effective Throat Area
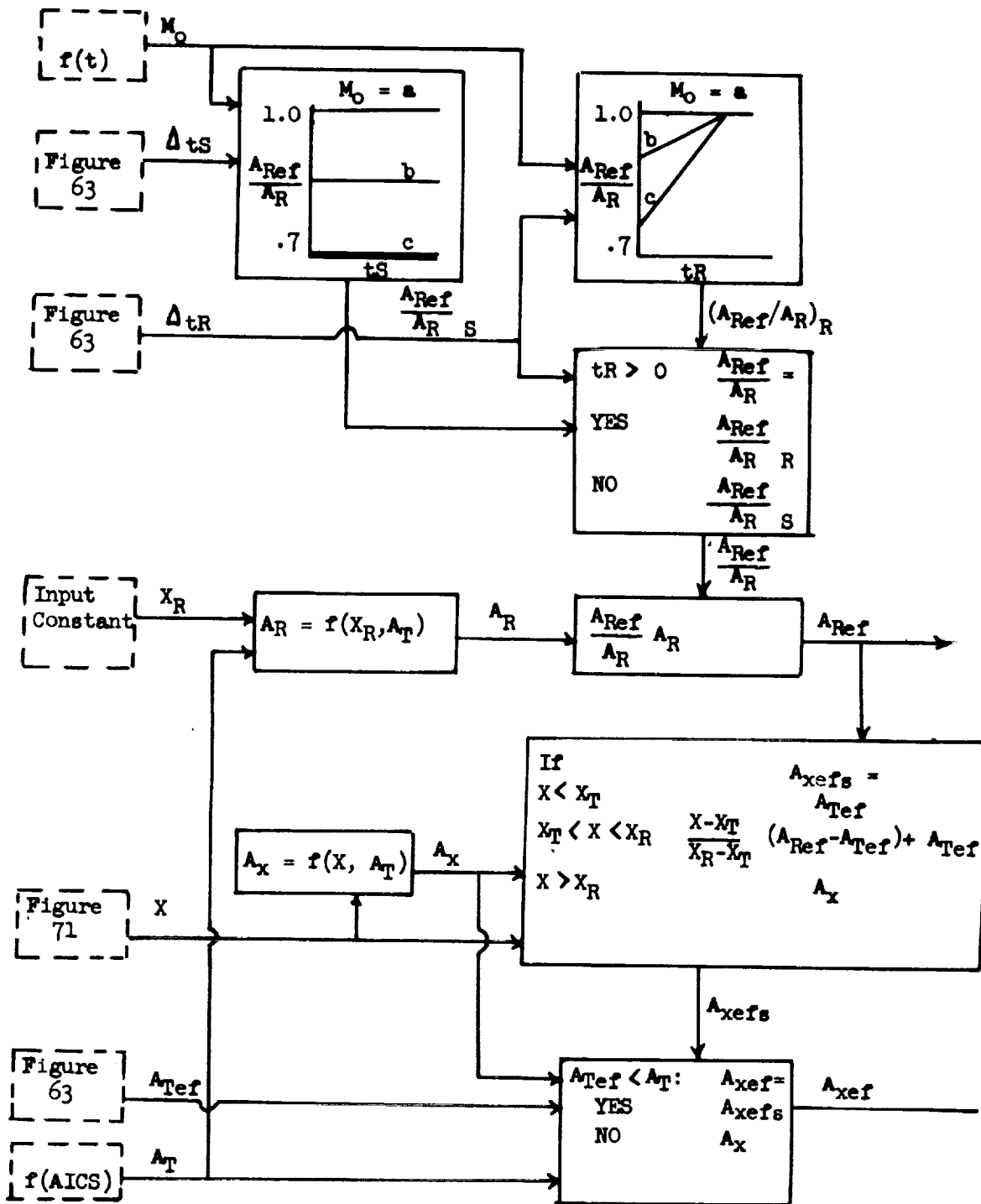
Figure 64. Empty-Fill Phase Effective Flow Area
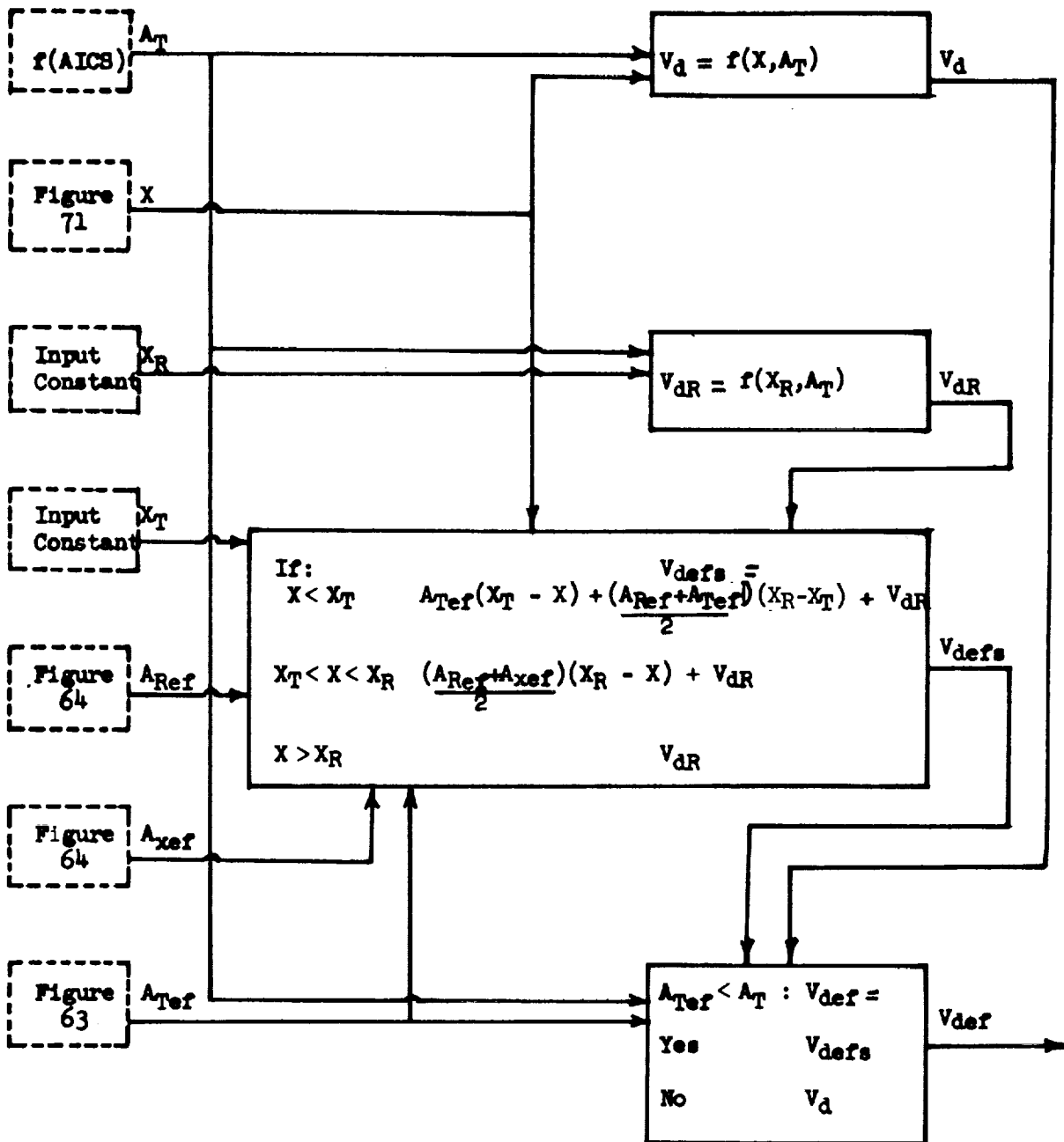
Figure 65. Empty-Fill Phase Effective Volume
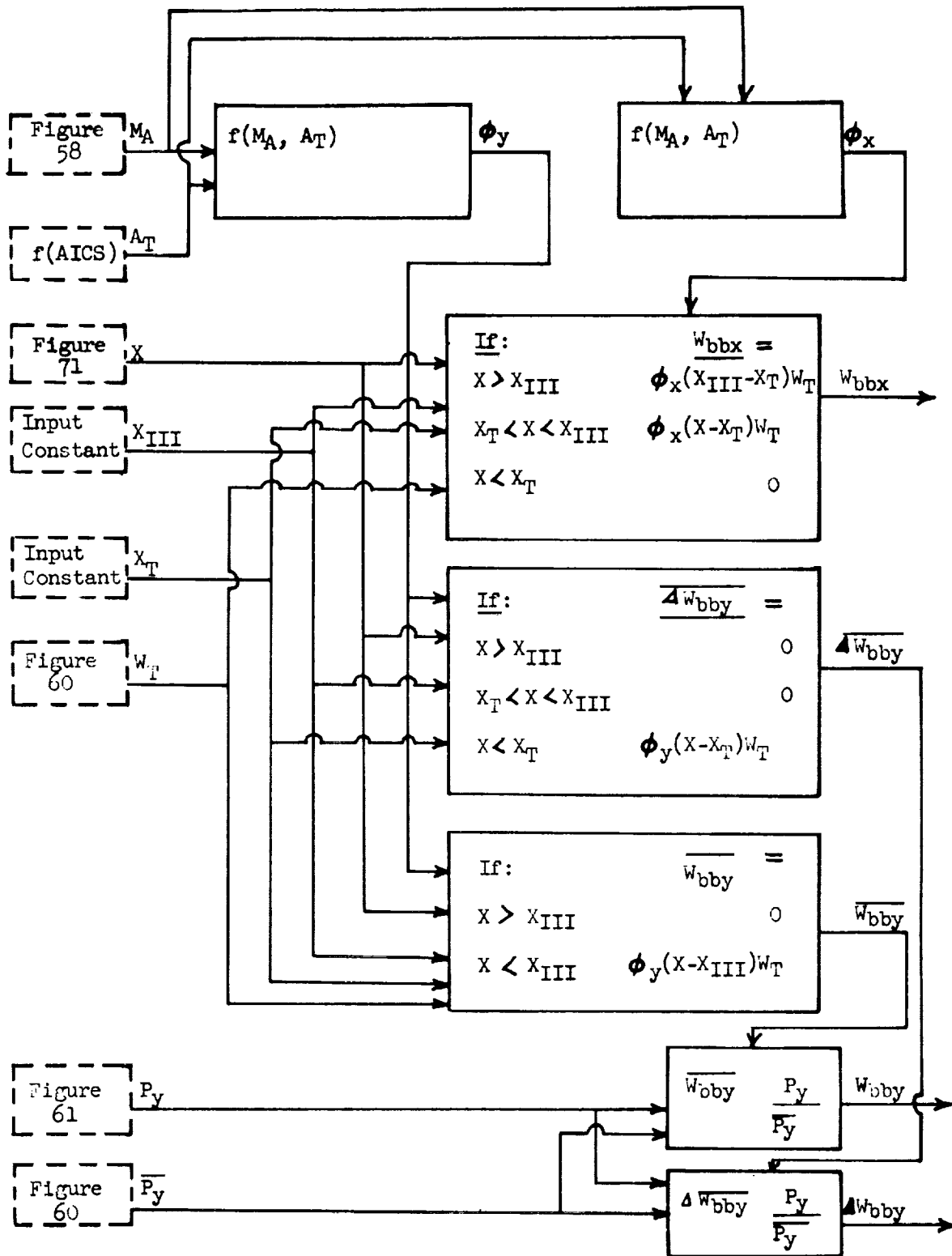
Figure 66. Empty-Fill Phase Boundary Layer Bleed Flows
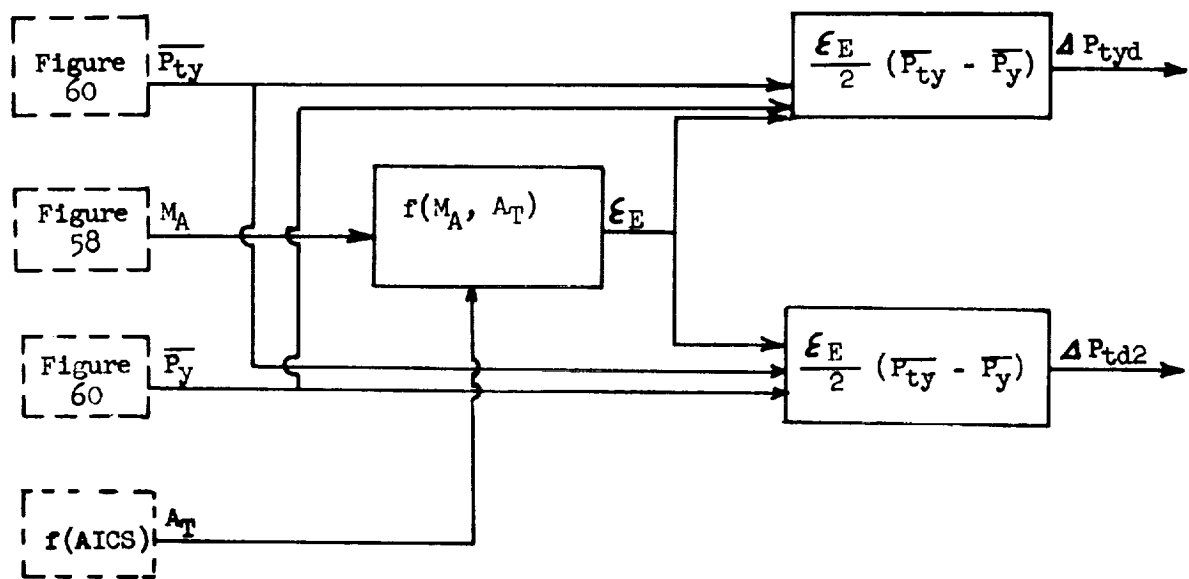
Figure 67. Empty-Fill Phase Duct Volume Total Pressure Losses
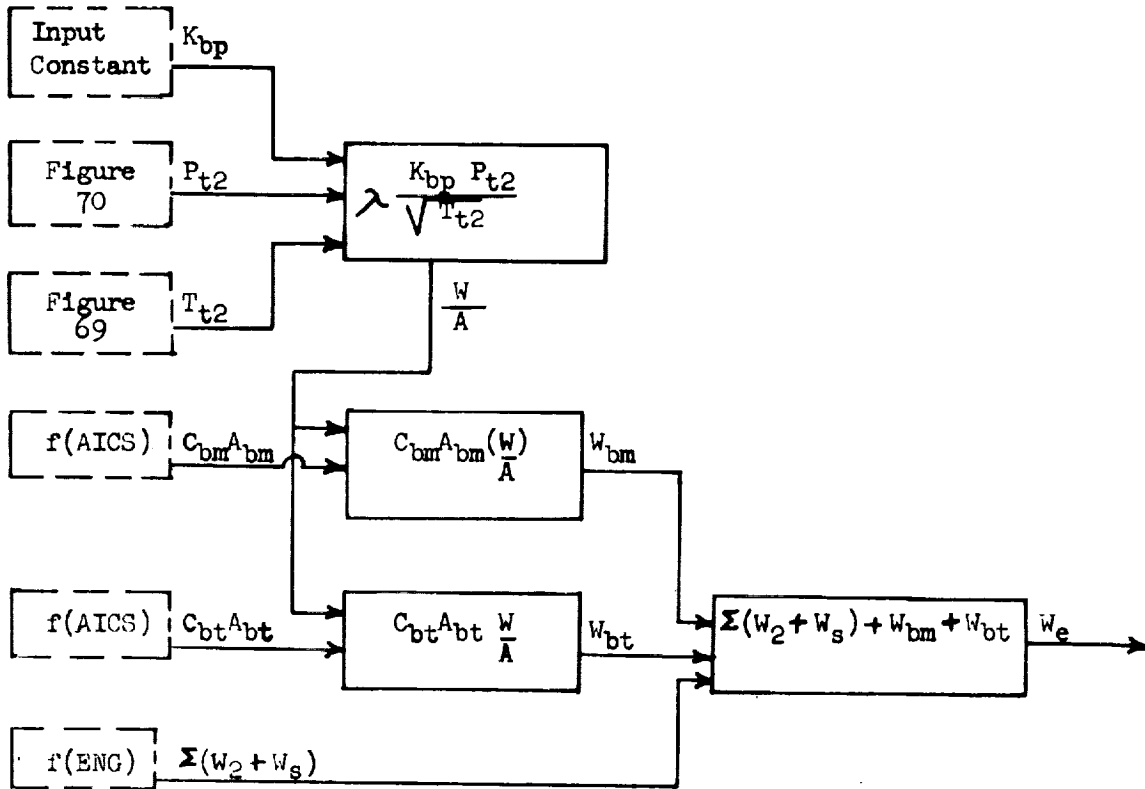
Figure 68. Empty-Fill Phase Bypass and Engine System Airflows
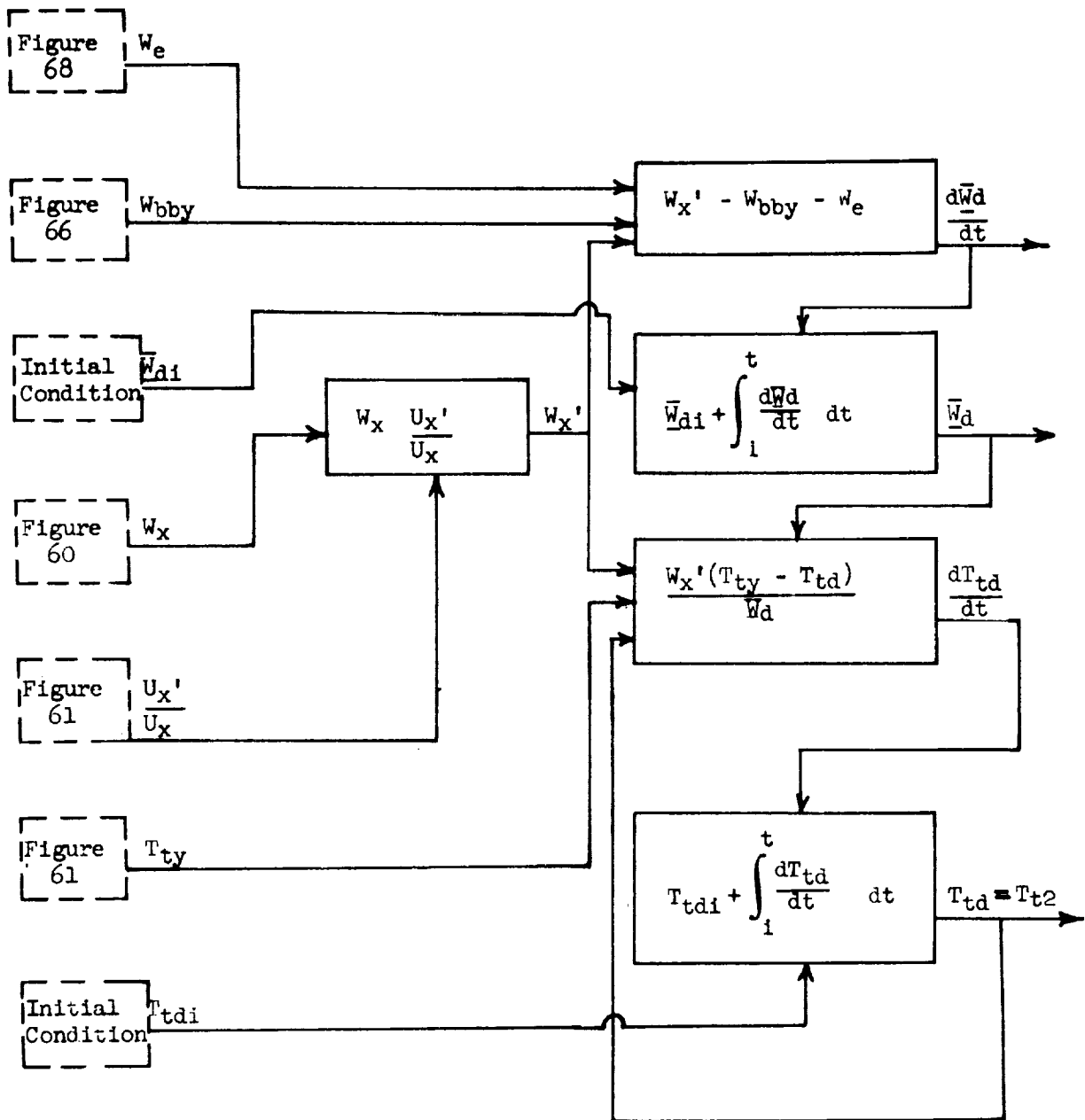
Figure 69. Empty-Fill Phase Duct Volume Mass and Total Temperature
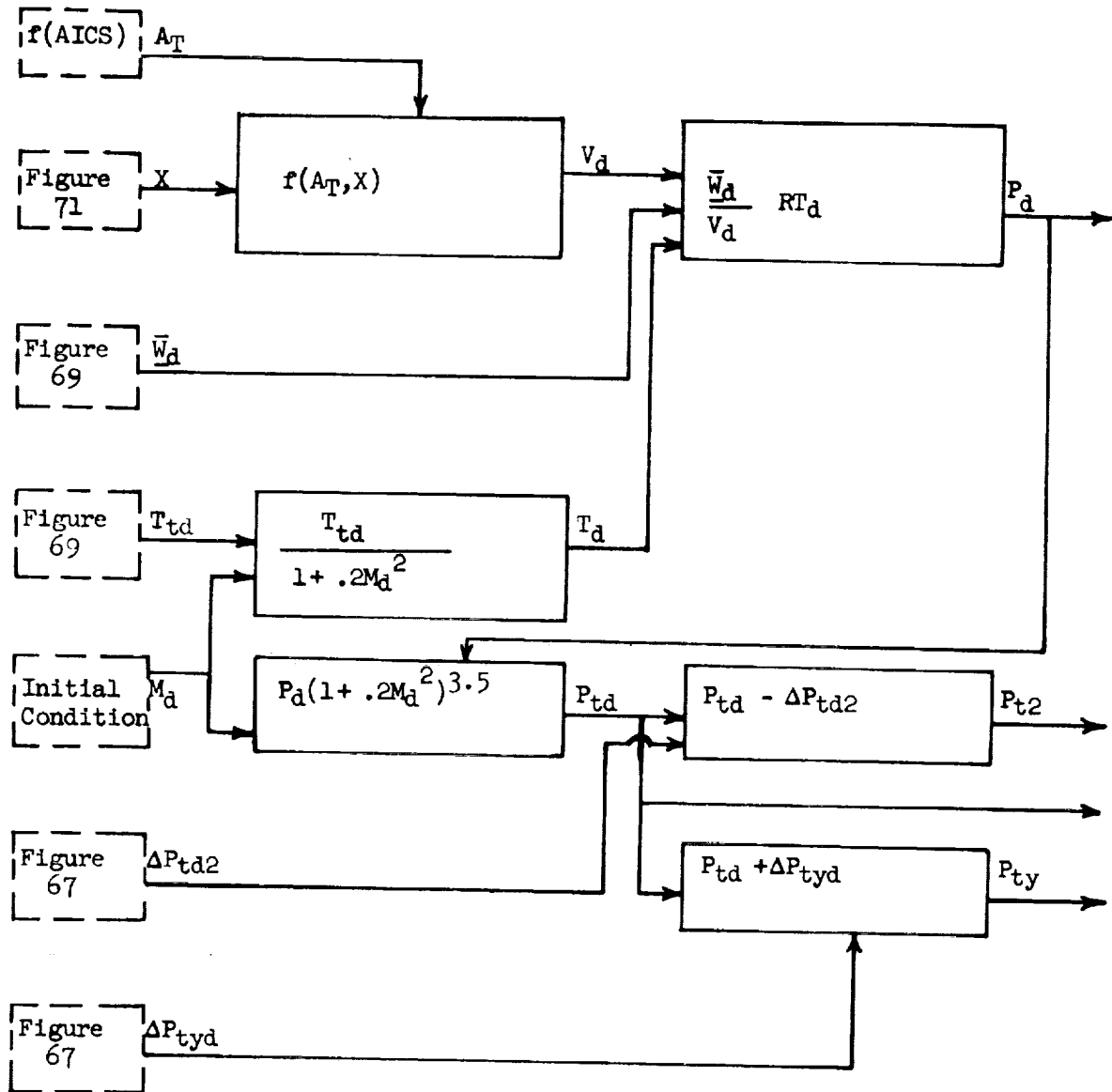
Figure 70. Empty-Fill Phase Duct Volume Total Pressure

174
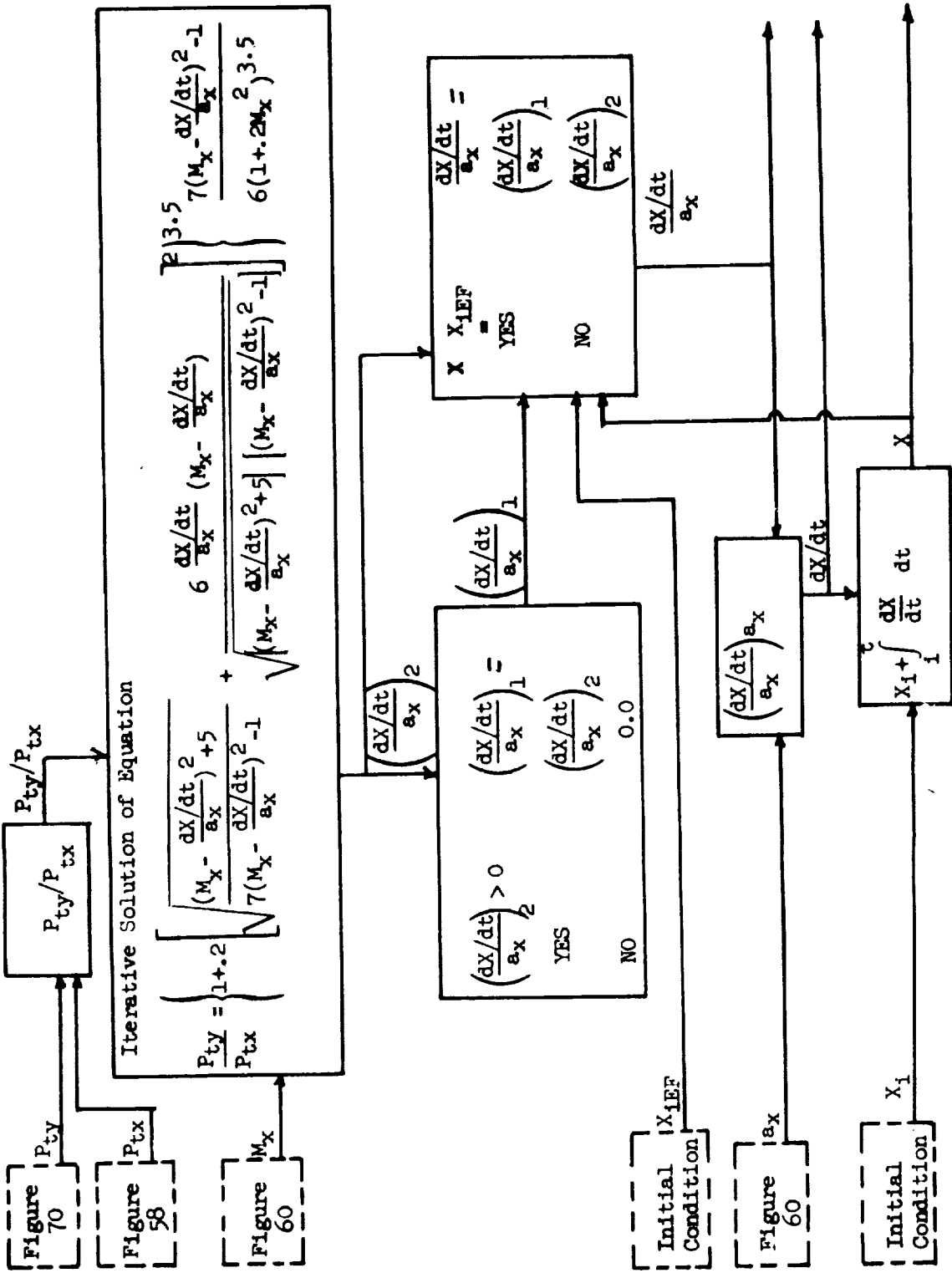
Figure 71. Empty-Fill Phase Duct Terminal Shock Velocity and Position

175

Figure 60 W_T

Figure 58 W_{II}

$f(t)$ M_O

$f(M_O)$ K_{RS}

WHEN

$$W_T \geq K_{RS}(W_{II})$$

SWITCH TO

Started Phase

Figure 68 W_e

$$\frac{\left(W_{e_{t-\Delta t}} - W_e\right)}{\left(W_{e_{t-\Delta t}}\right)(\Delta t)}$$ $\frac{dW_e/dt}{W_e}$

WHEN

$$\frac{dW_e/dt}{W_e} > K_{HS}$$

SWITCH TO

Hammershock Phase

Input Constant K_{HS}

$f(AICS)$ A_T

$f(M_O, A_T)$ $\left(\dfrac{W_I}{W_o}\right)_{buzz}$

WHEN

$$X < X_L \quad \&$$

$$\frac{W_e + W_{bby}}{W_o} < \left(\frac{W_I}{W_o}\right)_{buzz}$$

SWITCH TO

New
Empty-Fill Phase

Figure 71 X

Input Constant X_L

Figure 66 W_{bby}

Figure 58 W_o

WHEN

$$X < X_L \quad \&$$

$$\frac{W_e + W_{bby}}{W_o} > \left(\frac{W_I}{W_o}\right)_{buzz}$$

SWITCH TO
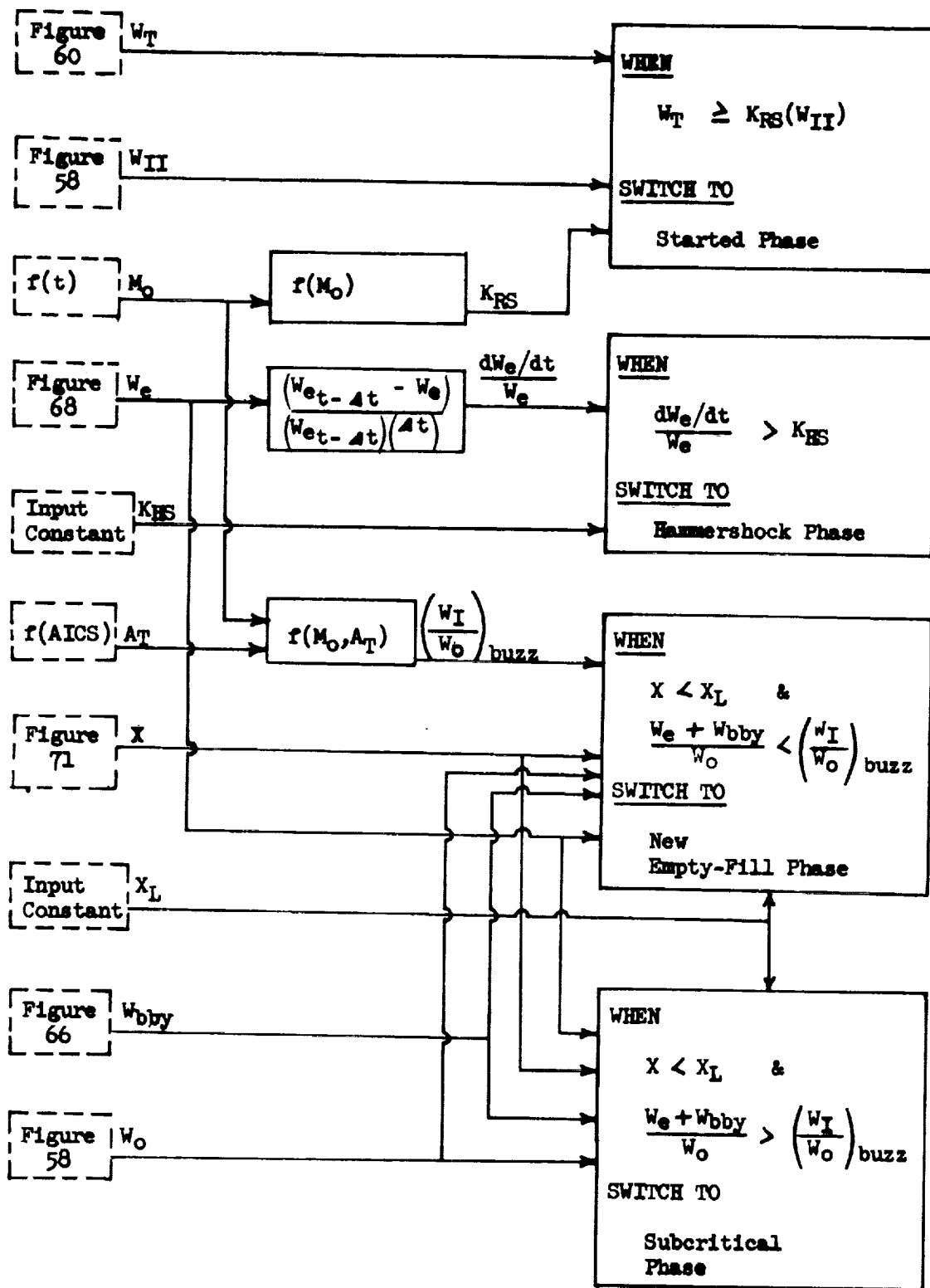
Subcritical
Phase

Figure 72. Empty-Fill Phase Phase Switches

176

PSEUDO-SURFACE

δ_{MAX}

h_x

M_x

h_1

h_2

ΔX

X_1

X_2
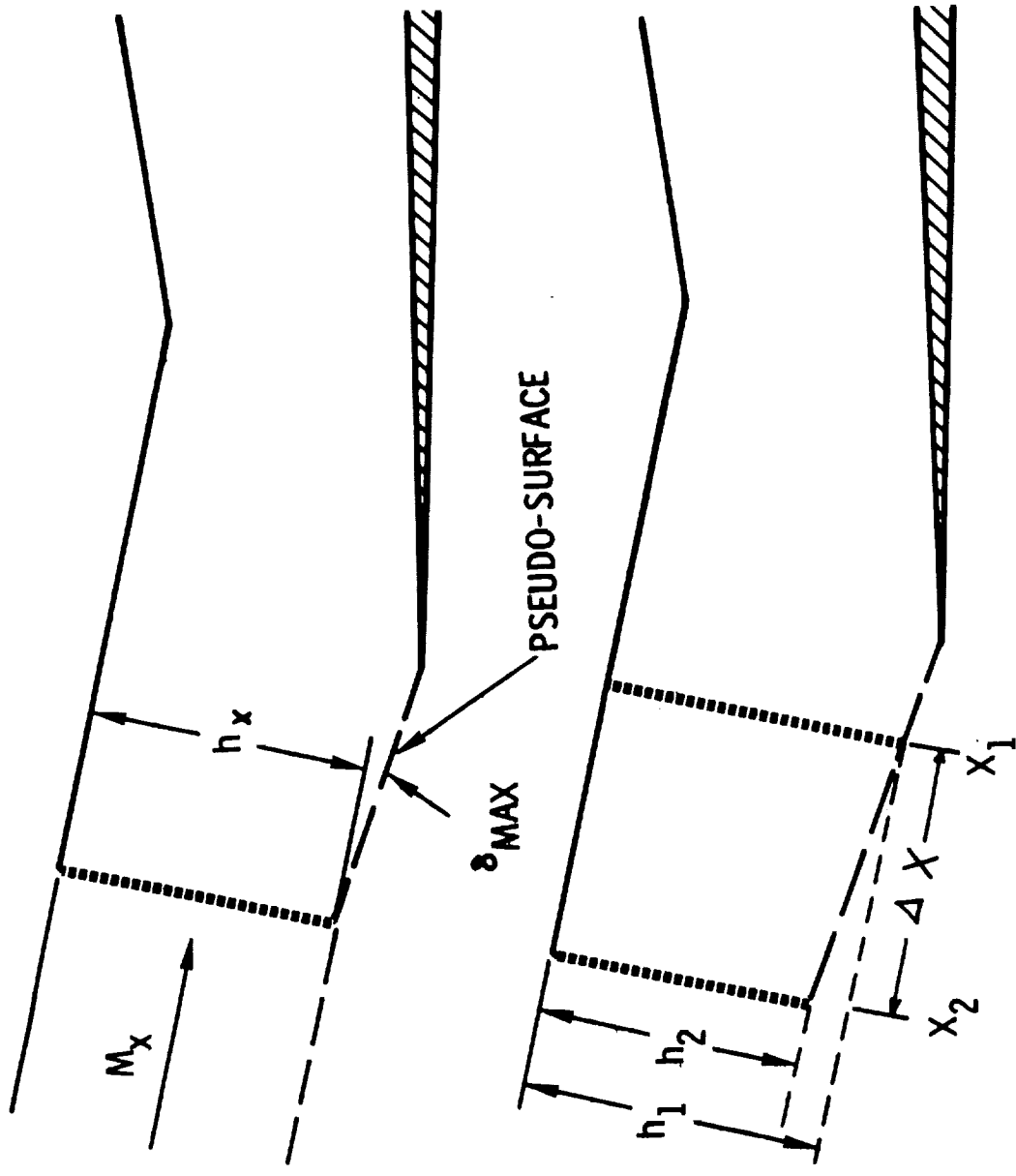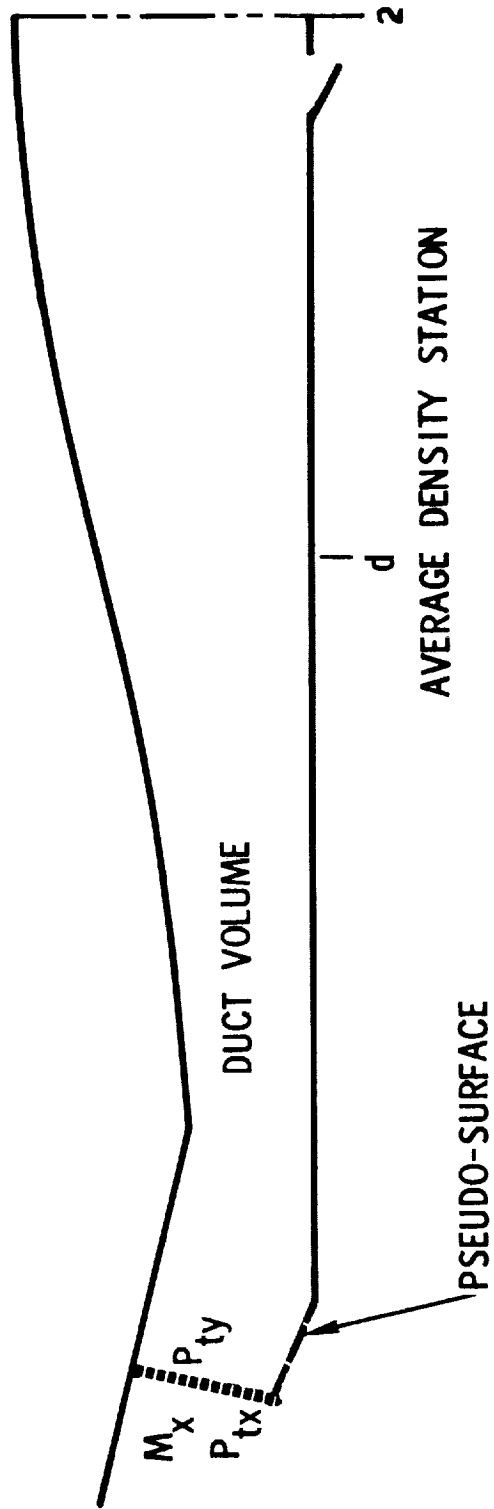
Figure 74. Subcritical Phase Simulation Model
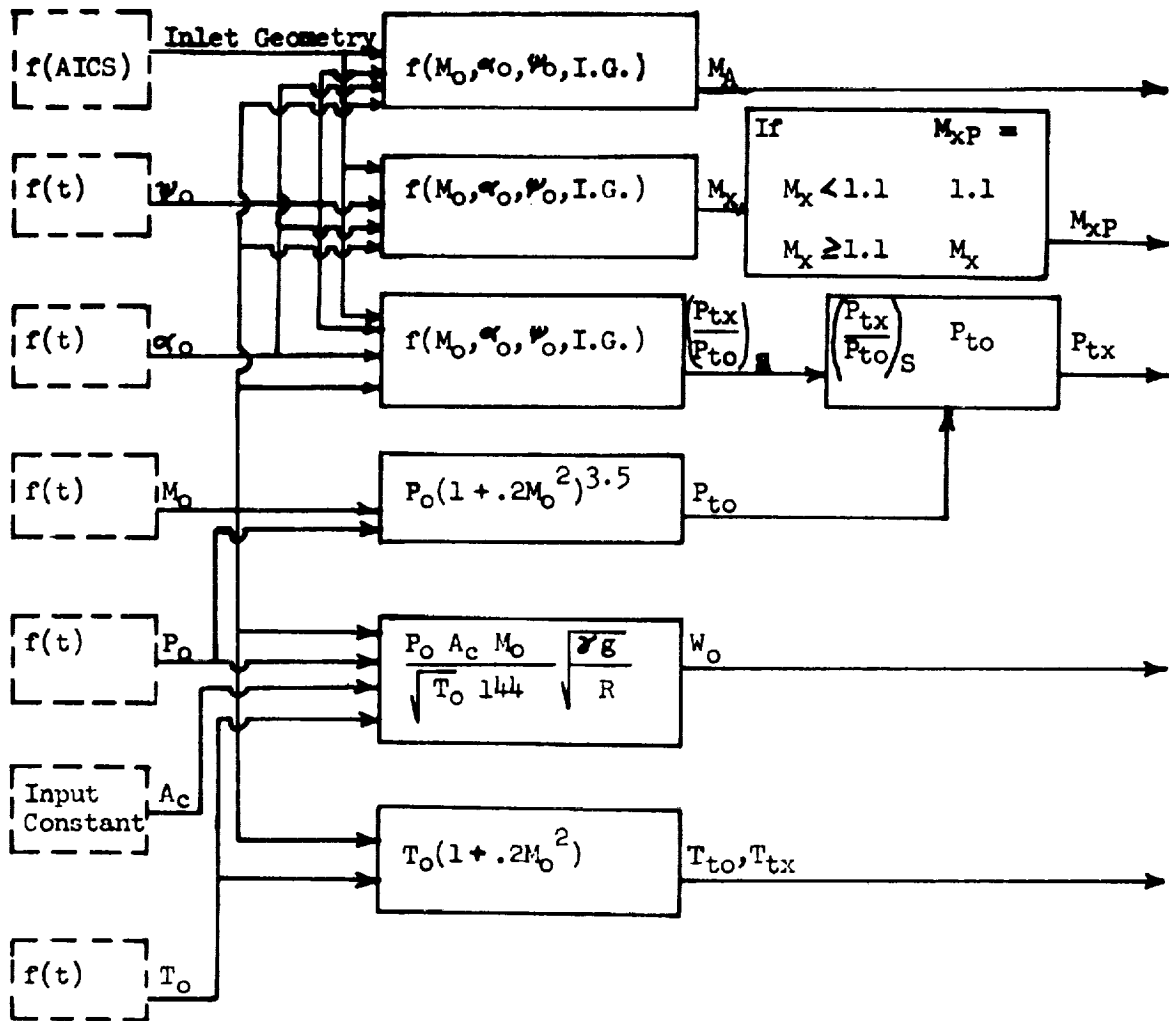
Figure 75a. Subcritical Phase Upstream Properties
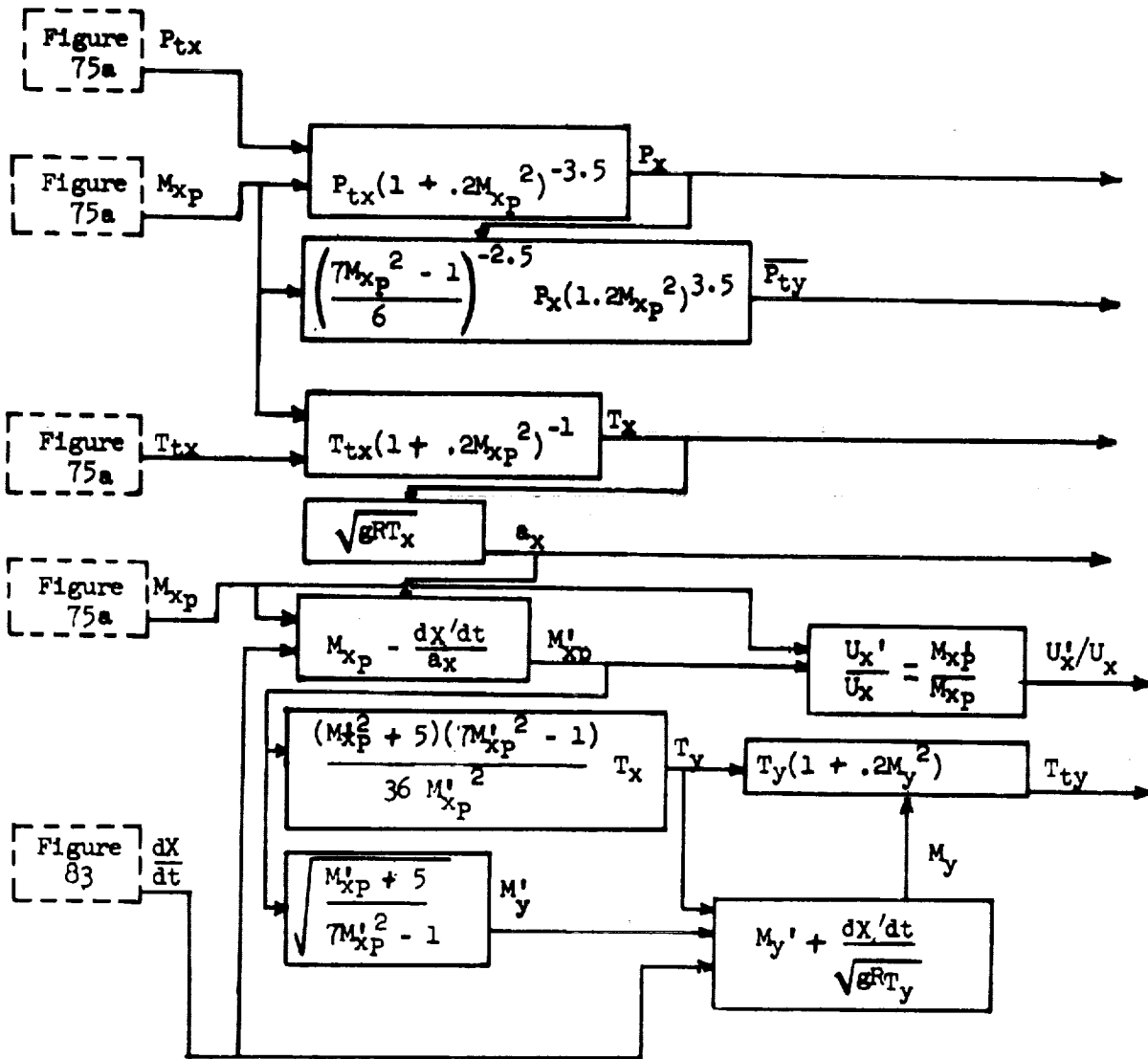
Figure 75b. Subcritical Phase Upstream Properties
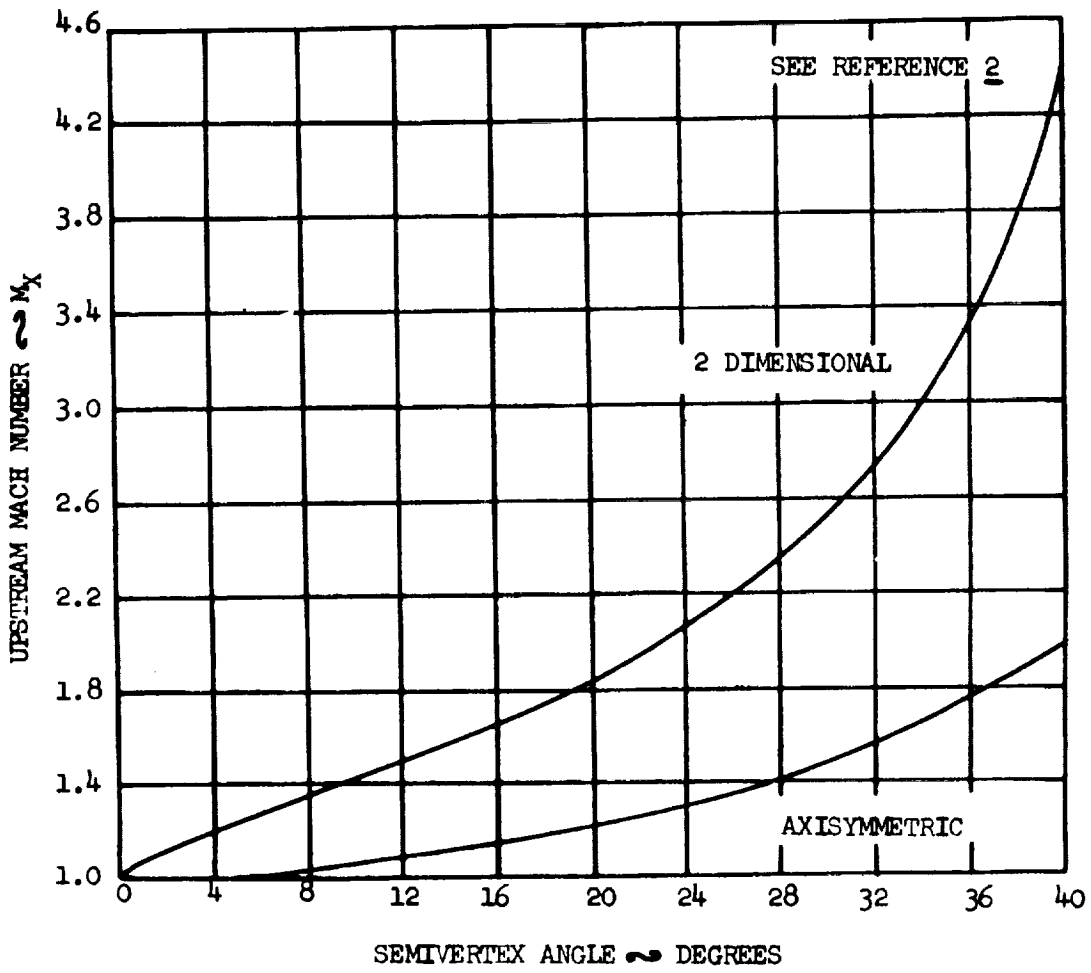
Figure 76. Subcritical Phase Maximum Deflection Angle for Attached Flow
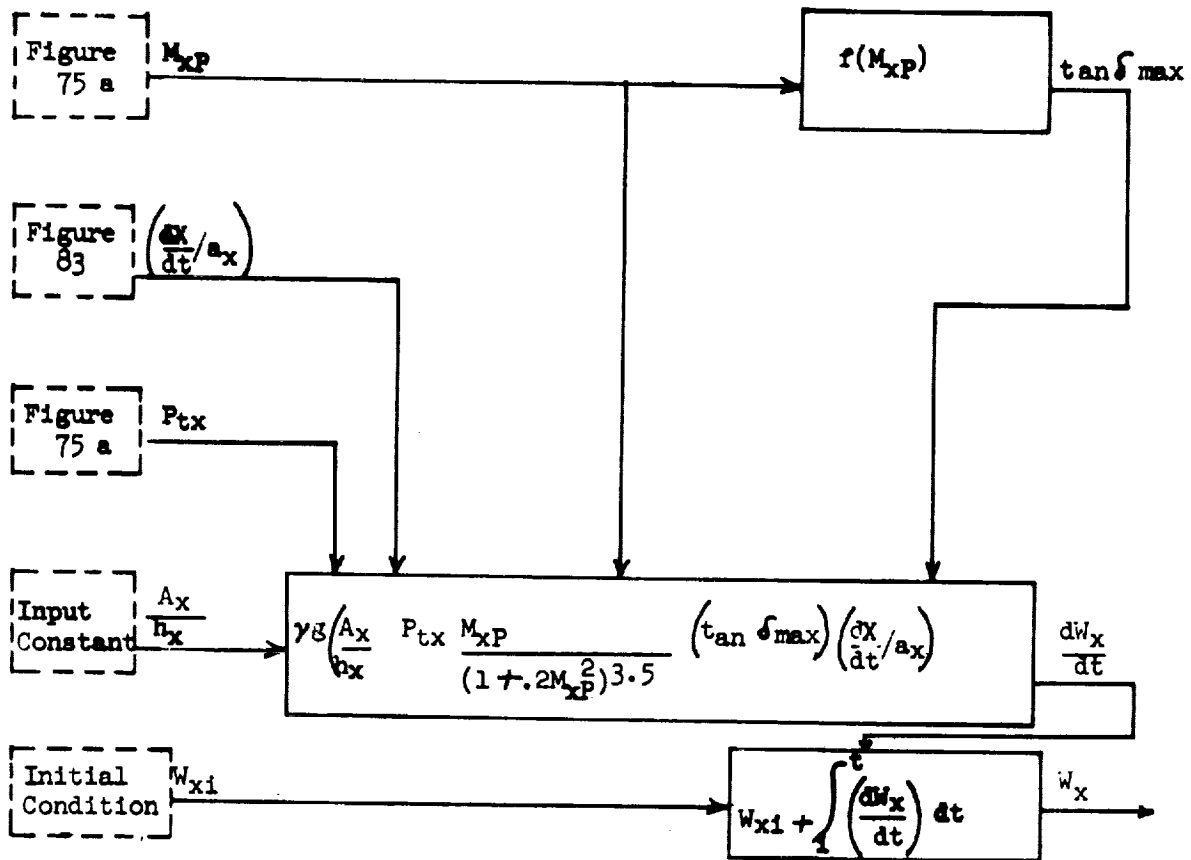
Figure 77. Subcritical Phase Inflow
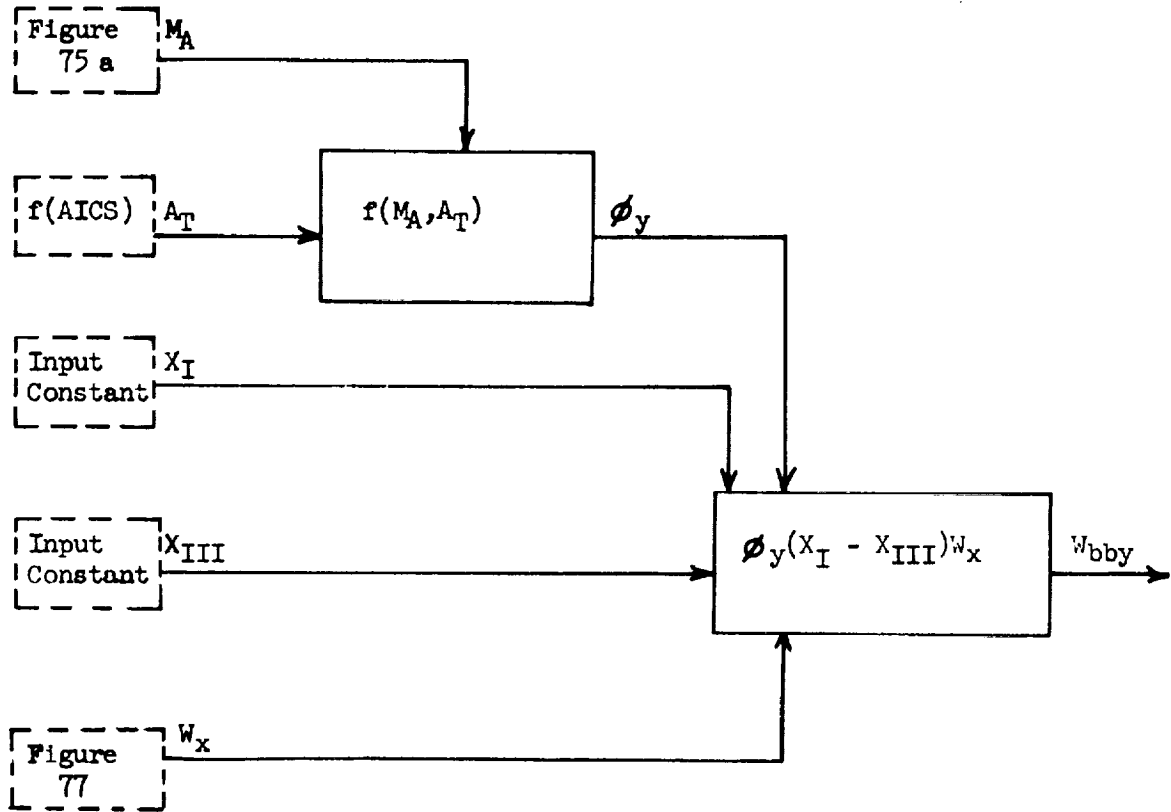
Figure 78. Subcritical Phase Boundary Layer Bleed Flow
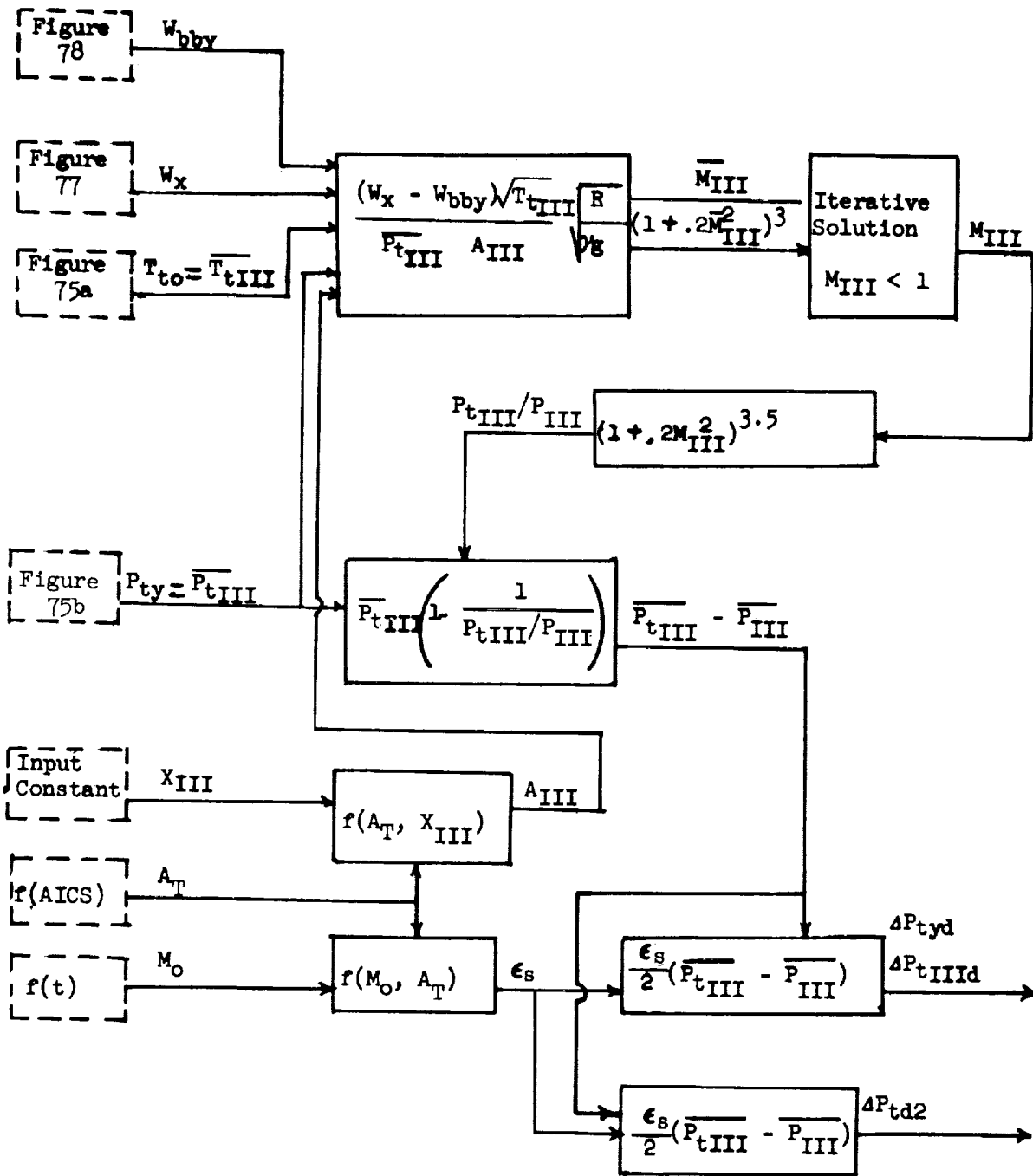
Figure 79. Subcritical Phase Duct Volume Total Pressure Losses

184
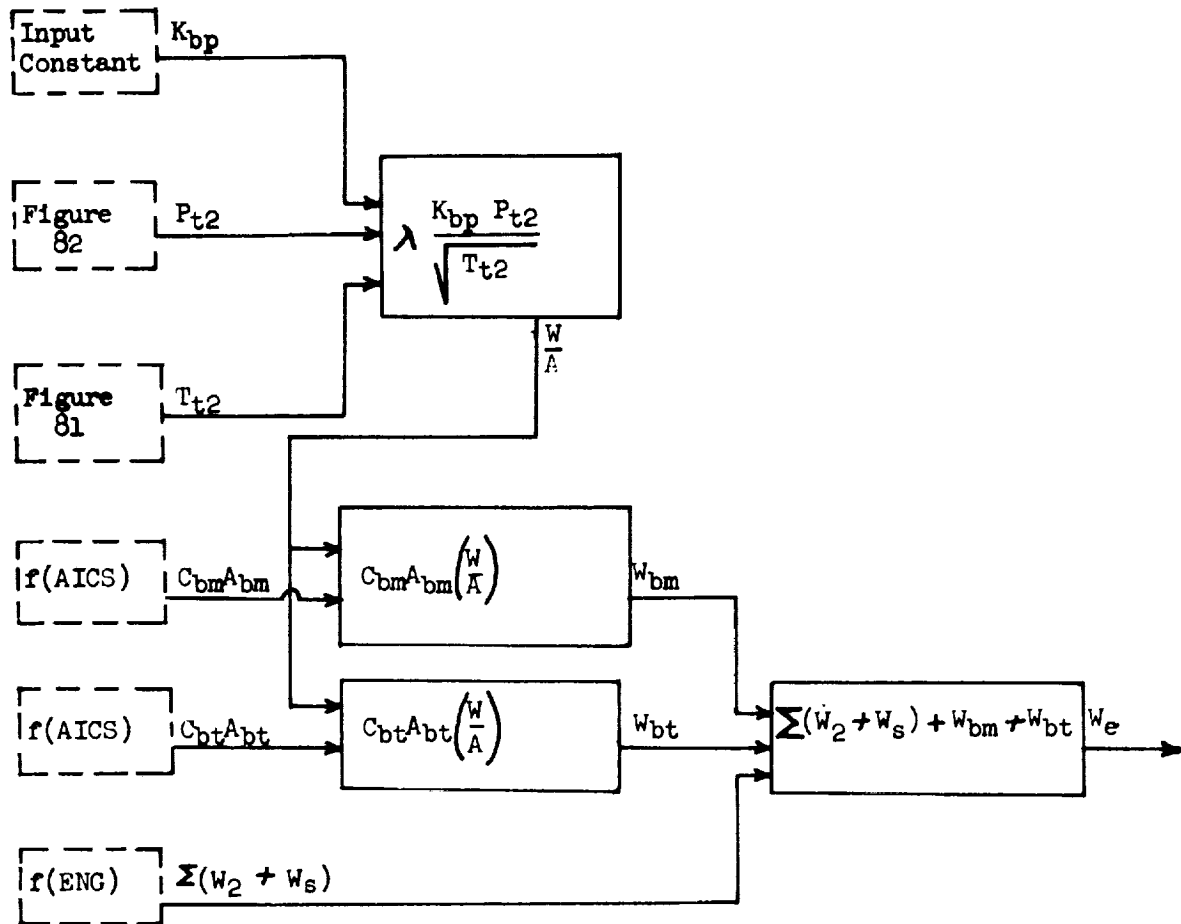
Figure 80. Subcritical Phase Bypass and Engine System Airflows
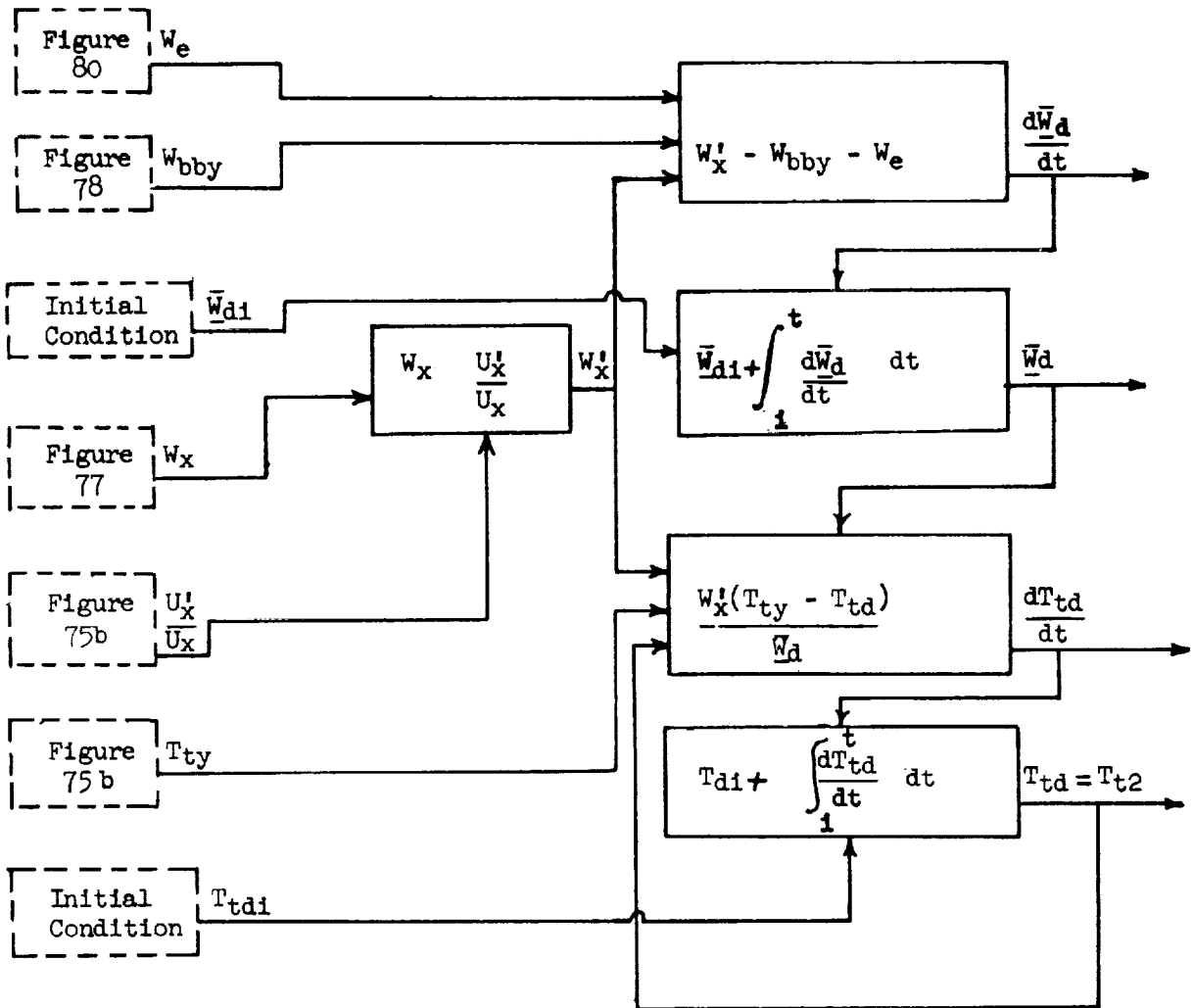
Figure 81. Subcritical Phase Duct Volume Mass and Total Temperature
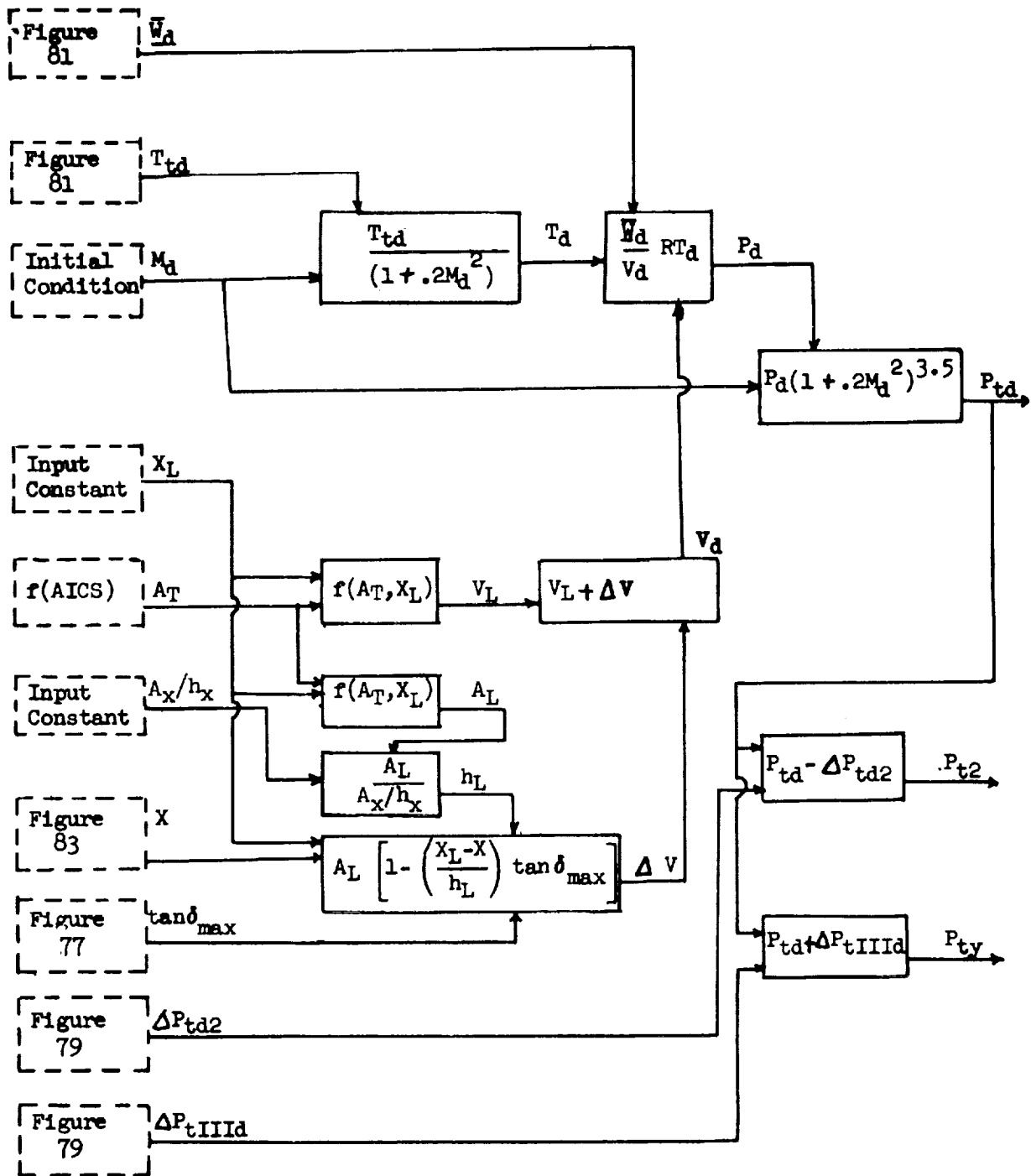
Figure 82. Subcritical Phase Duct Volume Total Pressure
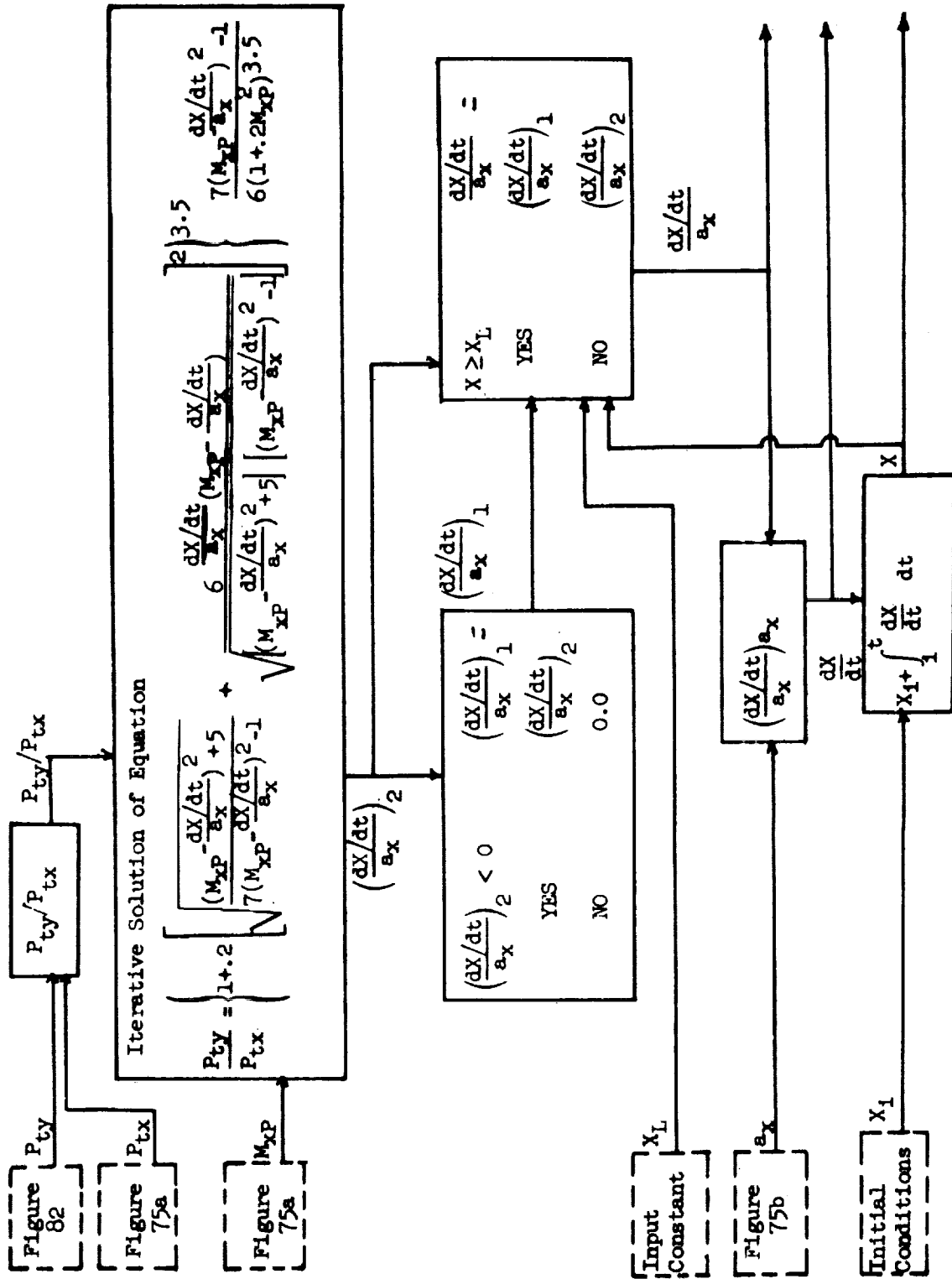
Figure 83. Subcritical Phase Terminal Shock Velocity and Position

188
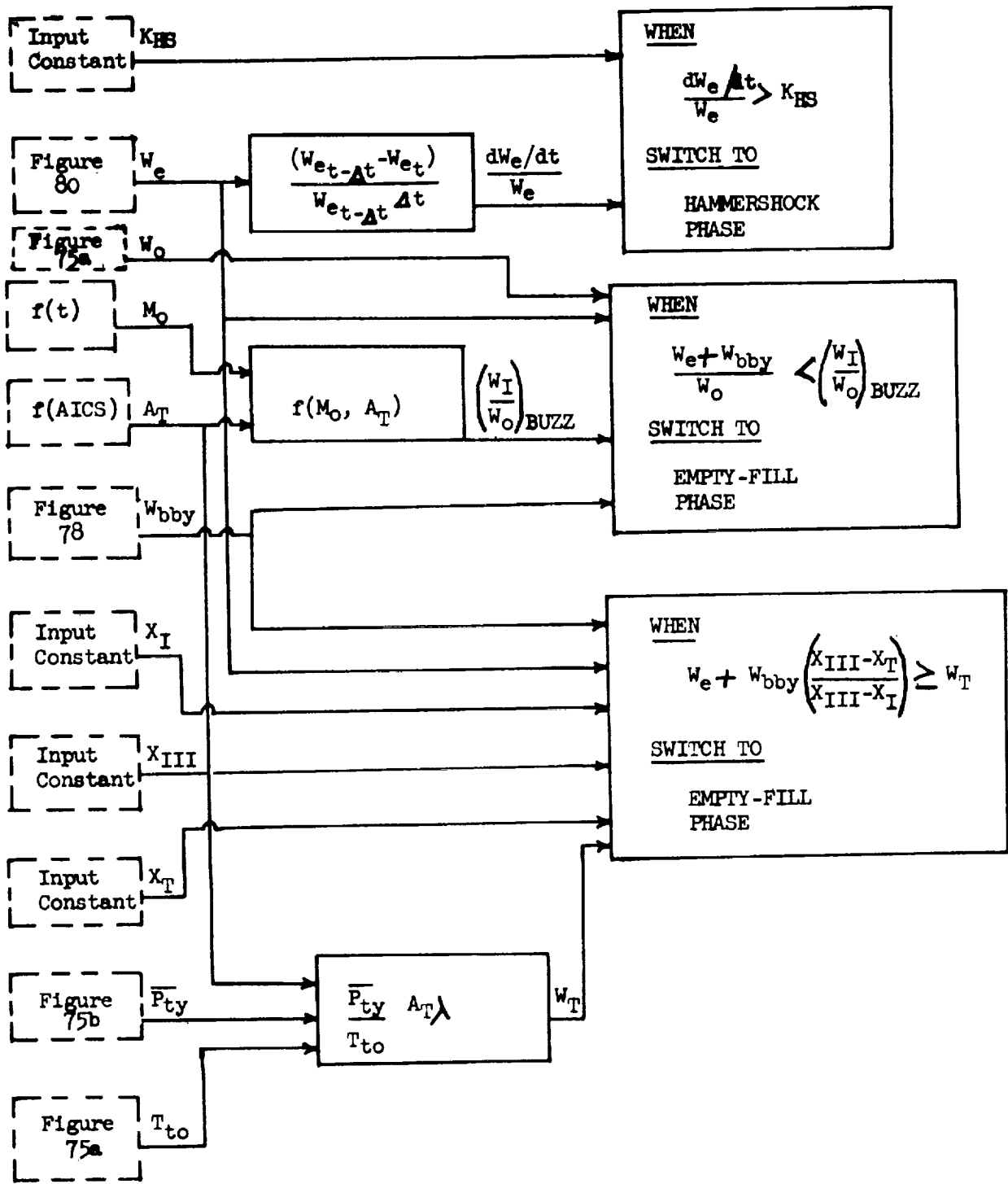
Figure 84. Subcritical Phase Phase Switches
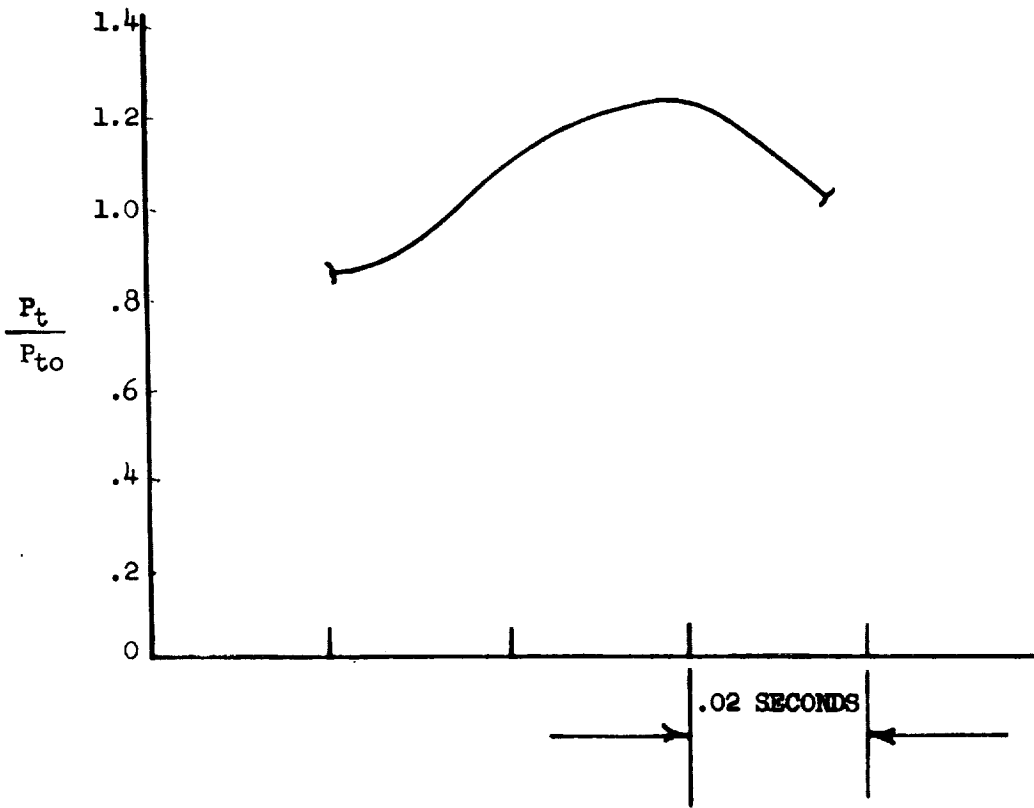
Figure 85. Hammershock Phase Hammershock Pressure Trace

190
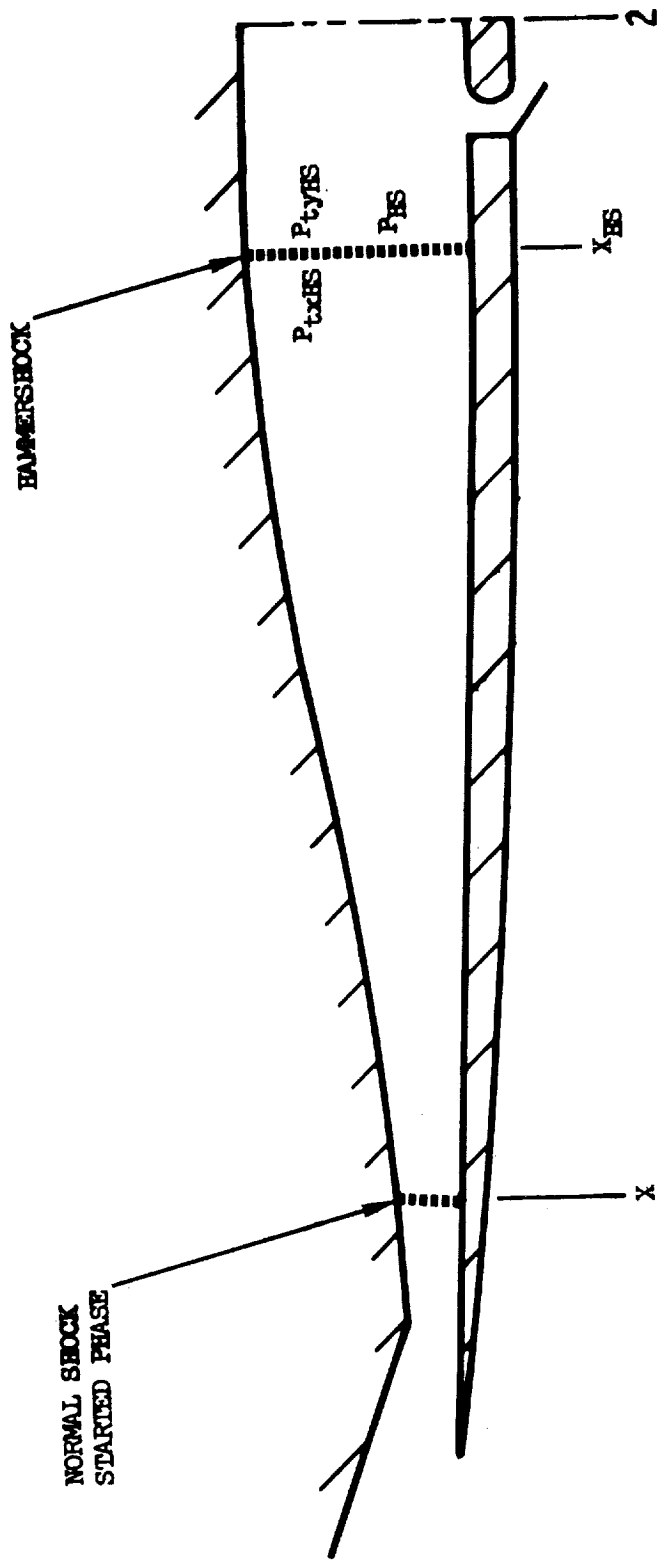
Figure 86. Hammershock Phase of Inlet Operation
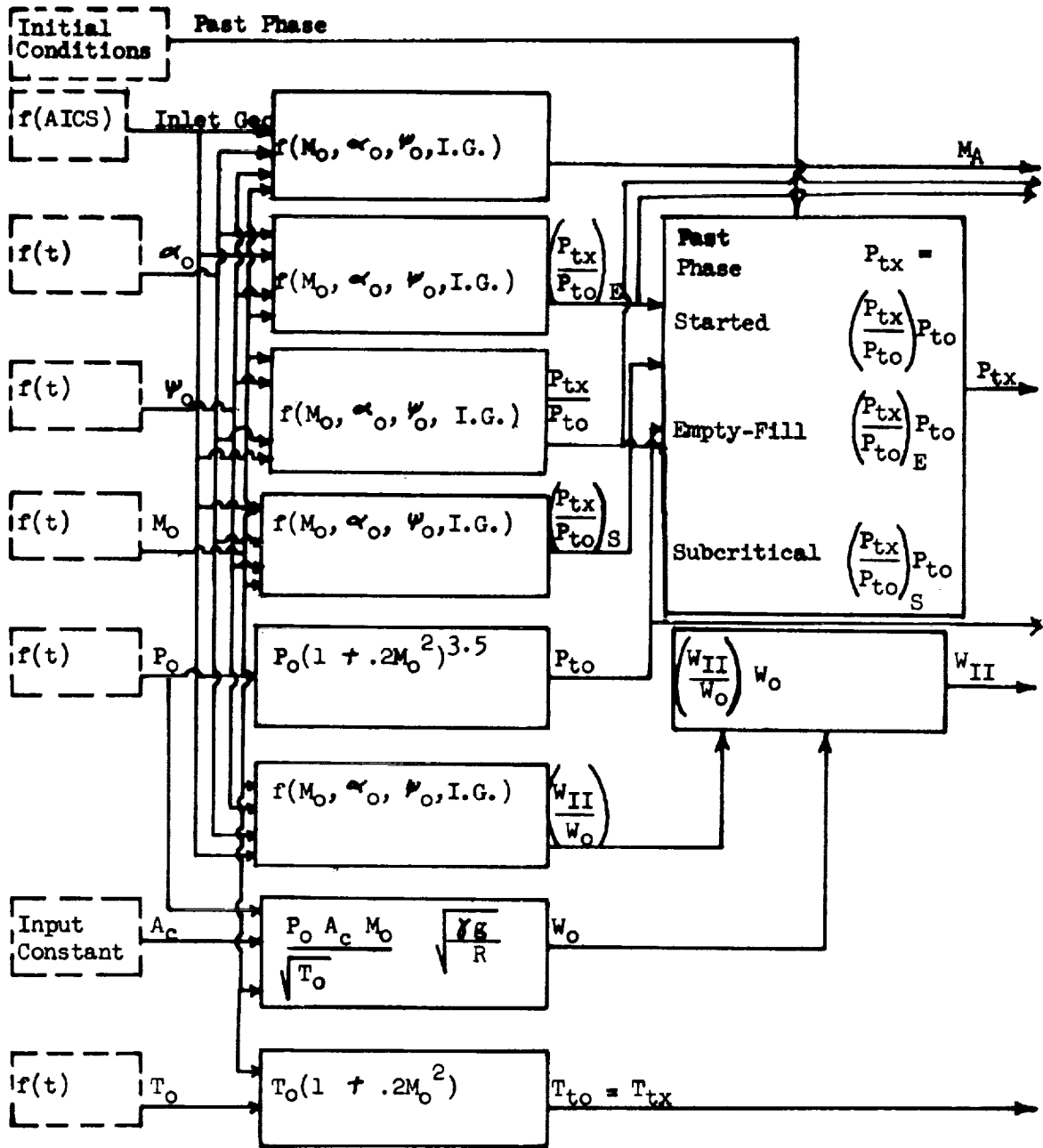
Figure 87. Hammershock Phase Upstream Properties
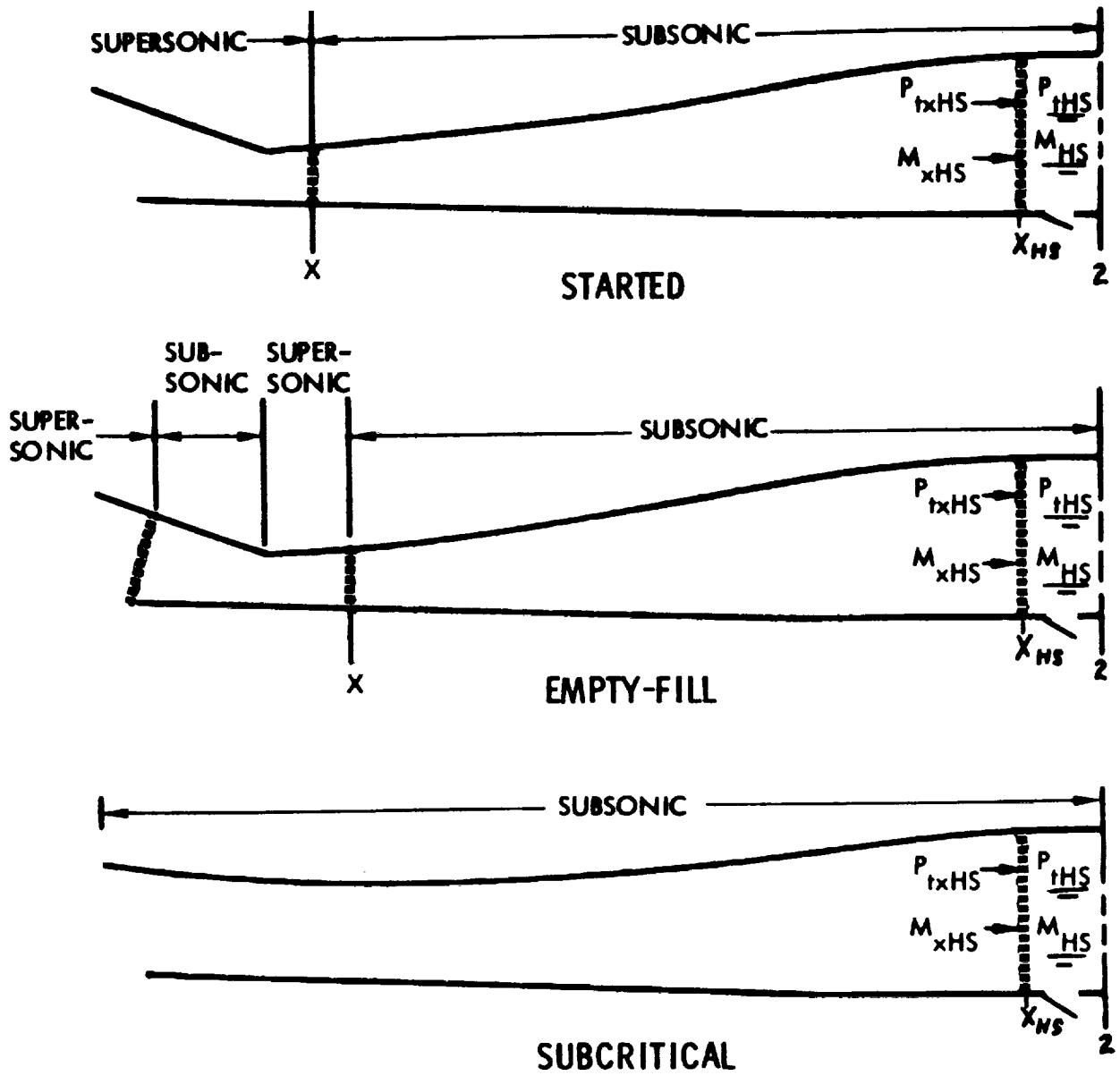
Figure 88. Hammershock Phase Simulation Models
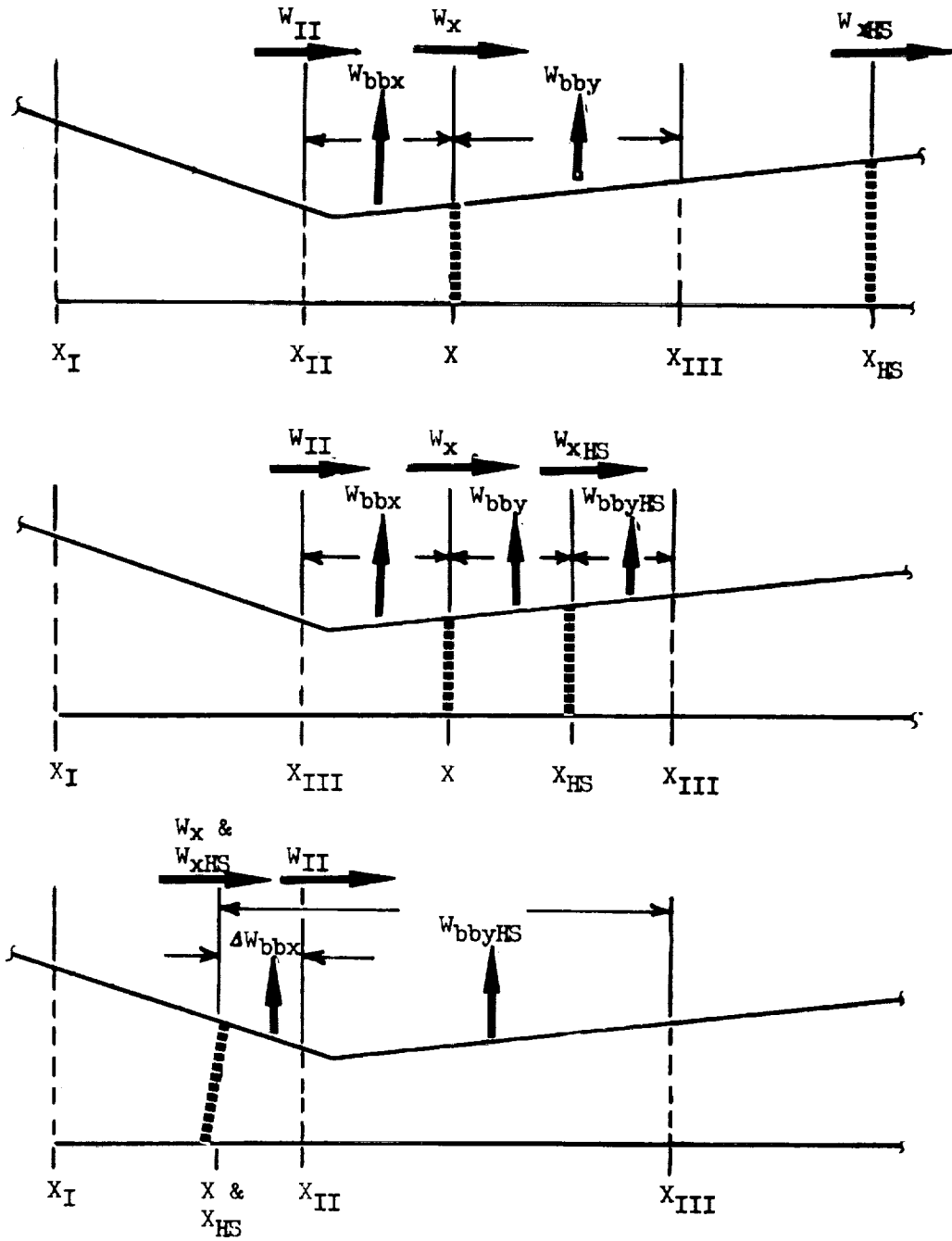
Figure 89a. Hammershock Phase Bleed Flow Schematic Diagram
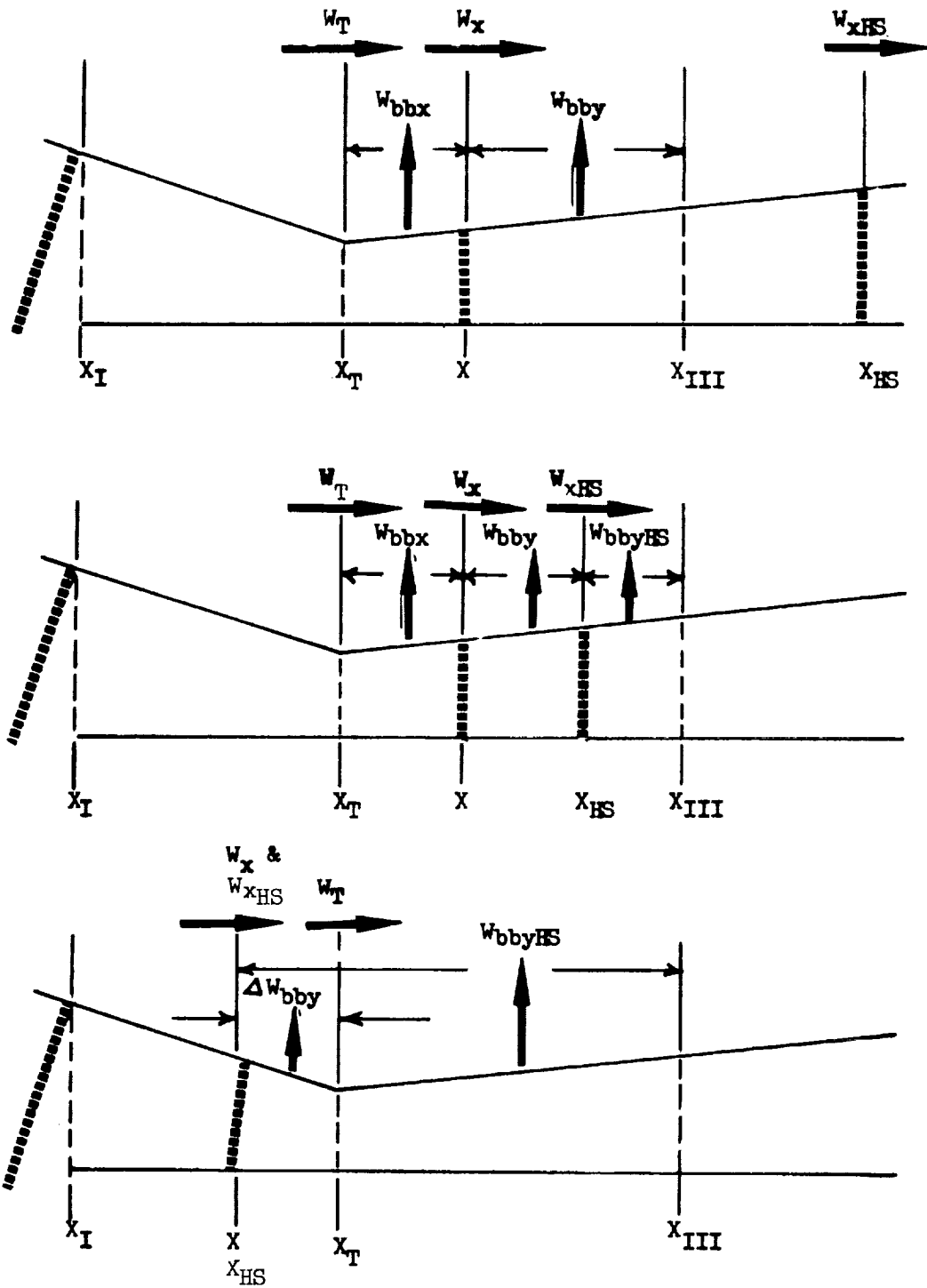
Figure 89b. Hammershock Phase Bleed Flow Schematic Diagram

195
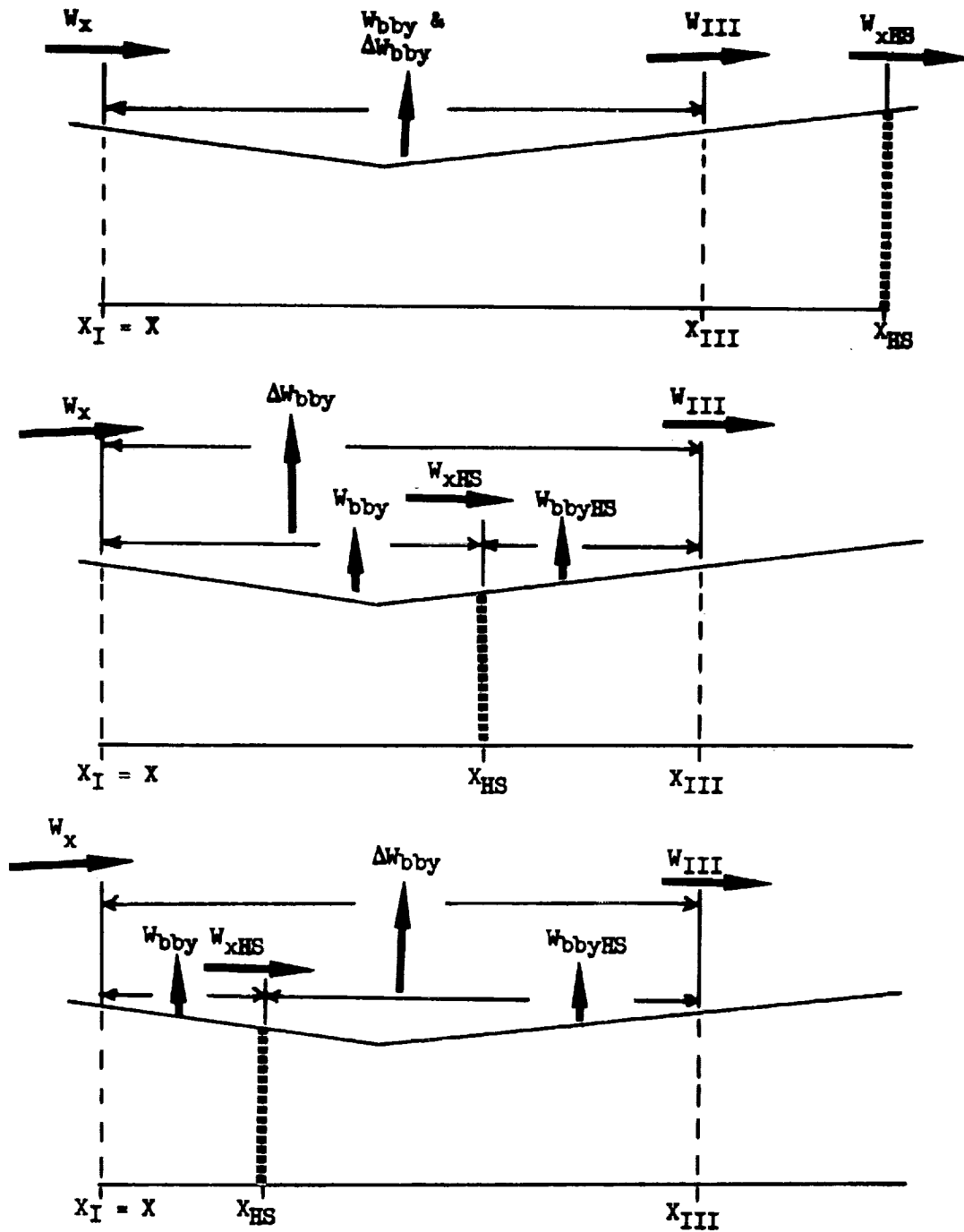
Figure 89c. Hammershock Phase Bleed Flow Schematic Diagram

Initial Condition — X_1

Input Constant — X_T

Figure 100 — X_{HS}

If: $(M_x)_1 =$

$X_{HS} > X_1$ < 1

$X_1 > X_{HS} > X_T$ > 1

$X_{HS} < X_T$ < 1

$(M_x)_1$

Past Phase: Iterative Solution For:

Started $M_x > 1$

Empty-Fill $M_x = (M_x)_1$

Subcritical $M_x < 1$

M_x

Initial Condition — Past Phase

Figure 93 — $A_{x_{ef}}$

Figure 87 — $T_{to} = T_{tx}$

$$\frac{W_x \sqrt{T_{to}}}{P_{tx} A_{x_{ef}}} \sqrt{\frac{R}{\gamma g}} \qquad \frac{M_x}{(1 + .2M_x^2)^3}$$

M_x: $\overline{P_{ty}} =$

> 1 $\left(\dfrac{6M_x^2}{M_x^2+5}\right)^{3.5} \left(\dfrac{6}{7M_x^2-1}\right)^{2.5} P_{tx}$

≤ 1 P_{tx}

$\overline{P_{ty}}$

Figure 87 — P_{tx}

M_x: $\overline{P_y} =$

> 1 $\left(\dfrac{7M_x^2-1}{6}\right)\left(\dfrac{5}{M_x^2+5}\right)^{3.5} P_{tx}$

< 1 $\dfrac{P_{tx}}{(1+.2M_x^2)^{3.5}}$

$\overline{P_y}$

Figure 93 — $A_{T_{ef}}$

$\sqrt{\dfrac{P_{tx}}{T_{tx}}} A_{T_{ef}}$ W_T

Figure 96 — $W_{III} = W_e$

Figure 87 — W_{II}

Figure 95 — ΔW_{bb}

Past Phase: $W_{base} =$

Started W_{II}

Empty-Fill W_T

Subcritical W_{III}

W_{base}

Figure 95 — W_{bbx}

$W_{base} - W_{bbx} + \Delta W_{bb}$ W_x

Figure 90. Hammershock Phase Properties at Station X
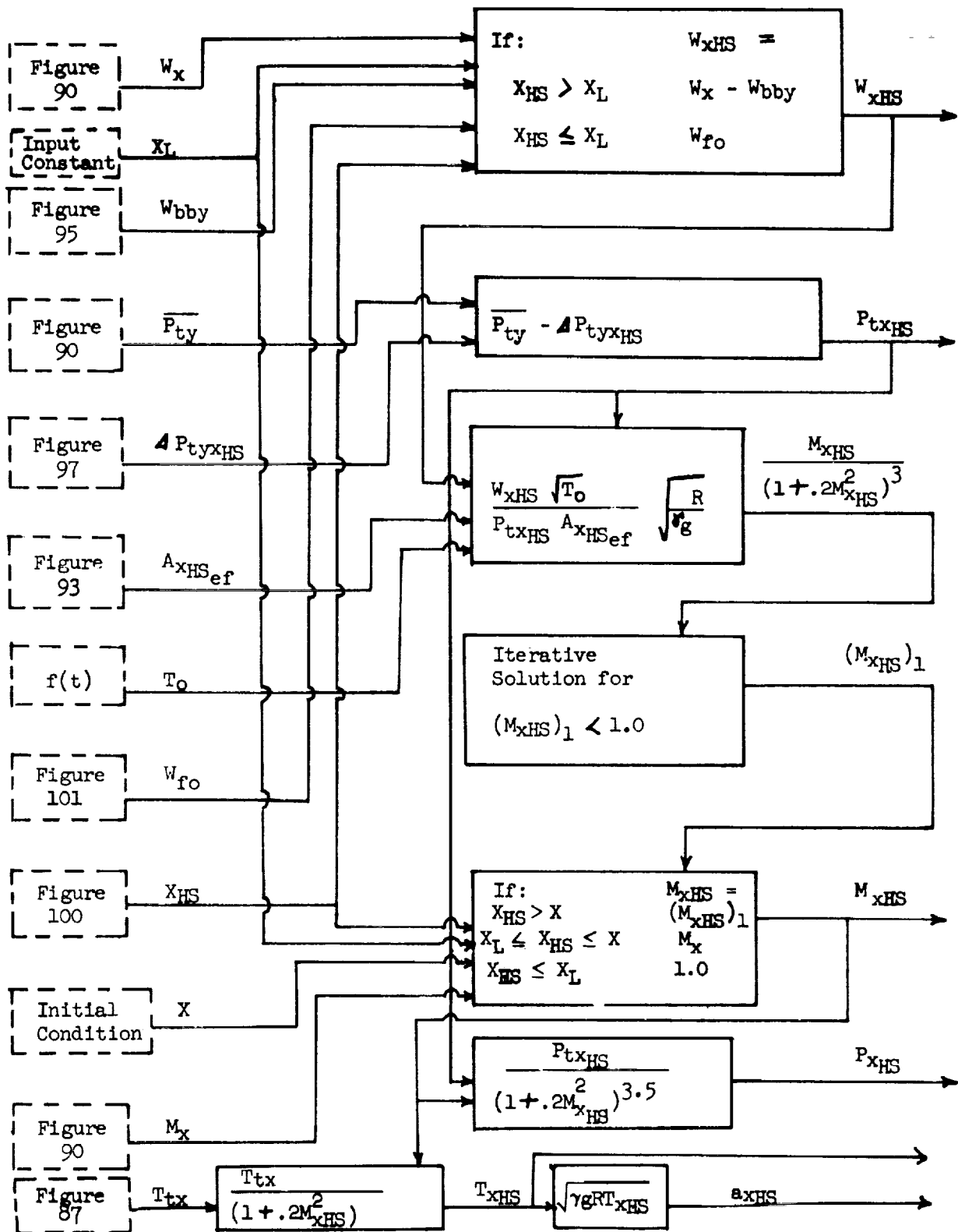
Figure 91. Hammershock Phase Properties at the Hammershock Station
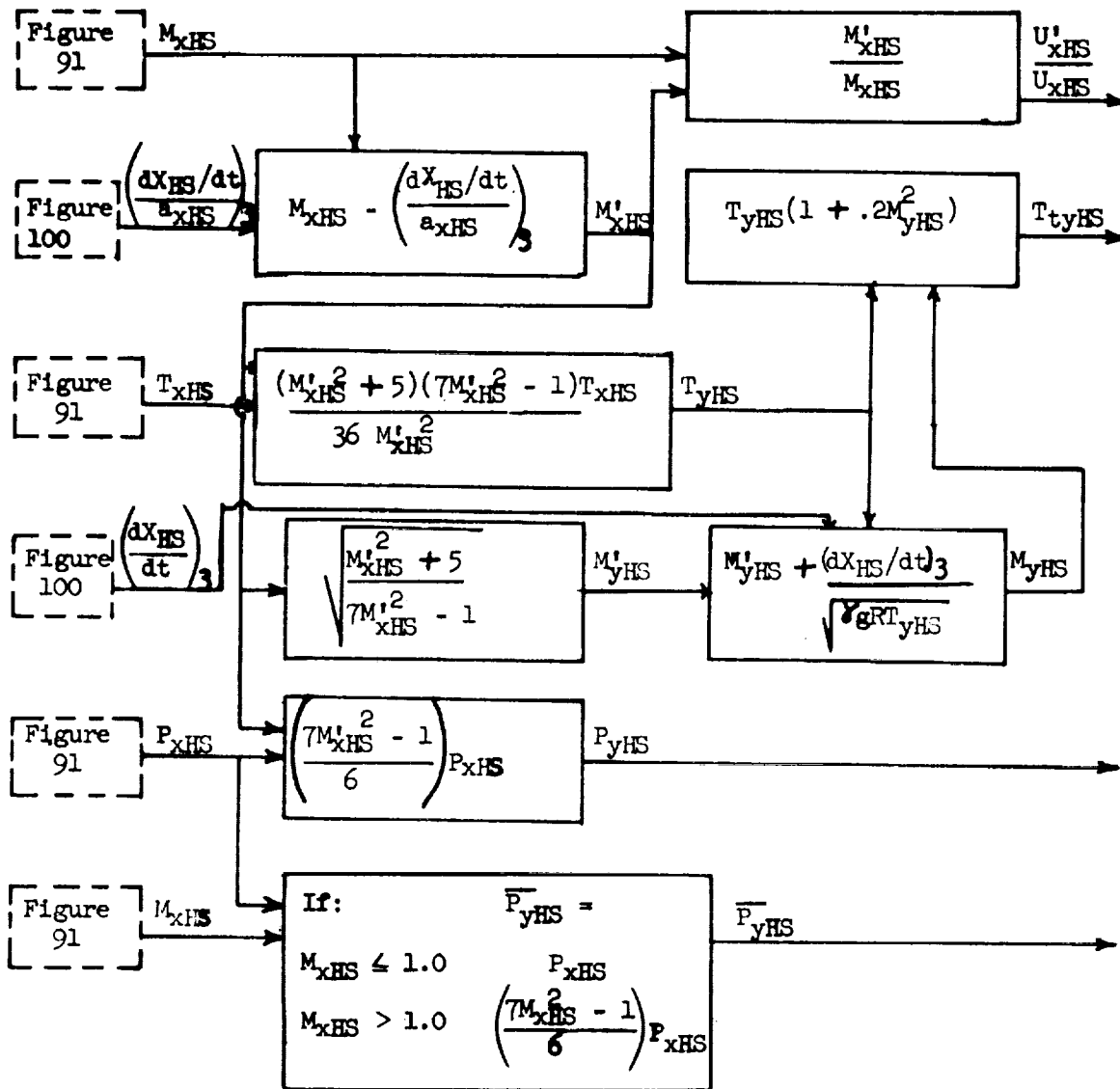
Figure 92. Hammershock Phase Properties Behind the Hammershock
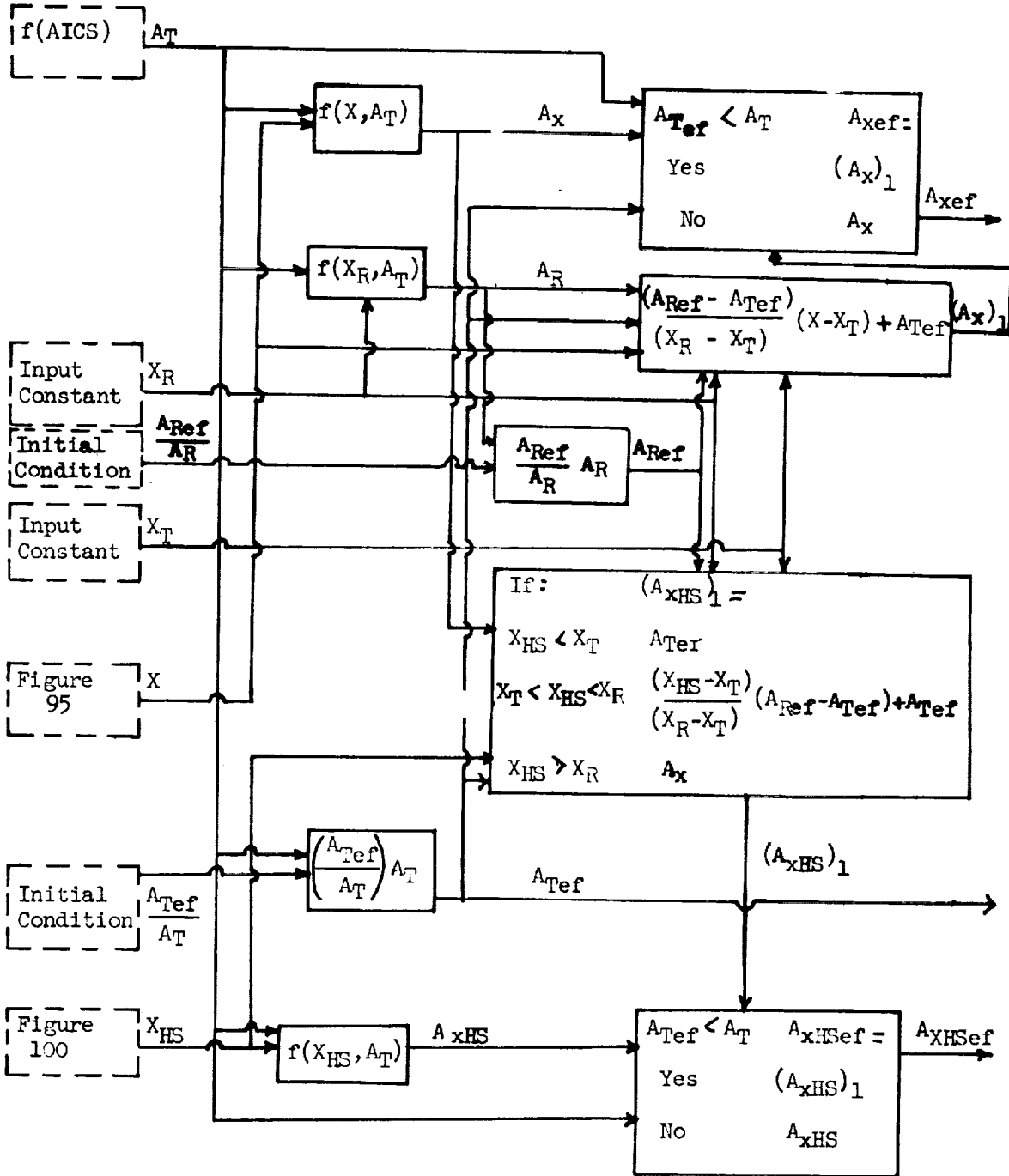
Figure 93. Hammershock Phase Effective Flow Area

Input Constant — X_R

$f(X_R, A_T)$ → V_R

Figure 93 — A_{xHSef}

Figure 93 — A_{Ref}

If:
$$V_{HSef} =$$

$$X_{HS} < X_T \quad A_{Tef}(X_T - X_{HS}) + \frac{(A_{Ref} + A_{Tef})}{2}(X_R - X_T) + V_R$$

$$X_T < X_{HS} < X_R \quad \frac{(A_{Ref} + A_{xHSef})}{2}(X_R - X_{HS}) + V_R$$

$$X_{HS} > X_R$$

V_{HS} V_{HSef}

Input Constant — X_T

Figure 100 — X_{HS}

$$V_{HS} = f(X_{HS}, A_T)$$ V_{HS}

Figure 93 — A_{Tef}

$f(AICS)$ — A_T

$A_{Tef} < A_T$	$V_{HSef} =$
YES	V_{HSef}
No	V_{HS}

→ V_{HSef}
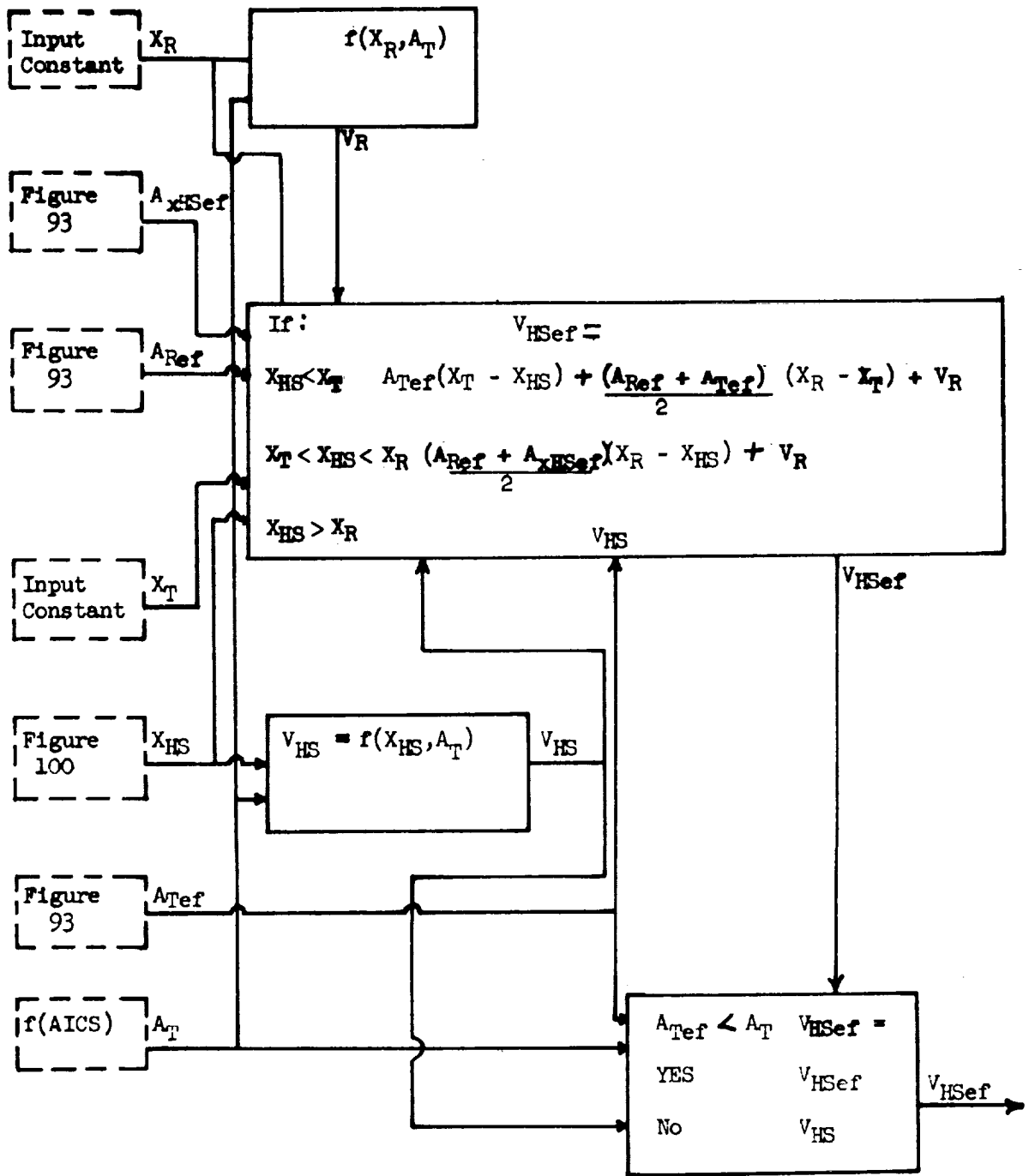
Figure 94. Hammershock Phase Effective Volume

201
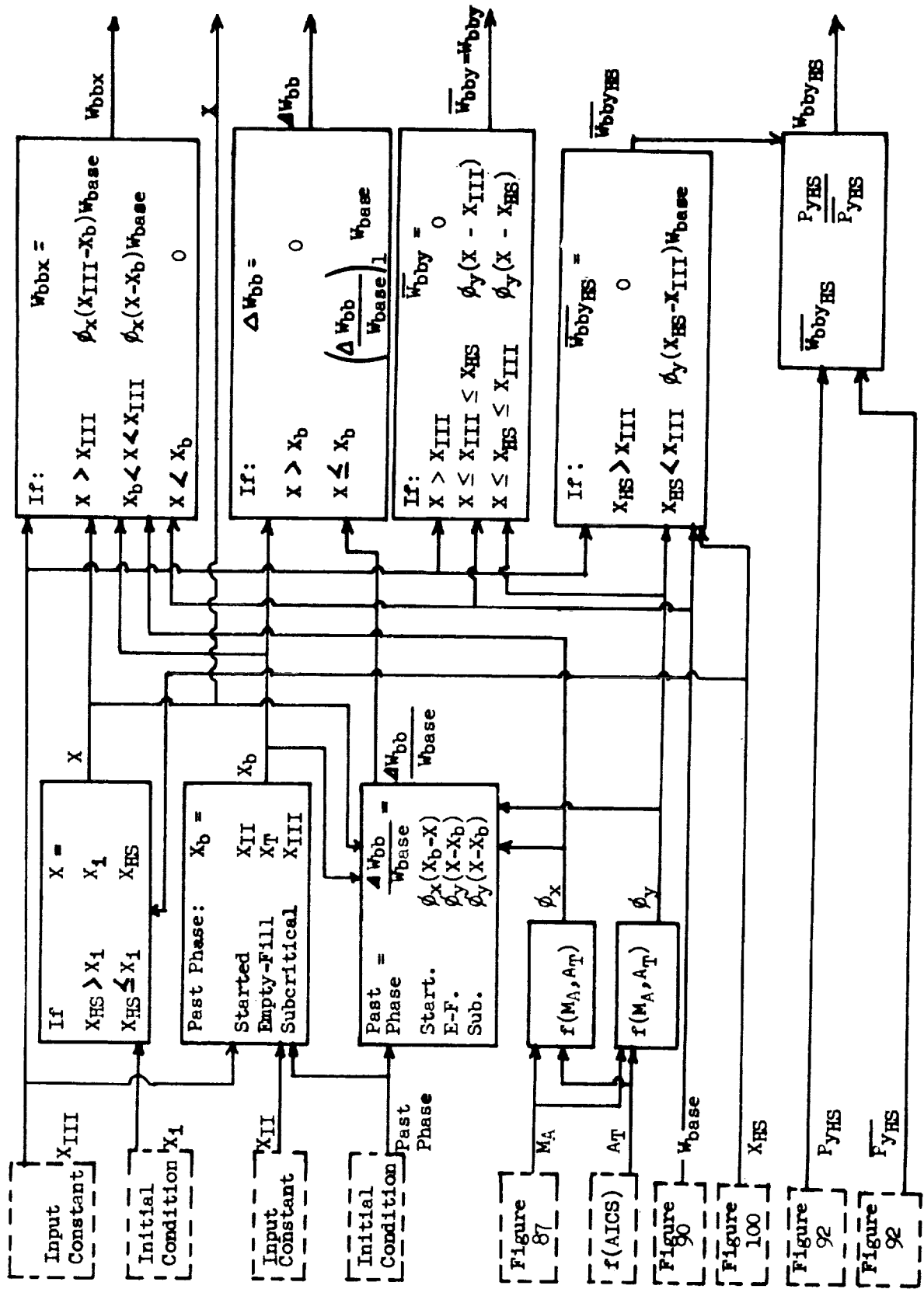
Figure 95. Hammershock Phase Bleed Flows

202
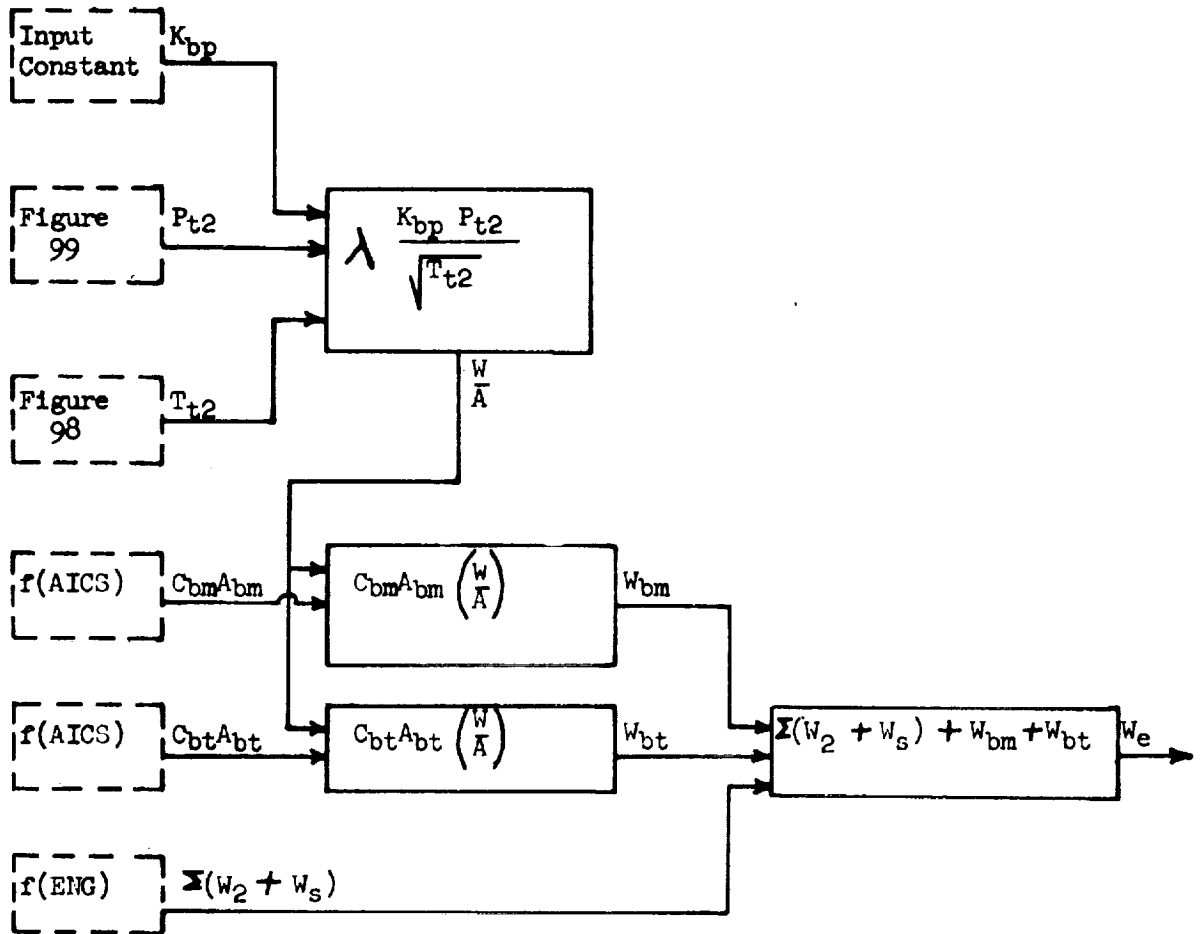
Figure 96. Hammershock Phase Bypass and Engine System Airflows
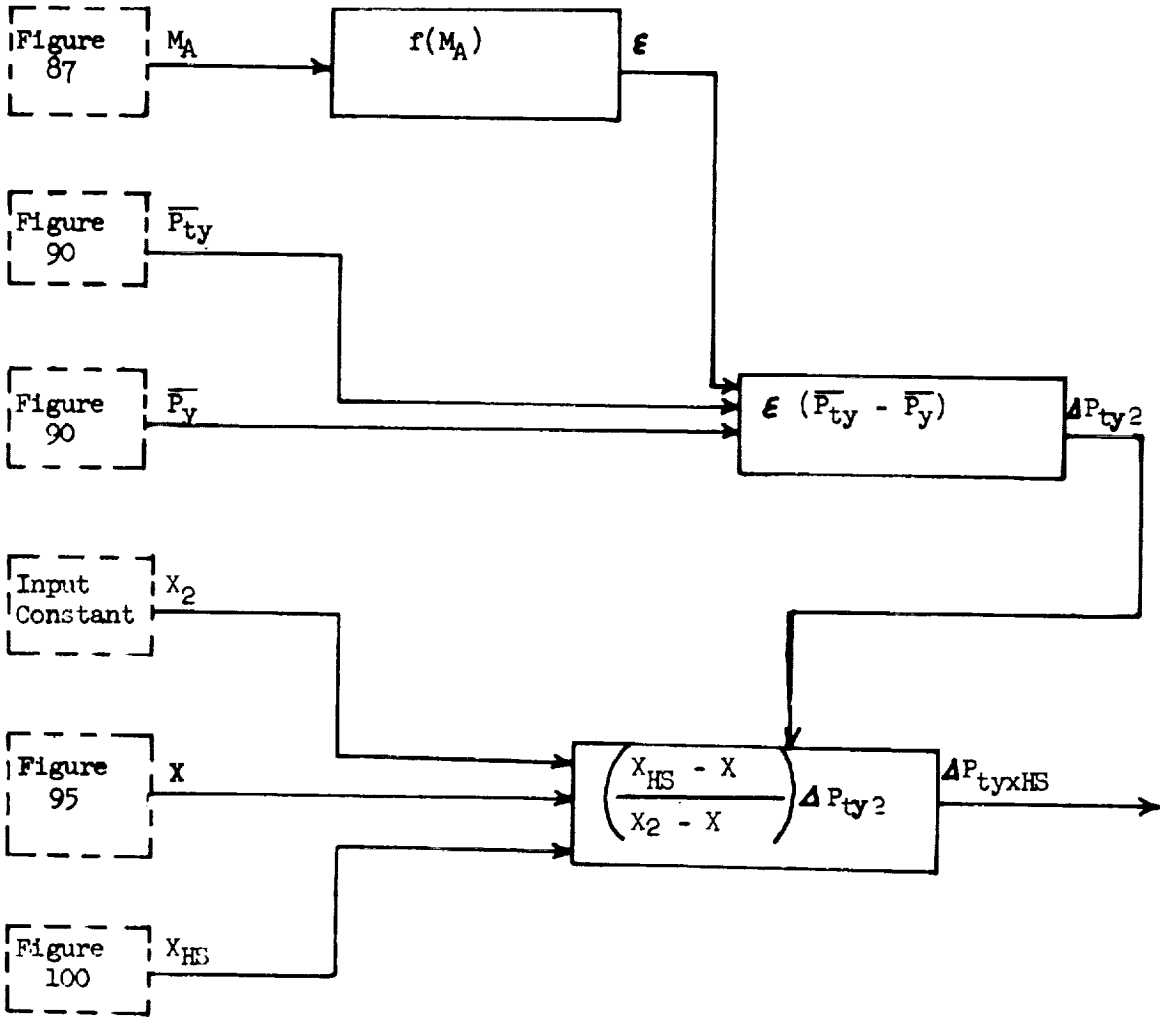
Figure 97. Hammershock Phase Subsonic Flow Total Pressure Loss

204
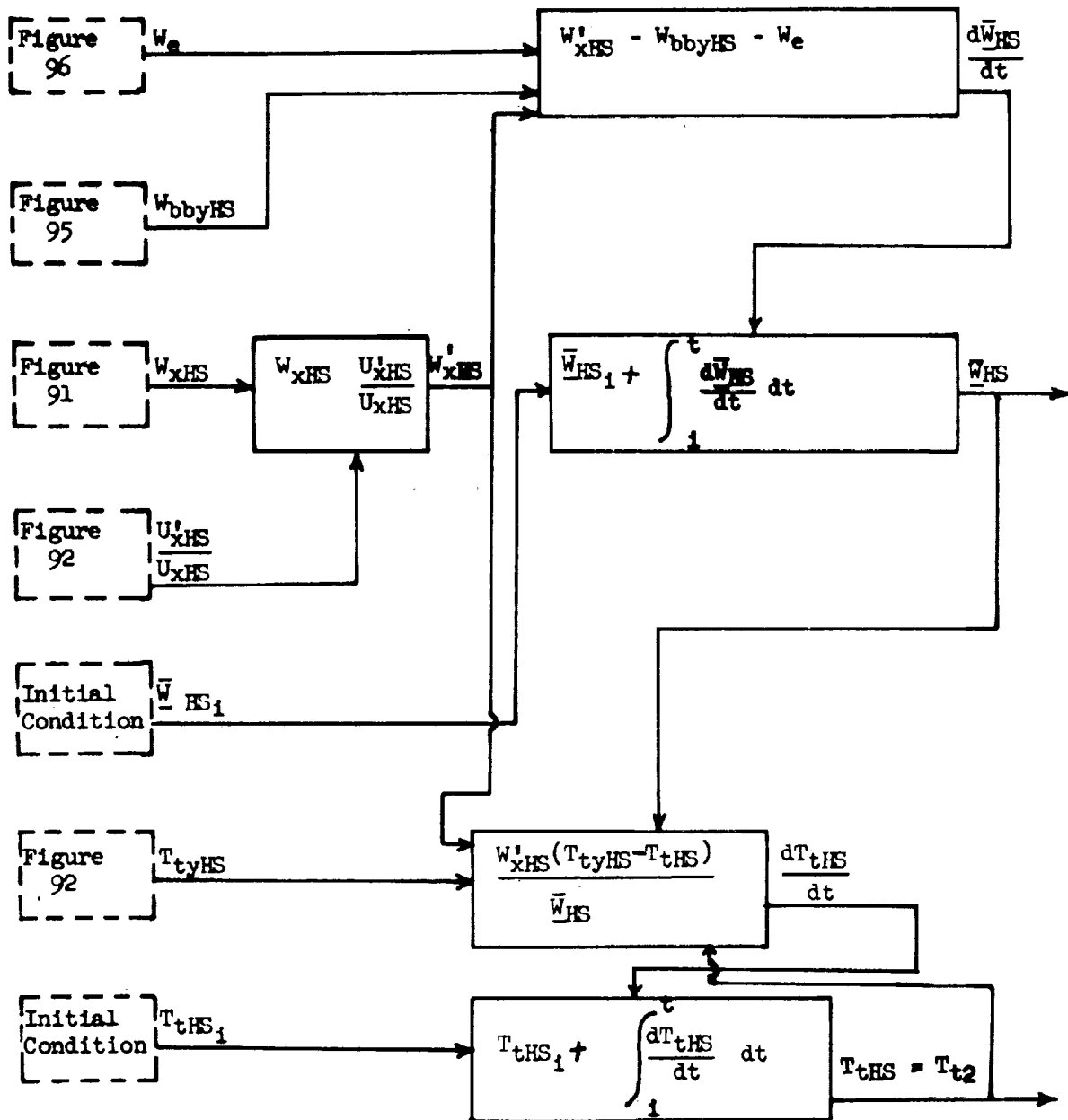
Figure 98. Hammershock Phase Hammershock Volume Mass & Total Temperature
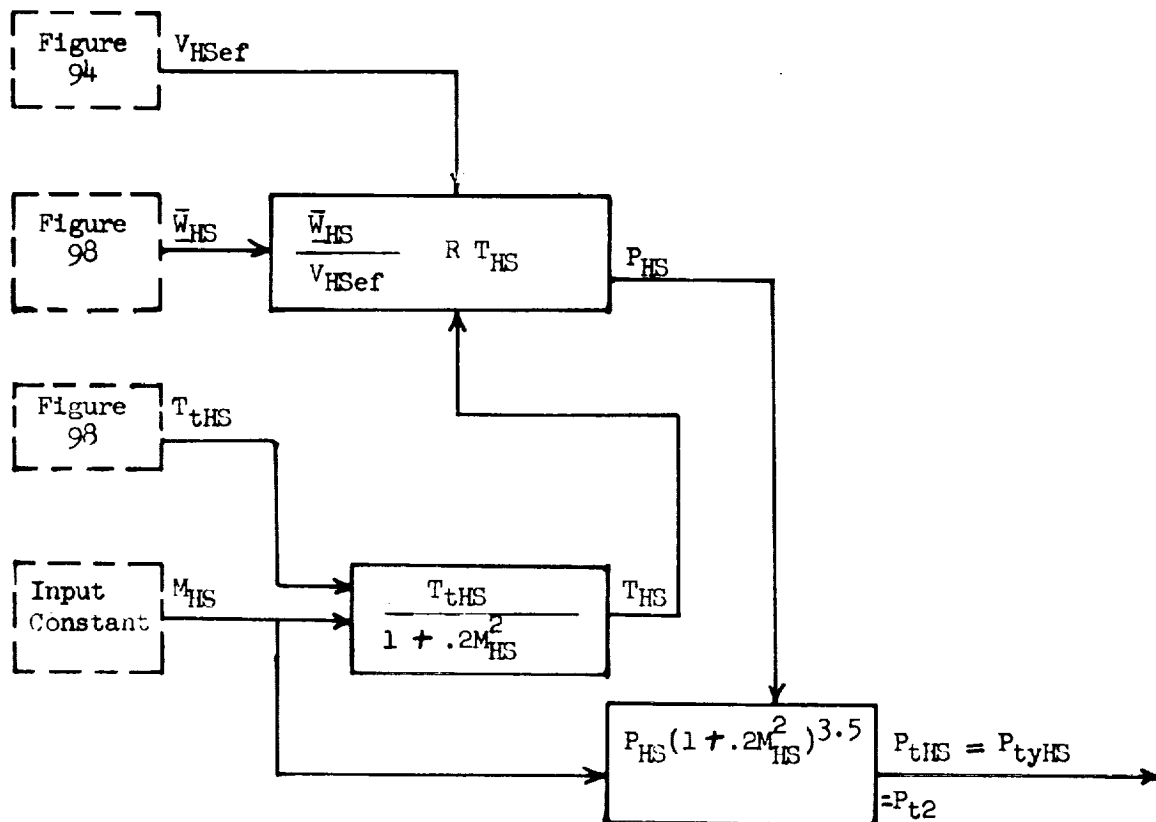
Figure 99. Hammershock Phase Hammershock Volume Pressures
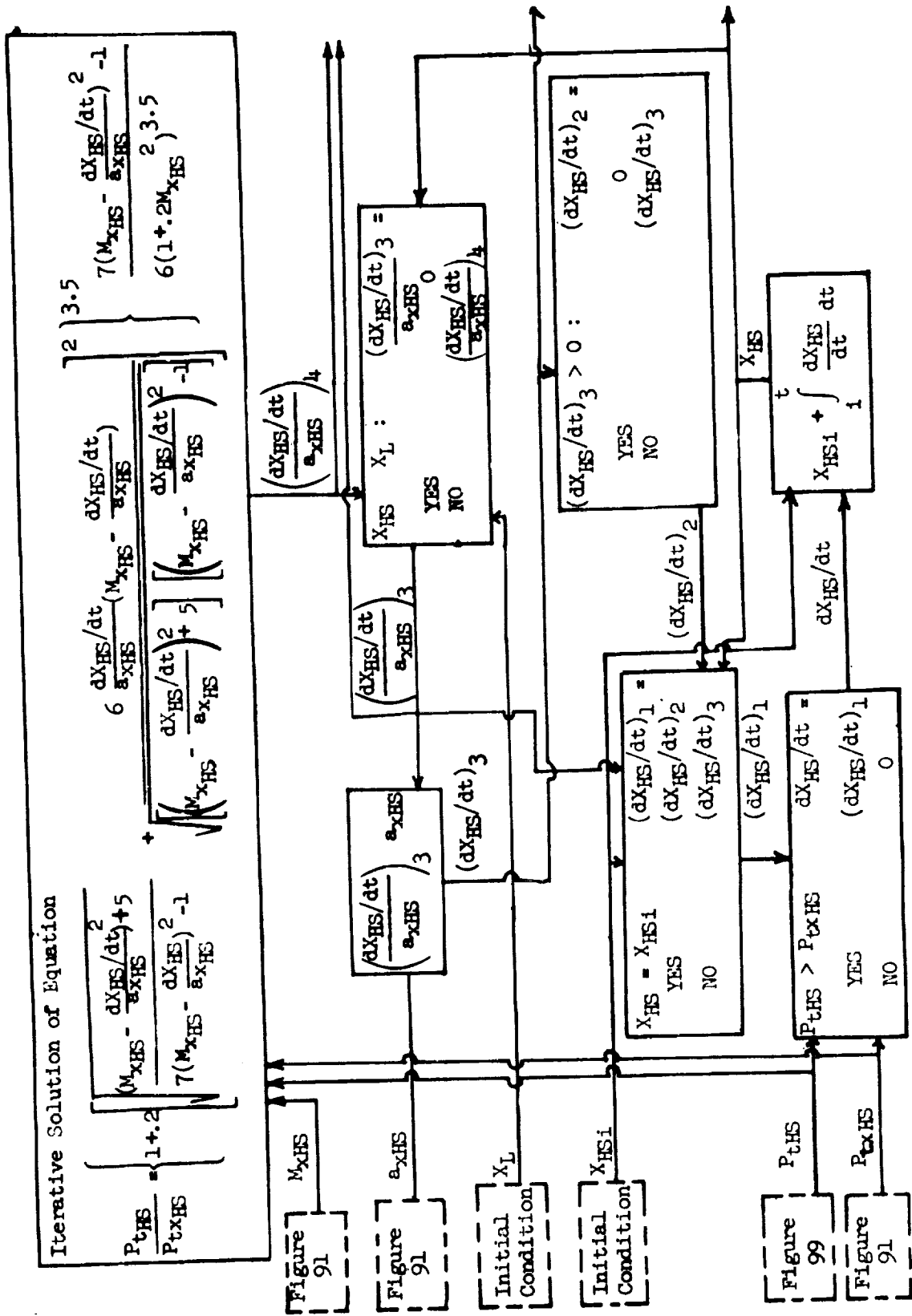
Figure 100. Hammershock Phase Hammershock Velocity and Position

207
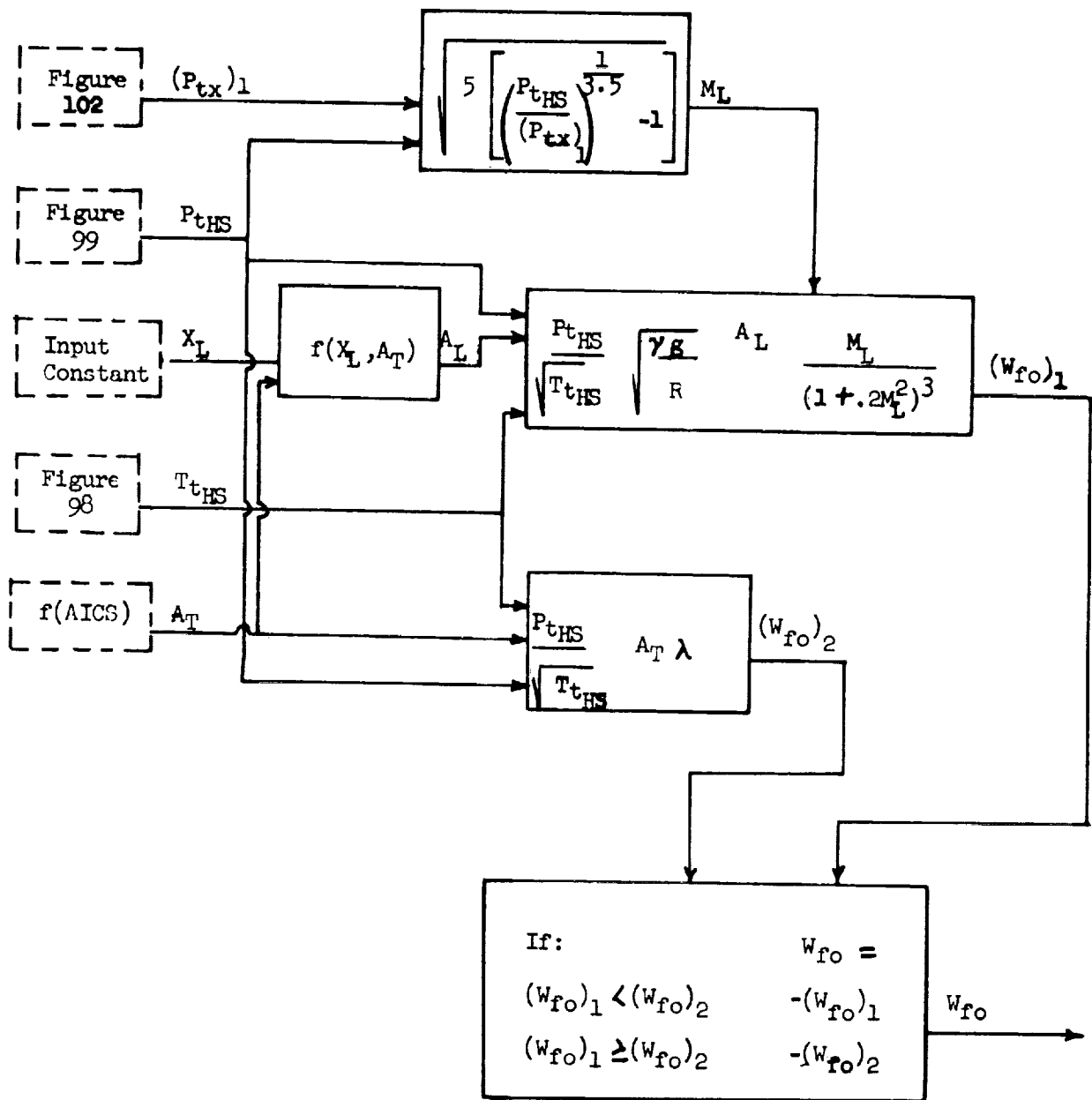
Figure 101. Hammershock Phase Forward Outflow
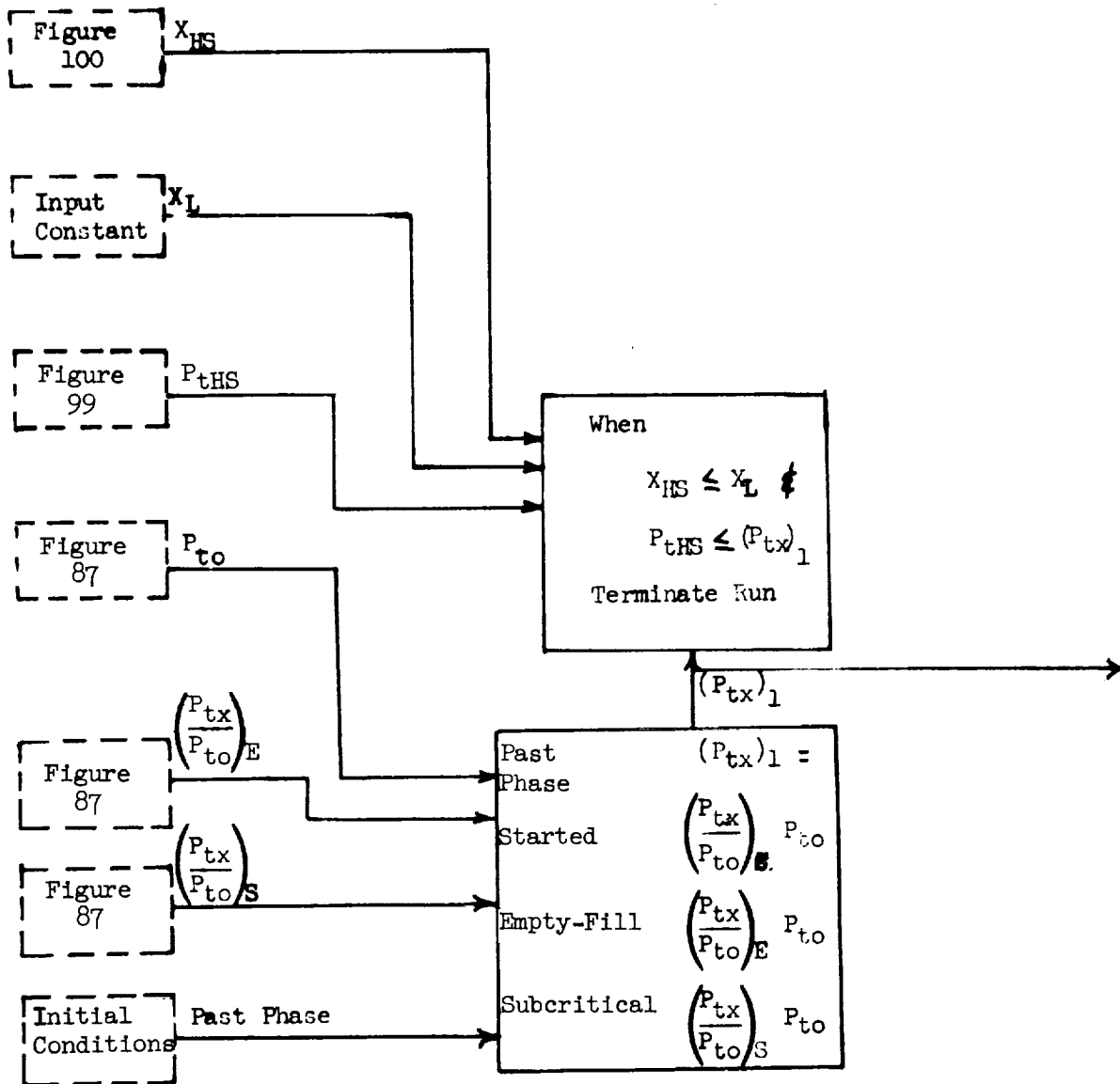
Figure 102. Hammershock Phase Phase Switches

209
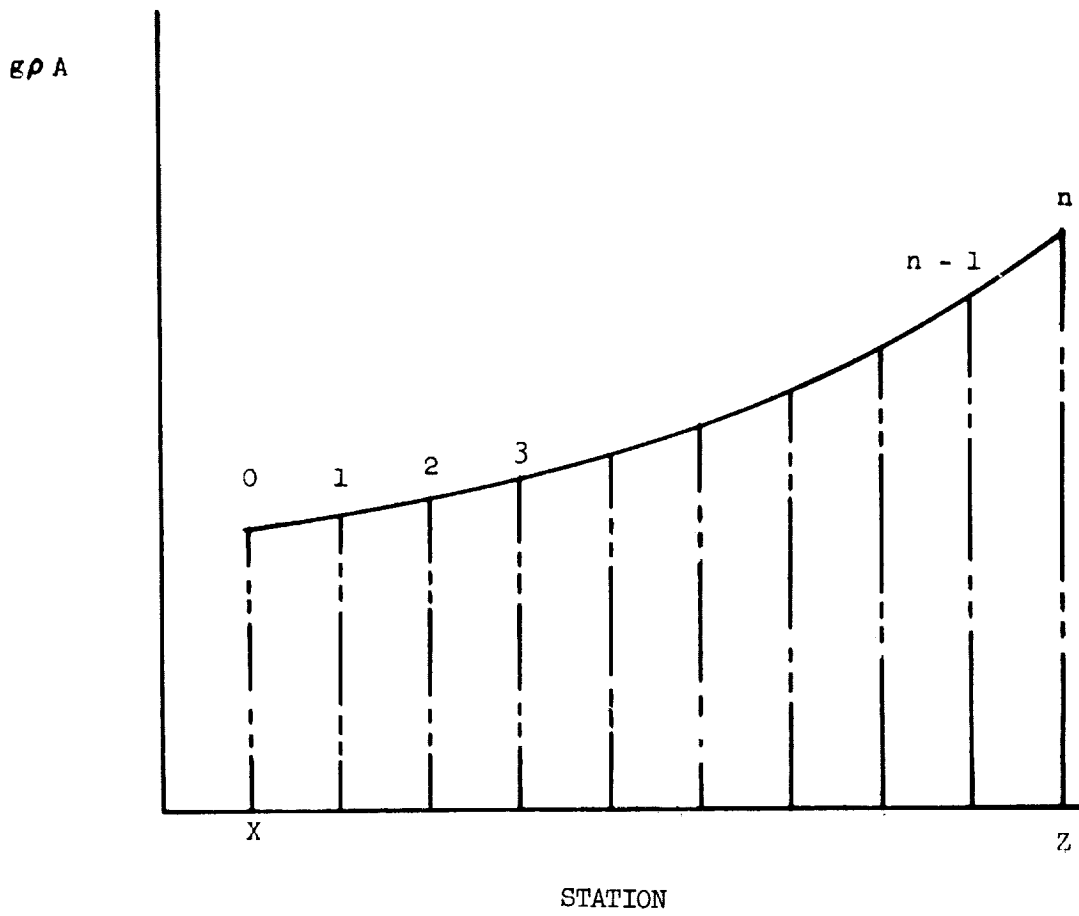
Figure 103. Initial Conditions - Simpson's Rule Determination of $\overline{W}_H$
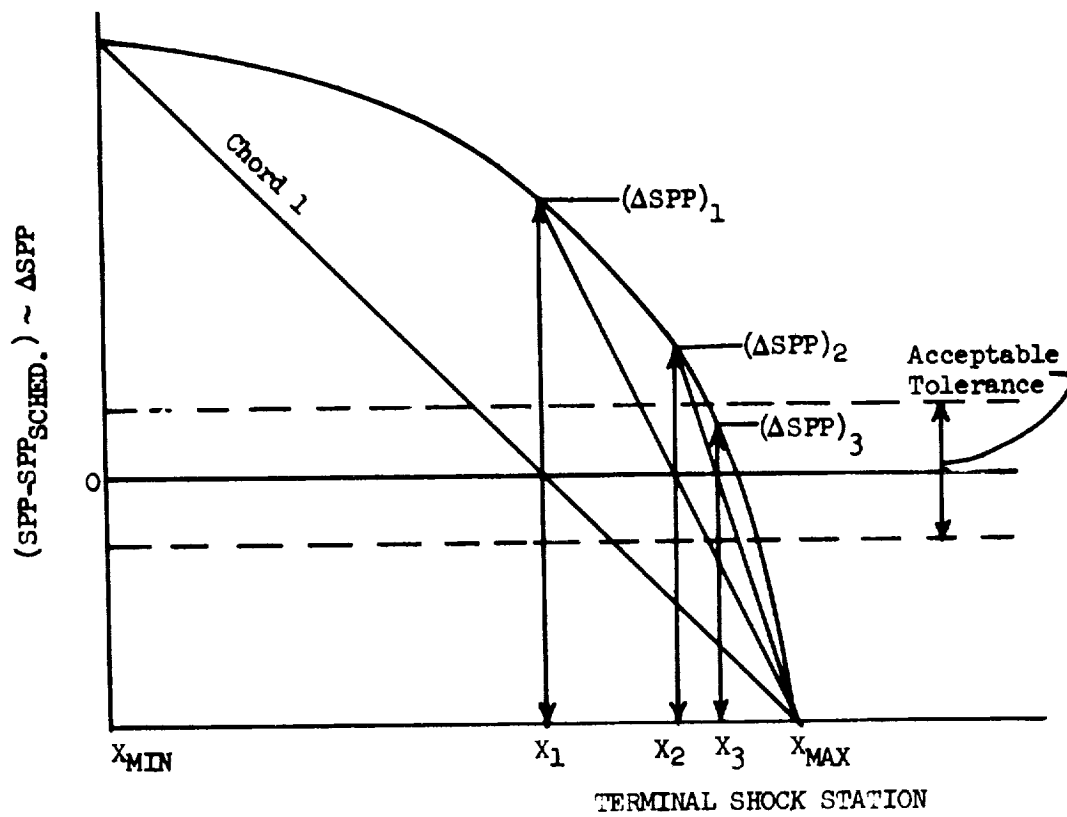
Figure 104. Initial Conditions - Slope Method of Successive Approximations

APPENDIX A

INSTANTANEOUS MOMENTUM SIMULATION MODEL FOR THE STARTED PHASE

The "instantaneous momentum" model differs from the "frozen plug" model described in the text only in the assumptions made relative to the Helmholtz Volume.

In the "frozen plug" concept, flow throughout the Helmholtz Volume is assumed to be in instantaneous equilibrium with conditions just downstream of the terminal shock. Consequently, P_{zH} , the pressure at the downstream face of the Helmholtz Volume, can be computed knowing only the upstream properties and the terminal shock velocity. P_{zD} , static pressure at the upstream face of the Duct Volume is then computed from continuity relationships. During non-steady state conditions, P_{zH} differs from P_{zD} . The difference of these pressures acting on the common interface provides an unbalanced force acting to change the momentum of the air in the Helmholtz Volume,

$$(P_{zD} - P_{zH}) \ A_z = \frac{d}{dt}\left(\frac{\overline{W}_H}{g} \ \frac{dX}{dt}\right)$$

By contrast, in the "instantaneous momentum" concept, the momentum equation for the air in the Helmholtz Volume is

$$P_y A_y + P_w A_w - P_z A_z + \frac{W_y U_y}{g} - \frac{W_z U_z}{g} = \frac{d}{dt}\left(\frac{\overline{W}_H}{g} \ \frac{dX}{dt}\right)$$

Figure A-1 illustrates the forces acting on the air in the Helmholtz Volume.

To evaluate the momentum equation, the assumption is made that P_w , the wall force pressure, is between and proportional to the static pressures

at the upstream and downstream faces of the Helmholtz Volume. Specifically, it is assumed that

$$P_W = KP_y + (1 - K)P_z$$

or

$$K = \frac{P_z - P_W}{P_z - P_y}$$

The further assumption is made that the factor K computed for quasi-steady state conditions is applicable to dynamic conditions. During quasi-steady state conditions,

$$\frac{d}{dt}\left(\frac{W_H}{g} \frac{dX}{dt}\right) = 0$$

Therefore

$$\overline{P_W} A_W = \frac{W_z U_z}{g} - \frac{W_y U_y}{g} + \overline{P_z} A_z - \overline{P_y} A_y$$

Inasmuch as $A_W = A_z - A_y$,

$$K = \frac{\overline{P_z} - \left(\dfrac{1}{A_z - A_y}\right)\left(\dfrac{\overline{W_z} \overline{U_z}}{g} - \dfrac{\overline{W_y} \overline{U_y}}{g} + \overline{P_z} A_z - \overline{P_y} A_y\right)}{\overline{P_z} - \overline{P_y}}$$

Then, for dynamic conditions

$$P_W A_W = P_z A_z - P_y A_y + \left(\frac{P_z - P_y}{\overline{P_z} - \overline{P_y}}\right)\left(\frac{W_z U_z}{g} - \frac{W_y U_y}{g}\right)$$

Substituting the wall force equation into the momentum equation,

$$\left(\frac{P_z - P_y}{\overline{P_z} - \overline{P_y}}\right)\left(\frac{\overline{W_z} \overline{U_z}}{g} - \frac{\overline{W_y} \overline{U_y}}{g}\right) - \left(\frac{W_z U_z}{g} - \frac{W_y U_y}{g}\right) = \frac{d}{dt}\left(\frac{\overline{W_H}}{g} \frac{dX}{dt}\right)$$

An alternate form of the above equation is

$$\frac{P_z - P_y}{\overline{P_z} - \overline{P_y}} \left(\overline{P_z} \gamma \overline{M_z}^2 A_z - \overline{P_y} \gamma \overline{M_y}^2 A_y \right) - \left(P_z \gamma M_z^2 A_z - P_y \gamma M_y^2 A_y \right)$$

$$= \frac{d}{dt} \left(\frac{W_H}{g} \frac{dX}{dt} \right)$$

Simulation runs have shown that the "instantaneous momentum" concept, as compared to the "frozen plug" concept, has the following characteristics.

1) The physically unrealistic discontinuity in pressures at the interface between the Helmholtz Volume and the Duct Volume is eliminated.

2) The dynamic response characteristics are much more sensitive to the selected length of the Helmholtz Volume. This factor enables better matching of test and simulation data, but introduces further uncertainties when test data is not available to help determine Helmholtz Volume length.

3) The simulation equations are more numerous, and the ratio of computer time to real time is greater.
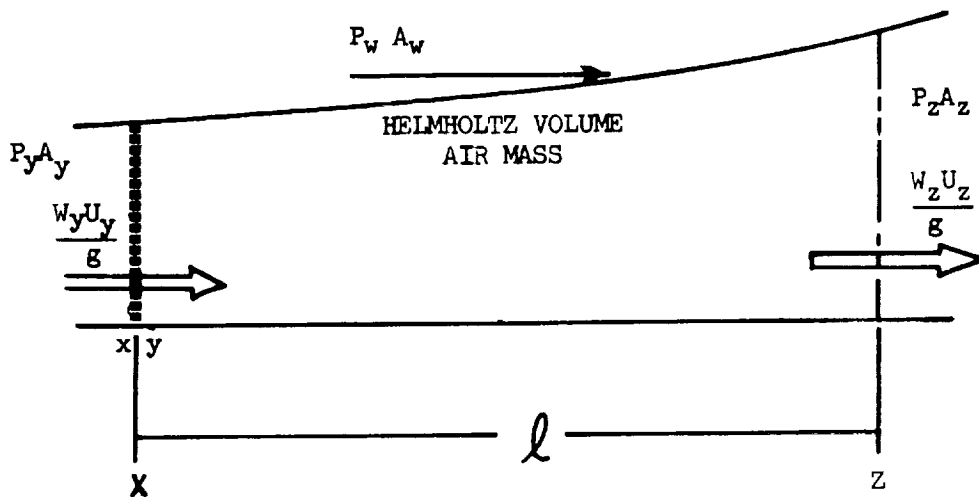
Figure A-1. Pressures Acting On The Helmholtz Volume Air Mass

REFERENCES

1. Martin, Arnold W.; Wong, H. W. : Propulsion System Dynamic Simulation Program User's Manual. NASA CR 73113

2. Ames Research Staff: Equations, Tables, and Charts for Compressible Flow. NACA Report 1135, 1953.

3. Martin. Arnold W. : Propulsion System Dynamic Simulation Data. NASA CR 73115

4. Moeckel, W. E. : Approximate Method for Predicting Form and Location of Detached Shock Waves Ahead of Plane or Axially Symmetric Bodies. NACA TN 1921, 1949.